

Northumbria Research Link

Citation: Omoware, Wisdom (2017) Wind Turbine Blades Made of Functional Materials. Doctoral thesis, Northumbria University.

This version was downloaded from Northumbria Research Link:
<http://nrl.northumbria.ac.uk/id/eprint/38080/>

Northumbria University has developed Northumbria Research Link (NRL) to enable users to access the University's research output. Copyright © and moral rights for items on NRL are retained by the individual author(s) and/or other copyright owners. Single copies of full items can be reproduced, displayed or performed, and given to third parties in any format or medium for personal research or study, educational, or not-for-profit purposes without prior permission or charge, provided the authors, title and full bibliographic details are given, as well as a hyperlink and/or URL to the original metadata page. The content must not be changed in any way. Full items must not be sold commercially in any format or medium without formal permission of the copyright holder. The full policy is available online: <http://nrl.northumbria.ac.uk/policies.html>



**Northumbria
University**
NEWCASTLE



UniversityLibrary

Wind Turbine Blades Made of Functional Materials

Wisdom Dadakpoye Omoware

A Thesis Submitted in Partial Fulfilment of the Requirements of
the
University of Northumbria at Newcastle for the Degree of
Doctor of Philosophy

A Research Undertaken in the Faculty of
Engineering and Environment

November 2017

DECLARATION

I hereby declare that the research work contained in this thesis has not been submitted for any other award and that it is my own work. I also confirm that this research work fully acknowledges the ideas, opinions and contributions from the work of others.

Name: Wisdom Dadakpoye Omoware

Signature:

Date:

ABSTRACT

Blades are designed to have good rigidity to be able to minimise the destruction that could be caused by rapid wind load and gust. The increase in length of the wind turbine contributes to the susceptibility of the wind turbine blade to the unpredictable destruction caused by random gusts. One of the ways to effectively increase the blade flexibility as well as increase its unloading effect led to the focus of this research on adaptive wind turbine blades. The project aims to investigate the potential benefits of flapping blades in the extraction of wind energy and proposing an analytical model for the prediction of the normalised induced twist with the sole purpose of having a robust tool for optimal design of adaptive wind turbine blades. In order to achieve these goals, the project is carried out in two aspects. Firstly, a proof of concept of a flapping blade; this report presents the preliminary results of the numerical simulation of a flapping-pitching rectangular flat plate in a uniform air flow. Various combinations of flapping amplitude, flapping frequency and pitching amplitude are analysed and their effect on the instantaneous and maximum lift coefficient is presented. The change in the flapping frequency and amplitude were shown to have considerable effect on the lift coefficient. It can be deduced from the results that the lift coefficient is influenced by the flapping frequency and flapping amplitude combination. The lift coefficient is most affected by the flapping amplitude when compared to the flapping frequency. The results indicate that the pitching amplitude initially enhances the lift coefficient. However, excessive pitching amplitude results in low lift coefficient.

The second aspect is to develop a robust analytical model for the prediction of the normalised induced twist of an adaptive blade. Wind turbine adaptive blade design is a coupled aero-structure (CAS) design process, in which, the aerodynamic performance evaluation requires structural deformation analysis of the adaptive blade. However, employing finite element analysis (FEA) based commercial packages for the structural deformation analysis as part of the aerodynamic objective evaluation process has been proven to be time consuming. In order to develop the robust tool for the prediction of the normalised induced twist, the effect of shell thickness distributions, fibre angle distributions and materials are investigated using arbitrary lay-ups configurations. The structural/material configurations and the analyses of the adaptive blades are performed using an auxiliary software tool developed via MATLAB codes for implementing structural deformation analysis. The results are generated in ANSYS Parametric Design

Language (APDL), which are read using ANSYS for the extraction of the results. Static and dynamic analyses are carried out for several cases, and the results are used to develop the analytical model for the prediction of the normalised induced twist. The proposed analytical model performance is validated by comparing the normalised induced twist predicted using the proposed model with those obtained using the ANSYS and the results suggest that the proposed model is efficient in predicting the normalised induced twist of an adaptive blade.

ACKNOWLEDGEMENTS

Firstly, I would like to express my sincere gratitude and appreciations to my principal supervisor Dr. Ulugbek Azimov, second supervisor Dr Martin Birkett and external supervisor Dr Alireza Maheri for their guidance and support throughout my postgraduate research programme.

Secondly, I would also like to extend my deepest gratitude to my lovely wife Mrs. Oyiye Omoware for her encouragement, financial support, emotional support, love and care in all aspect of my life. Also, appreciate my two beautiful daughters Ogheneghare and Oghenerukwe Omoware, for allowing me to do my research using father-kids time.

Thirdly, I would sincerely appreciate my parents Mr Jackson and Mrs Patience Omoware, and siblings for their encouragement and spiritual support throughout my research programme.

Fourthly, I would also like to extend my gratitude to the Amoebi Hardship Fund for International Students (AHFIS), The Douglas Bomford Trust, Pastor Bright Onoka, Mr Sunday Ebhohimen and Mr Charles Omoruan for their financial support.

Finally, my profound gratitude goes to God almighty for giving me the ability, strength and knowledge to carry out this research to completion.

Contents

DECLARATION	i
ABSTRACT.....	ii
ACKNOWLEDGEMENTS	iv
LIST OF FIGURES	viii
LIST OF TABLES	xiii
NOMENCLATURE	xiv
1 Introduction.....	1
1.1 Wind Energy: Trend.....	2
1.2 Wind Turbine Technology	2
1.3 Wind Turbine Design.....	3
1.3.1 Number of Blades Effect.....	3
1.3.2 Length of Blades Effect	3
1.3.3 Tower Height Effect.....	4
1.3.4 Shape of Blades Effect	4
1.4 Types of Wind Turbine	5
1.5 Wind Energy Challenges	8
1.6 State-of-the-Art of Smart Rotor Control for Wind Turbines	12
1.7 Wind Turbine Control Systems Advancement for Power Regulation & Load Alleviation.....	13
1.8 Aerodynamic Control Surfaces	14
1.8.1 Trailing Edge Flaps	15
1.8.2 Microtabs	16
1.8.3 Camber Control (Morphing)	17
1.8.4 Active Twist.....	18
1.8.5 Boundary Layer Control	19
1.9 Aim and Objectives.....	22
1.10 Structure of the Thesis	23
1.11 Summary	24
2 State-of-the-art of Flapping and Adaptive Blades	25
2.1 Challenges of Larger Blades	26
2.2 Smart Blades	28
2.3 Types of Smart Blades	29
2.4 Flapping Blades: Background.....	30
2.5 Adaptive Blades: Background	34
2.5.1 Geometrical Adaptiveness	34

2.5.2	Structural Adaptiveness	35
2.5.3	Bending/Twist Elastic Coupling	40
2.5.4	Induced Twist Elastic Determination.....	42
2.5.5	Classical Laminate Theory.....	43
2.5.6	High Performance Blade Modelling (HPBM)	44
2.6	Summary	46
3	Flapping Blades	48
3.1	Introduction.....	49
3.2	Flapping Wing Kinematics	51
3.3	Computational Fluid Dynamics of Flapping Flat Plate.....	52
3.3.1	2D Numerical Analysis.....	53
3.3.2	Results and Discussion.....	54
3.3.3	Effect of Flapping Amplitude	54
3.3.4	Effect of Flapping Frequency	57
3.3.5	3D Numerical Analysis.....	59
3.3.6	Results and Discussion.....	59
3.3.7	Effect of Flapping Amplitude	60
3.3.8	Effect of Flapping Frequency	61
3.3.9	Effect of Pitching Amplitude	63
3.4	Conclusion	64
4	Adaptive Blades: Extended Decoupled Design	65
4.1	Introduction.....	66
4.1.1	Implementing Elastic Coupling in Adaptive Blades.....	68
4.1.2	Adaptive Blades Integrated Design.....	69
4.1.3	Adaptive Blades Decoupled Design.....	71
4.2	Decoupled Design Method: Background Theory	73
4.3	Validation of HPBM.....	77
4.4	Normalised Induced Twist Analytical Model.....	83
4.4.1	Effect of Fibre Angle on β^* (NREL 5 MW Blade).....	87
4.4.2	Effect of Fibre Angle on β^* (AWT-27 Blade).....	91
4.4.3	Effect of Material on β^* (NREL 5 MW Blade)	94
4.4.4	Effect of Material on β^* (AWT-27 Blade).....	95
4.4.5	Effect of the variation of Shell Thickness Distribution on β^* (NREL 5 MW Blade) 96	
4.4.6	Effect of the variation of Shell Thickness Distribution on β^* (AWT-27 Blade) ..	99
4.4.7	Effect of the Shell Thickness on β^* (NREL 5 MW Blade).....	101

4.4.8	Effect of the Shell Thickness on β^* (AWT-27 Blade).....	102
4.5	Effect of Shear Webs on β^*	103
4.5.1	Effect of Fibre Angle variation distribution along the span on β^* (NREL 5 MW Blade)	104
4.5.2	Effect of Fibre Angle variation distribution along the span on β^* (AWT-27 Blade)	107
4.6	Extended Analytical Model for the blade Normalised Induced Twist.....	110
4.7	Conclusion	118
5	Adaptive Blades: Dynamic Analysis	120
5.1	Introduction.....	121
5.2	Aeroelasticity	122
5.2.1	Divergence	125
5.2.2	Flutter.....	129
5.2.3	Flutter Motion	129
5.2.4	Classical Flutter Instability Mechanism.....	130
5.3	Effect of the Fibre Orientation on the Natural Frequencies (NREL 5 MW Blade)	135
5.4	Effect of the Fibre Orientation on the Natural Frequencies (AWT-27 Blade).....	138
5.5	Effect of Unbalanced Layup Configuration on the Natural Frequencies (NREL 5 MW Blade)	140
5.6	Effect of Unbalanced Layup Configuration on the Natural Frequencies (AWT-27 Blade)	143
5.7	Conclusion	145
6	Summary and Conclusion	146
6.1	Summary	147
6.2	Achievements and Original Contribution	148
6.3	Critical Appraisal and Future Work.....	149
	References.....	151
	Appendix A	
	Appendix B	
	Appendix C	

LIST OF FIGURES

Figure 1.1. Historical development trend of Wind Turbines	2
Figure 1.2. Components of a Horizontal Axis Wind Turbine (HAWT)	6
Figure 1.3. Coefficient of Performance for a one, two and three-blades design	8
Figure 1.4. Evolution of the proportional cost for the different wind turbine subsystems, as size increases	11
Figure 1.5. Microtab concept	17
Figure 1.6. Camber control concept	18
Figure 1.7. Active twist concept [46].....	18
Figure 1.8. Schematic of DBD plasma actuator for flow control applications	21
Figure 1.9. Flowchart of the thesis structure.....	22
Figure 2.1. Types of Smart Blades	30
Figure 2.2. Layups for bending/twist and stretching/twist couplings	36
Figure 2.3. Flow Kinematic at a typical span location r	42
Figure 2.4. Showing the off-axis laminate	44
Figure 2.5. High performance finite element modelling and analysis of wind turbine blade	45
Figure 2.6. Flowchart of the blade modelling and analysis using commercial CAD/FEA software.....	46
Figure 3.1. Flapping Cycle	52
Figure 3.2. Flat plate with zero thickness in the fluid domain.....	544
Figure 3.3. Instantaneous lift coefficient for 20 Hz flapping frequency and different flapping amplitudes.....	55
Figure 3.4. Instantaneous lift coefficient for 40 Hz flapping frequency and different flapping amplitudes.....	555
Figure 3.5. Instantaneous lift coefficient for 50 Hz flapping frequency and different flapping amplitudes.....	56
Figure 3.6. Effect of flapping amplitude on maximum lift coefficient for various flapping frequencies	57
Figure 3.7. Instantaneous lift coefficient for 7.5 mm flapping amplitude and different flapping frequency	58
Figure 3.8. Effect of flapping frequency on maximum lift coefficient for various flapping amplitude.....	58
Figure 3.9. Flat plate in the fluid domain.....	60

Figure 3.10. Contours (a) velocity magnitude and (b) vorticity magnitude.....	60
Figure 3.11. Effect of flapping amplitude on maximum lift coefficient for various flapping frequencies (pitch amplitude 5 degrees)	61
Figure 3.12. Instantaneous lift coefficient for 40 Hz flapping frequency and different flapping amplitudes (pitch amplitude 5 degrees).....	61
Figure 3.13. Effect of flapping frequency on maximum lift coefficient for various flapping amplitudes (pitch amplitude 5 degrees).....	62
Figure 3.14. Maximum lift coefficient as a function of flapping frequency and flapping amplitude (pitch amplitude 5 degrees).....	63
Figure 3.15. Effect of pitch amplitude on maximum lift coefficient	63
Figure 4.1. Two types of elastic couplings: stretching/twist and bending/twist	68
Figure 4.2. (a) Sequential versus (b) Integrated design	69
Figure 4.3. Adaptive blade integrated design process	70
Figure 4.4. Decoupling design by VSDP	72
Figure 4.5. Variation of normalised flap-bending moment versus run conditions [pitch angle (deg.), Ω (rpm), V (m/s)]	75
Figure 4.6. Blade patches configuration	79
Figure 4.7. Stress and deformation results for HPBM and SOLIDWORKS/ANSYS	82
Figure 4.8. Normalised shell thickness distributions	84
Figure 4.9. Normalised fibre angle distributions	86
Figure 4.10. Case set 1 Induced twist for various fibre angle (NREL 5 MW Blade).....	88
Figure 4.11. Case set 2 Induced twist for various fibre angle (NREL 5 MW Blade)	88
Figure 4.12. Case set 3 Induced twist for various fibre angle (NREL 5 MW Blade)	89
Figure 4.13. Effect of fibre angle on β^* [Case Set 1 (NREL 5 MW Blade)]	89
Figure 4.14. (a) Effect of fibre angle on β^* [Case Set 2 (NREL 5 MW Blade)]	90
Figure 4.14. (b) Effect of fibre angle on β^* [Case Set 2 (25° to 75°) (NREL 5 MW Blade)].....	90
Figure 4.15. (a) Effect of fibre angle on β^* [Case Set 3 (NREL 5 MW Blade)]	91
Figure 4.15. (b) Effect of fibre angle on β^* [Case Set 3 (10° to 85°) (NREL 5 MW Blade)].....	91
Figure 4.16. Case set 4 Induced Twist for various fibre angle (AWT-27 Blade).....	92
Figure 4.17. Case set 5 Induced Twist for various fibre angle (AWT-27 Blade)	92
Figure 4.18. Case set 6 Induced Twist for various fibre angle (AWT-27 Blade)	93

Figure 4.19. Effect of fibre angle on β^* [Case Set 4 (AWT-27 Blade)]	93
Figure 4.20. Effect of fibre angle on β^* [Case Set 5 (AWT-27 Blade)]	93
Figure 4.21. Effect of fibre angle on β^* [Case Set 6 (AWT-27 Blade)]	94
Figure 4.22. Effect of material on the induced Twist (NREL 5 MW Blade).....	94
Figure 4.23. Effect of material on β^* (NREL 5 MW Blade)	95
Figure 4.24. Effect of material on the induced Twist (AWT-27 Blade).....	95
Figure 4.25. Effect of material on β^* (AWT-27 Blade).....	96
Figure 4.26. (a) Effect of variation of shell thickness distribution on β^* (NREL 5 MW Blade)	97
Figure 4.26. (b) Effect of linear variation of shell thickness distribution on β^* (NREL 5 MW Blade).....	97
Figure 4.26. (c) Effect of polynomial variation of shell thickness distribution on β^* (NREL 5 MW Blade)	98
Figure 4.26. (d) Effect of chord-wise shell thickness variation on β^* (AWT-27 Blade)..	98
Figure 4.27. (a) Effect of variation of shell thickness distribution on β^* (AWT-27 Blade).....	100
Figure 4.27. (b) Effect of linear variation of shell thickness distribution on β^* (AWT-27 Blade)	100
Figure 4.27. (c) Effect of polynomial variation of shell thickness distribution on β^* (AWT-27 Blade)	100
Figure 4.27. (d) Effect of chord-wise shell thickness variation on β^* (AWT-27 Blade)	101
Figure 4.28. Effect of shell thickness on the induced Twist (NREL 5 MW Blade)	102
Figure 4.29. Effect of shell thickness on β^* (NREL 5 MW Blade).....	102
Figure 4.30. Effect of shell thickness on the induced Twist (AWT-27 Blade).....	103
Figure 4.31. Effect of shell thickness on β^* (AWT-27 Blade)	103
Figure 4.32. Effect of shear webs on the induced Twist (NREL 5 MW Blade)	104
Figure 4.33. Effect of shear webs on β^* (NREL 5 MW Blade).....	104
Figure 4.34. Effect of variation of fibre angle distribution on the induced twist (NREL 5 MW Blade).....	105
Figure 4.35. (a) Effect of variation of fibre angle distribution on β^* (NREL 5 MW Blade)	105
Figure 4.35. (b) Effect of polynomial variation of fibre angle distribution on β^* (NREL 5 MW Blade).....	106

Figure 4.35. (c) Effect of linear variation of fibre angle distribution on β^* (NREL 5 MW Blade).....	106
Figure 4.35. (d) Effect of varying shell thickness and varying fibre angle distribution on β^* (NREL 5 MW Blade).....	107
Figure 4.36. Effect of variation of fibre angle distribution on the induced twist (AWT-27 Blade).....	108
Figure 4.37. (a) Effect of variation of fibre angle distribution on β^* (AWT-27 Blade).....	108
Figure 4.37. (b) Effect of polynomial variation of fibre angle distribution on β^* (AWT-27 Blade).....	109
Figure 4.37. (c) Effect of linear variation of fibre angle distribution on β^* (AWT-27 Blade).....	109
Figure 4.37. (d) Effect of varying shell thickness and varying fibre angle distribution on β^* (AWT-27 Blade).....	110
Figure 4.38. (a-j) Torsional stiffness/Fibre angles relations.....	112
Figure 4.39. Normalised tip induced twist.....	113
Figure 4.40. (a-j) Predicted normalised induced twist by Equation (4.16) and ANSYS (NREL 5 MW Blade).....	116
Figure 4.41. (a-j) Predicted normalised induced twist by Equation (4.16) and ANSYS (AWT-27 Blade).....	118
Figure 5.1. Collar aerodynamic diagram.....	123
Figure 5.2. The collar triangle modified with the control forces added.....	124
Figure 5.3. Simple aeroelastic model to demonstrate divergence phenomenon.....	126
Figure 5.4. Aerofoil motion demonstrating flutter.....	130
Figure 5.5. Blade section with 2 degrees-of-freedom.....	131
Figure 5.6. (a) Dynamic behaviour for a balanced layup configuration (NREL 5 MW Blade).....	136
Figure 5.6. (b) Effect of fibre orientation on the natural frequencies for a balanced layup configuration (NREL 5 MW Blade).....	137
Figure 5.7. (a) Dynamic behaviour for a “mirror” layup configuration (NREL 5 MW Blade).....	137
Figure 5.7. (b) Effect of fibre orientation on the natural frequencies for a “mirror” layup configuration (NREL 5 MW Blade).....	138
Figure 5.8. (a) Dynamic behaviour for a balanced layup configuration (AWT-27 Blade).....	139

Figure 5.8. (b) Effect of fibre orientation on the natural frequencies for a balanced layup configuration (AWT-27 Blade).....	139
Figure 5.9. (a) Dynamic behaviour for a “mirror” layup configuration (AWT-27 Blade)	140
Figure 5.9. (b) Effect of fibre orientation on the natural frequencies for a “mirror” layup configuration (AWT-27 Blade).....	140
Figure 5.10. (a-h) Dynamic behaviour for unbalanced and balanced layup configuration (NREL 5 MW Blade).....	142
Figure 5.11. (a-h) Dynamic behaviour for unbalanced and balanced layup configuration (AWT-27 Blade).	144

LIST OF TABLES

Table 4.1. Mechanical properties of the composite materials	77
Table 4.2. Case patches normalised coordinates.....	78
Table 4.3. The layup configuration for the NREL 5 MW Adaptive blade case	80
Table 4.4. Layup configurations	82
Table 4.5. Shell thickness distributions	84
Table 4.6. Layup fibre angle distributions	85
Table 4.7. Mechanical properties of the composite materials	86
Table 5.1. Layup configurations	135

NOMENCLATURE

A	Swept area	
A_{flap}	Amplitude of flapping motion	
A_{ij}	Extensional stiffness matrices entries	$i, j = 1, 2, 6$
B_{ij}	Coupling stiffness matrices entries	$i, j = 1, 2, 6$
C	Blade chord length	
C_D	Drag coefficient	
C_L	Lift coefficient	
C_M	Pitching moment coefficient	
C_{ij}	Stiffness matrices entries	$i, j = 1, 2, 3$
D_{ij}	Bending stiffness matrices entries	$i, j = 1, 2, 6$
e	Distance from aerodynamic centre to elastic centre, positive aft	
E_{11}	Longitudinal Young's modulus along the fibre direction	
E_{22}	Transverse Young's modulus perpendicular to the fibre direction	
E_{33}	Out-of-plane transverse Young's modulus (through-the-thickness)	
E_f	Young's modulus of fibre	
E_m	Young's modulus of matrix	
E_{xx}	Longitudinal Young's modulus in the global laminate coordinate system	
E_{yy}	Transverse Young's modulus in the global laminate coordinate system	
E_{zz}	Out-of-plane transverse Young's modulus in the global laminate coordinate system	
g	Coupling term	
G_f	Shear modulus of fibre	
G_m	Shear modulus of matrix	
G_{ij}	Shear moduli	$i, j = \{1, 2, 3, x, y, z\}$
h	Flap-wise translation DOF	
\ddot{h}	Second time-derivative of the flap-wise translation DOFs	
K	Effective stiffness at span location r	
K^*	Normalised effective stiffness	
k_f	Flap-wise stiffness	
k_t	Torsional stiffness	
K_{max}	Maximum effective stiffness of the blade	
K_α	Elastic spring constant	
L	Lift, net vertical force positive up	
mat_{ID}	Composite material identification	
m	Mass per unit length of the blade section	
M	Flap bending-moment at span location r	
M^*	Normalised flap bending moment	
M_b	Flap-wise bending moment	

M_t	Twisting moment	
M_y	Moment about the elastic centre or axis	
M_{AC}	Moment about aerodynamic centre, both moments are positive nose up	
M_{hub}	Flap bending at the hub	
$M^*(r^*)$	Normalised flap bending moment at span location r	
n	Number of fibre layers	
P	Power output	
p	Pitch angle	
q	Dynamic pressure	
q_D	Divergence dynamic pressure	
Q_{ij}	Reduced stiffness matrices entries	$i, j = 1, 2, 6$
\bar{Q}_{ij}	Transformed reduced stiffness matrices entries	$i, j = 1, 2, 6$
r	Radius of blade	
r_{CG}	Radius of gyration normalised by the blade chord length	
R_{hub}	Radius of hub	
R_{rotor}	Radius of rotor	
r^*	Normalised radial location	
S	Aerofoil area	
S_{ij}	Compliance stiffness matrices entries	$i, j = 1, 2, 6$
t_k	Thickness of k th ply	
t_{layer}	Lamina thickness	
t_{max}	Aerofoils maximum thickness	
t_s^*	Normalised shell thickness	
V_i	Wind speed	
ν_{ij}	Poisson's ratios	$i, j = \{1, 2, 3, x, y, z\}$
V_m	Volume fraction of matrix	
ν_f	Poisson's ratio of fibre	
V_f	Volume fraction of fibre	
ν_m	Poisson's ratio of matrix	
W	Relative inflow wind speed	
W_0	Steady-state relative inflow wind speed	
\bar{Z}_k	Distance of k th ply from the geometric mid-plane to the centre of the k th ply	
α	Angle of attack	
β	Induced twist	
β_0	Pretwist	
β^*	Normalised induced twist	

$\beta^*(r^*)$	Normalised induced twist at span location r	
ε_j	Strain component entries	$j = 1,2,3$
η	Power coefficient	
φ	Inflow angle	
ϕ	Instantaneous flapping angle	
$\dot{\phi}$	Flapping velocity	
ρ	Air density	
ρ_f	Density of fibre	
ρ_m	Density of matrix	
ρ_c	Density of composite	
σ_i	Stress component entries	$i = 1,2,3$
τ_{ij}	Shear stress component entries	$i, j = 1,2,3$
θ	Fibre angle	
θ_k	Angle of kth ply	
$\ddot{\theta}$	Second time-derivative of the torsional rotation DOFs	
ω	Angular velocity of rotor	
ω_f	Natural frequency flap-wise mode	
ω_t	Natural frequency torsional mode	
Ω	Rotor rotational speed	

TERMINOLOGY

Induced Twist: This is the torsional deformation of the blade that result from bending force on an unbalanced composite blade because some of the forces will be translated to the off-axis direction resulting to the blade twisting around the axis.

Normalised Induced Twist: This is the ratio of the induced twist at a particular blade location (r) to the maximum blade maximum induced twist which typically occurs at the tip of the blade.

1 Introduction

1.1 Wind Energy: Trend

Sources of alternative energy advancement has become of a need as the demand for energy is rapidly increasing and fossil energy resources are in a decline. Moreover, the wide use of fossil energy is polluting the environment and is causing issue of global warning. Thus, the need of wind and other renewable energy sources as viable option to fossil fuels [1]. Wind energy has the enormous potential to meet the world's energy needs. Cost effectiveness is the focus of the state-of-the-art technologies of wind turbines. In the past three decades, performance of wind and solar energy systems have continued to improve. Wind power generation is an established technology now that has been around so many decades. For instance, by 200 BC, that of the simple windmills used in China for pumping water [2]. The historical development trend of wind turbines is shown in Figure (1.1).

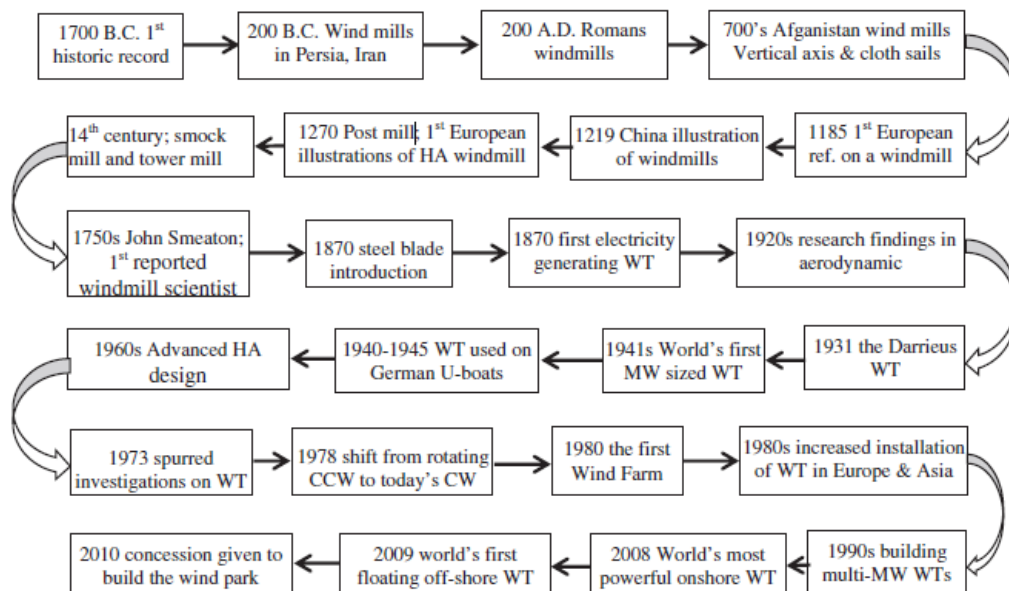


Figure 1.1. Historical development trend of Wind Turbines [3]

1.2 Wind Turbine Technology

Wind energy can be used directly as mechanical power like for pumping water and grinding of grain or indirectly by converting the wind kinetic energy into electrical energy like the wind turbine. The most important use of wind energy is the wind turbine, with the first wind turbine for electrical power generation developed in the early 20th century. The wind turbine technology is continuously improving with the attainment of significant advancement in recent years in the wind turbine design. To be specific, the current

technological advances and optimisations of a wind turbine system and the components have shown significant improvement in the generated power output and efficiency. Furthermore, with the use of power electronic devices, there are now some gearless turbine designs where the shaft of the rotor is directly attached to the generator to spin the blade.

1.3 Wind Turbine Design

The wind turbine design principal objective is to maximise the aerodynamic performance efficiency, or power that can be extracted from the wind. Nevertheless, this objective should be met by meeting the mechanical strength conditions and economical aspects. The number of blades, shape of blade, height of the tower and length of blade, all have an impact on the design of wind turbines [4].

1.3.1 Number of Blades Effect

The aerodynamic performance efficiency of a wind turbine increases with increase in the number of blades but in a diminishing way. Increasing the number of blades from two to three, gives an efficiency gain of about 3% while only a 0.5% gain is achieved when the number of blades increases from three to four. The cost of the wind energy system increases considerably with increase in the number of blades and the mechanical design of the blades becomes difficult. The blades have to be thinner as the number increases to be aerodynamically efficient. This will have adverse effect on the blade because the thinner portion at the root of the blade will experience high induced stress due to axial wind load. Thus, usually wind turbines with three blades are designed with a thicker root cross-section [4].

1.3.2 Length of Blades Effect

Another factor that affects the aerodynamic performance efficiency of a wind turbine is blade length. The governing equation for power extraction by a wind turbine is as shown in Equation (1.1) and thus, it is obvious that a longer blade will result to greater power extraction, $P \propto L^2$. This led to the current trend of increasing the length of turbine blades, as larger blades will have larger swept area, A , and yield greater power output, P . On the other hand, increase in length of the blade will result in an increase in the blade tip

deflection due to axial wind load. Therefore, calculated blade length increase is of a necessity to avoid the risk of collision of the turbine blade and tower.

$$P = \frac{1}{2} \eta \rho A V_i^3 \quad (1.1)$$

where

P = power output

A = swept area

V_i = wind speed

ρ = air density

η = power coefficient

Another effect, which goes against longer blades, is as the blade length increases, the tip velocity increases which produces noise because it is a function of the tip velocity. Furthermore, it leads to a requirement for huge mechanical structures resulting in a significant increase in cost [4].

1.3.3 Tower Height Effect

Another and very critical factor of the design of a wind turbine is determination of appropriate tower height. From Equation (1.1) it can be seen that the extracted power varies as the cube of wind speed. Therefore, little change in wind speed will have a massive effect on power extraction. Generally, wind speed increases from ground level. Therefore, from the perspective of power extraction, a high tower will be better but structural design difficulties and transportation need to be taken into consideration. Thus, the determination of the optimal tower height is crucial [4].

1.3.4 Shape of Blades Effect

The shape of the blade and its cross-section orientation have an effect on the aerodynamic performance efficiency of the wind turbine. The complete shape of the blade is greatly important in controlling the aerodynamic performance of the wind turbine. For proper turning of the rotor, the shape of the blade has to be designed to give adequate lift. The blade design is an aerofoil shape like that of an aeroplane wing, but the blades of large wind turbines are always in the form of a twist. Considering that the wind mostly comes from a steeper angle as it moves in the direction of the blade root, the rotor blade has to be

twisted in order to obtain an optimal angle of attack throughout the full length of the blade and thus adequate lift [5]. Wind condition is stochastic, thus, to achieve optimal angle of attack, the blade must be able to rotate about its axis in response to wind condition changes. This is referred to as pitching of wind turbine blades. The blade pitch angle is governed by an algorithm for maximum power extraction by using the wind turbine characteristics and wind conditions as inputs [4].

Designing an optimal blade is a complex problem as the multi-objectives for structure and aerodynamics of blades are often contradictory (i.e. decrease weight to reduce cost but maintain stiffness). Numerous researchers [6-31] have investigated wind turbine blade design by only considering aerodynamic or structural optimisation. However, aerodynamic and structural performances are dependent of each other. For instance, blade deflection results from the combination of the aerodynamic (and other) load distribution over the blades span and the blades structural properties.

In 1996, Seki et al [6] studied a method to find the optimum blade shape for the horizontal axis wind turbines (HAWT) rotor of several hundred mega-Watts. Jureczko [9] in 2005 developed a computer program package that would support optimisation of wind turbine blades with respect to a number of criteria. Designing a wind turbine is with the aim to achieve the optimum power output under specified atmospheric conditions. Technically, this depends on the shape of the blade. The change of the shape of blade is one of the methods to modify stiffness and stability, but it may influence aerodynamic efficiency of wind turbine/aerodynamic surfaces [9].

Mendez et al [10] in 2006 developed a method to achieve optimal chord and twist distributions in wind turbine blades by using genetic algorithms. To optimise chord and twist distributions, Blade element momentum theory (BEMT) was used [11-13]. With respect to computational cost, the BEMT has shown to give good accuracy.

1.4 Types of Wind Turbine

Wind turbines are divided into two core categories: Horizontal axis wind turbines (HAWTs) and Vertical axis wind turbines (VAWTs), with the Horizontal Axis type being the common type. HAWTs have the main rotor shaft and generator at the tower top and are pointed into the wind while VAWTs have the main rotor shaft arranged vertically.

VAWTs, are designed to extract wind energy for areas with lower wind speed [5]. There are two distinct types of VAWTs namely the Darrieus and the Savonius types. The Darrieus turbine is composed of several curved vertically oriented aerofoil blades mounted on a vertical rotor. It requires a small powered motor to start its rotation. When enough speed is attained, the wind passing through the aerofoils produces torque and consequently, the wind drives the rotor around. The lift forces created by the aerofoils then powers the Darrieus turbine. The Darrieus turbine reaches speeds that are greater than the actual speed of the wind through the help of the blades. This makes them suitable to generate electricity when the wind is turbulent. The Savonius turbine is a drag-type that comprises of two to three scoops. Because of the curved nature of the scoop, the drag is greater when it is moving with the wind than when it is moving against it. The differential drag causes the Savonius turbine to spin. The Darrieus turbine extracts more wind power than the Savonius turbine.

HAWTs are built with the purpose of extracting energy from wind with high speeds. HAWTs core components are as shown in Figure (1.2):

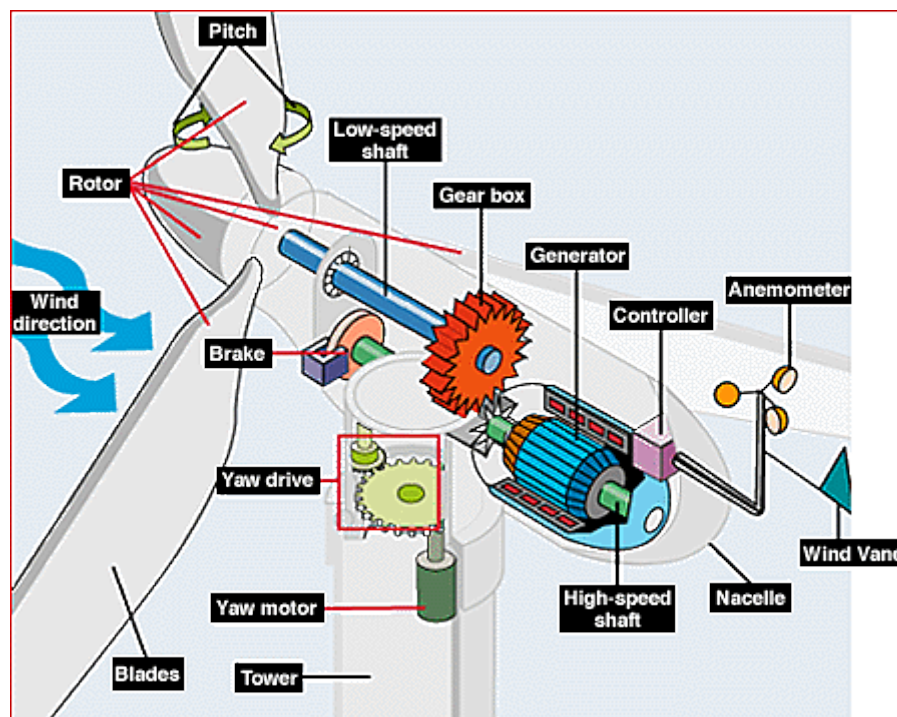


Figure 1.2. Components of a Horizontal Axis Wind Turbine (HAWT) [5]

HAWTs are either positioned away from the wind which are called downwind turbines (the rotor is on the back side of the turbine) or oriented into the wind which are called upwind turbines (the rotor is in the front of the turbine). The downwind turbine rotor blades can be flexible as there is no risk of a tower strike. This blade flexibility has two main advantages that is they are less expensive to make and can alleviate stress on the tower during windy conditions since the flexibility allows the distribution of some aerodynamic load on the blades instead of transferring directly to the tower. The disadvantage of the downwind turbine is tower shadow as the rotor blade passes behind the tower which could result to high turbulence and increased fatigue of the turbine. The upwind turbines have reduced tower shading as an advantage, but the disadvantage is the blades must be rigid to avoid bending back into the tower which could result to high stress at the point where the blade is attached to the rotor hub during gusty conditions. Another disadvantage of the upwind turbine is that an extended nacelle is needed to position the rotor away from the tower to avoid the danger of a blade strike.

The wind turbine could also be divided into aerodynamic drag and aerodynamic lift turbines considering the working function of the energy conversion system. However, the aerodynamic lift is the most predominant in modern wind turbines [3]. Wind turbines are also categorised by the number of blades. Determination of the number of blades involves consideration of the aerodynamic efficiency, system reliability and component costs [3].

The key factors pivotal in making decisions on the number of blades include the effect on the coefficient of power, the yawing rate (to reduce gyroscopic fatigue) and the design tip speed ratio (TSR) [32].

Attempts were made in the 1980s and early 1990s to commercialize one and two bladed wind turbine designs; though, three bladed designs are mostly used in modern wind turbines [3, 33]. The single bladed design has the greatest blade section dimensions which makes it the most structurally efficient because all the blade surface area is in a single beam [3]. It saves the cost of one blade and weight; however, it has rotor balancing difficulties. This necessitates the use of a counterweight on the other side of the hub to balance the rotor. This perceptibly negates the weight savings compared to a two-bladed design. Supersonic tip speed is also possible with the use of a single bladed design resulting to high pulsating torque which causes extreme vibrations [33].

However, increased aerodynamic efficiency is obtained with increase in the number of blades. There is about 6% increase in the aerodynamic efficiency when the number of blades is increase from one to two and a further 3% increasing it to three blades. It seems reasonable to assume increasing it more will increase the aerodynamic efficiency, but it is not the case. Addition of more blades increases the resistance in the pathway of the airflow. Though there is a slight increase in the rotor efficiency increasing the number of blades from three to four, but it will result to increase in the rotor weight and a drop in the rotational speed at which peak power would be achieved which in turn increases the rotor torque [3, 34]. Figure (1.3) shows the coefficient of performance of a two and three blade design.

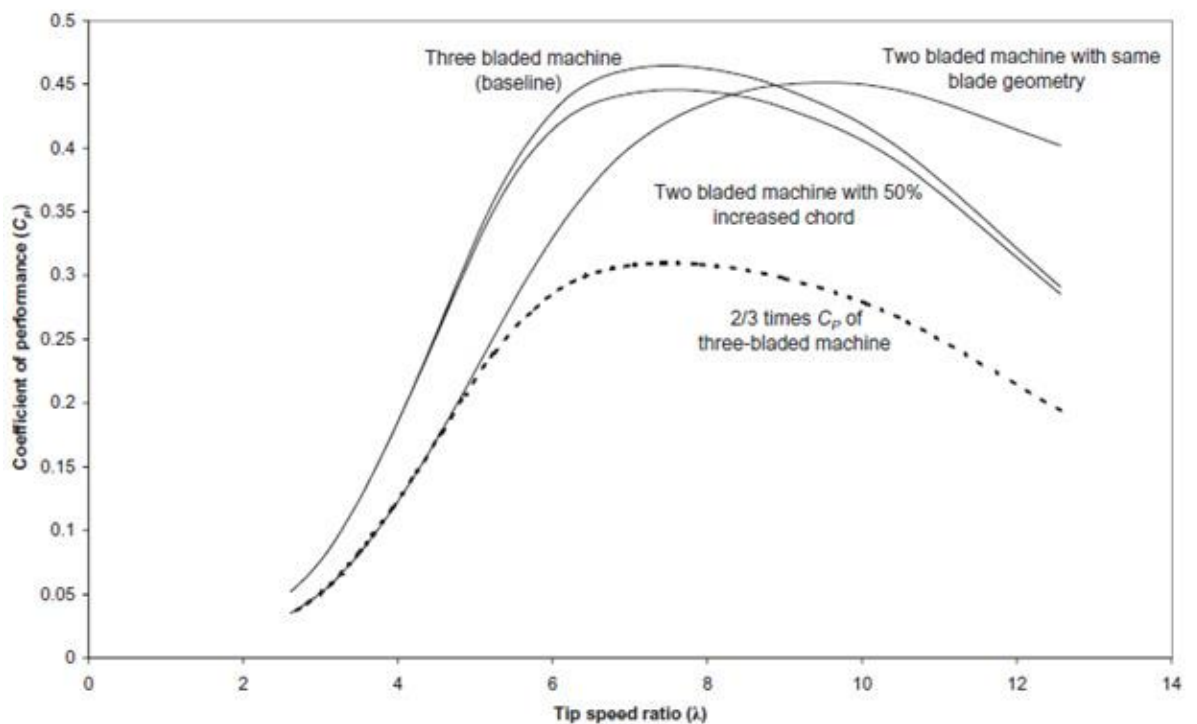


Figure 1.3. Coefficient of Performance for a two and three-blades design [32]

1.5 Wind Energy Challenges

Since resurgence in the renewable energy industry, the use of wind energy has become a focal point in the research of sustainable energy sources with the recent swift advancement of wind turbine technologies and significant installation of wind turbine worldwide. Optimisation of the extraction of the maximum wind power from the available wind is the focal point. However, wind energy system has some challenges; these include economic,

social, technical, and environmental challenges. Some of the challenges are discussed below:

Economic challenges

High cost per MW installed capacity: Wind energy system start-up cost is very high, and it generally needs very large investment. The capital cost includes manufacturing of the turbine, foundation, and transportation to the site. Thus, the wind turbine installation phase requires a substantial amount of capital. For wind energy systems to be globally acceptable, they must be able to compete on cost with other energy sources [1]. At the moment, the conventional energy sources (fossil fuels) for electricity generation are more reliable and available at cheaper prices. Nevertheless, wind energy prices are steadily on the decrease. Considering the long term, wind power will have better return on investment taking into consideration all subsidies and other incentives when compared over a lengthy period of time [1].

Environmental challenges

Spinning wind turbine blades could cause damage to the lives of birds and bats but some conventional sources of generating electricity still causes more harm to wildfire by polluting the air and water causing loss of animal life through acid rain. According to [1], in Canada each year about 20,000 to 28,300 birds are killed as a result of wind turbine striking which is just about ratio 1 bird killed by wind turbine to 2118 birds killed by fossil fuel powered plants. Wildlife killed by spinning wind turbine blades has significantly reduced by virtue of appropriate siting of wind turbines or technological development. At the present, the NREL's National Wind Technology Centre (NWTC) is assisting wildlife technology research validation in the reduction of wildlife fatalities at wind turbine sites [1].

Social challenges

Wind turbines might cause noise, but they have moderately little impact on the communities and environment compared to conventional power plants, though concern does exist over the sound produced by the turbine blades [1].

Technical challenges

The size of wind power plants poses significant challenges in terms of materials for producing the wind turbine blades and the design of the blades to enhance the capture of

energy, ensuring cheaper energy prices. Also, the larger turbine blades present transportation challenges because constraint of length of goods transported by rail and truck. One of the approaches of overcoming this is to manufacture the blades in sections and assemble them onsite like the Gamesa's InnoBlade segmented design concept or the multiple-part system from Enercon [35]. Another approach, which might not be suitable for all locations is by transporting the blades over water. It has generally been agreed by experts that the increase in weight of the nacelle and rotor will require a crane that will be suitably developed by or with wind turbine manufacturers. This entire process of installation will involve a progressively intricate logistical coordination [36].

According to Mckenna et al [36], material used for the manufacture of wind turbine blades is trending towards fully carbon fibre. Indeed, the rotor diameter and hub height have increased dramatically in the recent times. The main driving purpose of the increase in size is because of the levelized costs of energy generation (i.e. the sum of the turbine lifetime cost including operations and maintenance divided by the sum of the lifetime electrical energy generated) and possibly multi-objective optimisation criteria which includes total mass and annual energy production (AEP). Wind turbine optimisation includes maximisation of the aerodynamic performance efficiency and extreme load alleviation. Achieving little structural improvement and increase in aerodynamic performance efficiency can achieve an increase in the AEP and consequently, lower the cost of energy.

Under development are new forms for aerofoils, for instance the CAS- W1, with very good aerodynamic properties but it has a disadvantage of increasing blade thickness, thus, an increase in structural load on the turbine [37]. Furthermore, for large wind turbines, blades are being developed with vortex generators. This vortex generators allow the aerofoil stall speed to be reduced and are employed already in aircraft [38].

Another approach of alleviating the high loads resulting from larger rotor diameters is the use of active load control of turbine blades. This approach includes trailing edge flaps and the use of shape memory materials i.e. Smart Structure Principle. This has the tendency to respond to the aerodynamic loading effect by changing shape. One other load reduction option is use of pitch control. Employing pitch control can achieve between 20–30% aerodynamic load reductions. Furthermore, an additional 15% load reduction can be achieved by using a dual pitch control. This is done by pitching the blade tip twice as much as the root [35]. For monitoring of the aerodynamic load along the span of the blade, fibre

optics embedded in laminates or piezoelectrics are used. Also, microtabs are small tabs for actively mitigating aerodynamic loads on the blade by temporarily adapting the shape of the aerofoil [39]. Moreover, individual pitch control (IPC), which is a more intelligent pitch control system can be deployed to mitigate the aerodynamic load on the turbine whilst maximising the power output as opposed to using the conventional approach of symmetric blade pitching [40].

The attention of researchers now is the proliferation of the power output of the wind turbine in order to make it cheaper and competitive with other sources of energy. The Siemens SWT-6.0-154 and SWT-7.0-154 offshore wind turbines which have a rotor diameter of 154 m and blade length of 75 m have nominal power outputs of 6 MW and 7 MW respectively [41]. For improving wind turbine performance such as power quality, efficiency and control complexity, Vestas Wind Systems latest modern wind turbines are of height 140 m and have larger rotors that radically change the economics of wind power. In some countries there is a restriction on the maximum height of wind turbines. For example, the UK has a tip-height restriction of 125 m [42]. In order to overcome height limitations and other technological limitations, focus is placed on the blade design. The blades, tower and the gearbox are the most expensive components of the wind turbine. These three items put together account for around 50% to 60% of the cost of the wind turbine [43] and could be seen in Figure (1.4). Therefore, the design of cost efficient wind turbine blades to effectively increase energy capture, alleviate the blade load and also have structural balance of rigidity and flexibility is of great significance. Where the challenge lies is developing a large wind turbine blade that integrates the best promising combination of capability, weight and cost.

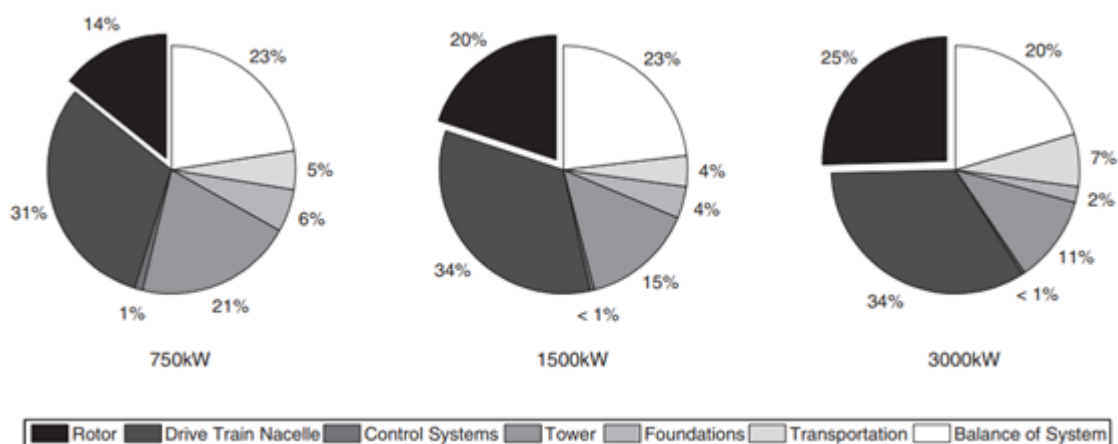


Figure 1.4. Evolution of the proportional cost for the different wind turbine subsystems, as size increases [data compilation (NREL 2005)]

1.6 State-of-the-Art of Smart Rotor Control for Wind Turbines

As the size of wind turbine blades is steadily increasing, there is the necessity for more sophisticated methods for aerodynamic load control. This has encouraged the interest for localised distribution of aerodynamic control devices with built-in intelligence on the blades. This concept is popularly known as ‘smart rotor control’ or ‘smart structures’.

At present, rotors of more than 120 m diameter are in the prototype phase. With the goal of cost per kWh reduction, the principal research and development target has been on technological improvements and new trends. Wind turbine blade cost reduction influences the energy cost, but it is only a minimal fraction of the total cost. However, with an innovative turbine blade design that is capable of alleviating the aerodynamic load, the total cost will reasonably reduce, as the loads on the rotor affect the loading of other components like the tower and drive train of the wind turbine. The design loads on a wind turbine are divided into fatigue loads and ultimate loads. The fatigue loads are a main factor when designing a wind turbine blade, thus reduction in the fatigue load will decrease maintenance cost and improve system reliability. This will significantly reduce the total cost. There are two principal methods considered for load alleviation namely; passive and active load control. With the active control, the blade adapts by altering its aerodynamic properties i.e. change in the lift coefficient and angle of attack by utilising appropriate sensor inputs. The most advanced active load control used nowadays is the individual pitch control (IPC). Passive load control is achieved by virtue of the anisotropic properties of the material and its configuration responding to the changes in the aerodynamic loading on the turbine blade. The conventional passive control based on aerodynamics is the stall control, which is used for power regulation. Other passive control solutions are based on aeroelastic tailoring, namely stretching/twist coupling, bending/twist coupling and pressure/twist [44, 45]. Many researchers are investigating the advanced concept of active control with the focus on considerably faster and more comprehensive load control. In an ideal situation, for each blade at any azimuthal position and also any span-wise location, there should be the possibility of control by aerodynamic load control devices with built-in intelligence which are distributed along the blade span. This suggests the implementation of effective and innovative actuators combining sensors which drive the aerodynamic surfaces to provide load control. This concept is known in rotorcraft research as ‘smart rotor control’. The smart rotor control comprises of distributed actuators, sensors and microprocessors to analyse the sensors responses and employ integrated control theory

to actuate the actuators to employ localised strains/ displacements to adjust the system response [46]. The aim of this wind turbine rotor control application is the alleviation of fluctuating aerodynamic loads on the rotor blades in a more comprehensive way than contemporary blade pitch control.

1.7 Wind Turbine Control Systems Advancement for Power Regulation & Load Alleviation

Wind turbine blades operate under turbulent and erratic environmental conditions where the efficiency and reliability depend highly upon a very good design. Research works are being performed in order to improve the overall blades aerodynamic performances and efficiently control the aerodynamic surfaces to be adaptive to the changing aerodynamic operating conditions. In order to achieve this, different concepts have been proposed and tested.

Over the years, wind turbine blade load control systems have advanced significantly as the size of the rotor is on the upscale [47]. Due to its simplicity, in the early times with smaller commercial turbines, the ‘Danish Concept’ was in use for the control, this is considered as a stall controlled three-bladed rotor with a fixed hub (the blades cannot be rotated around their axes). It permits the use of an asynchronous generator. The power limitation during stormy conditions is achieved by the stall effect [48]. These days, large wind turbines use a variable rotational speed pitch-controlled system to optimise the energy capture and control of the loads. This does not only help in power regulation but significantly aids the construction of lighter blades as a result of the reduced load spectrum, consequently a reduced torque peak thus, a lighter gear box can also be used [46].

The pitch control could be either collective which adjusts the pitch angle collectively or an advanced form which is individual pitch control where the pitch angle is controlled per blade. The individual pitch control alleviates the loads in an optimised way because of the fact that on a large wind turbine, the wind speed effect on each blade at any instant may vary significantly. However, there must be some measures in place to achieve any valuable advantage. The measures should be for the controller to distinguish the different blades, so it can produce the proper individual demand signals [49].

The simplest measure in achieving this is using the rotor azimuth angle. Though in turbulent wind conditions, the wind speed differences across the rotor are not mostly

dependent on the azimuth, there are some effects like wind shear, upflow, shaft tilt and tower shadow which cause systematic azimuth dependent variation in the aerodynamic load conditions at any point on the blade. Theoretically, each blades pitch could be altered as a function of azimuth to minimise the loading variations, which resulted from these effects, providing the effects are constant. In reality, upflow and wind shear fluctuate significantly depending on the environmental conditions though there is the possibility of correlating the direction of the wind. In reality, to realise any actual gain in this manner is very difficult due to the wind stochastic characteristics which are dominant. However, if additional load sensors are introduced to measure the asymmetrical loading, there is the possibility of using the individual pitch control to achieve significant load alleviation [49].

Larsen et al [50] demonstrated a new aerodynamic load mitigating control strategy for individual pitch control, based on the concept of local blade inflow measurements. This concept offers the possibility of significant load alleviation without power production loss as seen in other advanced load reducing control. This approach measures the local inflow angle and each of the blade's relative velocity and does the appropriate pitch angle adjustment for an optimised result. Hand et al [51] proposed the use of light detection and ranging system (LIDAR) to measure the upwind inflow field directly and react with the pitch system. Smart rotor control can positively affect the power generation, tower load and pitch system. The advances in material and control systems have contributed to the advancement of systems that can respond fast to the stochastic wind characteristics.

1.8 Aerodynamic Control Surfaces

Aerodynamic control surfaces act as an input surface or device on the blade for varying the local aerodynamic characteristics and providing suitable control responses.

To successfully employ active control, the aerodynamic control devices on the blades should either have the capability of varying the angle of attack or altering specific sections of the blade characteristic $C_l - \alpha$ curve. The aerodynamic control devices are set close to the blade tip to efficiently control the fluctuating loads on the root of the blade because a larger moment arm will be realised in this manner. The aerodynamic control devices should provide efficient load alleviation to justify their contribution in the increase in the total cost of the wind turbine. The aerodynamic performance of these control devices is strongly dependent on the turbine characteristics and operating conditions. The aerodynamic

control surfaces should have the capability of changing the angle of attack in order to compensate for the variations. Some aerodynamic control devices are trailing edge flaps, microtabs, camber control, active twist and boundary layer control. These aerodynamic control devices are briefly discussed below.

1.8.1 Trailing Edge Flaps

Trailing edge flaps were inspired by technology that is already in existence in the aircraft and rotorcraft industry. The trailing edge flap on wind turbine blades has been investigated for several years and it has shown great potential on alleviating load variations under proper control algorithms [46, 52]. The trailing edge flap produces great alteration in the lift coefficient of the aerofoil (i.e. maximum lift variation, zero-lift angle of attack and lift curve slope) by varying the pressure distribution along the chord of the blade. This is achieved by increasing or decreasing the aerofoil camber when deployed on the suction side. [46].

This device can produce substantial lift variation over the blade by means of small surface deflections. Due to the surfaces low inertia, high frequency control can be achieved, and these devices can be easily combined with smart materials for actuation. Trailing edge flaps can be either discrete trailing edge flaps or continuous deformable trailing edge.

The discrete trailing edge flaps are conventionally used in aircraft. They are known also as ailerons that are mounted on the blade (hinged) and for the required position to be achieved, a moment is needed over the hinge [46]. They provide great advantages in terms of regulation of power and alleviation of load but pose certain disadvantages such as kinks of the aerofoil contour that reduce the lift to drag ratio and concentrated mass. Moreover, the discontinuity of the surface causes stall and poses the concern of noise. Continuous deformable trailing edge, which is a variable trailing edge geometry, shows a smooth variable in the shape, which tends to increase its effectiveness in the lift variation and lift-drag ratio [46]. This is a simple and uniform part that is an integrated solution for an aerodynamic control surfaces. The actuation requires a bending moment to be exerted on the trailing edge. Depending on the material, this type of aerodynamic control works against the structural stiffness of the trailing edge and the probability of the skin being subject to fatigue. The trailing edge flap concept combines the ideas of aileron and camber control, which is based on skin deformation, using a small part of the turbine blade.

Wilson et al [53] did a research work on active aerodynamic blade control design for load reduction on large wind turbines. A numerical simulation was carried out which uses trailing edge flaps as the active control. A 20-32% reduction was realised in the blade root flap bending moments. This allows the blade lengths to be increased without the original fatigue damage on the system exceeded; which would result in a larger swept rotor area. While Frederick et al in 2010 [54] performed gust alleviation using rapidly deployed trailing-edge flaps. The study was numerical and experimental using small, rapidly actuated trailing-edge flaps to alleviate the unsteady loading experienced by the wind turbine blades due to the wind turbulence. A significant reduction in the unsteady loading was perceived.

1.8.2 Microtabs

The Microtabs concept was derived from the concept of Gurney flaps. They are small tabs proposed and comprehensively studied by Yen et al [55] which are deployed near the aerofoil trailing edge and are used to modify the flow kinematics locally [56]. The use of microtabs in improving the aerofoils aerodynamic performance is a relatively new field of research when compared to the use of trailing edge flaps, which have been comprehensively investigated for helicopter blades applications. They are used as aerodynamic load control devices on wind turbine blades. Deployment of microtabs changes the flow development (Kutta condition) at the trailing edge of the wind turbine blade [46]. The microtabs are deployed just about normal to the blade surface on the pressure and suction sides at height of about 1-2% of the localised chord length as shown in Figure (1.5) [56]. Enhancement of lift is achieved by installing the microtabs on the pressure side (lower surface) of the aerofoil, while reduction of lift is achieved by installing the microtabs on the suction side (upper surface) of the aerofoil. The lift reduction can still be achieved by mounting the microtabs close to the onset of pressure recovery to incite flow separation. The function of microtabs is primarily on-off, because the effective camber of the aerofoil is changed by varying the trailing edge point, so the lift is not altered proportionately as achieved when trailing edge flaps are deployed [46]. These microtabs are Micro Electrical Mechanical tabs (MEM tabs) that are actuated and controlled by small integrated electronic circuits [46]. The tabs give faster response times due to the miniscule size, and use of smart feedback control, and can generally reduce the weight, complexity

and cost of the system. From literatures, it been found that fitting of the lower and upper microtabs close to the blade trailing edge, typically yields an increment in the coefficient of lift to a value of $\Delta Cl = 0.3$ for a microtab height to chord ratio $T_h/c = 1\%$ and obtains a maximum increase of $\Delta Cl = 0.4$ for a tab height to chord ratio $T_h/c = 2\%$. Mounting of the upper tab at the onset of the pressure recovery can yield values of about $\Delta Cl = 0.55$ [46].



Figure 1.5. Microtab concept [46]

In 2008, Wilson et al [57] studied the optimal deployment of the microtabs in conjunction with individual and collective pitch control to provide effective load alleviation for the NREL Controls Advanced Research Turbine (CART) in Colorado. It was observed to have up to a 70% potential theoretical upper-bound reduction in the root bending moment.

1.8.3 Camber Control (Morphing)

Camber control which could be called morphing is an effective technique of regulating the aerodynamic loads by directly varying the aerofoil shape as shown in Figure (1.6) [46]. The force distribution on the blade can be directly influence by this action, thus load mitigation can be realised by utilising this technique. This can be realised by fitting smart materials inside the skin of the turbine blade or the use of a structure that internally deforms. The aerodynamic loads, dynamic and structural forces of the aerofoil need to be overcome for such actuation processes to occur. For the actuation, several concepts have been proposed, extending from construction of deformation of the centre part of the chord to bending of the aft section or bending of the trailing edge [46]. Deformation of the centre part can be achieved by internal framework actuation utilising smart materials or discrete actuators. This kind of framework is often known as a ‘compliant mechanism’ and it is used to offer load carrying paths. The major challenge with this concept is that large strains in the skin are required, thus skin sections that are partially weaker are utilised for the camber control. In order not to compromise the turbine blade integrity, it is a reasonable technique for small surfaces of variable geometry.

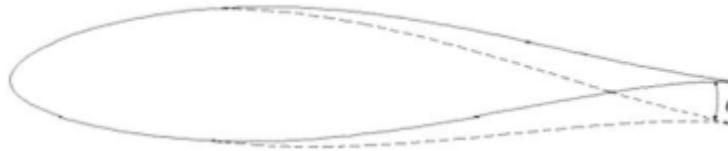


Figure 1.6. Camber control concept [46]

Morphing aerofoils are seen also to be capable active flow controllers. The main challenge of morphing aerofoils is how to manufacture a blade structure that is flexible enough to morph without losing its capability of withstanding aerodynamic loads. [58-77].

1.8.4 Active Twist

The active twist control concept utilises piezoelectric fibre composite actuators such as Active Fibre Composite (AFC) or Macro Fibre Composite (MFC), which are implanted within the blade structure to actively cause twisting deformation of the blade as shown in Figure (1.7) [78].

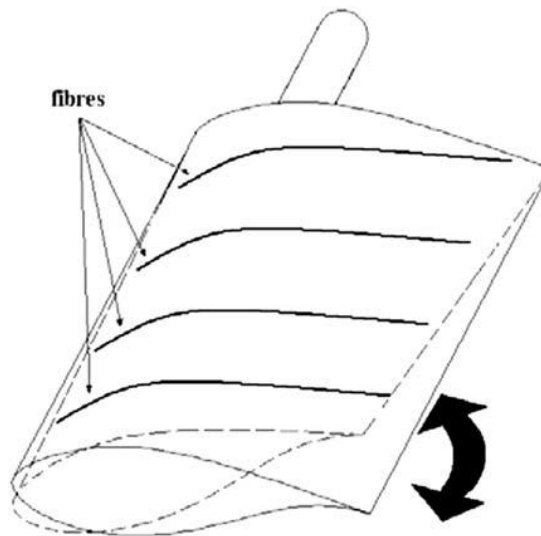


Figure 1.7. Active twist concept [46]

The twisting results in alteration of the local angle of attack. The largest change in pitch is realised at the blade tip, which gives an effective aerodynamic control of the blade [46]. Apparently, with active twist control, span-wise distributed control is not possible. The active twist control concept is based on actively controlled stretching-twist or bending-twist coupling. This concept research for rotorcraft applications has shown efficient aerodynamic control. It is shown to effectively mitigate vibrations and noise in helicopters. Strain levels of five times larger than those obtained from conventional piezo-ceramics can be achieved using single crystal piezoelectric materials [78]. Park and Shin [79] proposed

a new concept of developing a new active twist rotor blade that integrates single crystal MFC. The concept is known as the Advanced Active Twist Rotor (AATR) blade. This has been demonstrated to be more efficient in vibration mitigation and improve acoustic characteristics of the rotorcraft [79].

One of the disadvantages of the active twist control is evident when employed in large wind turbine blades due to relatively large inertia, and as such control concept response times will not be fast enough. Another pitfall of this concept is the control forces and strains required to twist the entire blade have been estimated to be very high. The major issue with respect to using active twist control would be the large scale embedding of smart materials in the complete blade structure. Particularly when piezoelectric fibre composites are used, it would result to an expensive and heavy structure. An obvious advantage of the active twist control concept is that a smooth blade is gotten which does not alter the aerodynamic characteristics of the original blade design [46].

1.8.5 Boundary Layer Control

Another approach is the boundary layer control approach proposed for aerodynamic load control on turbine blades. This technique is achieved by influencing the flow close to the aerofoil surface resulting to change in the total characteristics of the flow around the aerofoil, thus affecting the aerofoil aerodynamic characteristics [46]. This method is developed to manipulate the boundary layer either to decrease the drag or increase the lift. Most commonly known techniques are vortex generators, boundary layer suction/blowing, plasma actuators and synthetic jets. Conventionally these techniques are boundary layer influencing concepts. They are mounted on the surface of the aerofoil and used for flow separation control at large or moderate angles of attack, thus, greatly varying the pressure distribution of the aerofoil. Furthermore, the boundary layer control devices can be used at small angles of attack for camber control.

The boundary layer control by suction on aerofoils is an old concept. It progressed during the last century and several experimental aircraft applications have been investigated [46]. The boundary layer control by suction is achieved by sucking the low momentum layers from the bottom of the boundary layer into the suction slots [80]. From the outer layers, it sucks the higher energy air closer to the aerofoil surface. The development of boundary

layer by a suction system is relatively complex because it involves consideration of the optimal slot placement, the amount of suction, power system, and structural modifications etc [46]. The chief purpose of this separation control by suction is the elimination of flow separation and drag mitigation with the use of actively controlled suction, the aerofoil virtual shape can be changed, thus, theoretically control in lift can be realised.

Vortex generators are aerodynamic devices that can help to delay local flow separation aerodynamic stalling by mixing fluid with high momentum from the outer flow with fluid with low momentum next to the aerofoil surface, thereby increasing the surface effectiveness. This process is also known as re-energising of the boundary layer [46, 80]. Fixed or static vortex generators which are also known as passive vortex generators have been explored in the past for flow separation control in wind turbine blades. They produce vortices and interfuse the low momentum boundary layer with the high momentum air above, resulting in energising of the slow boundary layer. Thus, the boundary layer flow separation can be controlled at high angles of attack [81]. The use of fixed vortex generators is limited due to a pitfall of causing a permanently increased drag thereby reducing the efficiency [81]. Another technique is flow driven oscillating vortex generators (FDOVGs). These oscillate at certain frequencies to induced vortical flows. The length scales of these vortical flows are of the order of the aerodynamic surface scale. Power is received from the mean flow for the operation of the FDOVGs and generates the large amplitude oscillations required for controlling the dynamics of the boundary layer [82]. Though, for a wide range of speed, optimising poses further challenges [83].

Another approach is the synthetic jets approach which employs an oscillatory surface inside a cavity to create zero-net mass flux. This is achieved by momentarily interchanging of fluid ejection and suction across an orifice and is completely created from the controlled fluid. Thus, no fluid ducting is needed [46]. In this approach, during the suction phase, there is removal of low momentum flow from the boundary layer and perpendicular to the surface, high momentum flow is blown out resulting to a change in direction and net momentum addition. It was revealed that modification of the flow field on length scales of one to two orders of magnitude bigger than the characteristic jet length scale can be achieved with the synthetic jets [46]. In comparison with a small Gurney flap, the drag penalty is extremely reduced for a continuous jet [46, 84]. Synthetic jets permit simpler construction since no continuous pumping is required and at a lower momentum coefficient, they are still very effective.

Another boundary layer control is the plasma actuators concept which was recently proposed for wind turbine blades. The actuators are made up of two thin electrodes of typical thickness of around 1 mm, one bigger than the other, which are separated by a dielectric insulator [46, 85]. The plasma actuator is usually encapsulated within a surface with one of the electrodes left exposed to the airflow. Ionisation of the air is done by supplying high voltage ac potential to the electrodes. The ionisation occurs in the region of the highest ac potential, all that is needed is having a high electric field produced by the electrodes that is sufficient to cause the ambient air atoms to electric dissociation [85]. These actuators are very simple, fast-acting and can be produced in sheets that can be affixed on the desired surface [86]. Unlike synthetic jets, plasma actuators have no moving parts as shown in Figure (1.8) and they operate at frequencies usually ranging between 50 Hz and 500 kHz.

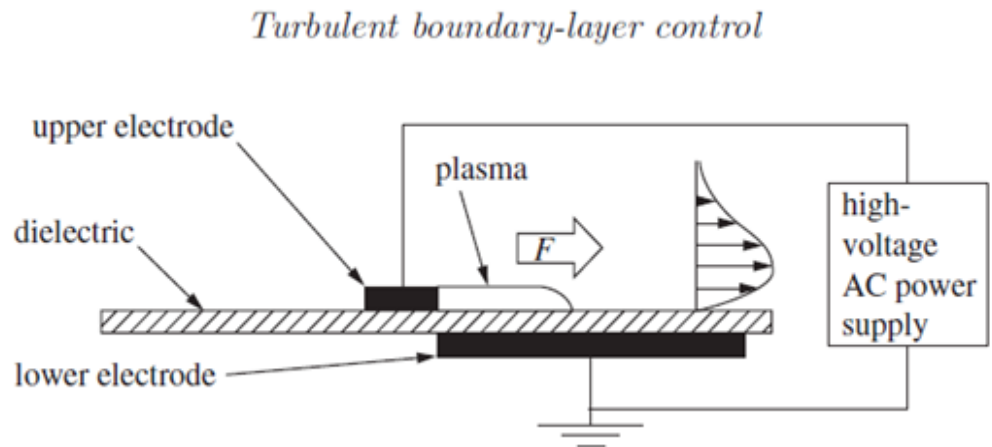


Figure 1.8. Schematic of DBD plasma actuator for flow control applications [86]

Locating the plasma actuators near the trailing edge has shown to be more effective in delaying flow separation and stalling at high angles of attack and it also affects the lift at low angles of attack.

All past and ongoing research works are to improve on the energy capture, power regulation and load alleviation on the blades to increase the fatigue life. Researches are focus towards the use of larger blades which has some challenges and also smart blades. The challenges of larger blades and smart blades are discussed in Chapter 2. Manufacturers and researchers are always seeking to develop more efficient way to design the blade, thus, the focus of this research work on ways of improving existing approaches.

1.9 Aim and Objectives

In view of the above, smart blades are significantly more efficient in producing flexible, reliable and load alleviation. In the context of wind turbines, flapping blades and adaptive blades (bend/twist elastic coupling blades) lead to more efficient capturing of wind energy and therefore cheaper energy. On other hand, high controllability makes these types of aerodynamic surfaces more efficient in alleviating stochastic loads.

The aim of this research is to explore the potential benefits of flapping blades and adaptive blades in extracting wind energy. To achieve this aim, the following objectives are defined and thesis structure is shown in the flowchart, Figure (1.9):

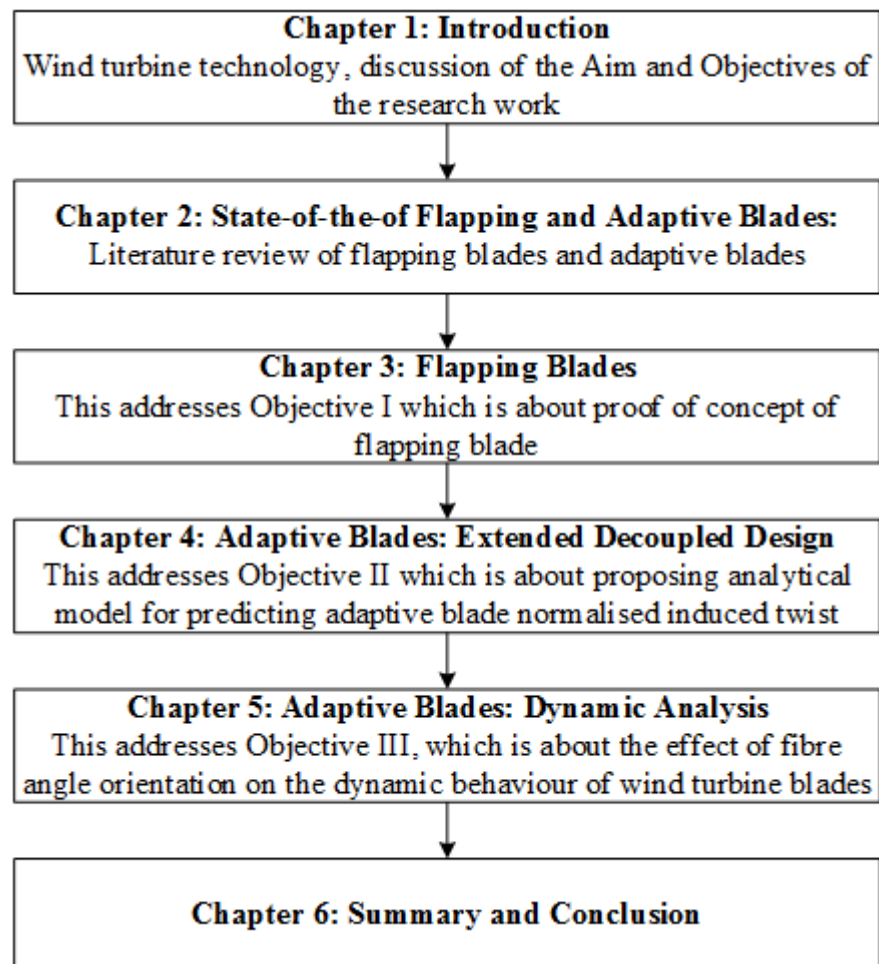


Figure 1.9. Flowchart of the thesis structure

Objective I

To perform aerodynamic analysis for establishing “proof of concept” for flapping blades towards obtaining the aerodynamic characteristics (lift coefficient C_L , drag coefficient C_D and pitching moment coefficient C_M) of a rotating flapping blade in terms of rotor rotational speed (Ω) as well as flapping frequency (ω) and wind flow field characteristics (e.g. turbulence)

Objective II

To establish an extended analytical model for adaptive blades to generalise it towards removing the limitation of the decoupled design model of predicting the normalised induced twist

Objective III

To perform dynamic characteristic analysis of adaptive blades aerodynamics for cases studied in Objective II

1.10 Structure of the Thesis

This thesis consists of six chapters. Chapter 1 is dedicated to the background and trend of wind energy, the design of wind turbine and the advancement of wind turbine technology. It also presents the types of wind turbines, wind energy challenges, state-of-the-art of smart rotor control for wind turbine and aerodynamic control surfaces. Chapter 2 discusses the challenges of larger blades, smart blades and types of smart blades. Also, the background of flapping blades and adaptive blades are discussed. Furthermore, it covers the description of an auxiliary tool developed using MATLAB codes for a high performance blade modelling and analysis. Chapter 3 discusses the flapping wing kinematics and flapping blade proof of concept which addresses objective I. Chapter 4 starts with the description of the decoupled design method of adaptive blades established by other authors and then it extends the application of this method to establishing a general analytical model for the determination of wind turbine normalised induced twist for cases of varying structural characteristics and also presents the validation of the HPBM. Objective II is addressed in this chapter. Chapter 5 which addresses Objective II, discusses aeroelasticity, types of aeroelasticity and then dynamic behaviour of adaptive blades. Chapter 6 is the summary of the research results obtained, recommendation, and highlights of the original contribution.

1.11 Summary

In this Chapter the structure of the Thesis, the objectives and methodology of the research were discussed. The resurgence in the renewable energy industry with wind energy as the major source has led to rapid technological advancement in the wind turbine industry. With the advancement, the research focus is to increase the energy power and aerodynamic load alleviation. To achieve the optimum power extraction and cost effectiveness of wind turbine, research for designing the wind turbine to be more efficient are being investigated with key focus on the blades, being the major component of the wind turbine for power extraction. Furthermore, different types of aerodynamic control surfaces for altering the aerodynamic characteristics at specific locations and providing the appropriate control responses were discussed. The challenges of having larger blades for increasing energy capture are discussed in Chapter 2.

2 State-of-the-art of Flapping and Adaptive Blades

2.1 Challenges of Larger Blades

The size of blade in wind turbine system determines the output power of the turbine. With the upsurge in the wind turbine industry, the power output of commercial wind turbine blade has risen to 5 MW and the blade length of over 100 m [87]. Large blades design is chiefly considered these days in order to enhance the extraction of wind energy. Due to the length and flexibility of Megawatt wind turbine, aeroelasticity is a critical concern [88]. Severe challenges are confronted in the design and manufacture of large scale wind turbine which results to the focus of researchers on the wind turbine blade design.

In design considerations, the blade should be of good rigidity to mitigate the destruction that could result from the wind load randomness and gust. Increasing the length of the blades make the blades move vulnerable to destruction by wind gust. According to Kensche [89], the length and weight of blade have increasing impact on the bending load that the blade can internally withstand. As the size of blade increases, it becomes more difficult for the blades which could be subjected to adverse environmental conditions to meet design requirements of 20-year basic fatigue life [89]. He made research on the S-N curve of the off-axis fibre which bears the shear load for more accurate prediction of the fatigue life of larger blades. Some researchers like Samborsky [90] and Sakin [91] investigated the fatigue and the interlayer destruction mechanism of carbon and glass fibres and they found out that the blade fibre manufacturing technology and the adaptability of the blade have an essential effect on the fatigue life of the blade. Therefore, with increase in the size of the blade, the more difficult it is to maintain the rigidity of the blade. Wind turbine blades are mostly subjected to stochastic conditions, which generates varied load on the blade as a result increasing the fatigue damage probability of the wind turbine blade. The blade failing to instantaneously adapt to the varying load will make it vulnerable to damage and thus reducing the fatigue life. Therefore, it is imperative the flexibility of the blade is increased as well as its unloading effect is improved.

Furthermore, increasing the size of the wind turbine blade requires better material because glass fibre can now barely meet the structure reliability requirements. Carbon fibre has light weight and good mechanical properties which made researchers to focus on hybrid fibres [87]. This gives the combination of high stiffening and strengthening potential of the carbon fibres with cheaper glass fibres

Recent research focuses are load alleviation on the blade, to improve the blade reliability, increase the fatigue life as well as the power output stability. This research focus is on blade adaptability to the wind load with the blade sections twisting accordingly in response to the load acting on it as a result unloading some of the force acting on it and controlling the power output.

At the Sandia National Laboratories (SNL), an advanced concept for enabling the use of longer blades with the weight reduced was developed by Ashwill and Laird [9]. These blades are more aerodynamically and structurally efficient. An approach to change the mechanical properties and dynamic behaviour of wind turbine blade is the modification of the composite material which the blade is made of. That is the use of smart materials.

Nowadays the blades are so long that the blades not only experience different wind conditions, but the wind conditions vary along each blade. Wind turbine blades load alleviation systems are mainly designed to redistribute the loads acting upon each wind turbine blade when the load factor upsurges. This control can be either passive or active. Several load alleviation control strategies are being explored in order to reduce the loads to avert damage/increase the fatigue life of the blades. These include; individual pitch control, trailing-edge flap, morphing aerofoil and microtabs.

Limitations in the present blade technology constitute technological barrier in upscaled wind turbines for cheaper construction that would reduce cost of energy production [92]. With increase in the turbines sizes, the turbine blade design and savings in the weight become of foremost importance. The concept of intelligent or smart blades that can adapt themselves to the stochastic aerodynamic loading and eliminate or reduce the use of an active control system becomes the focus for the future of wind turbine blade technology. The concept is not entirely new, it has been around for about three decades. In achieving these goals, some control systems have been proposed using either purely- active, purely-passive or a combination of active and passive control. Blade adaptiveness can be realised by the material layup influences the coupling among modes of the blade deformation. In designing of aircraft wings, the analysis of coupled modes has been long analysis in aeroelastic problems because coupled modes could be potentially dangerous if not appropriately considered at the design stage. Nevertheless, currently the aeroelastic effect is being used in developing adaptive blades by means of increasing the elastic coupling among the deformation modes of the blade which are normally slightly coupled [92]. For

instance, mitigation of extreme loads and vibration, control of power generation and improving of fatigue performance can be achieved by elastic coupling between bending and twisting [92]. For the bending/twist coupling, as the blade bend as a result of the aerodynamic load, a twist is induced by flexo-torsional modes resulting to a change in the angle of attack on the aerofoil sections. This reduces the lift force exerted on the blade.

2.2 Smart Blades

Researchers are focusing on achieving wind turbine blades that will be robust, reliable and cost effective that could have intelligent aerodynamic control. Smart blades are intended for improving the efficiency of the blade by adjusting or adapting with respect to the rapidly stochastic wind conditions. Wind turbine nowadays are designed to exploit technologies that are improved in blade aerodynamics, control, materials, and innovations to make it cheaper and as well as to increase the turbine yearly operational hours [93]. The systems life cycle costs are lowered with the support of these technologies. Aerofoils design for the aviation industry made by the National Advisory Committee for Aeronautics (NACA) were used for most horizontal axis wind turbines (HAWTs) in the mid-1970s. Because the NACA aerofoils were designed for aeroplanes, the Reynolds number operating range is usually much higher than that experienced by wind turbine blades, this results to terrible performance degradation from the leading edge of the blades when the wind turbine operates at much lower Reynolds number. Tangler et al [94] discuss the advancement of aerofoils used by the wind energy industry. The use of NACA aerofoils in wind turbine blade design led to aerodynamic performance loss which resulted in substantial annual energy losses. The National Renewable Energy Laboratory (NREL) and also the European research centres in the mid-1990s, sponsored the designing of a new type of aerofoil sections to be suitable for stall, variable rpm and variable pitch regulated wind turbines. Tangler and Somers did an estimation of the use of the NREL aerofoils and established that annual energy improvements for stall, variable rpm, and variable pitch regulated wind turbines of (23-35%), (8-10%), and (8-20%) could be achieved respectively. [93].

In the last twenty years, the blade loading control on large wind turbines has also significantly changed. Most wind turbine until 1990s were designed to control power output and blade loading using passive control mechanism by stall regulation. Stalling of

the blades begin as the wind speed increases in a stall regulated wind turbine. As the drag is increased, the wind turbine becomes less efficient thus regulating the power extracted by the wind turbine. This necessitates the design of larger wind turbines in the 1990s to make use of active control in the regulation of the speed of the rotor and power output via controlling the angle of the wind turbine blade pitch. The ability to control the angle of the blade pitch enables more blade load control and efficient operation. Furthermore, the application of active load control allowed designers the opportunity to use turbine blades with lighter weight.

Some of the challenges the wind turbine designers are facing include; alleviation of large transient blade loadings, a steady power output provision with time and regulation of the power output in high winds. It has been perceived that smart blades would offer the potential of enhancing the wind turbine performance through increasing the operating wind range, regulating the unsteady loads on the blade and increasing the fatigue life of the blade [93].

In order for an optimal performance improvement to be achieved in a velocity field that fluctuates both temporally and spatially across the blade, the localise blade pitch angle across the blade of the turbine need to be able to be adjusted. Distribution of active flow control system can be utilised to optimize the system extraction of wind energy and the moderation of the loading of the blade across the blade span. [93]. This can also be done using passive flow control which is a function of the material used and layup configuration.

2.3 Types of Smart Blades

There are several types of smart blades which are in used today. The smart blades of wind turbine can be classed into two major groups; extrinsically and intrinsically smart blades. The extrinsically smart blade (active) is basically blade that has actuators implanted in the material for the generation and controlling of the blade elastic deformation. The intrinsically smart blades (passive) are those made up of integrated anisotropic composite materials with the layup configuration generating and controlling the blades elastic deformation. Figure (2.1) shows the different types of smart blades. The types of smart blades that will be focused on in this research are the flapping blades and adaptive blades.

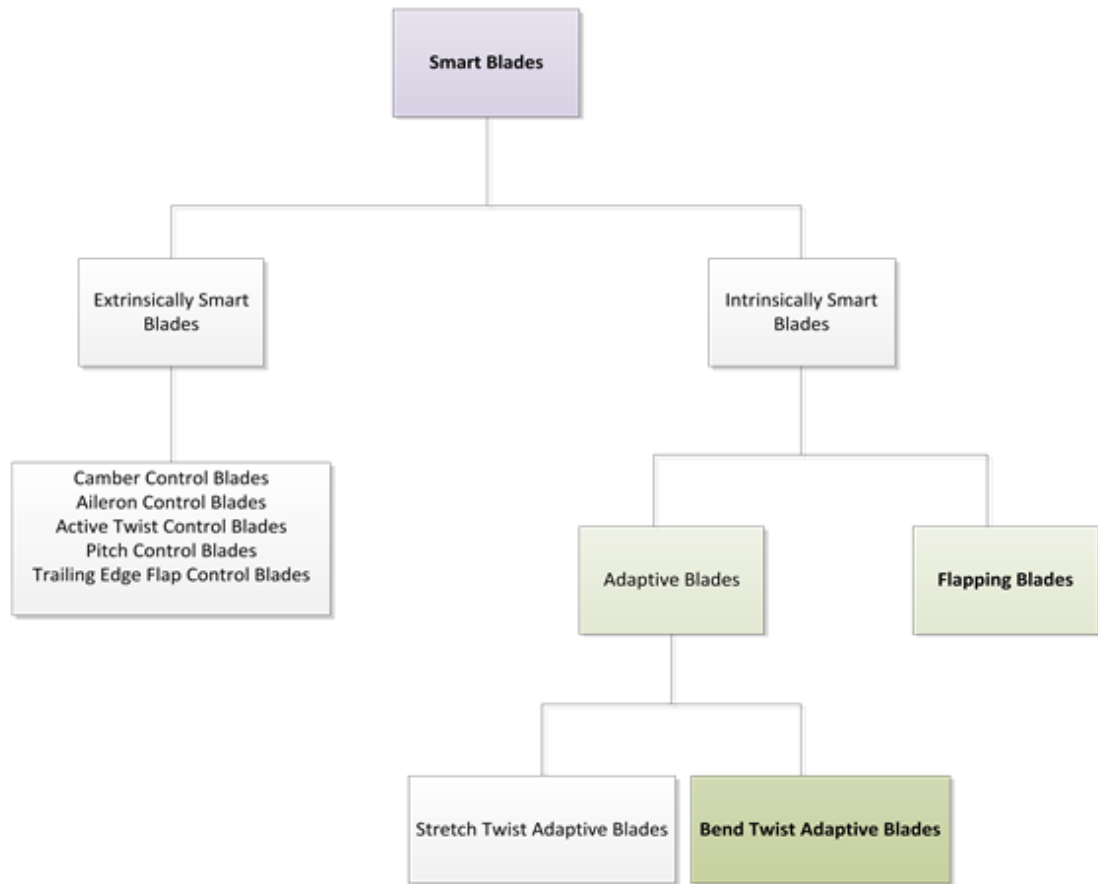


Figure 2.1. Types of Smart Blades

2.4 Flapping Blades: Background

Flapping wings generate high lift and forces necessary to support the weight and to perform rapid manoeuvres. Flapping wings sweep through the air as they translate with moderately slow changes in the angle of attack, which is followed by rapid rotations at the end of each stroke. The flight kinematics of most of flying insects comprises of three distinct motions, namely, flapping (up and down wing motion), lagging (forward and backward wing motion) and feathering or pitching (angular movement about the wing longitudinal axis) [95, 96]. The insects wing pronation (upstroke to downstroke) and supination (downstroke to upstroke) transition allows the maintenance of positive angle of attack and to lift generation [97]. The Weis-Fogh mechanism explains that pronation or supination generates large circulation and continue through the subsequent stroke [98].

Desire to mimic flying creatures such as birds and insects through engineering to meet human necessities has been in existence for hundreds of years and was firstly inspired by

Leonardo Da Vinci. His flapping wing studies were summarised in a book manuscript named “*Sul volo degli Uccelli*”. Little advancement was made by the Wright brothers when they successfully developed a powered human flight in 1903. The development and research of fabricated flapping wing vehicles were discouraged following the Wright Flyer sustained flight in 1903 and the later swift progress of fixed-wing aeroplanes in conjunction with the clear mechanical complications presented by flapping wings.

Knoller in 1909 and Betz in 1912 carried out an independent study and observed that a wing flapped in a free stream flow will result in an effective angle of attack with a normal force vector comprising both thrust and lift components. This phenomenon is known as the Knoller-Betz effect [99 & 100].

In 1922, Katzmayr carried out experimental validation of Knoller-Betz effect using the wind tunnel tests. Instead of flapping the aerofoil, Katzmayr did a sinusoidal oscillation of the free stream velocity and measured an average thrust. Katzmayr’s measurements shown that an aerofoil mounted in a wind stream that is oscillating experienced a thrust force. In 1924, a solution was developed by Prandtl’s student, Birnbaum, for an incompressible flow past flapping aerofoils and the conditions that lead to thrust or flutter generation were observed. He as well proposed the usage of a flapping (heaving) wing using a sinusoidal motion as a substitute to the conventional propeller [99 & 100].

In 1935, an analytical method was published by Theodorsen for estimating the moment and unsteady lift of harmonically oscillating aerofoils. In developing this method, the assumptions of an inviscid and incompressible flow were used by Theodorsen. Theodorsen assumed that the aerofoil wake would take the form of a continuous vortex sheet of varying strength of sinusoidal motion, which stretch from the trailing edge to infinity in the downstream direction [58 & 100].

This bio-inspired (biomimetics) research has played a key role in the advancement of many evolutionary engineering applications. The study of birds and insects (e.g. dragonfly and hummingbird) gives insights on the generation of high lift by the wing-created vortical formation, the relationship between aerodynamic parameters and flapping frequency, flapping amplitude, flapping wing kinematics and morphological parameters [101-110]. This study has provided us with valuable insights into the complex aerodynamics of moving wings with many applications including Micro Air Vehicles (MAVs), for example see [111 & 112].

As cited in [99 & 100], von Karman and Burgers presented the first theoretical explanation of drag and thrust production based on the observed location and orientation of the wake vortices in the year 1935. Burgers and von Karman experimentally perceived that a wake consisting of two rows of counter-rotating vortices could create a thrust force on an aerofoil in an incompressible flow. Later, in 1936, Garrick used Theodorsen's inviscid, incompressible, oscillatory, flat plate theory for the prediction of thrust and propulsive efficiency of harmonically plunging or pitching aerofoils. He discovered that to generate lift by pure pitch oscillations, comparatively high frequency value has to be exceeded.

Theodorsen oscillatory thin-aerofoil theory was replaced by an approach that allows the computation of incompressible potential flow past oscillating aerofoils of arbitrary shape by the placement of sources and vortices on the aerofoil surface rather than along the chord line. Giesing established the so-called panel method; he generalised the Hess and Smith method for steady aerofoil flow. More at a recent time, 2D unsteady panel methods have been employed for predicting the flapping wing MAV propulsion [113]. Three-dimensional methods also have been employed to the prediction of the forces acting on insect wings.

Some current works using Navier-Stokes solvers include the research work done by Young and Lai [114], where it is made known that the vortical structure in the wake, and the thrust and lift characteristics of a heaving aerofoil are strongly determined by the oscillation amplitude and frequency.

Isogai et al. [115] performed Navier-Stokes computations to ascertain the effect of dynamic stall on propulsive efficiency and thrust of flapping aerofoil. They calculated the propulsive efficiency and thrust for several combinations of frequency and phase difference, and a comprehensive analysis of the dynamic stall phenomena effects on the behaviour of the thrust and the propulsive efficiency was given. High efficiency was observed for the situation in which the pitching oscillation advances 90° ahead of the heaving oscillation and the reduced frequency is at some optimal value, for which there seems no significant flow separation in spite of large-amplitude oscillations. For reduced frequency and phase angles frequency other than this optimum condition, there is rapid degrading of efficiency by the occurrence of the large-scale leading edge separation.

In a subsequent work, Isogai et al did an investigation of the dragonfly aerodynamic performance, for which they made more comprehensible the fundamental mechanism of

the dragonfly hovering flight [116]. Three-dimensional Navier-Stokes solver was used by Liu et al. [117] to successfully model the powered Hawkmoth hovering mode. Lewin et al [118] studied the propulsive characteristics of an aerofoil heaving in sinusoidal motion over certain heave amplitudes and frequencies range in order to correlate viscous flow structures to generation of thrust.

Pedro et al. [119] carried out a numerical study of a flapping hydrofoil propulsive efficiency at Reynolds number of 1100. In their study, Pedro et al. [119], aerofoils undergoing pure pitching motion and combined pitching-and-heaving motion were investigated and the sensitivity of thrust and efficiency to the phase angle, maximum pitch angle and the Strouhal number was showed. Hover et al. [120] used non-sinusoidal and sinusoidal effective angle of attack variations in time to study the aerofoil propulsive performance of the aerofoil experiencing combined pitch and heave oscillations.

Tuncer et al. [121-123] carried out Navier-Stokes computations to investigate the flow separation effects on the propulsive efficiency and the thrust of a flapping aerofoil in combined heave and pitch oscillations.

Koochesfahani [124] experimentally studied the wake structure behind a flapping aerofoil and found out that the flapping amplitude, flapping frequency and oscillation waveform shape have great effect on the wake structure. It was also observed that there exists an axial flow in the cores of the wake vortices and estimate of the magnitude suggest linear dependence on the oscillation amplitude and frequency [99, 100]. Anderson et al. [125] carried out experiments and they found out that the phase angle between heave and pitch oscillations plays an important part in the propulsive efficiency maximisation. The experimental investigation by Jones et al. [126] established that two aerofoils organised in a biplane configuration and oscillating in counter-phase display substantial benefits of propulsive efficiency and thrust compared to a single flapping aerofoil.

Ho et al in 2003 [127] investigated flow control and unsteady aerodynamics for flapping wing flyers and observed mechanisms such as unsteady leading edge vortex, wake capture and rotational circulation do seem to properly account for the aerodynamics forces.

Some research works investigated the oscillation frequency and amplitude effects on the wake of a plunging aerofoil (for example see [124-134]). It is well known that the vortical wake structures, and the lift and thrust characteristics of a heaving aerofoil strongly depend on the oscillation frequency and amplitude. Therefore, beating the wings at certain

frequency will produce high vortex circulation and if properly phased, the vorticity around the wing edges will generate high lift.

Wind energy industry is highly under the influence of the advances in aerospace, particularly in design of intrinsically or extrinsically smart blades (for example see [135-140]).

2.5 Adaptive Blades: Background

Blades are designed to have good rigidity to be able to reduce the destruction that could be caused by rapid wind load and gust. The increase in length of the wind turbine blade boosts energy capture but contributes to the susceptibility of the blade to the unforeseeable destruction caused by random gusts [141]. The design of blades to respond to the changes in the aerodynamic loads led to the focus on blade adaptiveness. There are basically two major approaches in realising blade adaptiveness which result to having either geometrical or structural adaptiveness. The two types of blade adaptiveness are discussed here with major focus on structural adaptiveness.

2.5.1 Geometrical Adaptiveness

Geometrical tailoring is a concept that originated from aeronautics. This is achieved by fine tuning of the relative distance between the blade aerodynamic centre (usually located at the quarter of the chord length for typical aerofoils and the structural torsional centre of the blade section. This is one of the key principles of swept wings to self-adapt the angle of attack on the wing sections and preventing structural divergence. This could be achieved by modifying the blade geometry. Geometrical adaptive blades have a curved outboard towards the trailing edge. In theory, the outer parts of the blades pitching arm increases thus, resulting to higher pitching moment in the inboard sections [92]. As a result of this, the blade responds to changes in aerodynamic loads, is possible. On swept wings, there are two configurations that are possible; the backwards sweeping and the forward sweeping. The major characteristics of the backward sweeping is having the aerodynamic coefficient reference point located behind the torsional centre of the wing section which results in a nose-down motion of the aerofoil section thus causing a decrease in the angle of attack with increasing aerodynamic loads. For the forward sweeping, the aerodynamic coefficient

reference point is located forward of the torsional centre of the wing section resulting in a nose-up motion of the aerofoil section which cause an increase in the angle of attack as the aerodynamic loads increase. In addition to the adaptiveness effects, the swept wings help to delay the increase in drag caused by the compressibility of the fluid at high Mach number regimes. The swept-wind concept motion can be applied to the wind turbine blade design by geometric modification of the blade planform.

2.5.2 Structural Adaptiveness

Wind turbines blades might look like slender structures, but they are usually complex structural members as a result of the inhomogeneous material properties distribution and the cross sections complexity. In complex beams, because of their non-homogeneous sections, the matrix is not diagonal resulting to coupling between different deformation modes [92]. These types of couplings are referred to as non-conventional couplings. Most of the modern wind turbine blades are made from fibre reinforced laminates and they are certainly inclined to exhibit non-conventional couplings due to the anisotropic stiffness properties. Thus, the adaptiveness of the blade comes from the orthotropic stiffness of the laminates and the material distribution over the blade sections.

Recent research has been focussing on using adaptive composite materials to produce wind turbine blades with flexibility capability to mitigate the load effect on the blade and to increase the efficiency of the wind turbine [33, 135, 136, 143-155]. Adaptive composite, sometimes referred to as a smart material or intelligent material is a structure tailored composite to exhibit desirable elastic deformation behaviour not necessarily proportional to the imposed load [143]. Unique structural responses can be exhibited by the tailoring of composite laminates which are not achievable with isotropic materials. Specific composite layup configurations can determine the type of elastic couplings produced.

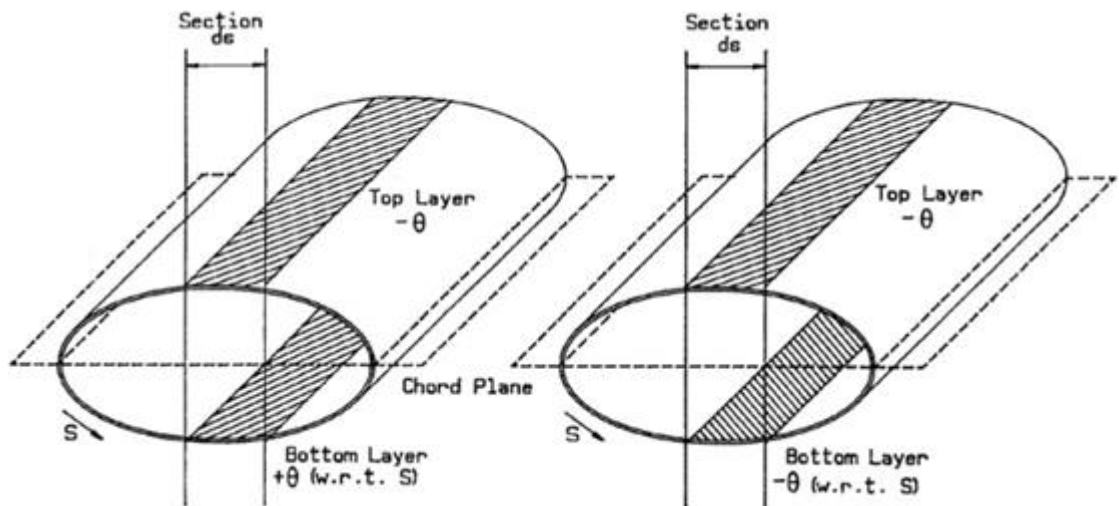
According to Karaolis et al. [162], there are three possible ways of elastic couplings with the objective of achieving some desired adaptive behaviours:

Bending/twist coupling: A mirror lay laminate configuration when subjected to bending moment produces bending/twist elastic deformation. For bending/twist coupling, the flap-wise aerodynamic load component is the most important contributing load to the bending of the blade [92]. This coupling basically depends on the rotational and wind speeds, thus,

is ideal for controlling the power output and as a sensor of the working condition [92]. For wind turbines, the predominant force is the bending moment, thus the bending/twist elastic coupling is most suitable elastic coupling [144]. The layup of the laminate configuration for a bending/twist coupling is shown in Figure (2.2.a).

Stretching/twist coupling: A helical layup composite configuration produces a stretching/twist elastic deformation when subjected to axial loading. For stretching/twist coupling, the centrifugal force is the most important contributing load to the stretching of the blade. The stretch twist elastic coupling blades are usually suitable for helicopter where the predominant force is the centrifugal force. In the situation of a blade having a stretching/twist coupling, the rotor speed can be utilised to make changes to the twist angle and accordingly alter the angle of attack, eventually controlling the aerodynamic load on the blade.

This elastic coupling was proposed for variable speed rotors control or as an emergency system for variable and fixed speed rotors. The layup of the laminate configuration for a stretching/twist coupling is shown in Figure (2.2.b).



(a) "Mirror" layup for bending/twist coupling [θ changes sign below chord]	(b) "Helical" layup for stretching/twist coupling [θ has same sign around S]
---	---

Figure 2.2. Layups for bending/twist and stretching/twist couplings [162]

Pressure/twist coupling: Another coupling which was proposed by Karaolis et al [162] as well was to pressurise the blade interior as a mean of controlling the blade twist angle. This type of control does not actually fit into the smart blade or adaptive blade concept because the lowering or increasing of the internal pressure needs to be commanded externally.

Of the three strategies, the most promising for wind turbine blade is the bending/twist coupling and most researchers focus on its advancement. The blade twist under increasing load can be either increasing the angle of attack which is towards stalling or decreasing the angle of attack which is towards feathering. The type of control behaviour desired and variables to be optimised determines the more appropriate twist (twist sense) either towards stalling or feathering [92].

It has been shown that bending force on an unbalanced composite blade will result to torsional deformation of the blade because some of the forces will be translated to the off-axis direction resulting to the blade twisting around the axis. This twist is known as induced twist. Adaptive wind turbine blades from preliminary studies have shown to reduce thrust loading on the blade and increase energy capture. This adaptability capability helps the blades to deform in response to the load changes. The shape of the blade spontaneously adapts to the stochastic inflow air which could help to increase the energy capture and reduction in blade surface cavitation. This type of control which is known as passive control could be achieved from the laminate configuration. The directionality of anisotropic composite material is exploited to achieve this passive control which is determined by the level of elastic coupling. The level of elastic coupling of the composite is dependent on the ply angle configuration in the laminate structure. Several studies have been carried out studying the effect of elastic coupling. It has been proven that bending/twist elastic can help in load alleviation and improve fatigue performance [33, 135, 136, 143-155]. The elastic coupling capability of the blade reduces the effect of the vagarious nature of the load on the blade by adapting the blade twist and angle of attack. The blade twist changes as the load changes which will make it not to be optimum. The blade twist is optimised by the induced twist which is a function of the elastic coupling of the blade. For adaptive blade, the blade twist angle could be expressed as a combination of the pitch angle, pre-twist and the induced twist which is a function of the elastic coupling and aerodynamic loading on the load [136]. The induced twist is a variable that is a function of the turbine running condition, the inflow air, the material properties and the blade fibre layup configuration. This implies the adaptive blade will have a dynamic topology which adjusts with the aerodynamic loading and rotor

angular velocity. The load reduction depends on the elastic coupling level and the twist distribution along the blade length. This bending/twist coupling has influence on the power output and the fatigue damage on the blades [141]. The concept of employing biased fibre layup blade skins configuration to achieve various types of elastic twist coupling for wind turbine applications was presented by Karaolis et al [90, 154, 155]. This is attainable by changing the blade skin from orthotropic blade skin to a biased fibre layup blade skins configuration that can be aerodynamically adapted with little alteration to the beam stiffness properties. This modification affects the aerodynamic performance and the aeroelastic instability of the blade [142-162].

Kooijman [163] investigated the aeroelastic tailoring, which is the term use to describe the design process where the effects of intended anisotropic mechanical properties of the structure are considered to control the aeroelastic deformation, either static or dynamic. He came to the conclusion that the use of the effect of elastic coupling is a promising way of improving wind turbine blade design. Some of his findings show that the bending/twist coupling provides the potential for a few percentage rise in energy yield and also the elastic coupling is best realised with hybrid carbon/glass reinforcement in the cross ply direction [154, 163]

Lobitz et al [Lobitz 1996] studied using the adaptive blade for the enhancement of HAWT's and observed that increase of about 5-10% in energy capture can be realised with about 2 degrees of blade twist. The adaptive blades respond to the aerodynamic loads by twisting elastically which could promote stall [164]. Several researchers' studies show that bending/twist elastic coupling of wind turbine blades towards stall yields significant reduction in fatigue damage on the blade.

Lobitz et al [154] investigated the use of aeroelastic tailoring as a passive control means for load mitigation, cost-effective and shaping of the power curve. Their main results could be as summarised be:

- Twisting the blade moderately toward stall and as well increasing of the rotor diameter will result to the annual energy significantly increased.
- With regard to classical flutter (twist to feather) and divergence (twist to stall), twist coupled blades have the tendency to be less stable though not in excessive.
- The fatigue damage is significantly increased by twist coupling to stall and could promote stall flutter.

- The fatigue damage is significantly decreased without power output reduction by twist coupling to feather especially at the lower wind speeds.
- Twist coupling to feather for variable speed pitch-controlled rotors significantly decreases the fatigue damage without the reduction of power output for all wind speeds condition.

Classical flutter and divergence are the two most common aerodynamic constraints and were investigated by Lobitz and his colleagues [153, 154]. From their studies, they concluded that divergence is a condition where the blade twists in response to increasing aerodynamic load in a direction that increases the load further [153, 154]. This usually happens when the blade rotational speed leads to a condition where it cannot withstand the increasing aerodynamic loading that is caused by the corresponding state of the blade deformation [92]. Resonant condition in classical flutter is realised for a certain phasing between the fluctuations in the elastic deformation and the aerodynamic load. In the case of wings, for each wing, there is particular speed where flutter will start, that is flutter boundary while for wind turbine blades, the flutter boundary is defined as the rotational speed at which the turbine blade flutter in still air, that is assuming zero wind flow. The stability margin is referred to as the difference between the normal operating speed and the flutter speed. Flutter involves the instability of the blades that twist toward feather while divergence involves twist toward stall with the divergence end of the spectrum being significantly more critical than the flutter end.

Due to their anisotropic mechanical properties, fibre reinforced plastics, which are the primary materials used in blade fabrication, allow the designer to vary the stiffness in different loading directions developing what is called bending/twist coupling effects. To define coupling levels, a parameter, α , is defined to indicate the proportion of the theoretically possible coupling. The coupling terms are generated starting with beam stress-strain relations. For bending/twist coupling the stress-strain relations at a point along the blade span, x , are given by:

$$\begin{bmatrix} EI & -g \\ -g & GJ \end{bmatrix} \begin{bmatrix} \frac{\partial \theta}{\partial x} \\ \frac{\partial \varphi}{\partial x} \end{bmatrix} = \begin{bmatrix} M_b \\ M_t \end{bmatrix} \quad (2.1)$$

where $\theta = \partial v / \partial x$ is the flap-wise slope of the blade (v is the flap-wise displacement), M_b is the flap-wise bending moment, M_t is the twisting moment, φ is the blade twist, and the quantities GJ and EI are the torsional stiffness and flexural rigidity respectively. The coupling term g has zero value for standard beam since there is no coupling present. For a system to be certainly positive, g is taken to be:

$$g = \alpha \sqrt{EIGJ}, \quad -1 < \alpha < 1 \quad (2.2)$$

The ability to define the coupling level of the composite material helps in the determining the bending/twist elastic coupling of the wind turbine blade which has huge influence in the blade adaptability to the stochastic loading.

2.5.3 Bending/Twist Elastic Coupling

As manufactures are in search of ways for increasing energy capture and reducing the cost of energy, the size of turbines is increased. However, the weight and wind loads increase also making the durability of the turbines to be of concern [88, 165]. Researchers have established that passively alleviating the wind induced stochastic loads by introducing bending/twist elastic coupling in the blade is one of the most cost effective way of increasing the fatigue life of large wind turbine blades [165]. A wind turbine blade possessing the bending/twist elastic coupling feature is known as an adaptive blade.

Bending/twist coupling is intended to modify the wind turbine blade response under aerodynamic loads application by introducing a coupling between bending and twist of the wind turbine blade. This coupling connects the aerodynamic loads, which induce bending moment on the blade, with the twist of the blade. The blade twist is directly related to the blade angle of attack and as a result, the aerodynamic loads. Twisting towards lowering of the angle of attack by the coupling mechanism, supports the blade to self-alleviate abrupt airflow changes such as turbulent conditions or gust, as a result, leading to alleviation of fatigue loads. Bending/twist coupling can be realised either by sweeping the planform of the wind turbine blade (i.e. geometric coupling) or by exploiting the anisotropic properties of the blade material (i.e. material coupling) [166]. These could be realised by ply material, ply angle and ply thickness unbalances of the composite laminates [165].

Composite laminate is usually characterized in terms of their response to mechanical or thermal loading, which is normally associated with a description of the coupling behaviour described by the ABD matrix relation. The ABD matrix which is a 6×6 matrix serves as a link between the load applied on the laminate and the resulted strains in the laminate. It basically defines the elastic properties of the laminate. Elastic coupling in a blade could be in the form of stretching/twist where the blade twist is a function of axial load of the blade or bending/twist coupling is said to occur when a structure undergoes both bending and twisting due to pure bending load. Bending/twist coupling for wind turbine blade has been identified as a prospective method for load alleviation because it gives more flexibility [33, 135, 136, 143-155]. The material and stacking sequence of the laminae will determine the type and extent of coupling that will be achieved [156-160]. Tailoring of the bending/twist coupling could be used to improve the aerodynamic performance by controlling the coupling between the flap-wise bending and the span-wise twisting of the blades [161].

In adaptive blades, a controlled and torsional deformation is produced because of the elastic coupling in the blade, which response to the magnitude and direction of the aerodynamic loads on the blade.

The aerodynamic performance of blades is extremely influenced by the angle of attack along its span. The angle of attack depends on the other angles as expressed in Equation (2.3).

$$\alpha = \varphi - (\beta_e + \beta_0 + p) \quad (2.3)$$

where $\alpha, \varphi, \beta_e, \beta_0$ & p represent angle of attack, the inflow angle, the elastic twist, pre-twist and pitch angle respectively.

The simulation of the aerodynamic performance of wind turbine conventional blades involves only the aerodynamic characteristics of the blades while the simulation of the aerodynamic performance of wind turbine utilizing adaptive blades involves aerodynamic characteristics and structural characteristics [135]. This type of simulation is an aero-structure process. The induced twist of the bending/twist adaptive blades (BTABs) is a structural response of the aerodynamic characteristics of the blade which makes the simulation a coupled-aero-structure (CAS) process [136].

When incident wind causes the bend–twist coupled blade to bend in flap-wise direction, the induced twist changes the angle of attack of the blade aerofoils, subsequently, causing the aerodynamic loads to vary. Thus, the analysis of a bending/twist coupled blade must take into account the interaction between aerodynamic and structure responses [165].

2.5.4 Induced Twist Elastic Determination

When a blade is constructed with an unbalanced composite laminates configuration and the blade is subjected to aerodynamic loads, it will experience a torsional deformation known as induced elastic twist. The unbalanced laminates configuration and the anisotropic properties of the material determine the level of elastic coupling. The produced induced twist which is a function of the elastic coupling changes the effective angle of attack of the airflow. The angle of attack of the blade has significant impact on the magnitude and direction of the aerodynamic force and consequently the performance of the blade [143]. The relations of the different angles are shown in Figure (2.3)

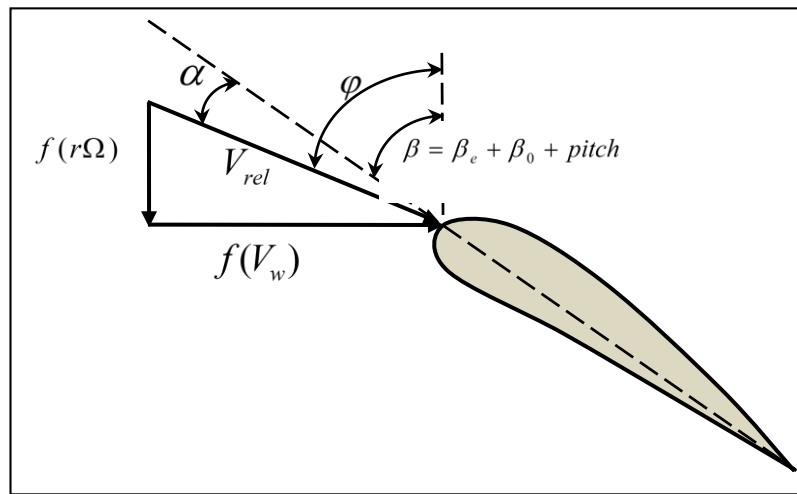


Figure 2.3. Flow Kinematic at a typical span location r [144]

The induced elastic twist in a bending/twist adaptive blade depends on some set of parameters: The aerodynamic characteristics, wind turbine run conditions, material & structural properties of the blade and material & structural configuration of the blade [135].

The induced elastic twists at different radial locations for the blade analysis carried out were simply calculated using the equation below

$$\beta_e = \tan^{-1}\left(\frac{\Delta Y_{t_e} - \Delta Y_{l_e}}{c}\right) \quad (2.4)$$

ΔY_{l_e} = leading edge displacement, ΔY_{t_e} = trailing edge displacement, c = location chord length.

The results will be used to develop a generalised equation for blades with varying material properties along the span.

In order to determine the material properties, the classical lamination theory was used which is discussed in Section (2.5.5).

2.5.5 Classical Laminate Theory

The classical lamination theory allows analytical stress-strain analysis of arbitrary laminated structures subjected to mechanical or thermal load. The classical lamination theory can be used for the stress-strain analysis taking into account arbitrary number of layers, layer thicknesses and material type. It is used to develop relationships for plates under in-plane loads. The classical lamination theory is a direct extension of classical plate theory and it is only valid for thin laminates. It enables the calculation of stresses and strains within layers, the apparent laminate properties and also the total deformation of the laminate (twisting, bending) [167, 168].

The classical lamination theory assumptions are [167, 168]:

1. The laminate comprises of perfectly bonded layers, i.e. there is no slip between the lamina interfaces
2. Each laminate is orthotropic or transversely isotropic
3. Each laminate is homogeneous such that its effective properties are known
4. The individual lamina is in a state of plane stress
5. The individual lamina is elastic
6. The line straight and normal to the mid-plane remain straight and normal to the mid-plane during deformation.
7. The displacements are continuous and small all the way through the laminate

The four bases of the classical lamination theory are the kinematic equations, constitutive equations, equilibrium equations and force resultant equations, with our focus on the

constitutive equations herein which describes the relationship between the stresses and strains within each lamina.

Transversely isotropic composite was considered for the bases of our analyses in order to determine the extensional (A), coupling (B) and bending (D) stiffness matrices. Several equations are related below from which the extensional, coupling and bending stiffness can be readily calculated for any fibre/matrix combination and angle-ply orientation. Figure (2.4) shows an off-axis laminate. This shows the relationship between the fibre-related axes in a lamina (123 coordinate) and that of the arbitrary coordinate (xyz).

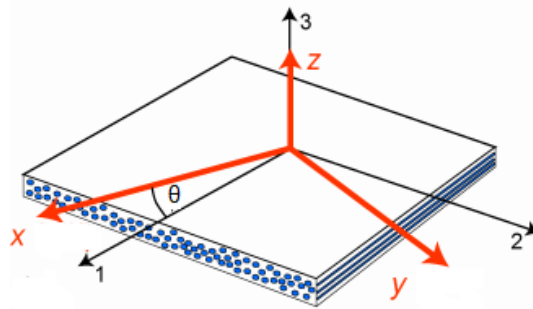


Figure 2.4. Showing the off-axis laminate [169]

The 123 Coordinate is the principal material coordinates since they are associated with reinforcement directions while the xyz is the off-axis coordinate system.

Systematically, the relations to determine the elastic engineering properties of an arbitrary laminate are derived and shown in Appendix B which will be used for defining the material properties for the blade analysis.

The modelling and analysis of the adaptive blade is done utilising an in-house tool by Dr Alireza Maheri with his permission. This high performance blade modelling tool (HPBMA) is discussed in section 2.5.6.

2.5.6 High Performance Blade Modelling (HPBM)

Blade modelling using commercial CAD/FEA software package has proven to be time consuming. In order to effectively and efficiently model and carry out finite element analyse of an adaptive wind turbine blade, an in-house tool, HPBM tool using MATLAB codes was used. The HPBM tool has been developed for deformation analysis of

aeroelastic tailored blades and wings made of composite materials. It involves the defining of the structural/material properties and the blade configuration (the composite material properties, blade topology and layup configuration) saved in MATLAB mat-file format. The sole aim of the HPBM is to have a robust tool that can be used to model wind turbine blade easily and with great time efficiency. Figure (2.5) shows the flowchart of the HPBM and Figure (2.6) shows the flowchart of using commercial CAD/FEA software.

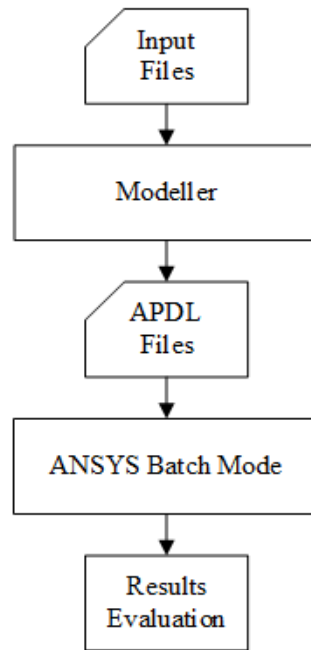


Figure 2.5. High performance finite element modelling and analysis of wind turbine blade

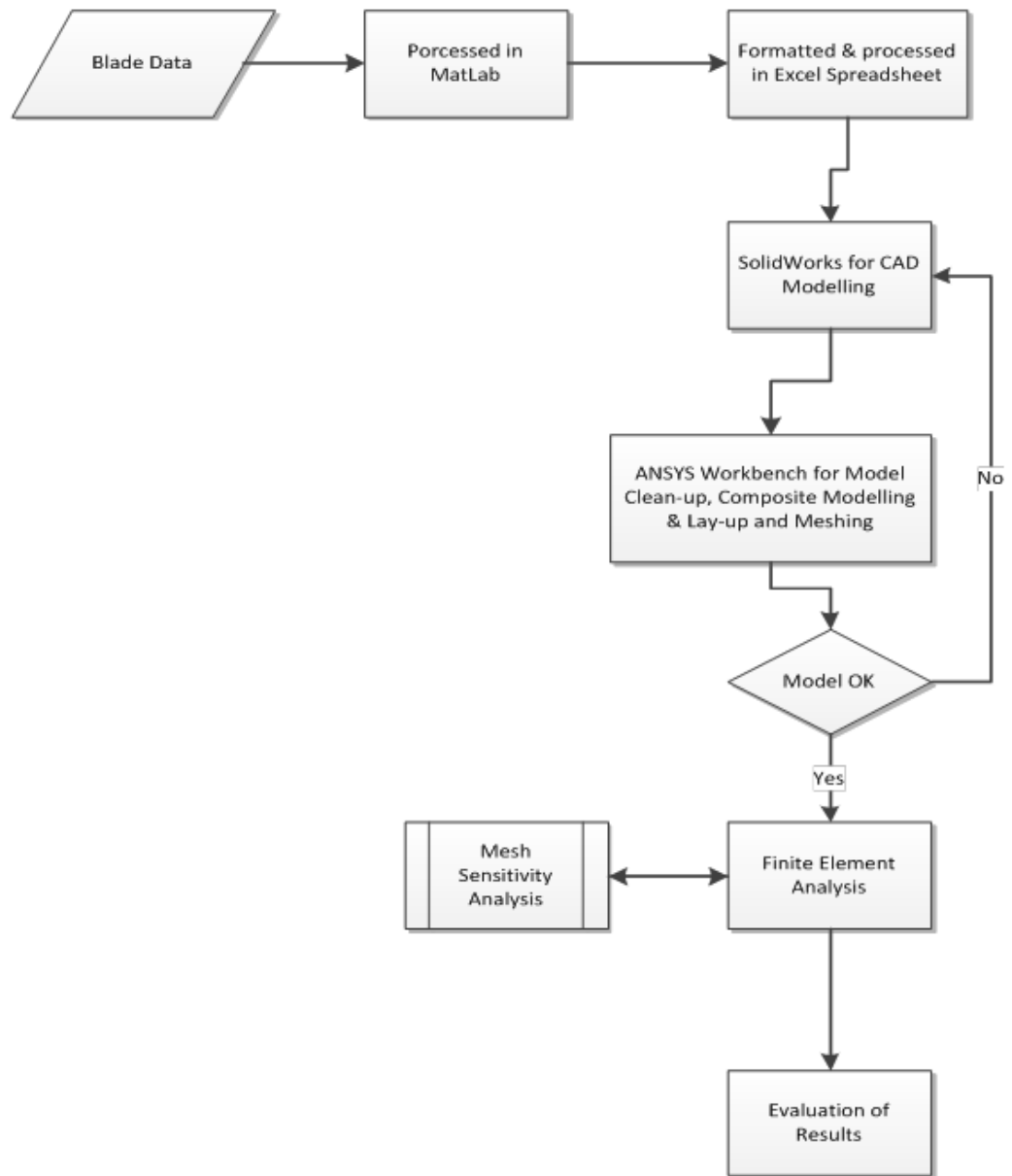


Figure 2.6. Flowchart of the blade modelling and analysis using commercial CAD/FEA software

The validation of the HPBM is done in section 4.3.

2.6 Summary

In endeavour to increase the energy capture, larger blades and smart blades are being exploited. As the blades increase in size, they become more flexible and susceptible to damage and pose some challenges. One of the ways of overcoming these challenges include the use of smart blades. The smart blades that are of focus in this research work are flapping blades and adaptive blades. As discussed, the blade adaptiveness could be

either geometrical or structural adaptiveness. Structural adaptiveness of the blade could be achieved by composite material configuration due to the anisotropic effect of the composite which, results to elastic coupling.

The level of elastic coupling of the blade is dependent on the fibre angle of the laminate, stacking sequence, and the material properties of the blade. An equation for the calculation of the induced elastic twist was established and how it affects the effective angle of attack of the blade.

Furthermore, the relationships for the determination of the laminate extensional, coupling and bending stiffness for any laminate configuration using the Classical Lamination Method were established in this Chapter and also the material properties of the laminate.

3 Flapping Blades

3.1 Introduction

Heathcote and Gursul [171] performed water tunnel experiments on a pitching and heaving flexible aerofoil for low Reynolds numbers. From the results of the experiment, it was perceived that the effect of chord-wise flexibility is of benefit for purely heaving aerofoils at low Reynolds number. Schouveiler et al. [172] using experiment, investigated an aquatic propulsion system performance inspired from the swimming mode of thunniform to study the flapping parameters effects on the hydro-mechanical efficiency and thrust force. In the computational area of flexible aerofoils/fins, Miao and Ho [173] investigated the effect of chord-wise flexure amplitude on the flapping aerofoils unsteady aerodynamic characteristics with several combinations of reduced frequency and Reynolds number. They found out that with flexure amplitude of 0.3 of the flapping aerofoil chord length, there is an enhancement in the propulsive efficiency and also, that the flow conditions that produce the highest propulsive efficiency correspond to a Strouhal number St of 0.255.

Notwithstanding the prospective of flapping wings for either pure propulsion or as an integrated lift/propulsion system, it was not attractive until very recent times. A sudden resumption of attention in the investigation of flapping wing flight phenomena happened in the late 1990s with the announcement of a key initiative by the United States of America Defense Advanced Research Projects Agency (DARPA) to inspire micro-air-vehicles (MAVs) development. The objective of the DARPA MAVs program was to establish whether progressing technologies could be satisfactorily incorporated into a mission capable flight system for military reconnaissance and surveillance applications. The only condition was that the dimension of the micro-air-vehicle should not be more than 15 cm. With dimension not more than 15 cm in length or span for a flapping wing vehicle is a clear alternative because of the low efficiency of conventional propellers and fixed wings at low Reynolds number. Therefore, the DARPA initiative ignited an enormous number of researches in the field of flapping wing propulsion.

Ansari et al [174] carried out study of aerodynamic modelling of insect-like flapping flight for micro air vehicles and he reviewed four core classes of methods: unsteady, semi-empirical, quasi-steady and steady state methods. Unsteady aerodynamic approaches eliminate small-angle approximations and attempt the modelling of all aspects of flapping flight of insect without employing experimental corrections and promise to be the most accurate. Truong et al [175] investigated an insect-mimicking flapping-wing system to

observe the generation of pitching moment. The study involved the development of a flapping wing system that generates the desired pitching moment during the flapping wing motion. Andro et al [176] investigated the effects of frequency on the aerodynamic mechanisms of heaving aerofoils in forward flight configuration. They observed that the contribution of the leading edge vortex, which forms and detaches on a time scale fixed by a global hydrodynamic instability, could be described by means of a quasi-steady analysis at low enough frequencies.

Amiralaei et al [177] performed a parametric research of the flow effects and system parameters on the lift, pitching moment coefficients, and drag as well as the vortical patterns around the aerofoil. It was found out that the mean angle of attack, the phase angle, and the pitching amplitude of oscillations significantly affect the force and moment coefficients.

Bos et al [178] did 3-D flow numerical simulations around a modelled insect wing to examine the flapping flight performance and to make available good understanding of the vortex dynamics and corresponding force generation. Different parameters relevant for a 3-D aerodynamics of flapping wing were investigated, notably the stroke kinematic pattern, the angle of attack in mid-stroke, the Reynolds number and the Rossby number. The leading-edge vortex is established to be significant for the lift gain.

Du et al [179] and Wang et al [180] investigated corrugation and deformation aerodynamic effects in hovering hoverflies flapping wings and observed flapping wings undergo time-varying deformation. It was also observed that corrugation gives a flapping wing the advantages of high stiffness, low mass and low membrane stress. This is as a result of the arrangement of the veins and in general, the flapping wing would predominantly have camber deformation and span-wise twist deformation. Ren et al, Mantia et al and Sun et al [181-183] studied the dragonfly wing structure effects on the dynamic performances. The experimental and numerical simulation results indicate that the netted veins with different tubular diameter and membrane with different thickness is essential structural feature. The wings corrugation along the chord-wise cross-section can considerably enhance the total wing stiffness to give enough flapping frequency, and the torsional deformation amplitude also significantly increase.

Pourtakdoust et al [184] developed a new aeroelastic model of a typical flexible Flapping Micro Air Vehicle (FMAV) to evaluate the propulsion system capabilities by utilising

quasi-steady aerodynamic model and the Euler-Bernoulli torsion beam. Stanford et al [185] studied the micro air vehicle nonlinear dynamics with flexible flapping wings to measure the role of wing planform, kinematic actuation and wing structure variables in obtaining MAVs with superior open loop characteristics and/or low-power requirements. Ghommem et al [186] carried out analysis on the shape optimisation of flapping wings in forward flight by combining a gradient-based optimiser with the unsteady vortex lattice method (UVLM). The analysis identifies the set of optimised shapes that maximise the propulsion efficiency.

3.2 Flapping Wing Kinematics

The wing kinematics is the most distinctive features in insect flight [110]. The flapping wing kinematics is not definitely periodic but characteristically recurrent. For example, the vertical position at the beginning of the downstroke is not precisely the same position for following strokes. This contributes to the difficulty of estimating flapping-flight aerodynamics [187].

The flapping wing kinematics consists of both translational and rotational motion of the wing. The insect flapping wing kinematics can be divided into four parts: downstroke, supination, upstroke and pronation. The downstroke is the translation of the wing at an angle of attack that is comparatively constant from its most aft position to its most forward position. Supination occurs at the completion of the downstroke, which is when the wing rapidly decelerates to a stop and simultaneously undergoing rotation along its span-wise axis to reverse its direction and angle of attack. This results to the wing underside becoming the topside for the following half stroke. At the end of the rotation phase, the upstroke starts which is the translation of the wing at an angle of attack that is comparatively constant back to its most aft position. Finally, the wing pronates at the end of the upstroke by rapidly decelerating to a stop and simultaneously undergoing rotation along its span-wise axis to reverse its direction and angle of attack. Supination and pronation can be either delayed or advanced by insects relative to stroke reversal to control aerodynamic forces. During the downstroke and upstroke, the angle of attack is constant except at the near the beginning and near the end of the stroke. The angle of attack changes with time as the stroke reversal (the rotation phase) is approached [109, 188].

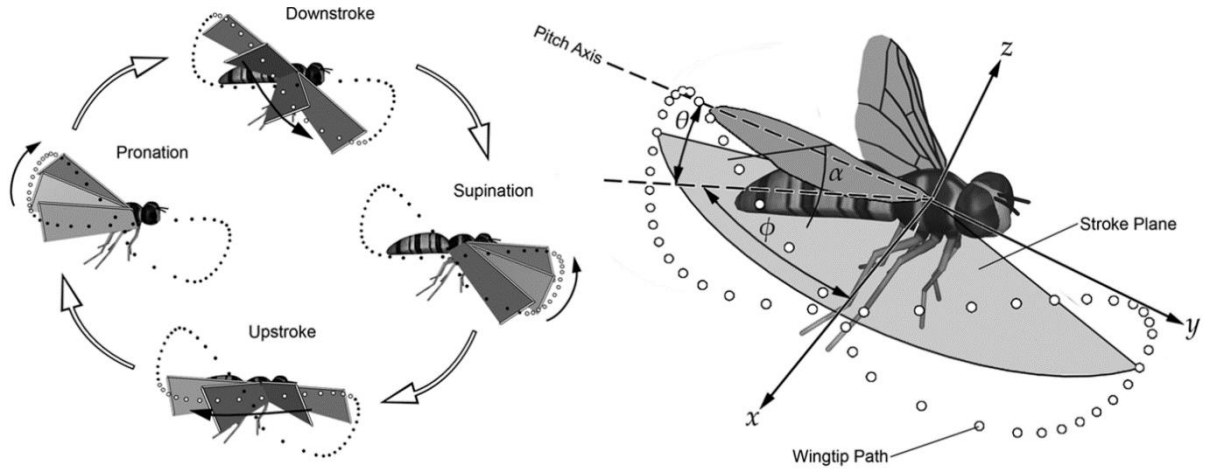


Figure 3.1. Flapping Cycle [109]

The flapping wing kinematics can be defined by three flapping angles and a general representation of the positional angle, the elevation (deviation) angle and the angle of attack (pitching) for a hovering fruitfly and hovering hawkmoth, all angles in radian, are expressed using the Fourier series as shown in Equations (3.1) to (3.3) below [106]

$$\phi(t) = \sum_{n=0}^3 [\phi_{cn} \cos(n\omega t) + \phi_{sn} \sin(n\omega t)] \quad (3.1)$$

$$\theta(t) = \sum_{n=0}^3 [\theta_{cn} \cos(n\omega t) + \theta_{sn} \sin(n\omega t)] \quad (3.2)$$

$$\alpha(t) = \sum_{n=0}^3 [\alpha_{cn} \cos(n\omega t) + \alpha_{sn} \sin(n\omega t)] \quad (3.3)$$

where, n is an integer varying from 0 to 3, ϕ is the positional angle, θ is the elevation angle, α is the angle of attack and the coefficients ϕ_{cn} , ϕ_{sn} , θ_{cn} , θ_{sn} , α_{cn} , α_{sn} can be determined from the empirical kinematic data [106, 189].

3.3 Computational Fluid Dynamics of Flapping Flat Plate

The flow around insects and birds' wings according to Wang [103] can be considered incompressible. The Mach number is usually about 1/300 with wingbeat frequency of about the range of 10-10³ Hz. The governing equations are then incompressible Navier-Stokes equations subject to no-slip boundary condition [103]:

$$\frac{\partial \mathbf{U}}{\partial t} + (\mathbf{U} \cdot \nabla) \mathbf{U} = -\frac{\partial p}{\rho} + \nu \nabla^2 \mathbf{U} \quad (3.4)$$

$$\nabla \cdot \mathbf{U} = 0 \quad (3.5)$$

where,

- \mathbf{U} = flow velocity
- p = pressure
- ρ = density of the fluid
- ν = kinematic viscosity

The ability of insects and birds to produce lift by flapping is beyond estimation from a steady state theory; it is a result of a complex aerodynamic setup. The modelling of a flapping wing is a complex kinematic mechanism, therefore a design of the fundamental dynamics involved can benefit from simplified simulations.

In order to have illustrative models, 2D and 3D models of a flapping flat plate were analysed using ANSYS FLUENT. The analyses were performed using an incompressible Navier-Stoke solver because the Mach number of the flow over insects and birds is about 1/300 with flapping frequency of about 10-10³ Hz [103].

3.3.1 2D Numerical Analysis

A 2-D model of a flat plate was done using ANSYS FLUENT and a C++ Language to write the user defined function (UDF) for the dynamic mesh to simulate the flapping of the flat plate. A flat plate of set dimension 1000 mm length and zero thickness was modelled in a fluid domain size of 2000 mm×520 mm resulting to about 226,000 mesh cells. A wind free stream velocity of 10 m/s was used for the simulation. A 2D transient turbulent k-epsilon model, Pressure-velocity Coupling and SIMPLEC Scheme was carried out using a time step of 0.001s [190].

For this simulation, a simple harmonic equation was used for the flapping motion and the equation is shown below:

$$y = A \sin(\omega t) \quad (3.6)$$

leading to the instantaneous flapping angle and flapping velocity

$$\phi = A_{flap} \sin(\omega t) \quad (3.7)$$

$$\dot{\phi} = A_{flap} \omega \cos(\omega t) \quad (3.8)$$

where, ϕ and $\dot{\phi}$ are instantaneous flapping angle and flapping velocity respectively, A_{flap} represents the amplitude of flapping motion and ω is the angular velocity of the wing along the flap axis.

3.3.2 Results and Discussion

The Navier-Stoke computations were carried out for comprehensive range of flapping frequency and amplitude. All the analyses were performed using free stream velocity of 10 m/s with varied flapping frequency and flapping amplitude to investigate the effect of flapping frequency and amplitude on the aerodynamic characteristics for a 2D model. Figure (3.2) below show the flat plate in the fluid domain.

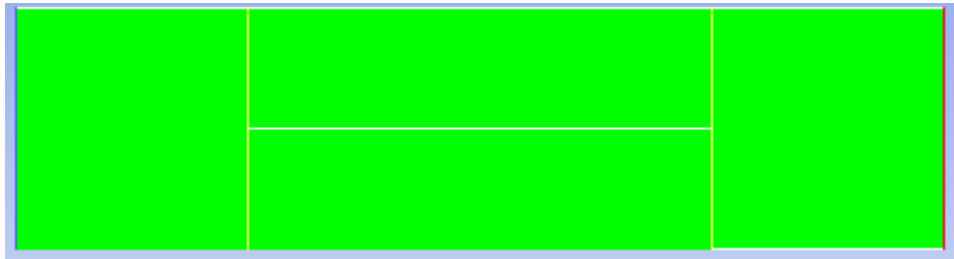


Figure 3.2. Flat plate with zero thickness in the fluid domain

3.3.3 Effect of Flapping Amplitude

This section objective is to investigate the effects of the flapping amplitude on the lift coefficient. A rectangular flat plate was analysed by varying the amplitude of flapping at different frequency 20 Hz, 40 Hz and 50 Hz, and the changes were observed. For a particular flapping frequency, flapping amplitude of 2.5 mm to 7.5 mm in increment of 2.5 mm were investigated. The effect of changing the flapping amplitude can be seen in Figure (3.3) to Figure (3.6) below which show the variation of the lift coefficient with respect to the changes in the flapping amplitude at the different flapping frequencies.

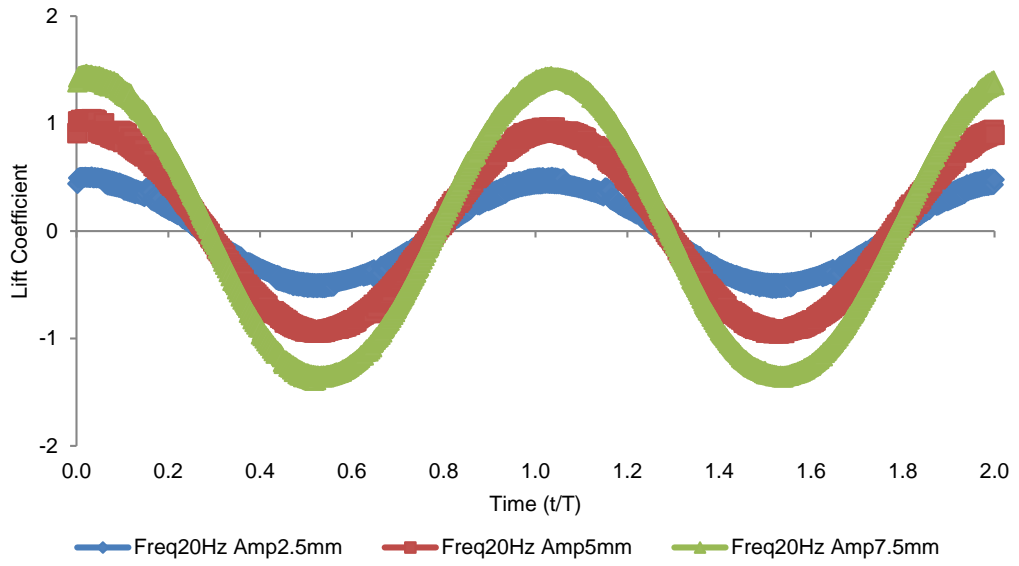


Figure 3.3. Instantaneous lift coefficient for 20 Hz flapping frequency and different flapping amplitudes

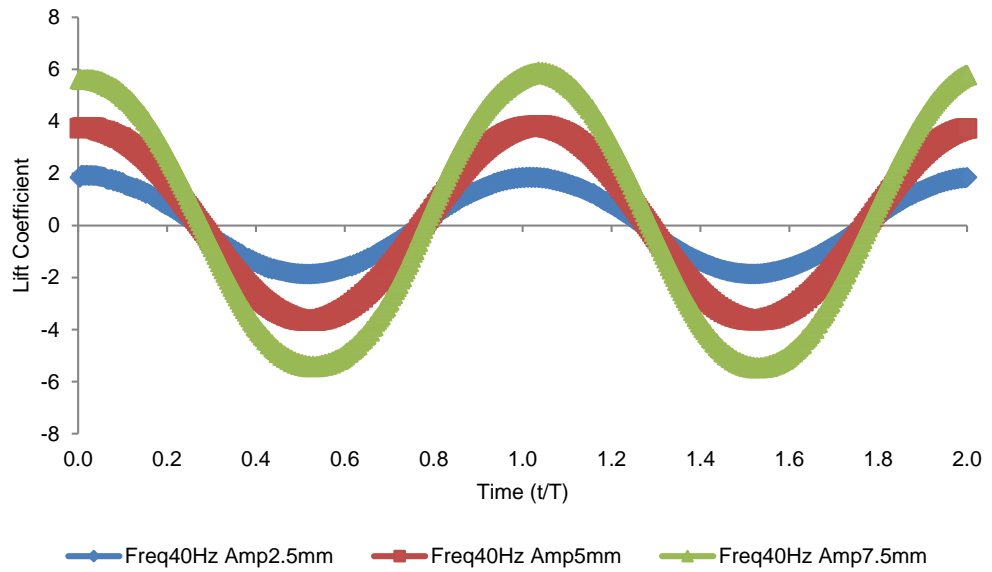


Figure 3.4. Instantaneous lift coefficient for 40 Hz flapping frequency and different flapping amplitudes

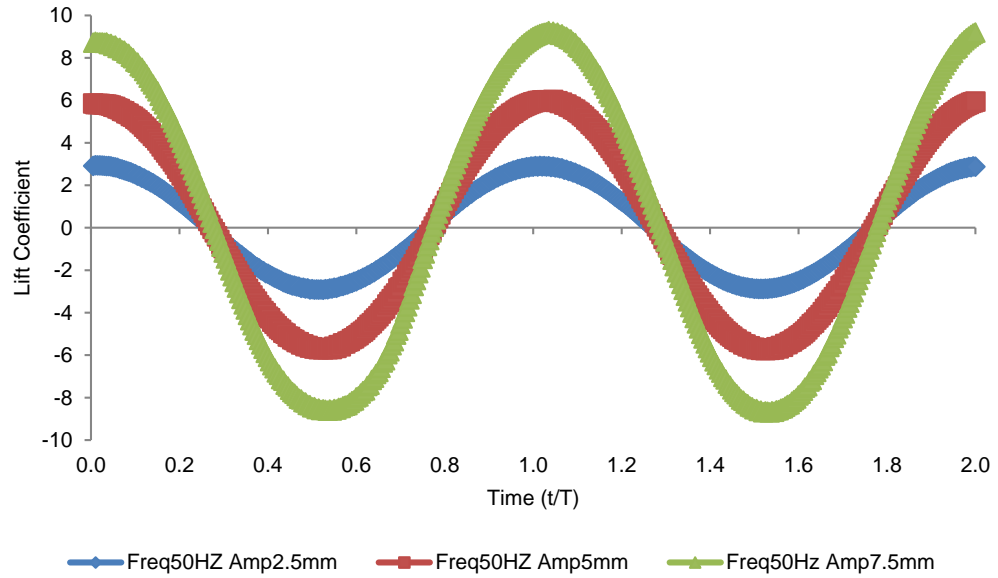


Figure 3.5. Instantaneous lift coefficient for 50 Hz flapping frequency and different flapping amplitudes

Figure (3.3) to Figure (3.5) show the curve of the instantaneous lift coefficient as the lift coefficient changes with varying the flapping amplitude. In order to properly capture the flat plate instantaneous lift coefficient, very small time step which was mentioned in Section 3.3.1 was used resulting to many points compressed in Figure (3.3) to Figure (3.5). Thus, the compressed points make the curves of Figure (3.3) to Figure (3.5) look thick. The curves indicate they have common feature of increasing lift coefficient as the flapping amplitude is increased.

Figure (3.6) shows a trend for the different curves indicating increase in the maximum lift coefficient as the flapping amplitude is increased.

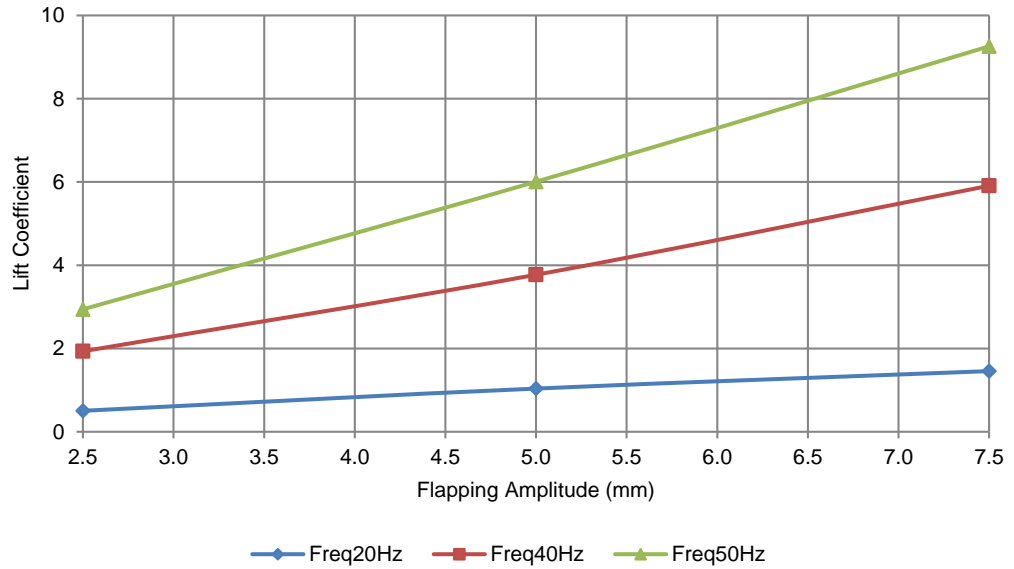


Figure 3.6. Effect of flapping amplitude on maximum lift coefficient for various flapping frequencies

3.3.4 Effect of Flapping Frequency

In order to gain insight into the effects of flapping frequency on the lift coefficient, analyses for three flapping amplitude 2.5 mm, 5 mm and 7.5 mm were performed by varying the flapping frequency and frequencies 20 Hz, 40 Hz and 50 Hz were used for the analyses. Figure (3.7) shows the instantaneous lift coefficients for flapping frequencies 20 Hz, 40 Hz and 50 Hz with flapping amplitude 7.5 mm. As shown in Figure (3.7), the curves Freq20HzAmp7.5mm, Freq40HzAmp7.5mm and Freq50HzAmp7.5mm have common features i.e. the lift coefficient increases with increase in flapping frequency.

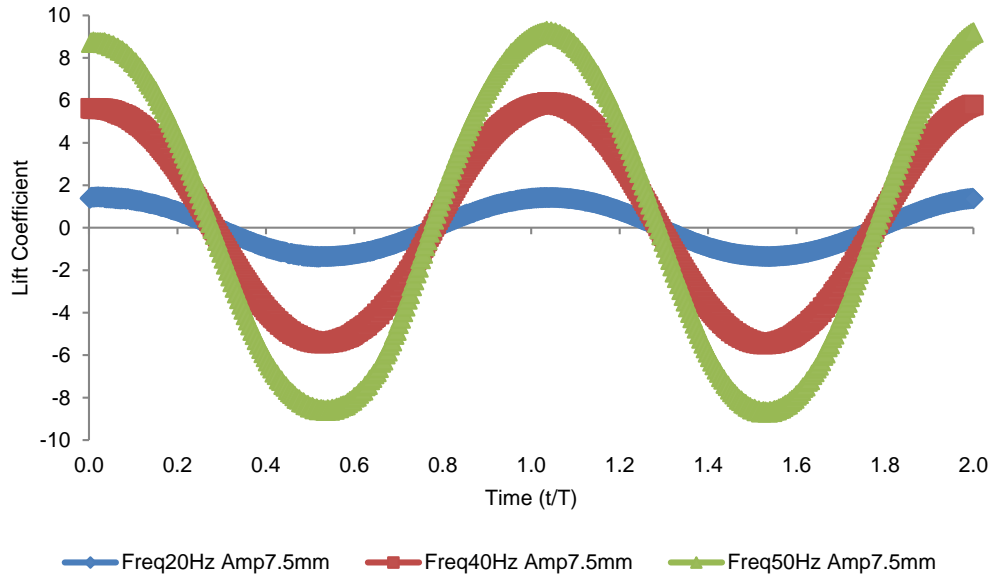


Figure 3.7. Instantaneous lift coefficient for 7.5 mm flapping amplitude and different flapping frequency

As it could be seen in Figure (3.8), the trend for varying the flapping frequency shows that the maximum lift coefficient increases with increase in the flapping frequency.

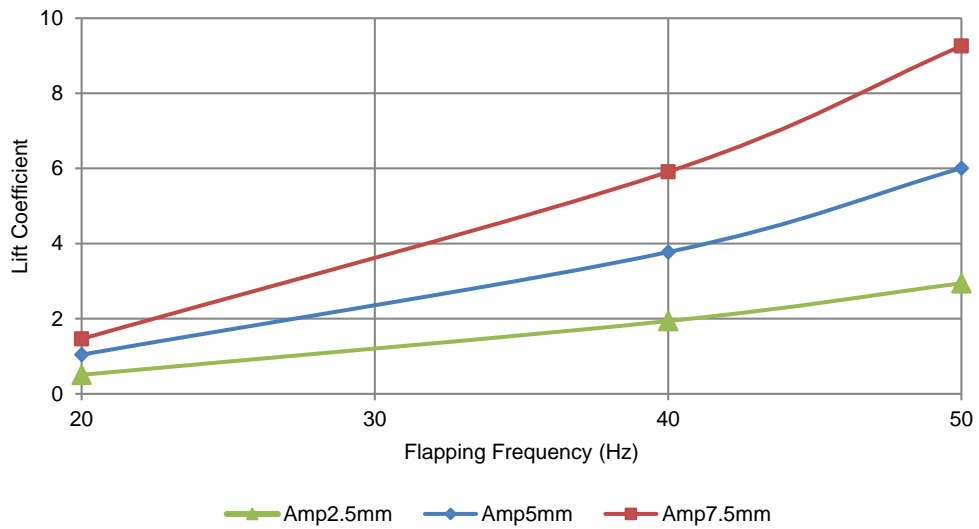


Figure 3.8. Effect of flapping frequency on maximum lift coefficient for various flapping amplitude

3.3.5 3D Numerical Analysis

In order to have a simplified model to investigate the effect of flapping frequency, amplitude and pitching angle on the aerodynamic characteristics, a flat plate was modelled and analysed using ANSYS FLUENT. A flat plate of finite dimension 1000 mm×100 mm×1 mm was modelled in a fluid domain size of 1500 mm×1000 mm×800 mm. The distance from the inlet is 350 mm to the centre of the flat plate while 650 mm from the centre of the plate to the outlet. It was meshed to have fine mesh around the flat plate and coarser mesh in the outer part of the domain resulting to about 574,119 cells. The choice of the dimension of the flat plate was to simulate a flapping blade for a small wind turbine. The simulation was done using a wind free stream velocity of 10 m/s resulting to Reynolds number (Re_x) of 6.85×10^4 at the end of the plate and boundary layer thickness (δ) of 26 mm using the turbulent boundary layers equation over a flat plate $\delta \approx 0.38x/Re_x^{1/5}$ [191]. A 3D transient turbulent model, Pressure-velocity Coupling and SIMPLEC Scheme was performed using a time step of 0.001s.

For the CFD meshing, in order to simulate the flapping motion using ANSYS FLUENT, UDF was written for the dynamic mesh in C++. The UDF was defined to simulate flapping and pitching. For the 3D motion of the flat plate, coordinate transformation from global to local similar to Euler transformation was done. The displacement motion of the rectangular flat plate is the same as that used for the 2D analysis.

3.3.6 Results and Discussion

Figure (3.9) shows the flat plate in the fluid domain and Figure (3.10) shows the contour plots for velocity and vorticity magnitudes for the case of flapping frequency and amplitude of 40 Hz and 10 degrees respectively. The pitching amplitude is 5 degrees the free stream velocity is 10 m/s.

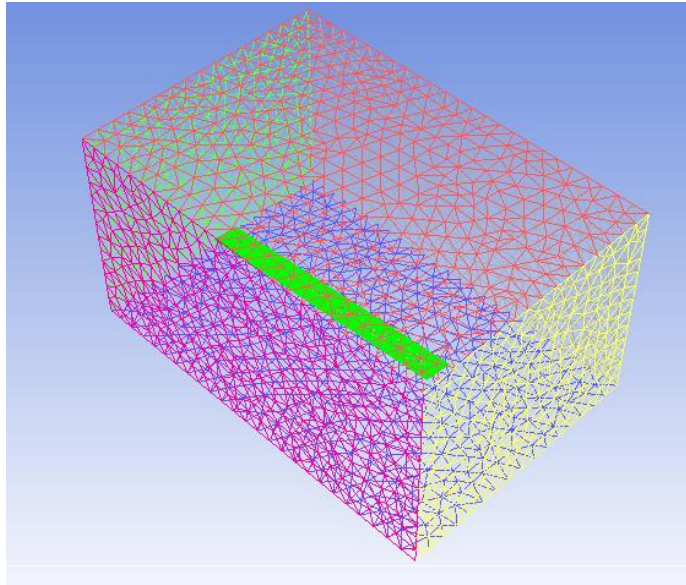


Figure 3.9. Flat plate in the fluid domain

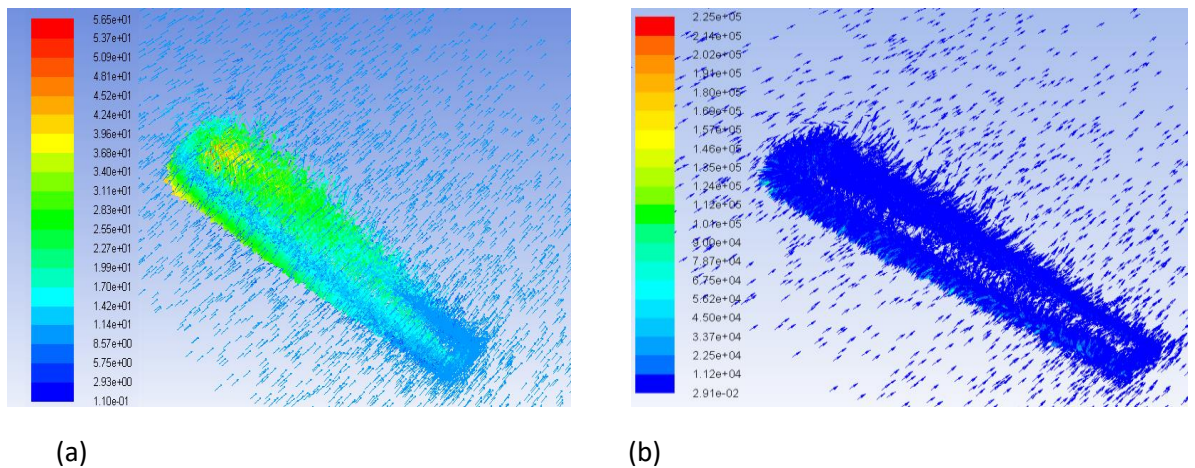


Figure 3.10. Contours (a) velocity magnitude and (b) vorticity magnitude

3.3.7 Effect of Flapping Amplitude

In this research work, flow past a flapping and pitching flat plate was simulated by setting a uniform inlet velocity of 10 m/s and a pitching angle of 5 degrees. The simulations were carried out for a constant flapping frequency and varying flapping amplitude. Analyses were carried out for frequency 20 Hz, 40 Hz and 60 Hz by varying the flapping amplitude from 5 degrees to 15 degrees in increment of 5 degrees. The analyses were performed using the

same flapping and pitching frequency. It was observed from the result (Figure (3.11)) that as the flapping amplitude increases, the vorticity magnitude around the leading and trailing edge increases and the lift coefficient significantly increases.

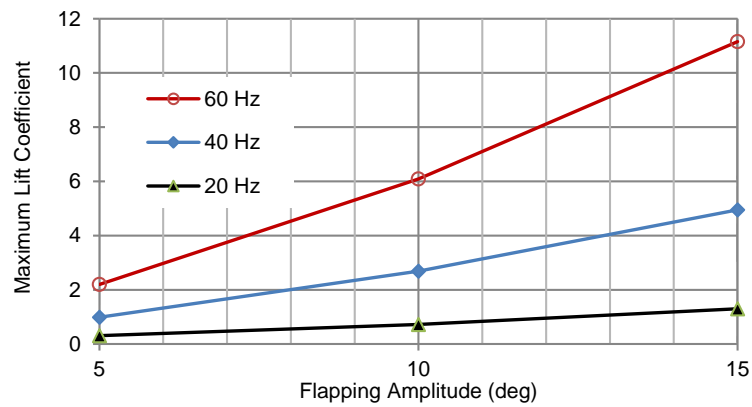


Figure 3.11. Effect of flapping amplitude on maximum lift coefficient for various flapping frequencies (pitch amplitude 5 degrees)

The trend of the result observed from Figure (3.12) suggests that the flapping amplitude positively influences the lift coefficient. The fluid dynamic pressure during the upstroke is lower at the lower surface due to the flapping motion and higher during the downstroke. Therefore, generating higher lift coefficient during downstroke and lower during the upstroke. The initial upstroke high negative lift is due to non-convergence of the initial result (between time 0.001-0.002 sec).

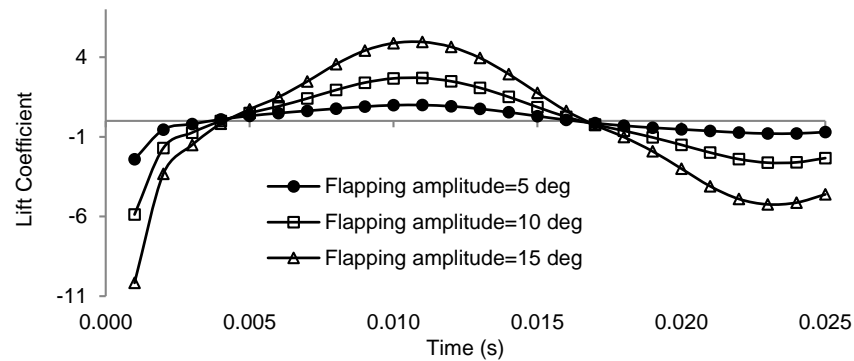


Figure 3.12. Instantaneous lift coefficient for 40 Hz flapping frequency and different flapping amplitudes (pitch amplitude 5 degrees)

3.3.8 Effect of Flapping Frequency

With other parameters kept constant, analyses were performed for flapping amplitude 5 to 15 degrees by changing the flapping frequency from 20 Hz to 60 Hz in increment of 20 Hz. The effect of the variation of flapping frequency on the lift coefficient is shown in Figure

(3.13). It can be observed that as the flapping frequency increases, the lift coefficient increases. This is due to increase in total air velocity and its influence on the aerodynamic forces and vorticity magnitude around the rectangular flat plate edges.

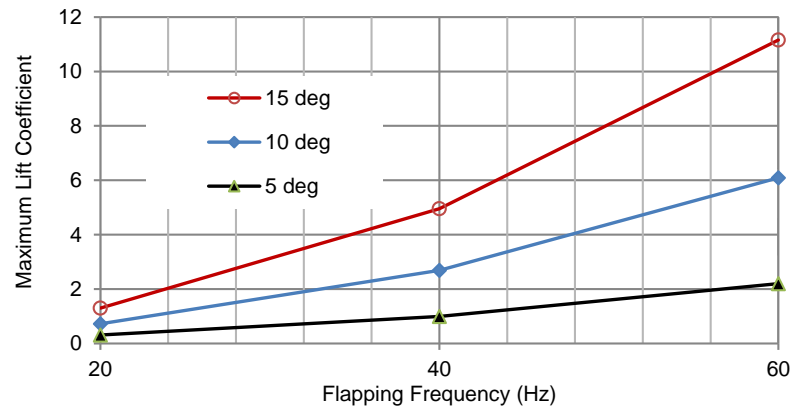


Figure 3.13. Effect of flapping frequency on maximum lift coefficient for various flapping amplitudes (pitch amplitude 5 degrees)

These results also displayed that at flapping frequency 20 Hz and flapping amplitude 15 degrees, the lift coefficient was higher than that of 40 Hz and 5 degrees flapping amplitude at the same pitching amplitude. This indicates that the lift coefficient also depends on how the flapping frequency and flapping amplitude are combined. The 3D surface plot shown in Figure (3.14) shows the effect of flapping frequency and amplitude on the flow characteristics. At flapping frequency 40 Hz and flapping amplitude 10 degrees, the lift coefficient is higher than that of flapping frequency 60 Hz and flapping amplitude 5 degrees of the flat plate at the same pitching amplitude.

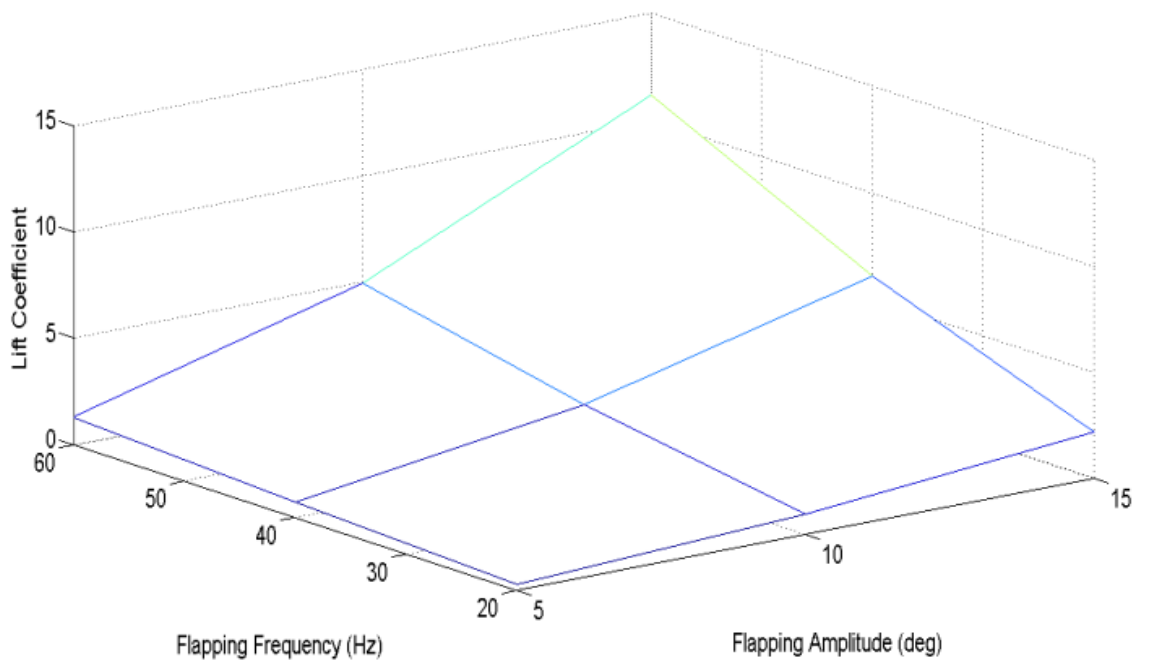


Figure 3.14. Maximum lift coefficient as a function of flapping frequency and flapping amplitude (pitch amplitude 5 degrees)

3.3.9 Effect of Pitching Amplitude

Figure (3.15) shows the effect of pitch amplitude on the maximum lift coefficient. This figure is based on a flapping frequency of 40 Hz, flapping amplitude of 10 degrees and flow speed of 10 m/s. The results show that small pitch of up to about 10 degrees leads to some enhancement on the maximum lift coefficient but as the pitching amplitude increase the maximum lift coefficient decreases, due to flow separation.

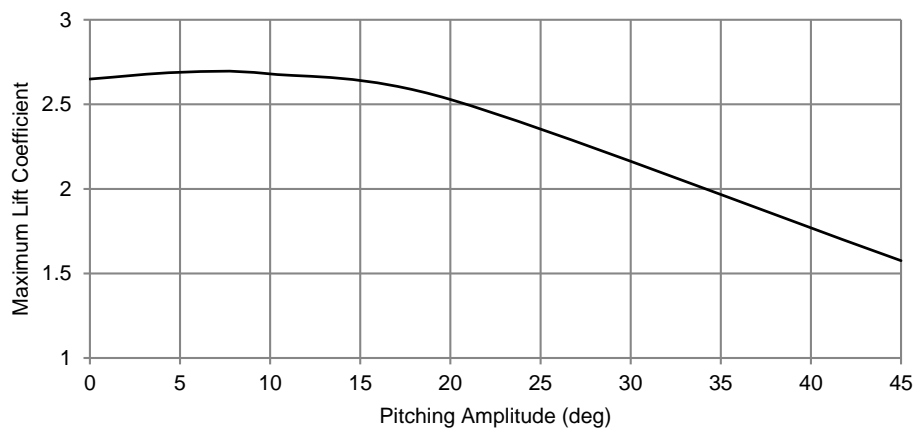


Figure 3.15. Effect of pitch amplitude on maximum lift coefficient

3.4 Conclusion

The flat plate undergoing a flapping and pitching motion was simulated by varying the flapping frequency and amplitude. 2D and 3D analyses were performed. The variation in the flapping frequency and amplitude were shown to have significant influence on the lift coefficient. It can be deduced from the results that the lift coefficient is influenced by the flapping frequency and flapping amplitude combination. For the size and geometry presented in this report, the lift coefficient is most influenced by the flapping amplitude when compared to the flapping frequency. The results indicate that the pitching amplitude initially enhances the lift coefficient. However, excessive pitching amplitude results in low lift coefficient.

The flapping blade is in the conceptual investigative phase and the analysis for could not be completed due to the non-availability of capable workstation for the analysis. Thus, because of the analyses were not completed, reasonable size and topology could not be defined to produce a flapping blade.

4 Adaptive Blades: Extended Decoupled Design

4.1 Introduction

Adaptive blades produce controlled torsional deformation in response to changes in the wind turbine run conditions. This method the blade itself serves as the controller, it detects the wind velocity and response by adjusting its aerodynamic characteristics to influence the wind turbine performance [144]. The variation of the induced twist along the span of the blade due to the bending/twist elastic coupling in the wind turbine adaptive blade, significantly affects its aerodynamic performance [136].

Blade aerodynamic performance at a span location r is a function of the blade angle of attack at that location. The angle of attack is a function of pre-twist, the inflow angle, the pitch angle and the elastic twist and as expressed by Equation (2.3) and shown in Figure (2.3) in Chapter 2.

The inflow angle φ is determined by the wind turbine run conditions. The blade pre-twist β_0 is fixed. The pitch angle p can be actively controlled or fixed which depends on the usage or non-usage of a pitch control system. In adaptive blades, the elastic twist β_e is intended to be treated as a controlling variable which passively influences the angle of attack in response to the changes in the aerodynamic forces.

The elastic twist in conventional wind turbine blades is solely as a result of pitching moment and has no significant influence on the aerodynamic performance of the blade. For the blade elastic twist to be treated as a controlling variable, its effect needs to be enhanced through making it a stronger function of the aerodynamic forces, which has considerably higher values compared to aerodynamic pitching moment [144]. This can be achieved by two methods, namely geometric type and elastically coupled type of adaptive blade. Geometric type adaptive blades have a curved outboard towards the trailing edge. In theory, this increases the pitching arm of the blade outer parts, thus higher pitching moment is produced in the inboard sections. Therefore, allowing the blade to respond to the fluctuations in aerodynamic loads

Knight and Carver [14] developed a sweep-twist adaptive rotor blade (STAR) for Sandia National Laboratories that reduced operating loads, in order to achieve a larger rotor blade that is more productive. The blade design adopted outer blade sweep to create twist

coupling without the use of angled fibre. They successfully designed the blade and prototype was produced, tested and evaluated through laboratory and field tests.

Karaolis et al [162] and later Kooijman (1996) [163, 164] proposed the move from the use of conventional control methods to the utilisation of aeroelastic tailoring of fibre reinforced composite blades. Composite laminates can be intended to exhibit unique structural responses by virtue of the layup configuration which cannot be achieved using isotropic materials. Elastic couplings are produced by specific layup configurations. A simple illustration is shown in Figure (4.1) showing how unbalanced layups in a blade shell produces different elastic couplings. A bending/twist elastic coupling is produced by mirror layup configuration, while a helical layup produces a stretching/twist coupled structure. By implanting bending/twist elastic coupling in a wind turbine blade, the induced twist becomes a function of the blade bending moment due to aerodynamic lift and drag forces. In case of stretching/twist coupled blades, the axial force due to weight and centrifugal forces produces the induced twist. Stretching/twist elastic coupling is more suitable for helicopter blades and small wind turbines with higher rotor speeds in which the centrifugal forces are dominated. Bending/twist is suitable for large wind turbines which run at low rotor speeds. The term adaptive blade in this chapter refers to the bending/twist coupled adaptive blades.

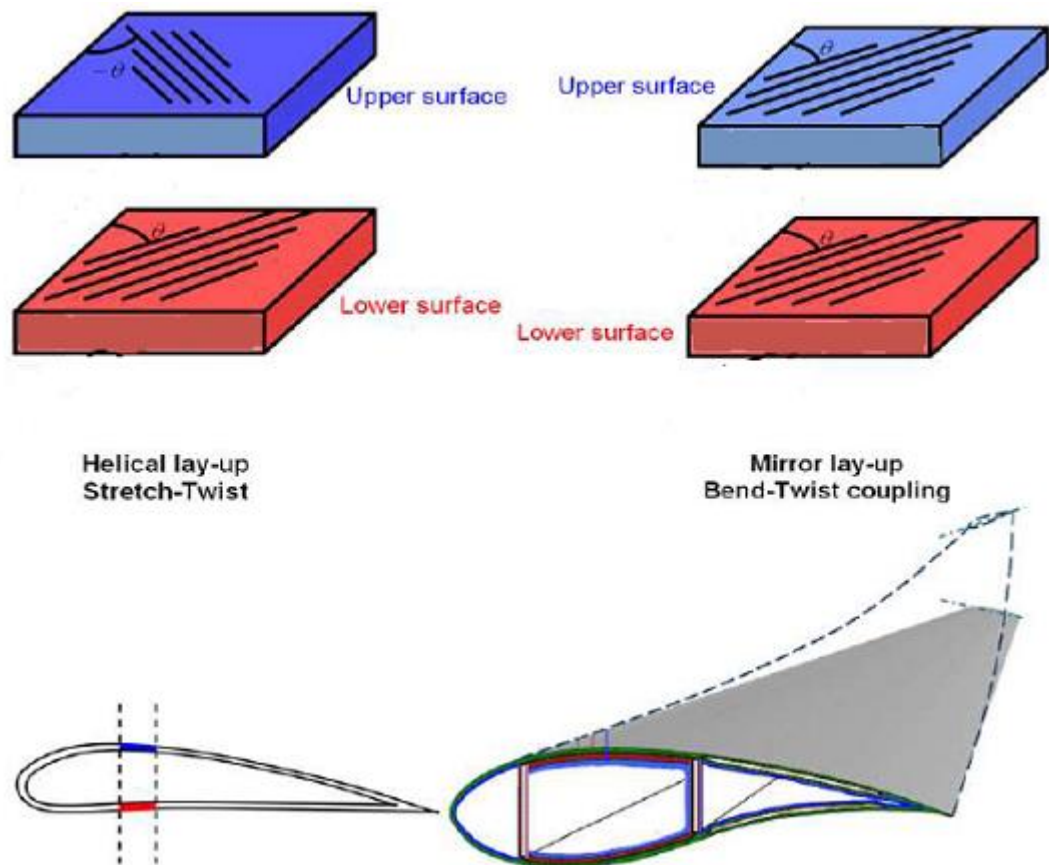


Figure 4.1. Two types of elastic couplings: stretching/twist and bending/twist [144]

4.1.1 Implementing Elastic Coupling in Adaptive Blades

In spite of the fact that aeroelastic tailoring of the blade has potential benefits, the level of elastic coupling that could be realised with asymmetric fibre layups is limited [144]. The fibre and matrix properties determine the maximum coupling achieved and best direction. It was figured out by Karaolis et al. [162] that the best combination for optimum blade twisting could be realised with the off-axis orientation of the fibres at about 20-degrees to the blade longitudinal axis, which was also recommended by Kooijman [163] for reinforcement. The type of elastic coupling to be achieved determines the type of layup configuration and manufacturing process. Fibre winding is well appropriate for the manufacturing of stretching/twist coupling in a spar while manufacturing of bending/twist coupling, clam-shell construction with the bottom and top skins produced separately is best suited [144].

4.1.2 Adaptive Blades Integrated Design

Maheri [149] showed that wind turbines simulation when a bending/twist adaptive blade is used is an iterative coupled-aero-structure (CAS) process. For this reason, the conventional blades design methods are not appropriate for designing of bending/twist adaptive blades [149] with figure of bending/twist adaptive blade shown in Figure 4.1.

When performing the aerodynamic performance simulation of wind turbine with conventional blades, it is only the blades aerodynamic characteristics that are involved. Thus, the aerodynamic design of conventional blades can be carried out without direct participation of the structure configurations and the material properties of the blade. The structural and aerodynamic design phases of conventional wind turbine blades take place in a sequence. In the case of adaptive blades, for the aerodynamic performance simulation of the wind turbine, the blade structural characteristics must be also known. Thus, the structural and aerodynamic design phases are integrated in nature (See Figures (4.2) and (4.3)).

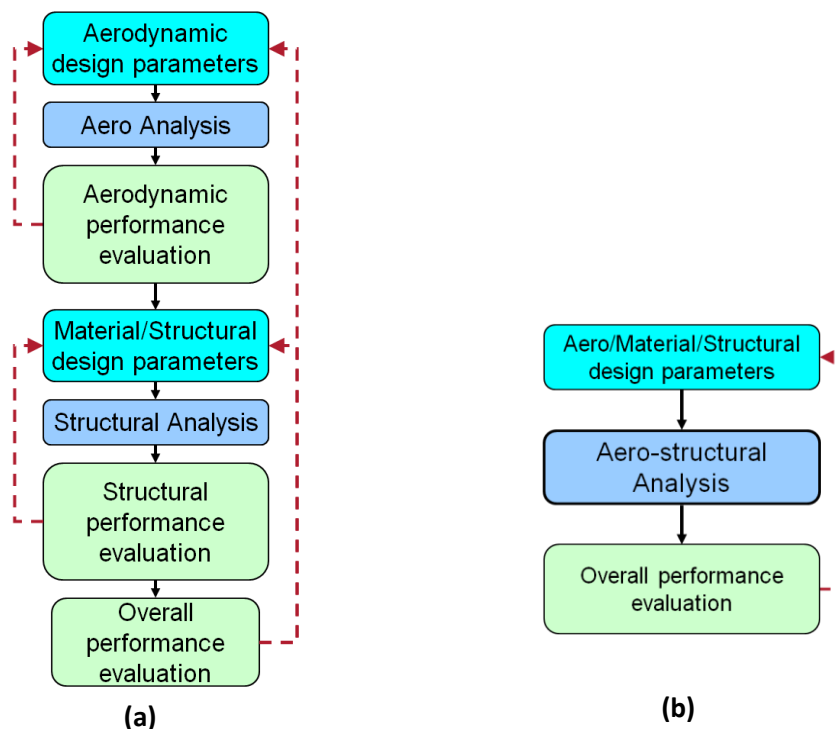


Figure 4.2.(a) Sequential versus (b) Integrated design [144]

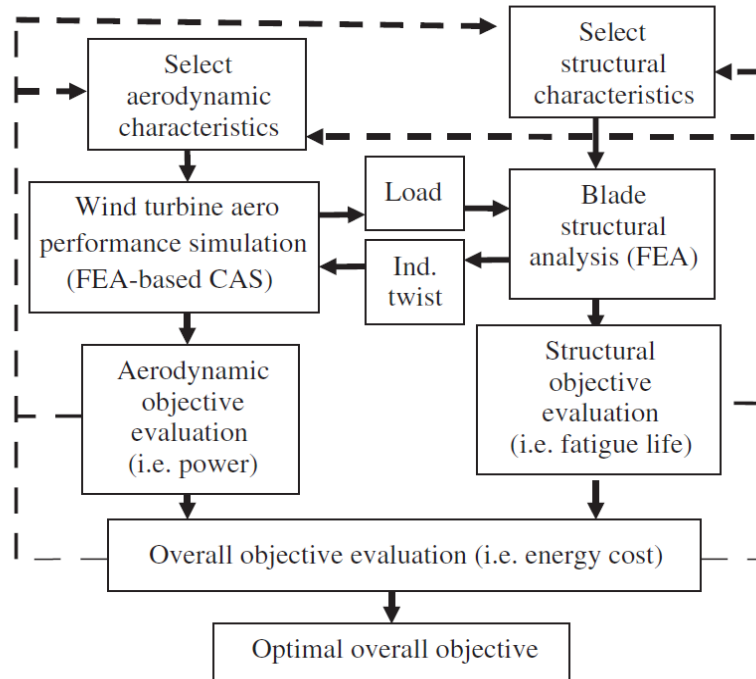


Figure 4.3. Adaptive blade integrated design process [135]

According to Lobitz and Veers [155], an induced twist as small as 1 degree at the tip of the blade can have considerable effect on the aerodynamic performance of the wind turbine. Thus, evaluating of the elastic induced twist accurately becomes the key concern in the design and analysis of wind turbine adaptive blades. Maheri et al. [146, 148 & 192] developed an auxiliary software tool for aero-structure analysis of adaptive blades. With the purpose of reducing the computational time, while maximising the structural analysis accuracy, a wind turbine simulator with a built-in FEA-based structural analyser and an adaptive mesh generator was developed. In a further step towards minimising the computational time, a hybrid analytical/FEA method was developed for the simulation and design of adaptive blades [33 & 145]. This method brings in the flap bending moment at the hub of the blade and the induced twist distribution predicted through a FE-based structural analysis at a reference run condition of the wind turbine adaptive blade to define the turbine performance at other run conditions. Thus, the FE-based structural analysis will be performed only once, thereby making the method to significantly reduce the computational time and resulting to more efficient aerodynamic simulation of bending/twist adaptive blades [145].

In 2012, Maheri [193], did a further work on integrated design of adaptive blades using FE-based methods can be seen in Maheri (2012) [194] and Nicholls-Lee et al [143]

developed a fluid-structure coupled tool for passively adaptive blade design. The structural analysis was performed by FEA and was coupled with fluid dynamic model for fluid-structure interaction analysis. The results compared well to the earlier work done by Nicholls-Lee and Turnock [195] and indicated that an increase in the turbine coefficient of power could be realised by means of appropriately designing of the bending/twist coupled blades.

4.1.3 Adaptive Blades Decoupled Design

According to Maheri et al [135], the degree and distribution of the induced twist in a bending/twist adaptive blade depends on the following parameters:

- Wind Turbine run-condition (wind speed, rotor speed and blade pitch angle)
- Aerodynamic characteristics (aerofoil, pre-twist and chord distributions, etc.)
- Material and structural properties of the blade (mechanical properties of the material, shell thickness, fibre angle, etc.)
- Material and structural configurations of the blade (span-wise variations of mechanical properties of the blade material, shell thickness, fibre angle, etc.)

These set of parameters makes the aerodynamic performance evaluation of wind turbine to be an iterative coupled-aero-structure (CAS) process and as a result making the design of adaptive blades integrated in nature.

Maheri et al. [135] are of the opinion that the integrated design of adaptive blades using FEA-based structural analyser is not efficient. They point out that carrying out a coupled aero-structure design process for adaptive blades has two key drawbacks. Firstly, wind turbines with bending/twist adaptive blades simulation is a CAS process, and in order to realise reliable results for the blade induced twist, the structural analyser must be based on FEA. Using a FE-based code as a part of a design objective evaluator, makes the evaluation of aerodynamic objective very time consuming [135]. The second drawback is that, in the evaluation of the aerodynamic objective, many structural and material parameters are also involved in addition to the aerodynamic parameters. Therefore, the number of parameters making the design space increases and as a result, the number of required evaluations will exponentially increase [135].

Maheri et al [135 & 147] proposed a design method by making the aerodynamic design phase to be decoupled from structural design phase in order to make the adaptive blade design more efficient and flexible. This was done by using the concept of “variable state design parameters” (VSDP) which is illustrated schematically in Figure (4.4). The induced twist is considered as an aerodynamic design variable in the decoupled design approach while its reliance on the blade structural characteristics is considered by imposing an adequate constraint on the structure design [147]. The aerodynamic design is separated from the structural design by treating the induced twist as a variable state design parameter. The chief advantage of this method is the substantial reduction in the aerodynamic evaluation time by avoiding carrying out a structural analysis for each aerodynamic performance evaluation that is time consuming. This is achieved by replacing a FEA-based CAS simulation in the aerodynamic objective evaluation by a non-FEA-based CAS simulation [147]. However, by use of the decoupled design method, in the structure design part, the structural and material configurations selection for producing the planned induced twist must be met in the aerodynamic design process. Therefore, the planned induced twist as a design parameter must be realistic and realisable [135].

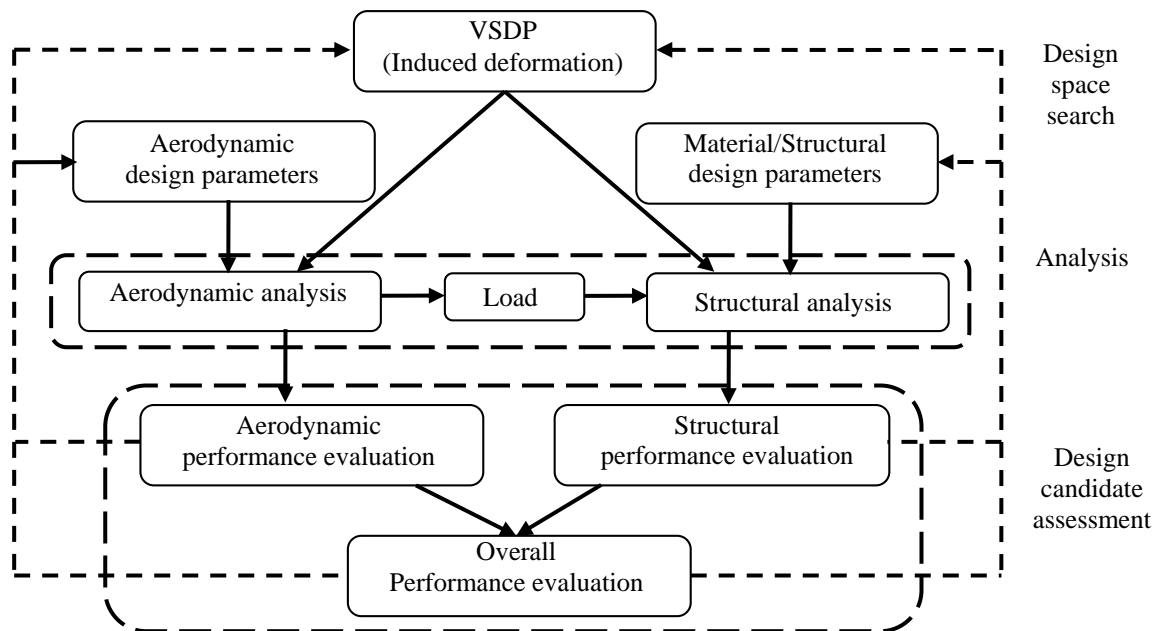


Figure 4.4. Decoupled design by VSDP [147]

4.2 Decoupled Design Method: Background Theory

Maheri et al [145] began with the force-displacement relationship for bending/twist coupled composite closed thin-/thick-walled beams using Equations (4.1) and (4.2) as reported by Kim and White [196], and with the application of the following two basic assumptions:

- The blade edge-wise slope is negligible ($\theta_z \approx 0$)
- The internal torque contribution due to the blade off-axis aerodynamic loading of the blade, in comparison with the torque produced due to elastic coupling is negligible.

$$\begin{Bmatrix} F \\ V_y \\ V_z \end{Bmatrix} = \begin{bmatrix} K_{11} & K_{12} & K_{13} \\ K_{21} & K_{22} & 0 \\ K_{31} & 0 & K_{33} \end{bmatrix} \begin{Bmatrix} u'_0 \\ v'_0 - \theta_z \\ w'_0 - \theta_y \end{Bmatrix} \quad (4.1)$$

$$\begin{Bmatrix} T \\ M_y \\ M_z \end{Bmatrix} = \begin{bmatrix} K_{44} & K_{45} & K_{46} \\ K_{54} & K_{55} & 0 \\ K_{64} & 0 & K_{66} \end{bmatrix} \begin{Bmatrix} \beta' \\ \theta'_y \\ \theta'_z \end{Bmatrix} \quad (4.2)$$

in which, T , M_y , θ_y and β are twisting moment, flap-wise bending moment, flap-wise slope and the coupling induced twist respectively. Applying the first assumption, Equation (4.2) reduces into the following form [145].

$$\begin{Bmatrix} T \\ M_y \end{Bmatrix} = \begin{bmatrix} K_{44} & K_{45} \\ K_{54} & K_{55} \end{bmatrix} \begin{Bmatrix} \beta' \\ \theta'_y \end{Bmatrix} \quad (4.3)$$

Recalling the bending moment produces the induced torque in the case of circumferentially asymmetric stiffness, by the second assumption, the induced torque, T , can be expressed as a fraction of the flap bending moment, M_y , as follows:

$$T = \varepsilon M_y \quad (4.4)$$

The application of the second assumption to Equation (4.3) gives:

$$M_y = M_{flap} = K \partial \beta / \partial x \quad (4.5)$$

where

$$K = \frac{K_{44}K_{55} - K_{45}K_{54}}{\varepsilon K_{55} - K_{45}} \quad (4.6)$$

Using normalised flap bending moment M^* , normalised radial location r^* and normalised effective stiffness K^* , Equation (4.5) can be re-written as:

$$\beta(r^*) = \frac{M_{hub}}{K_{max}} \int_0^{r^*} \frac{M^*(r^*)}{K^*(r^*)} dr^* \quad (4.7)$$

in which:

$$M^* = \frac{M}{M_{hub}} \quad (4.8)$$

$$K^* = \frac{K}{K_{max}} \quad (4.9)$$

$$r^* = \frac{r - R_{hub}}{R - R_{hub}} \quad (4.10)$$

In the above equations K_{max} is the maximum effective stiffness of the blade, M_{hub} is the flap bending at the hub, R_{hub} and R are hub and rotor radius respectively. K and M are the effective stiffness and the flap bending-moment at span location r respectively [145].

They also demonstrated that the normalised bending moment M^* is not a function of the wind turbine run-condition which is shown in Figure (4.5). Figure (4.5) shows the normalised flap bending moment for a variety of AWT-27 wind turbine run-conditions [145].

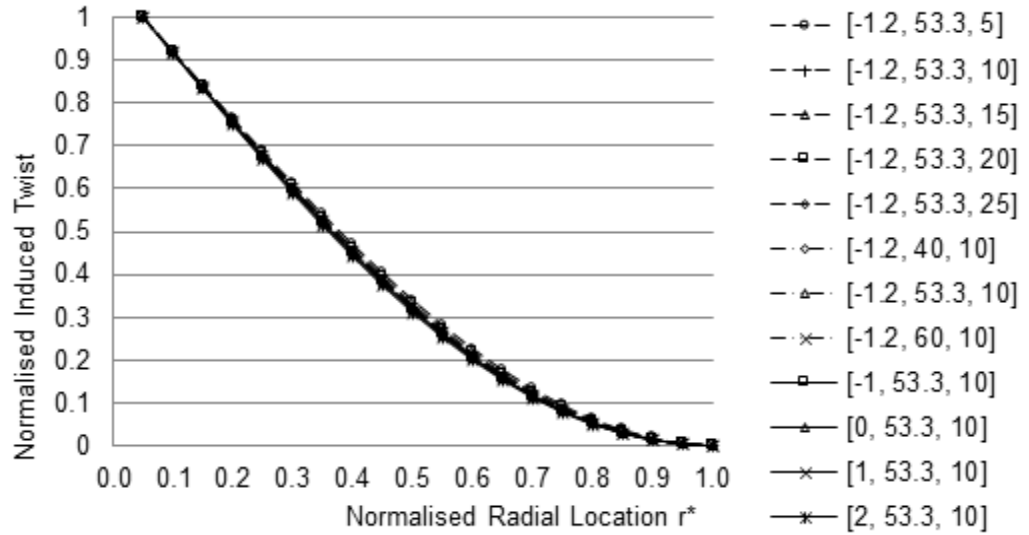


Figure 4.5. Variation of normalised flap-bending moment versus run conditions [pitch angle (deg.), Ω (rpm), V (m/s)] [149]

Then they came to the conclusion that since the effective stiffness distribution only depends on the blade structural characteristics and not the run-condition of the wind turbine run, so once calculated at a particular wind turbine run-condition using either FEA or an analytical model, the value can be used at other run-conditions as well [145].

Having M^* and K^* as not a function of wind turbine run-condition, the term

$\int_0^{r^*} \frac{M^*(r^*)}{K^*(r^*)} dr^*$ in Equation (4.7) becomes invariant to the wind turbine run-conditions.

This leads to Equation (4.11), which relates the distribution of the induced twist at a general run-condition $\beta(r^*)$ to the induced twist at a reference run-condition $\beta(r^*)_{ref}$ [145].

$$\beta(r^*) = M_{hub} \frac{\beta(r^*)_{ref}}{M_{hub,ref}} \quad (4.11)$$

Equation (4.11) is the basis of the decoupled design method and the variable state design parameter (VSDP) proposed by Maheri et al [135 & 147], as explained below.

Normalising the distribution of the induced twist using its maximum value of the induced twist occurring at the blade tip β_T and substituting into Equation (4.7) gives:

$$\beta^*(r^*) = \frac{\beta(r^*)}{\beta_T} = \frac{\int_0^{r^*} \frac{M^*(r^*)}{K^*(r^*)} dr^*}{\int_0^1 \frac{M^*(r^*)}{K^*(r^*)} dr^*} \quad (4.12)$$

Combining Equations (4.10) and (4.11) results to:

$$\beta_T = M_{hub} \frac{\beta_{T,ref}}{M_{hub,ref}} \quad (4.13)$$

In decoupled design method, $\beta_{T,ref}$ is considered as an independent design parameter, which is required to be obtained such that the wind turbine aerodynamic performance is optimised. Having optimised $\beta_{T,ref}$ for wind turbine aerodynamic performance, then the elastic coupling in the blade should be applied such that the exact amount of blade tip induced twist at reference run-condition is produced [144].

So, when a value is assigned to the reference tip induced twist $\beta_{T,ref}$, the induced twist at blade tip at other run-conditions, β_T can be determined using Equation (4.13) [144]. The simulation of the wind turbine with adaptive blade requires the actual distribution of induced twist. To determine the actual induced twist at each run-condition, the normalised induced twist β^* is also required:

$$\beta = \beta^* \beta_T \quad (4.14)$$

The normalised induced twist can be determined by either analytical model or by employing FEA.

A simple model (Equation (4.15)) was produced by Maheri et al [135] for modelling constant shell thickness distribution problems and it is capable of simulating the normalized induced twist only based on geometry information with the assumption of the blade having uniform material and it does not require any knowledge about the blade material. However, for variable shell thickness distribution under various constant layup configurations, the validity of this simple model is certainly unknown.

$$\beta^*(r^*) = \frac{\int_0^{r^*} \frac{M^*(r^*)}{t_{\max}^3(r^*)} dr^*}{\int_0^1 \frac{M^*(r^*)}{t_{\max}^3(r^*)} dr^*} \quad (4.15)$$

where

t_{\max} = the aerofoils maximum thickness,

$\beta^*(r^*)$ = normalised induced twist,

$M^*(r^*)$ = normalised flap bending moment.

To establish an analytical model for variable shell thickness and variable fibre angle, several finite element analyses for different blade configurations are carried out. For efficient and effective modelling and analysing of the adaptive blade, the HPBM is used. The validation of the HPBM is presented in section 4.3.

4.3 Validation of HPBM

Using the same running condition of wind speed 10 m/s and wind turbine rotor speed of 53.3 rpm, the blade analyses are carried out using the HPBM which was discussed in section (2.5.6) and the commercial CAD/FEA software was employed to validate the results.

In modelling of the wind turbine blade for the analysis, the blade structure is defined by the combination of different ‘Patches’. A ‘Patch’ is a four-sided figure defined by coordinates of its four corners. For the purpose of validation of the HPBM, Table 4.1 presents composite materials, a simple ‘Patch’ coordinates are shown in Table (4.2), Table (4.3) presents the material layup configuration and the blade patches configuration is presented in Figure (4.6).

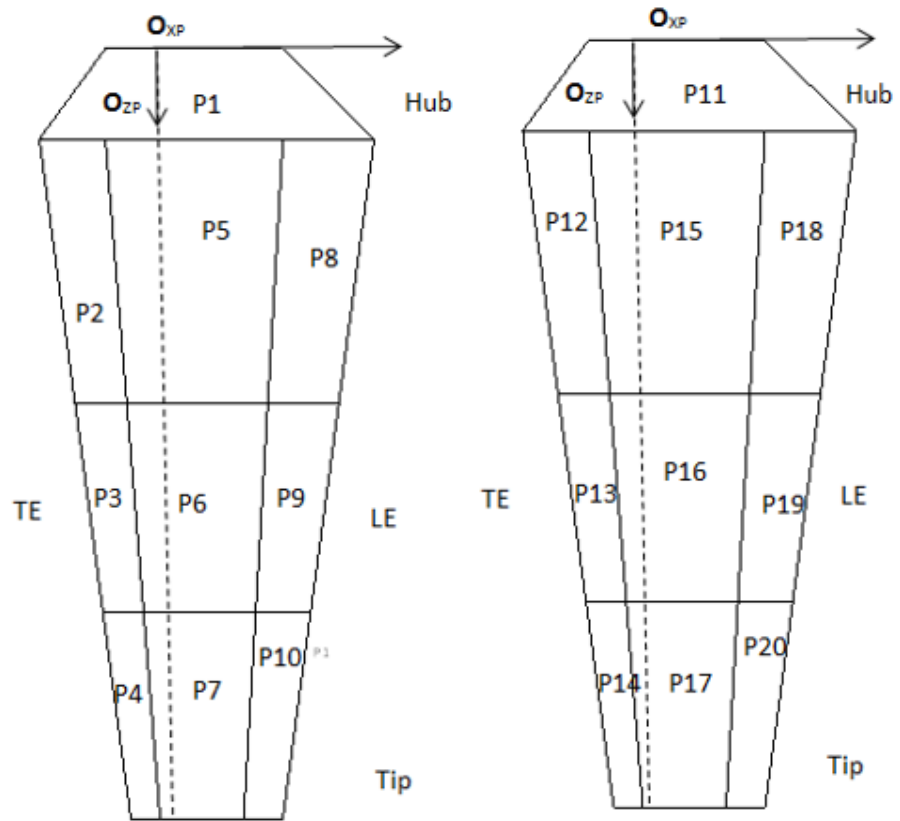
Table 4.1- Mechanical Properties of the Composite Materials

	E_x (GPa)	E_y (GPa)	E_z (GPa)	G_{xy} (GPa)	G_{yz} (GPa)	G_{xz} (GPa)	ν_{xy}	ν_{yz}	ν_{xz}	Density (kg/m ³)	mat_{ID}
EpoxyCarbonHM_50	197.25	5.1429	5.1429	5.2174	3	5.2174	0.375	0.4	0.375	1525	1
EpoxyEglass_40	32.3	7.2078	7.2078	4.6875	3	4.6875	0.34	0.4	0.34	1782	2

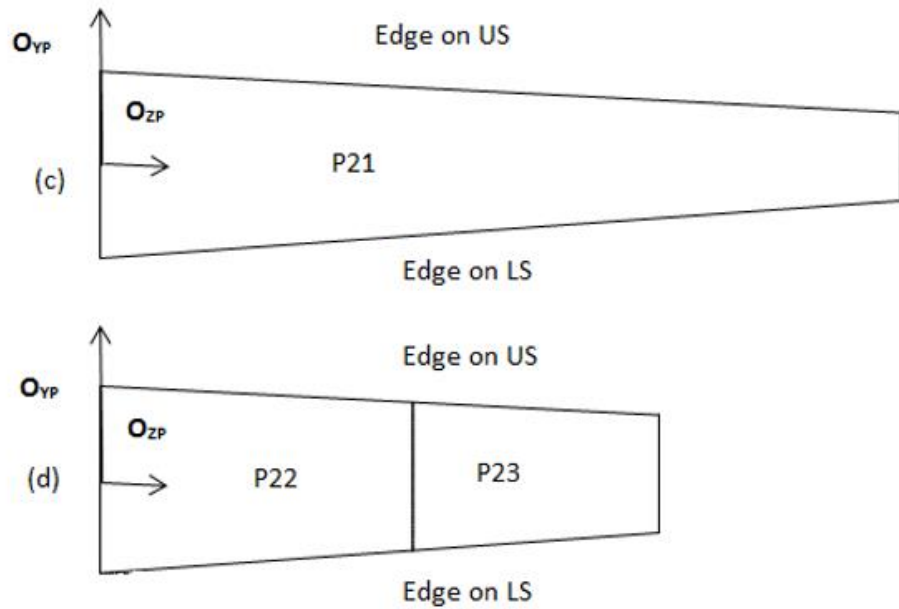
EpoxyCarbonHM_50 is composite material having 50% volume fraction of high modulus carbon fibres and EpoxyEglass_40 having 40% volume fraction of E-Glass fibres.

Table 4.2- Case Patches Normalised Coordinates

Patch	x _p	y _p	z _p	Patch	x _p	y _p	z _p	Patch	x _p	y _p	z _p	Patch	x _p	y _p	z _p
1	0	-	0	2	0	-	0.133	3	0	-	0.4	4	0	-	0.7
	1	-	0		0.2	-	0.133		0.2	-	0.4		0.2	-	0.7
	1	-	0.133		0.2	-	0.4		0.2	-	0.7		0.2	-	1
	0	-	0.133		0	-	0.4		0	-	0.7		0	-	1
5	0.2	-	0.133	6	0.2	-	0.4	7	0.2	-	0.7	8	0.7	-	0.133
	0.7	-	0.133		0.7	-	0.4		0.7	-	0.7		1	-	0.133
	0.7	-	0.4		0.7	-	0.7		0.7	-	1		1	-	0.4
	0.2	-	0.4		0.2	-	0.7		0.2	-	1		0.7	-	0.4
9	0.7	-	0.4	10	0.7	-	0.7	11	0	-	0	12	0	-	0.133
	1	-	0.4		1	-	0.7		1	-	0		0.2	-	0.133
	1	-	0.7		1	-	1		1	-	0.133		0.2	-	0.4
	0.7	-	0.7		0.7	-	1		0	-	0.133		0	-	0.4
13	0	-	0.4	14	0	-	0.7	15	0.2	-	0.133	16	0.2	-	0.4
	0.2	-	0.4		0.2	-	0.7		0.7	-	0.133		0.7	-	0.4
	0.2	-	0.7		0.2	-	1		0.7	-	0.4		0.7	-	0.7
	0	-	0.7		0	-	1		0.2	-	0.4		0.2	-	0.7
17	0.2	-	0.7	18	0.7	-	0.133	19	0.7	-	0.4	20	0.7	-	0.7
	0.7	-	0.7		1	-	0.133		1	-	0.4		1	-	0.7
	0.7	-	1		1	-	0.4		1	-	0.7		1	-	1
	0.2	-	1		0.7	-	0.4		0.7	-	0.7		0.7	-	1
21	0.25	0	0.133	22	0.5	0	0.133	23	0.5	0	0.5				
	0.25	1	0.133		0.5	1	0.133		0.5	1	0.5				
	0.25	1	1		0.5	1	0.5		0.5	1	0.7				
	0.25	0	1		0.5	0	0.5		0.5	0	0.7				



(a) Patch numbering on upper surface (b) Patch numbering on lower surface



(c) Web closer to LE (d) Web closer to TE

where LE is leading edge and TE is the trailing edge

Figure 4.6. Blade patches configuration

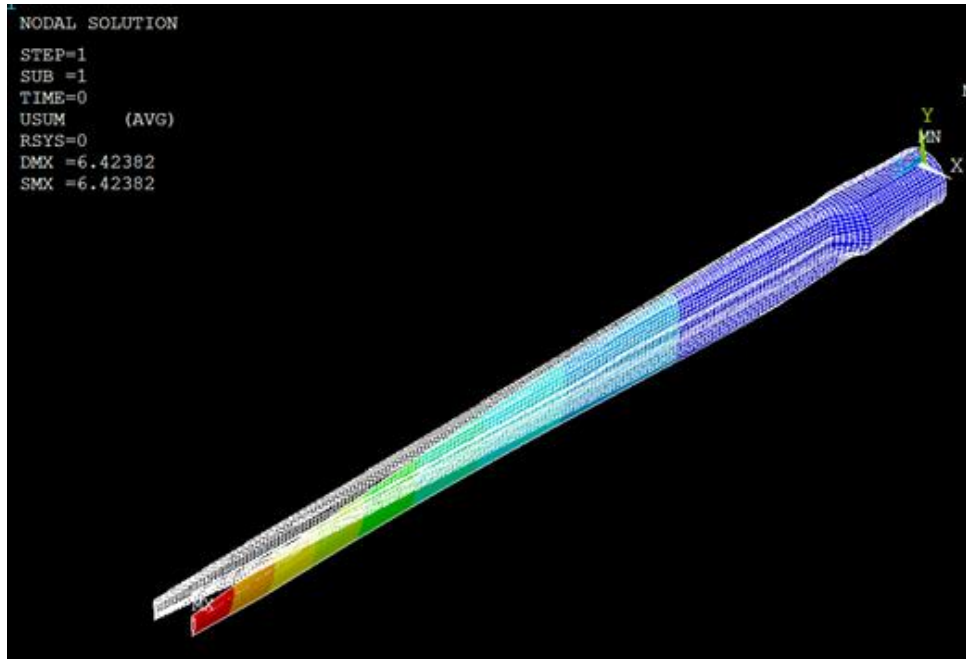
Table 4.3- The layup configurations for the NREL 5 MW adaptive blade case

Patch	Layup [mat_{ID}, θ_n]	Patch	Layup [mat_{ID}, θ_n]
1	[1, $\pm 45_{20}$]	2	[1, 0/90/ $\pm 45_{15}$ /0/90]
3	[1, 0/90/ $\pm 45_{12}$ /0/90]	4	[1, 0/90/ $\pm 45_{10}$ /0/90]
5	[2,0/90/ $\pm 45_{15}$][1, 65 ₃₀]	6	[2,0/90/ $\pm 45_{12}$][1, 65 ₂₀]
7	[2,0/90/ $\pm 45_{10}$][1, 65 ₁₀]	8	[1, 0/90/ $\pm 45_{15}$ /0/90]
9	[1, 0/90/ $\pm 45_{12}$ /0/90]	10	[1, 0/90/ $\pm 45_{10}$ /0/90]
11	[1, $\pm 45_{20}$]	12	[1, 0/90/ $\pm 45_{15}$ /0/90]
13	[1, 0/90/ $\pm 45_{12}$ /0/90]	14	[1, 0/90/ $\pm 45_{10}$ /0/90]
15	[2,0/90/ $\pm 45_{15}$][1, -65 ₃₀]	16	[2,0/90/ $\pm 45_{12}$][1, -65 ₂₀]
17	[2,0/90/ $\pm 45_{10}$][1, -65 ₁₀]	18	[1, 0/90/ $\pm 45_{15}$ /0/90]
19	[1, 0/90/ $\pm 45_{12}$ /0/90]	20	[1, 0/90/ $\pm 45_{10}$ /0/90]
21	[1, $\pm 45_{10}$]	22	[1, 0/90/ $\pm 45_{15}$ /0/90]
23	[1, $\pm 45_{10}$]		

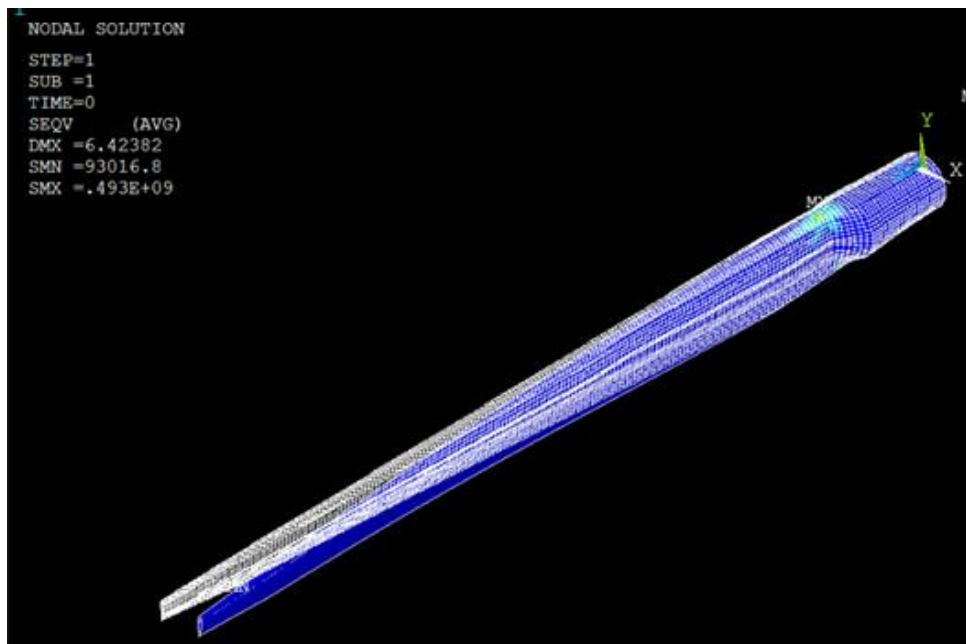
where n is the number of layers

Table 4.3 shows the blade material layup configuration with mat_{ID} indicating the material used and θ_n representing the fibre angle for each lamina.

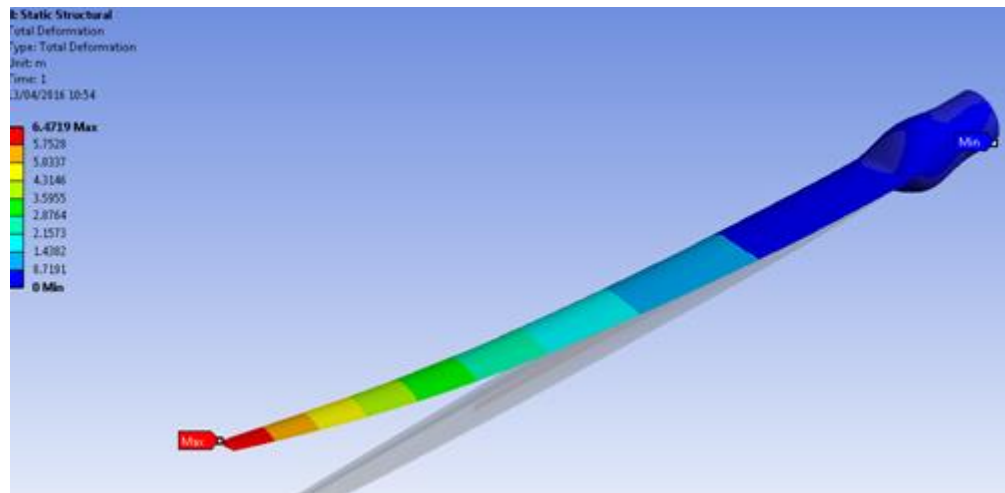
The NREL 5 MW blade with the configuration shown above was analysed using the CAD/FEA commercial software and the innovative approach. The deformation and equivalent stress responses under the aforementioned running conditions are obtained using the HPBM tool and the commercial software comparison in order to validate the results.



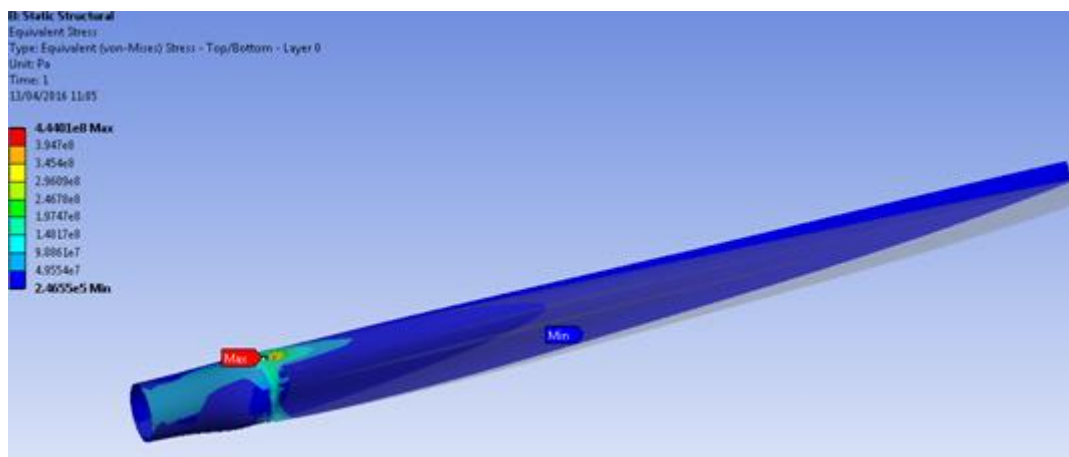
(a) Total Deformation using MATLAB coding



(b) Equivalent von Mises Stress using the MATLAB coding



(a) Total Deformation using SOLIDWORKS/ANSYS



(b) Equivalent von Mises Stress using SOLIDWORKS/ANSYS

Figure 4.7. Stress and deformation results for HPBM and SOLIDWORKS/ANSYS

Figure (4.7) shows the stress and deformation results using the HPBM and SOLIDWORKS/ANSYS. For the maximum deformation and stress results are presented in Table (4.4).

Table 4.4- Stress and deformation results

	Maximum Deformation (m)	Maximum Stress (GPa)
HPBM	6.424	0.493
ANSYS	6.472	0.444

From the results, it could be observed that HPBM analysis results are in good agreement with that obtained using SolidWorks/ANSYS.

The results show that the tool could be used for the modelling and analysis of NREL 5 MW adaptive wind turbine blade with the following below as advantage over using commercial software:

1. The time of modelling and analysing is drastically reduced
2. The ease of modelling using just writing of MATLAB codes for the patches configuration and material properties using the ‘innovative sophisticated’ tool as a platform for modelling the adaptive wind turbine blade with complex structural configurations.

4.4 Normalised Induced Twist Analytical Model

In order to propose generalised analytical model for predicting the normalised induced twist, the investigation of the effects of span-wise variation of fibre angle, shell thickness, the variation of the shell thickness distribution and shear webs on the normalised induced twist will be carried out. In this research work, the NREL 5 MW and AWT-27 wind turbine running at wind speed of 10 m/s are used.

The blade patches coordinates in 2D square system of coordinates for these analyses are shown in Table (A1), the patches configuration and the blade cross section are shown in Figure (A1-a) to (A1-d) and Figure (A2) respectively.

In simulation, the linear variations of thickness and layup have been replaced with a stepwise variation over blade’s segments from the root to tip and applied both upper and lower surface. Here, concept of normalized thickness distribution and fibre angle distribution is introduced and shown in Figure (4.8) and Figure (4.9). The equations of the normalised thickness distributions and fibre angle distributions are shown in Table (4.6) and Table (4.7) respectively.

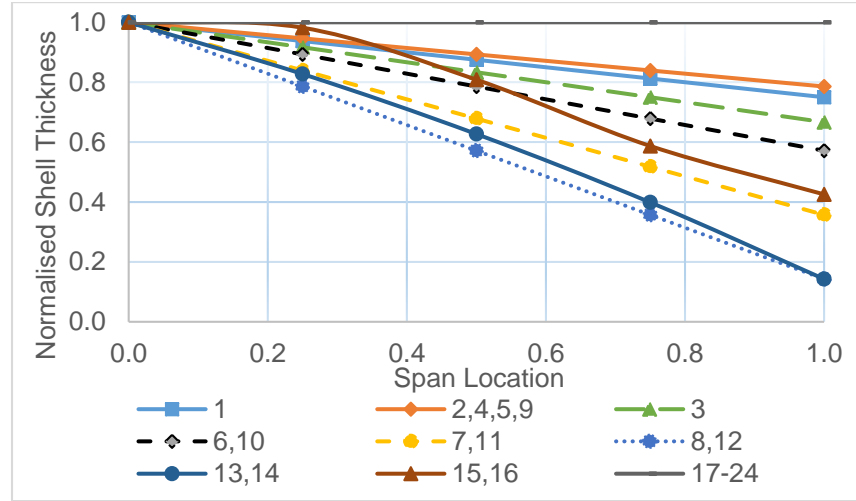


Figure 4.8. Normalised shell thickness distributions

Table 4.5- Layup Configurations

Case	Layup configuration, $\{[t_{layer}, mat_{ID}, \theta]_n\}$	Web 1	Web 2
1	$\{[1,3,0]_1, [1,2, \theta]_n\}$ mirror lower surface	$[\pm 45]_{16}$ @ x/c=0.25	$[\pm 45]_{16}$ @ x/c=0.55
2	$\{[1,3,0]_1, [1,1, \theta]_n\}$ mirror lower surface	$[\pm 45]_{16}$ @ x/c=0.25	$[\pm 45]_{16}$ @ x/c=0.55
3	$\{[1,3,0]_1, [1,2, \theta]_m, [1,1, \theta]_m\}$ mirror lower surface	$[\pm 45]_{16}$ @ x/c=0.25	$[\pm 45]_{16}$ @ x/c=0.55
4	$\{[1,3,0]_1, [1,2, \theta]_n\}$ mirror lower surface	–	–
5	$\{[1,3,0]_1, [1,2, \theta]_n\}$ mirror lower surface	$[\pm 45]_{16}$ @ x/c =0.38	–
6	$\{[1,3,0]_1, [1,2, \theta]_n\}$ mirror lower surface	$[\pm 45]_{16}$ @ x/c =0.46	–
7	$\{[1,3,0]_1, [1,1, \theta]_n\}$ mirror lower surface	$[\pm 45]_{16}$ @ x/c =0.46	–
8	$\{[1,3,0]_1, [1,2, \theta]_m, [1,1, \theta]_m\}$ mirror lower surface	$[\pm 45]_{16}$ @ x/c =0.46	–
9	$\{[1,3,0]_1, [1,2, \theta]_n\}$ mirror lower surface	$[\pm 45]_{18}$ @ x/c=0.25	$[\pm 45]_{18}$ @ x/c=0.55

where n is the number of layers and m is half the number of layers

Table 4.6- Shell Thickness distributions

Case	Variation type	Thickness range (mm)	Normalised thickness distributions
1	Linear (span-wise & chord-wise)	48 to 36	$t^* = -0.25r^* + 1$
2		56 to 44	$t^* = -0.23366 r^* + 1$
3		18 to 12	$t^* = -0.3333 r^* + 1$
4		28 to 22	$t^* = -0.23366 r^* + 1$
5	Linear (span-wise)	56 to 44	$t^* = -0.23366 r^* + 1$
6		56 to 32	$t^* = -0.42857 r^* + 1$
7		56 to 20	$t^* = -0.64286 r^* + 1$
8		56 to 8	$t^* = -0.88513 r^* + 1$
9		28 to 22	$t^* = -0.23366 r^* + 1$
10		28 to 16	$t^* = -0.42857 r^* + 1$
11		28 to 10	$t^* = -0.64286 r^* + 1$
12		28 to 4	$t^* = -0.88513 r^* + 1$
13	Quadratic (span-wise)	56 to 8	$t^* = -0.24336 r^{*2} - 0.66916 r^* + 1$
14		28 to 4	$t^* = -0.24336 r^{*2} - 0.66916 r^* + 1$
15	Third Degree (span-wise)	56 to 24	$t^* = 1.1498r^{*3} - 2.1078r^{*2} + 0.3833r^* + 1$
16		28 to 12	$t^* = 1.1498r^{*3} - 2.1078r^{*2} + 0.3833r^* + 1$
17	Uniform	56	$t^* = 1$
18		52	$t^* = 1$
19		48	$t^* = 1$
20		44	$t^* = 1$
21		28	$t^* = 1$
22		24	$t^* = 1$
23		20	$t^* = 1$
24		16	$t^* = 1$

Table 4.7- Layup Fibre Angle distributions

Case	Variation type	Angle range (deg.)	Normalised Angle distributions
1	Uniform	0	$\theta^* = 1$
2		5	$\theta^* = 1$
3		10	$\theta^* = 1$
4		15	$\theta^* = 1$
5		20	$\theta^* = 1$
6		25	$\theta^* = 1$
7		30	$\theta^* = 1$
8		35	$\theta^* = 1$
9		40	$\theta^* = 1$
10		45	$\theta^* = 1$
11		50	$\theta^* = 1$
12		55	$\theta^* = 1$
13		60	$\theta^* = 1$
14		65	$\theta^* = 1$
15		70	$\theta^* = 1$
16		75	$\theta^* = 1$
17		80	$\theta^* = 1$
18		85	$\theta^* = 1$
19		90	$\theta^* = 1$
20	Linear	45 to 0	$\theta^* = -r^* + 1$
21		50 to 38	$\theta^* = -0.2632 r^* + 1$
22		50 to 20	$\theta^* = -0.6452 r^* + 1$
23		50 to 8	$\theta^* = -0.840 r^* + 1$
24	Quadratic	50 to 8	$\theta^* = 0.2044 r^{*2} - 0.6401 r^* + 1$
25	Third degree	50 to 21	$\theta^* = 1.07325 r^{*3} - 2.0033 r^{*2} + 0.34651 r^* + 1$

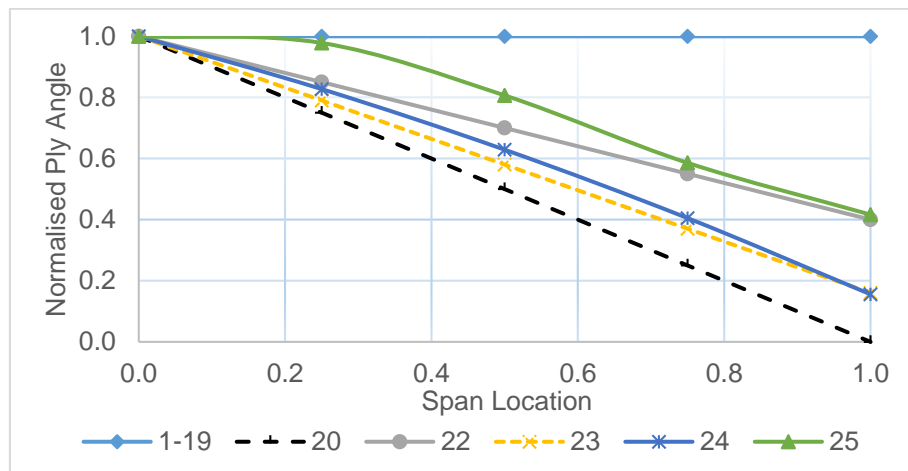


Figure 4.9. Normalised fibre angle distributions

Table 4.8- Mechanical Properties of the Composite Materials

Mat. ID	Mat. Name	Min. Thick. (mm)	Density (kg/m ³)	EL (Gpa)	ET (Gpa)	GLT (Gpa)	NuLT
1	EpoxyEglass_40	0.001	1782	32.3	7.2078	4.6875	.4
2	EpoxyCarbonHM_50	0.001	1525	197.25	5.1429	5.2174	.4
3	Gel Coat	0.05	1235	3.44	3.44	1.38	0.3

Tables (4.5), (4.6) & (4.7) present the different layup configurations, different shell thickness distributions and fibre angle distributions respectively along the span of the blade while Table (4.8) shows the materials used for the analyses. From the Table 4.5, t_{layer} is the material thickness, mat_{ID} is used to identify the material used which could be found in Table 4.8 while θ is the fibre angle. Also, as stated before, n is the number of layers and m is half the number of layers

For convenience, each blade is represented by its corresponding [layup, thickness, angle] case. For example [4, 2, 6] refers to an adaptive blade made of the layup configuration 4, thickness distribution 2 and fibre angle distribution 6 while [4, 2/3/5, 6] could be expanded to be cases [4,2,6], [4,3,6] & [4,5,6].

Furthermore, these terms induced twist and normalised induced twist will be used frequently in this chapter and are defined below:

Induced Twist: This is the torsional deformation of the blade that result from bending force on an unbalanced composite blade because some of the forces will be translated to the off-axis direction resulting to the blade twisting around the axis.

Normalised Induced Twist: This is the ratio of the induced twist at a particular blade location (r) to the maximum blade maximum induced twist which typically occurs at the tip of the blade.

4.4.1 Effect of Fibre Angle on β^* (NREL 5 MW Blade)

The investigation of the effect of fibre angle on the normalised induced twist of the NREL wind turbine blade was performed using layup configuration shown in Table (4.5), (4.6) & (4.7). For these cases, the fibre angle range from 0° to 90° in an increment of 5° . This is considered in three case sets, each set comprising of 19 cases with the case sets having the

same layup configuration but of different materials. Case Sets 1, 2 & 3 are made using carbon fibre, glass fibre, and a combination of carbon and glass fibre respectively.

Figure (4.10) to (4.12), which are plots of the induced twist, show that the induced twists for angles 0° and 90° are negligible which is as a result of insignificant elastic coupling. Cases for 0° and 90° were not included in the normalised induced twist plots [Figure (4.13), Figure (4.14.a) & Figure (4.15.a)]. From the graphs, Figure (4.10) to (4.12), it can be seen that the fibre angle determines the magnitude of the induced twist but Figure (4.13), Figure (4.14.b) & Figure (4.15.b) show that the normalised induced twist is independent of fibre angle though for Case Set 2 and Case Set 3, it is between a certain range. For Case Set 2, it could be observed that between angles 15° to 80° that the normalised induced twist is independent of the fibre angle while Case Set 3, the angle range of which the normalised induced twist is independent of the fibre angle is 10° to 85° .

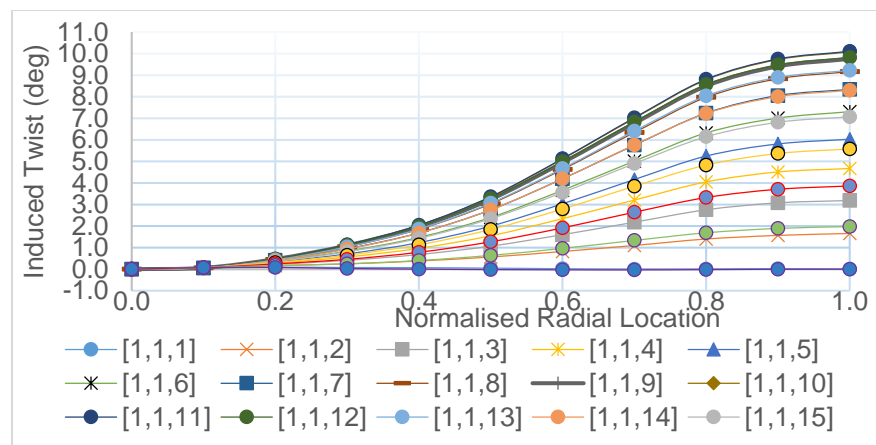


Figure 4.10. Case set 1 Induced twist for various fibre angle (NREL 5 MW Blade)

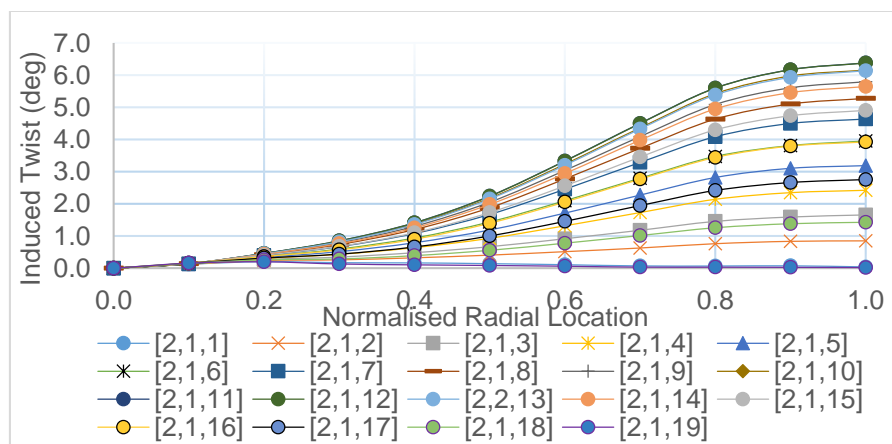


Figure 4.11. Case set 2 Induced twist for various fibre angle (NREL 5 MW Blade)

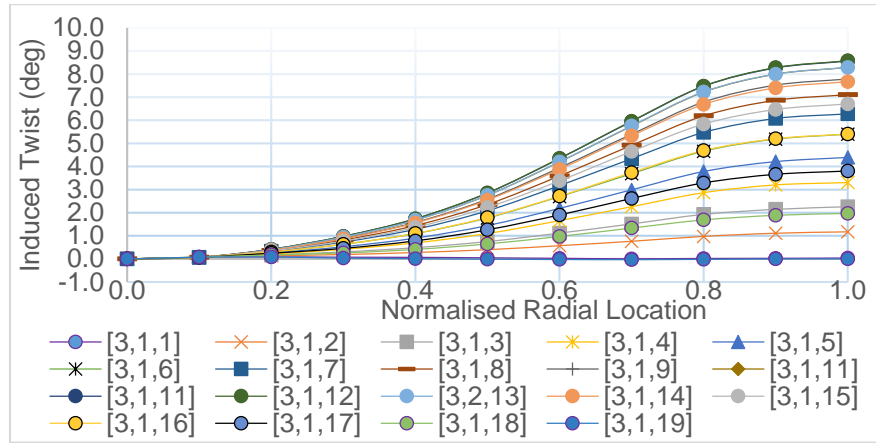


Figure 4.12. Case set 3 Induced twist for various fibre angle (NREL 5 MW Blade)

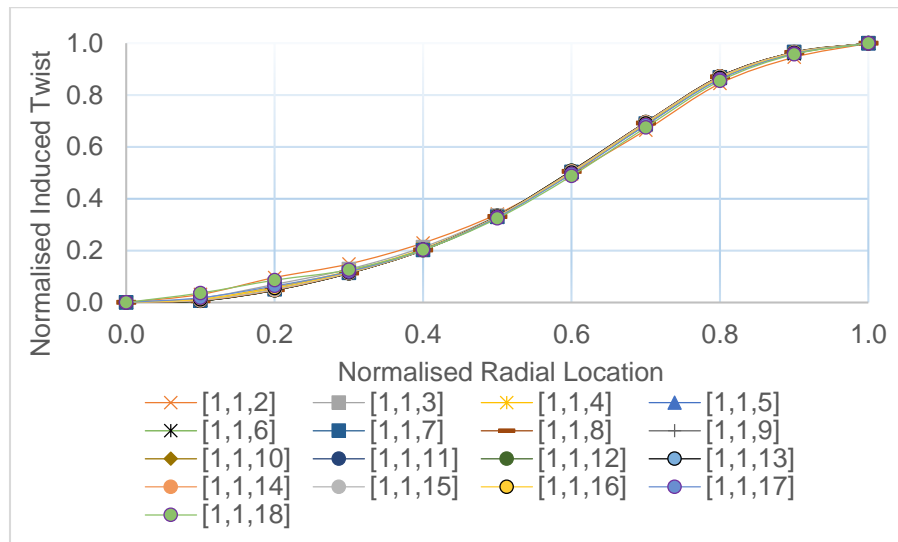


Figure 4.13. Effect of fibre angle on β^* [Case Set 1 (NREL 5 MW Blade)]

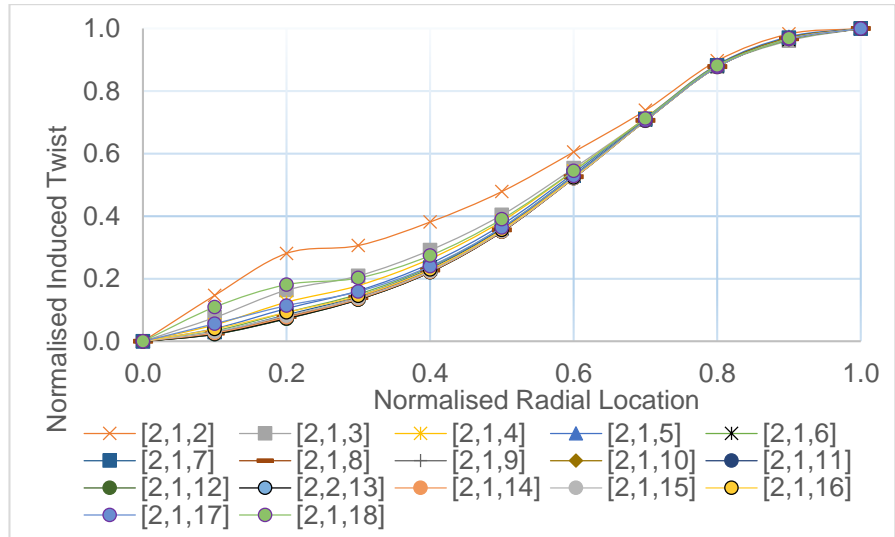


Figure 4.14.(a) Effect of fibre angle on β^* [Case Set 2 (NREL 5 MW Blade)]

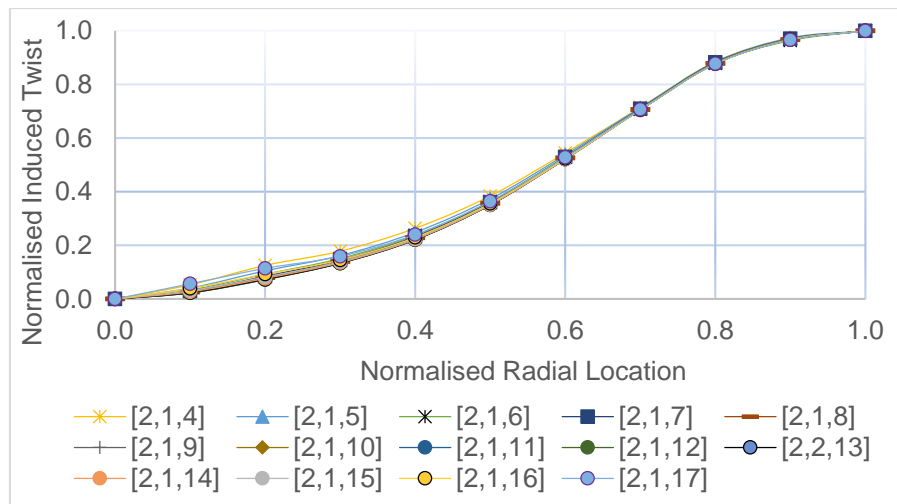


Figure 4.14.(b) Effect of fibre angle on β^* [Case Set 2 (15° to 80°) (NREL 5 MW Blade)]

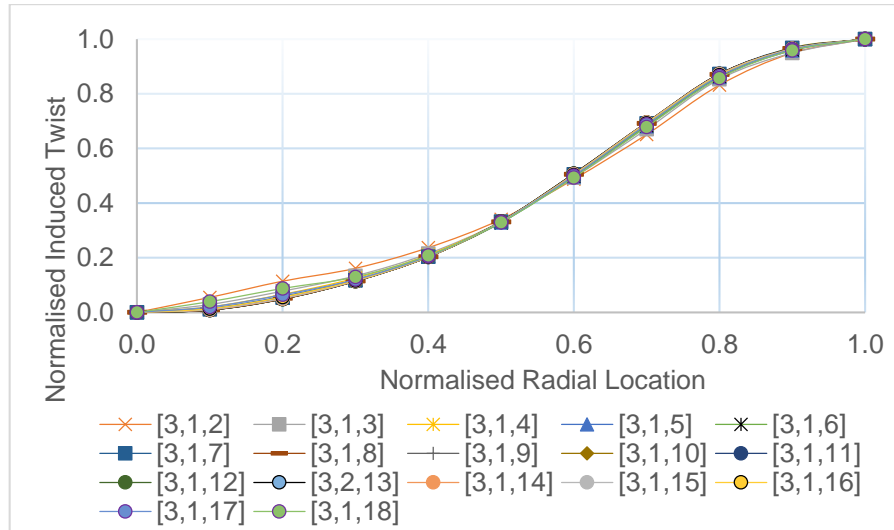


Figure 4.15.(a) Effect of fibre angle on β^* [Case Set 3 (NREL 5 MW Blade)]

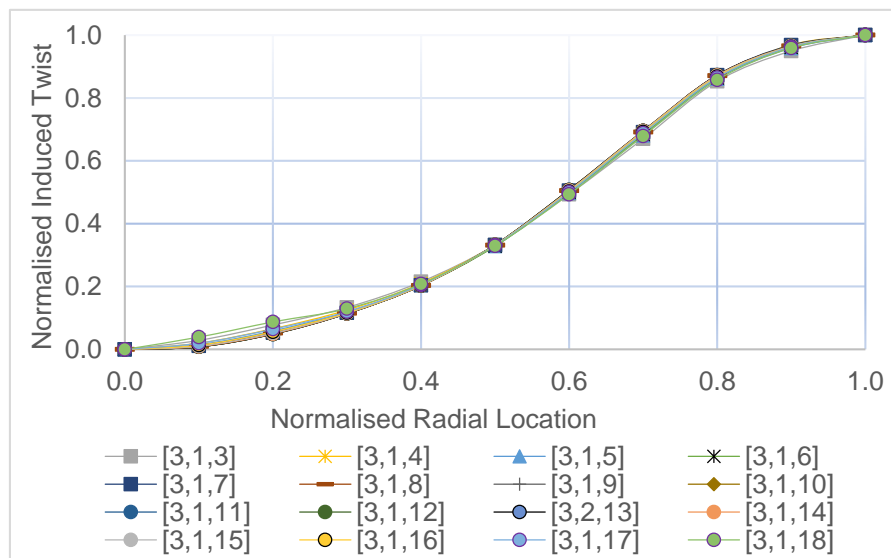


Figure 4.15.(b) Effect of fibre angle on β^* [Case Set 3 (10° to 85°) (NREL 5 MW Blade)]

4.4.2 Effect of Fibre Angle on β^* (AWT-27 Blade)

This section is same as section (4.4.1) but in this case the effect of fibre angle on the normalised induced twist is considered for an AWT-27 wind turbine blade. With the afore knowledge as we can see in section (4.4.1), that for very small angles and angles close to 90° , the induced twist is insignificant. Therefore, considering three Case Sets, with each

Case Set comprising of 10 cases for fibre angles 20° to 65° with blade configurations shown in Tables (4.5), (4.6) & (4.7). The three Case Sets are of the same layup configuration but of different materials. Case Sets 4, 5 & 6 are made using carbon fibre, glass fibre, and a combination of carbon and glass fibre respectively.

From the graphs, Figure (4.16) to (4.18), it can be seen that the fibre angle determines the magnitude of the induced twist but Figure (4.19) to (4.21) show that the normalised induced twist is not a function of the fibre angle for uniform fibre angle along the span of the blade.

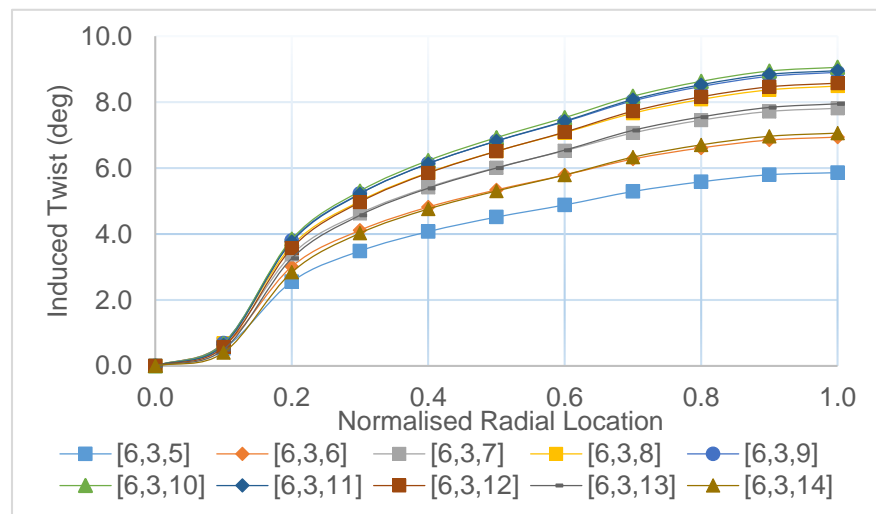


Figure 4.16. Case set 4 Induced twist for various fibre angle (AWT-27 Blade)

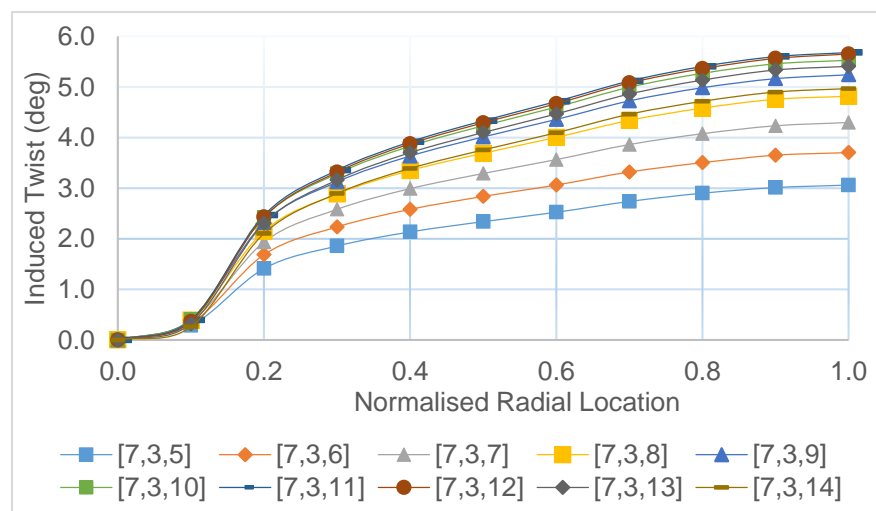


Figure 4.17. Case set 5 Induced twist for various fibre angle (AWT-27 Blade)

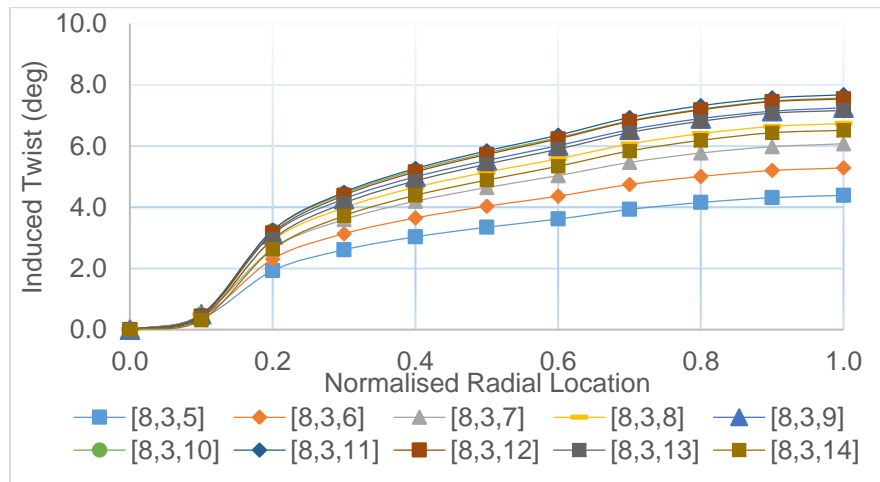


Figure 4.18. Case set 6 Induced twist for various fibre angle (AWT-27 Blade)

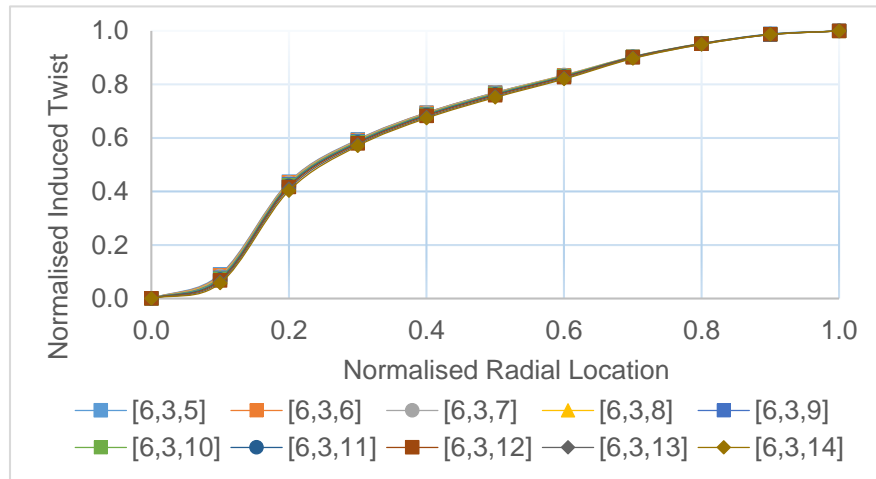


Figure 4.19. Effect of fibre angle on β^* [Case Set 4 (AWT-27 Blade)]

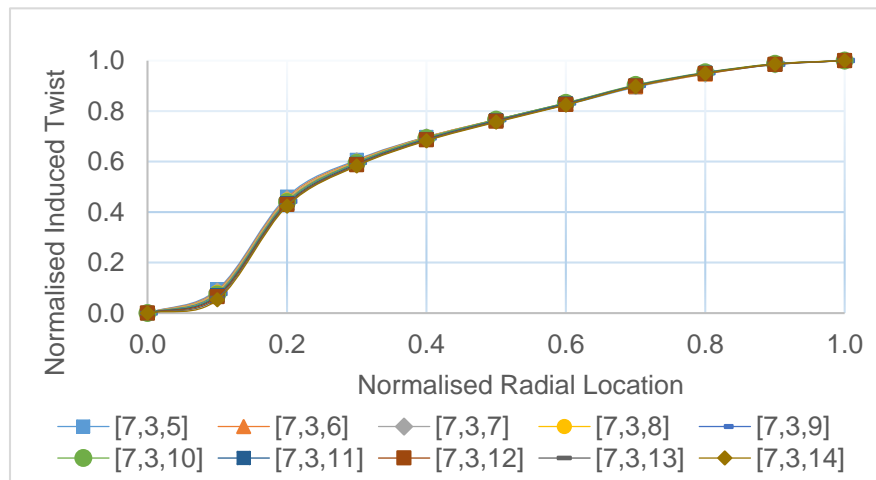


Figure 4.20. Effect of fibre angle on β^* [Case Set 5 (AWT-27 Blade)]

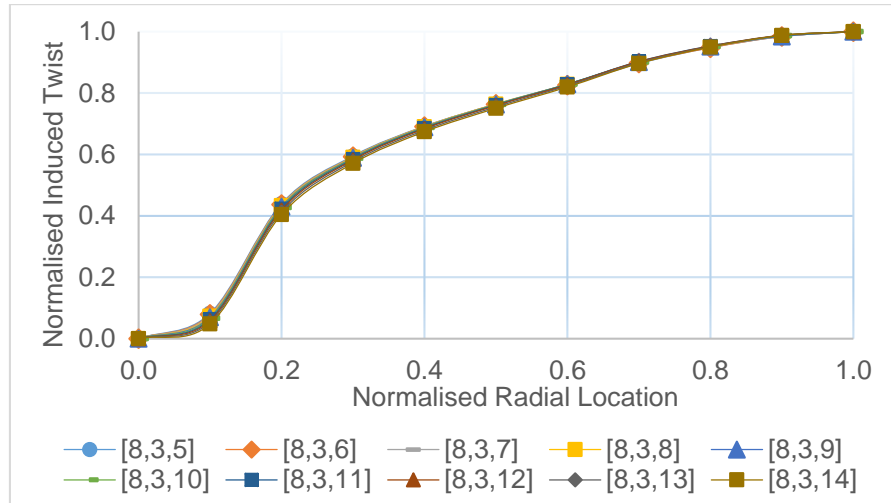


Figure 4.21. Effect of fibre angle on β^* [Case Set 6 (AWT-27 Blade)]

4.4.3 Effect of Material on β^* (NREL 5 MW Blade)

In order to investigate the effect of material on the normalised induced twist, Case Sets 1, 2 & 3 above were analysed, the normalised induced twist were plotted using cases ([1,1,11], [2,1,11], [3,1,11]) since from the previous analysis (section (4.4.1)), it could be concluded in these range of fibre angles, the normalised induced twist is independent of the fibre angles. Figure (4.22) shows that the induced twist is a function of the material. It could be seen from Figure (4.23), that there is no difference in the normalised induced twist for [1,1,11] & [3,1,11] but there is insignificant different with that of [2,1,11] from the other two aforementioned cases. To give a conclusion on the effect of materials on the normalised induced twist, cases using the AWT-27 blade will be investigated.

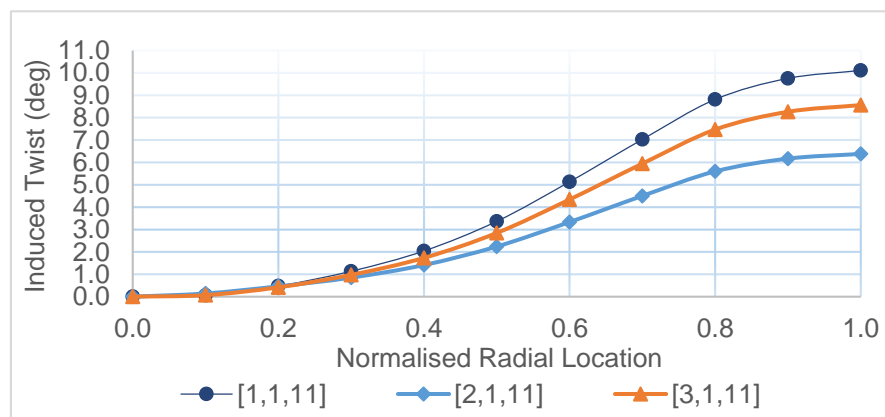


Figure 4.22. Effect of material on the induced twist (NREL 5 MW Blade)

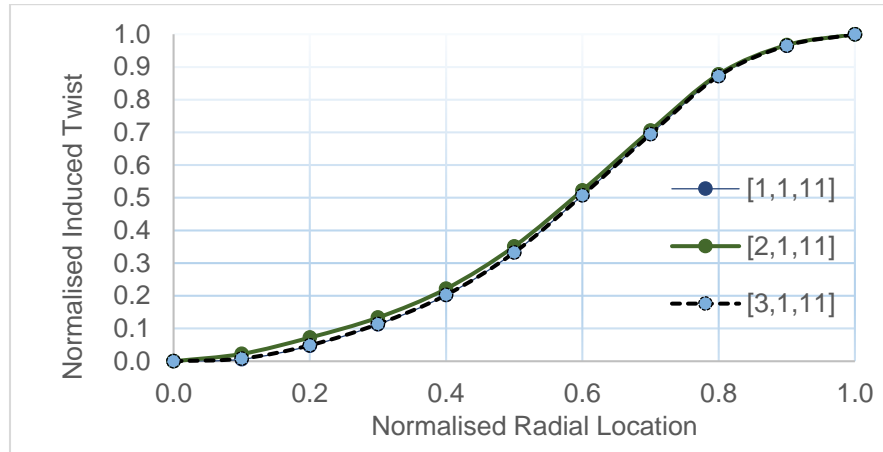


Figure 4.23. Effect of material on β^* (NREL 5 MW Blade)

4.4.4 Effect of Material on β^* (AWT-27 Blade)

Using same configuration as that in section (4.4.2), the effect of material on the normalised induced twist is analysed. Carbon fibre, glass fibre and a combination of carbon and glass fibre are used for the blade layups, the induced twist and the normalised induced twist are plotted for the cases ([6,3,10], [7,3,10], [8,3,10]) since it could be concluded that the normalised induced twist in these range of fibre angles, is independent of the fibre angles for a blade configuration with uniform angle. It could be seen from Figure (4.24) that the induced twist is a function of the material properties but, there is no difference in the normalised induced twist shown in Figure (4.25), which indicates that the normalised induced twist is not a function of the material properties.

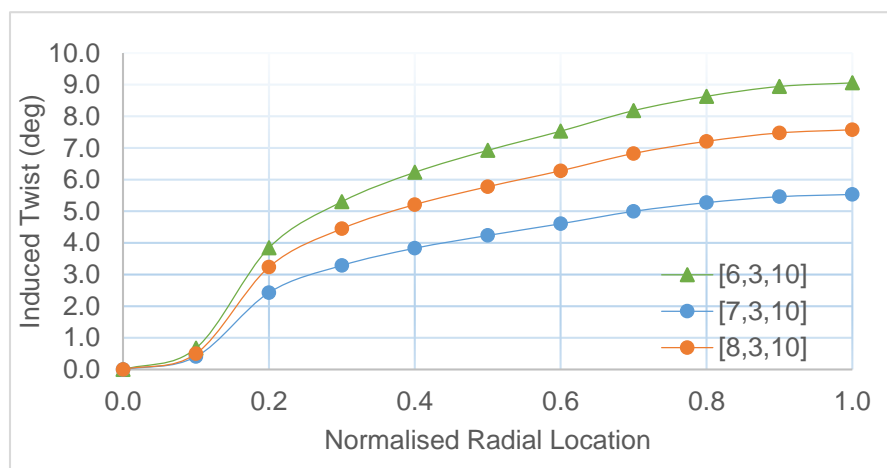


Figure 4.24. Effect of material on the induced twist (AWT-27 Blade)

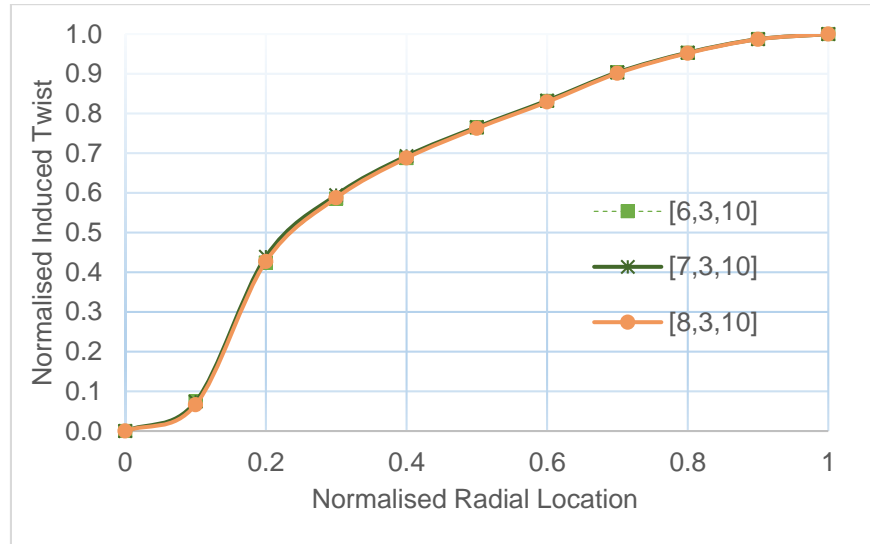


Figure 4.25. Effect of material on β^* (AWT-27 Blade)

This helps to draw to a conclusion that the material used only influences the magnitude not the trend of the normalised induced twist which, gives the same conclusion when investigated by Maheri et al [170]. This is expected as a result of bending/twist coupling which differs in the material since the materials have different orthotropic ratio.

4.4.5 Effect of the variation of Shell Thickness Distribution on β^* (NREL 5 MW Blade)

This section is the consideration of the effect of the variation of the shell thickness distribution along the span of the blade structure on the normalised induced twist. This investigation is done using layup configurations shown below:

Case [9,2,11]: Linear variation of shell thickness along the span and along the chord. This case has span-wise and chord-wise linear thickness variation of which at the root of the blade, chord-wise shell thickness distribution from the leading edge to the trailing edge varies from 56 mm to 40 mm and tip of the blade chord-wise distribution from leading edge to trailing edge varies from 44 mm to 28 mm.

Cases [9, 5/6/7/8, 11]: Linear variation of shell thickness along the span.

Case [9,13,11]: Quadratic variation of shell thickness along the span.

Case [9,15,11]: Third degree variation of shell thickness along the span.

Cases [9, 17/18/19/20, 11]: Uniform shell thickness along the span.

The blade configurations (layout, shell thickness distributions and fibre angle distributions) for these cases are shown in Table (4.5), (4.6) & (4.7).

Figure (4.26.a) shows that the trend of the normalised induced twist is a function of the variation of the shell thickness distribution along the span.

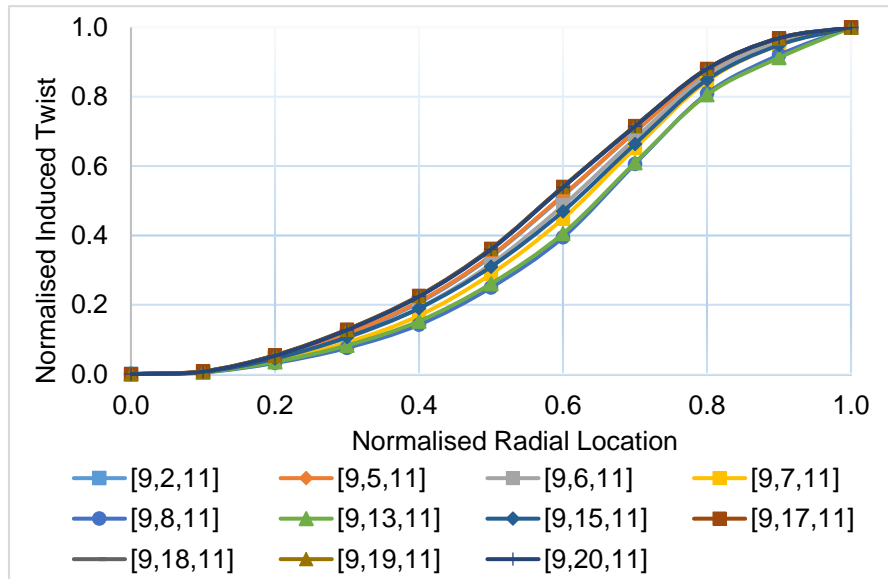


Figure 4.26.(a) Effect of variation of shell thickness distributions on β^* (NREL 5 MW Blade)

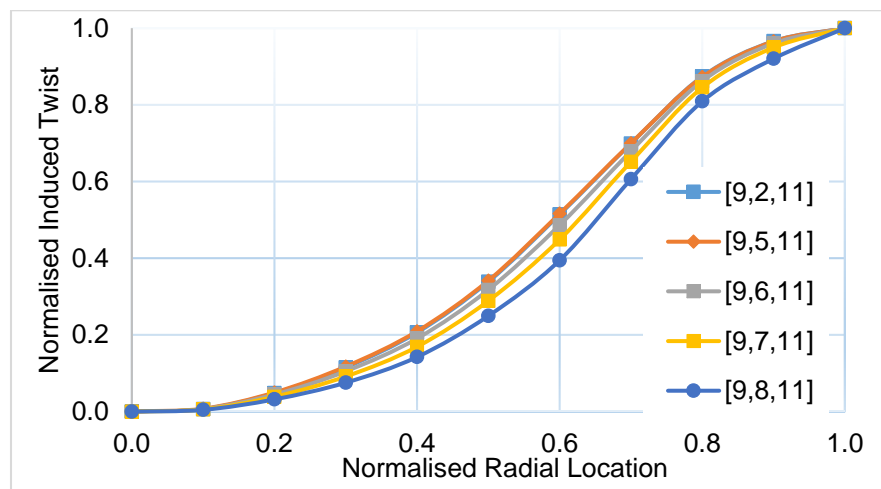


Figure 4.26.(b) Effect of linear variation of shell thickness distributions on β^* (NREL 5 MW Blade)

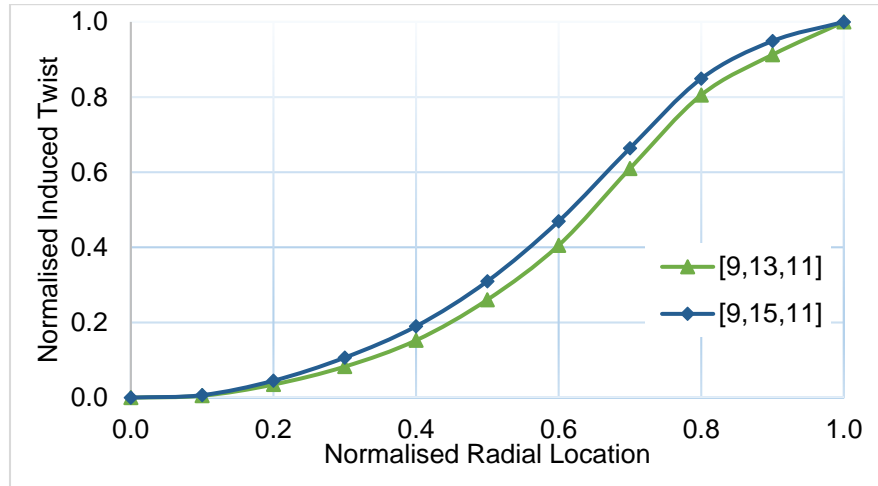


Figure 4.26.(c) Effect of polynomial variation of shell thickness distributions on β^* (NREL 5 MW Blade)

For shell thickness cases [9, 2/5/6/7/8, 11] all have linear gradient variation while cases [9, 13/15, 11] have polynomial slope with case [9,13,11] having a quadratic variation and case [9,15,11] having a third degree variation. The results shown in Figure (4.26.b) and Figure (4.26.c) show the normalised induced twist is a function of the variation of gradient of the shell thickness along the span of the blade.

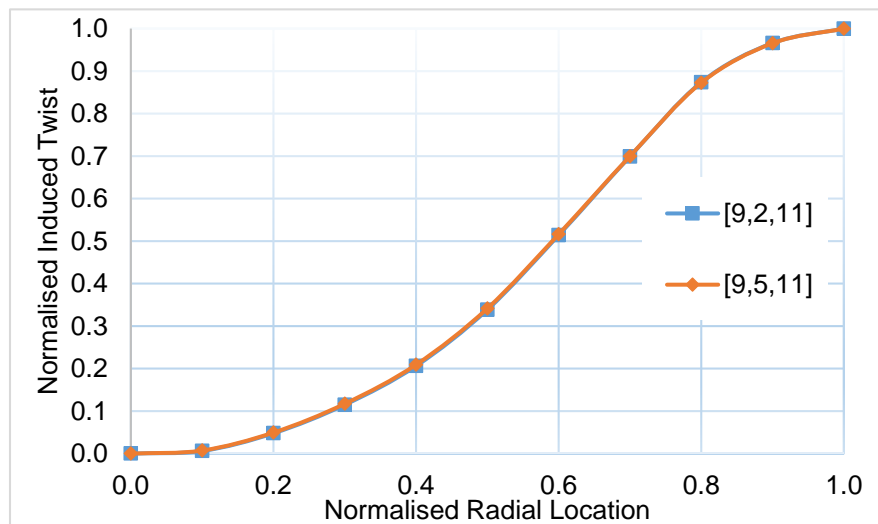


Figure 4.26.(d) Effect of chord-wise shell thickness variation on β^* (NREL 5 MW Blade)

Considering the effect of chord-wise shell thickness variation, using the same gradient of shell thickness distribution span-wise and chord-wise for Case [9,2,11]. The same span-

wise shell thickness distribution was used for Case [9,5,11] and result is shown in Figure (4.26.d), it can be observed that the chord-wise slope has no effect on the trend of the normalised induced twist for the same span-wise configuration.

4.4.6 Effect of the variation of Shell Thickness Distribution on β^* (AWT-27 Blade)

Using the AWT-27 blade, the effect of the variation of the shell thickness distribution along the span of the blade structure on the normalised induced twist is investigated. This investigation was done using layup configurations shown below:

Case [5,4,10]: Linear variation of shell thickness along the span and along the chord. This case has span-wise and chord-wise linear thickness variation of which at the root of the blade, chord-wise shell thickness distribution from the leading edge to the trailing edge varies from 28 mm to 20 mm and tip of the blade chord-wise distribution from leading edge to trailing edge varies from 22 mm to 14 mm.

Cases [5, 9/10/11/12, 10]: Linear variation of shell thickness along the span.

Case [5,14,10]: Quadratic variation of shell thickness along the span.

Case [5,16,10]: Third degree variation of shell thickness along the span.

Cases [5, 21/22/23/24, 10]: Uniform shell thickness along the span.

The blade configurations (layup, shell thickness distributions and fibre angle distributions) for these cases are shown in Table (4.5), (4.6) & (4.7).

Figure (4.27.a) shows that the trend of the normalised induced twist is a function of the variation of the shell thickness distribution along the span.

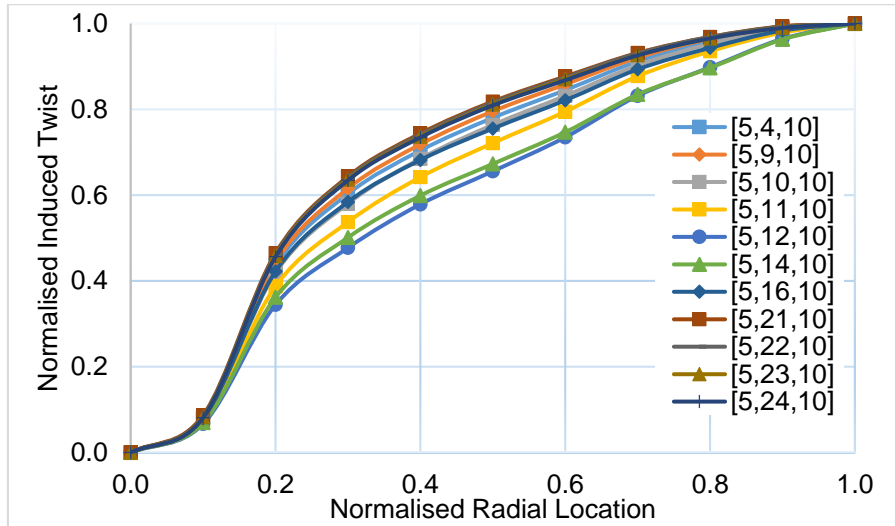


Figure 4.27.(a) Effect of variation of shell thickness distributions on β^* (AWT-27 Blade)

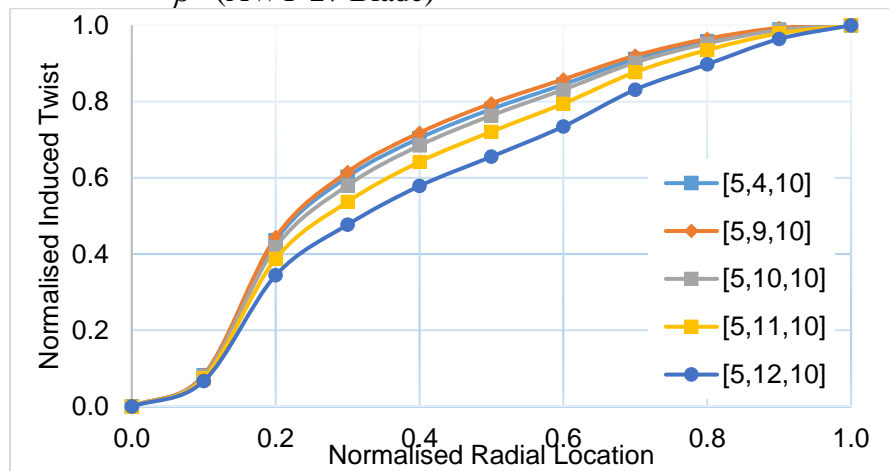


Figure 4.27.(b) Effect of linear variation of shell thickness distributions on β^* (AWT-27 Blade)

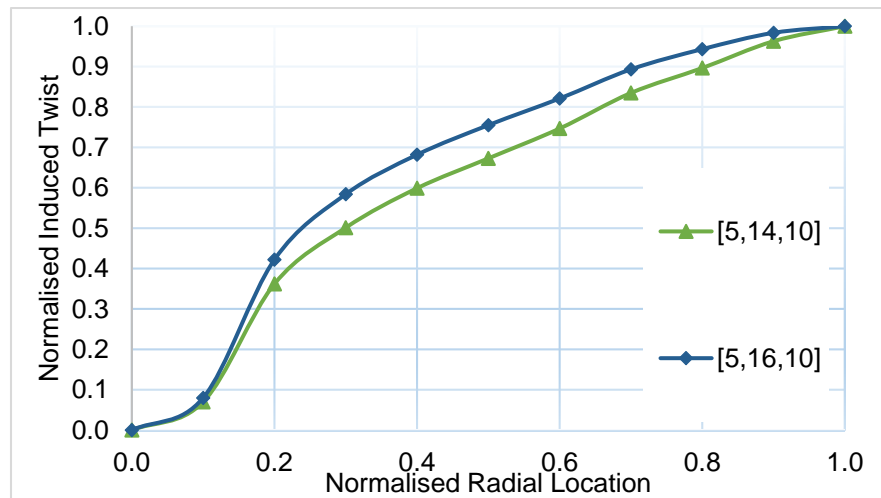


Figure 4.27.(c) Effect of polynomial variation of shell thickness distributions on β^* (AWT-27 Blade)

It could be observed from Figure (4.27.a) that the trend of the normalised induced twist is a function of the variation of the shell thickness distribution along the span.

Shell thickness cases [5, 4/9/10/11/12, 10] all have linear gradient variation while cases [5, 14/16, 10] have polynomial slope with case [5,14,10] having a quadratic variation and case [5,16,10] having a third degree variation. The results shown in Figure (4.27.b) & (4.27.c) show the normalised induced twist is a function of the variation of steepness of the shell thickness distribution along the span of the blade.

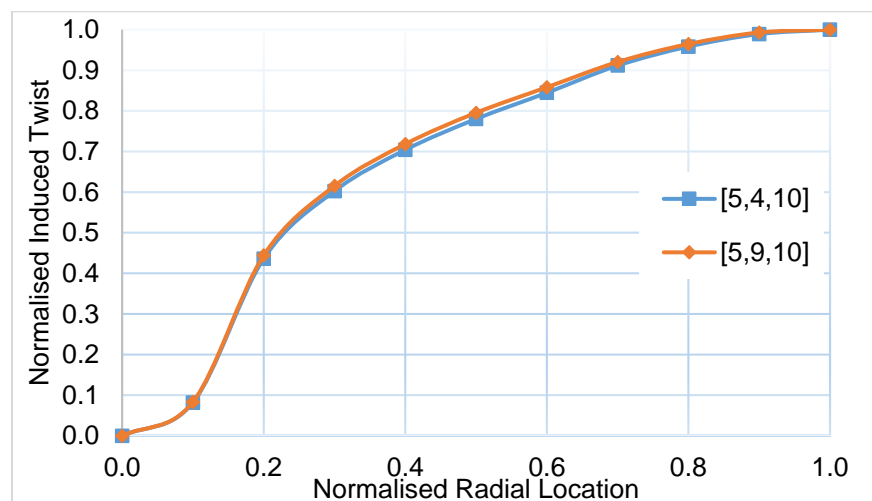


Figure 4.27.(d) Effect of chord-wise shell thickness variation on β^* (AWT-27 Blade)

Considering the effect of chord-wise slope, using the same gradient of shell thickness distribution span-wise and chord-wise for Case [5,4,10]. The same span-wise shell thickness distribution was used for Case [5,9,10] and result is shown in Figure (4.27.d), it can be observed that the chord-wise slope has no effect on the trend of the normalised induced twist for the same span-wise configuration.

4.4.7 Effect of the Shell Thickness on β^* (NREL 5 MW Blade)

The effect of the actual magnitude of the shell thickness on the normalised induced twist is investigated. It is examined using some cases [9, 17/18/19/20, 11] with uniform shell thickness distributions and uniform layup configurations in the blade structure. The actual shell thickness has an effect on the magnitude of the induced twist, which could be seen in Figure (4.28). Figures (4.29) shows that the actual shell thickness value for the uniform shell thickness along the span is not a determining factor for the normalised induced twist.

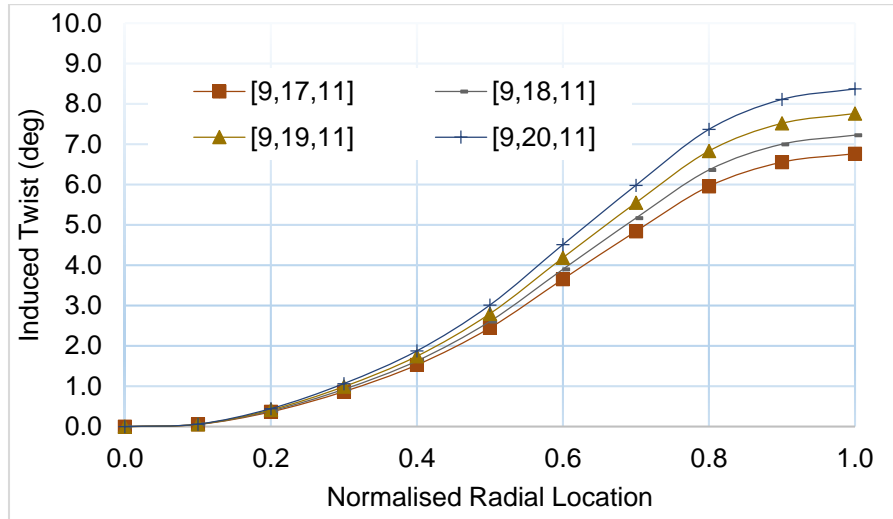


Figure 4.28. Effect of shell thickness on the induced twist (NREL 5 MW Blade)

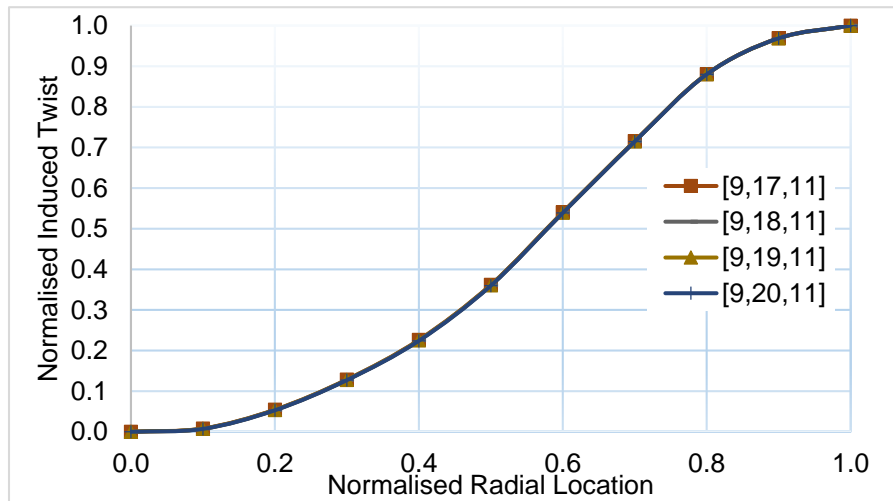


Figure 4.29. Effect of shell thickness on β^* (NREL 5 MW Blade)

4.4.8 Effect of the Shell Thickness on β^* (AWT-27 Blade)

The effect of the actual value of the shell thickness on the normalised induced twist is investigated. Cases [5, 21/22/23/24, 10] with uniform shell thickness distributions and uniform layup configurations in the blade structure are analysed. From the results, the actual shell thickness affects the magnitude of the induced twist, which could be seen in Figure (4.30). Figures (4.31) shows that the actual shell thickness value for the uniform shell thickness along the span is does not affect the trend of the normalised induced twist. The result is in accordance with the investigation of Zhang H [144].

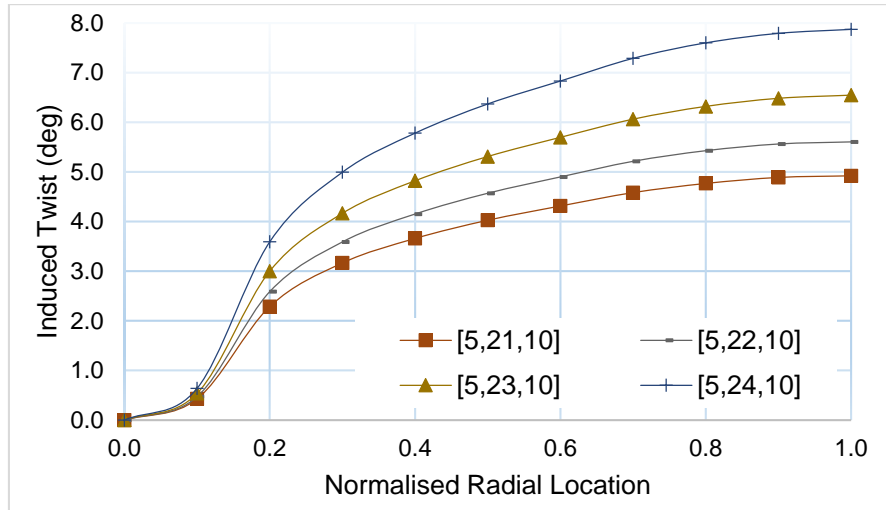


Figure 4.30. Effect of shell thickness on the induced twist (AWT-27 Blade)

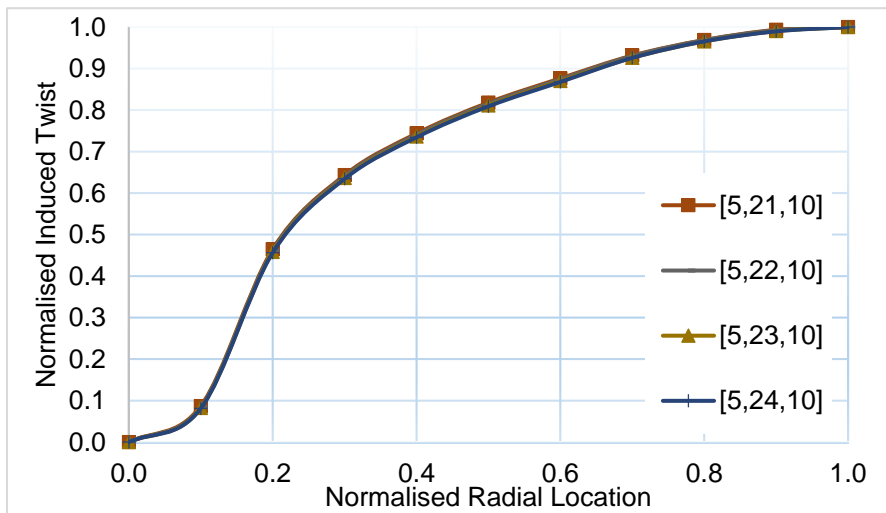


Figure 4.31. Effect of shell thickness on β^* (AWT-27 Blade)

4.5 Effect of Shear Webs on β^*

This section is to investigate the effect of shear webs on the normalised induced twist. This was carried out using carbon fibre considering no shear web case [4,2,11], single shear web case [5,2,11] and double shear webs case [9,2,11]. The case with the double shear webs has the webs at location 0.25 and 0.55 of the chord length while that of single shear web, the web is located at 0.38 of the chord length. The shear web thickness for these cases is 36 mm. Similarly, case [1,1,11], which has double shear webs of thickness 32 mm and located at 0.25 and 0.55 of the chord length likewise. Case [1,1,11] has the same shell thickness distribution with the aforementioned three cases but reduced number of layers.

These cases were analysed, and the normalised induced twist is shown in Figure (4.33). The Shear webs effect illustrated in Figure (4.32) is of mechanical advantage like influence on the torsional resistance of the blade, which, has little effect on the magnitude of the induced twist. It can be seen from the plots that the shear webs do not have any effect on the trend of the normalised induced twist of the blade.

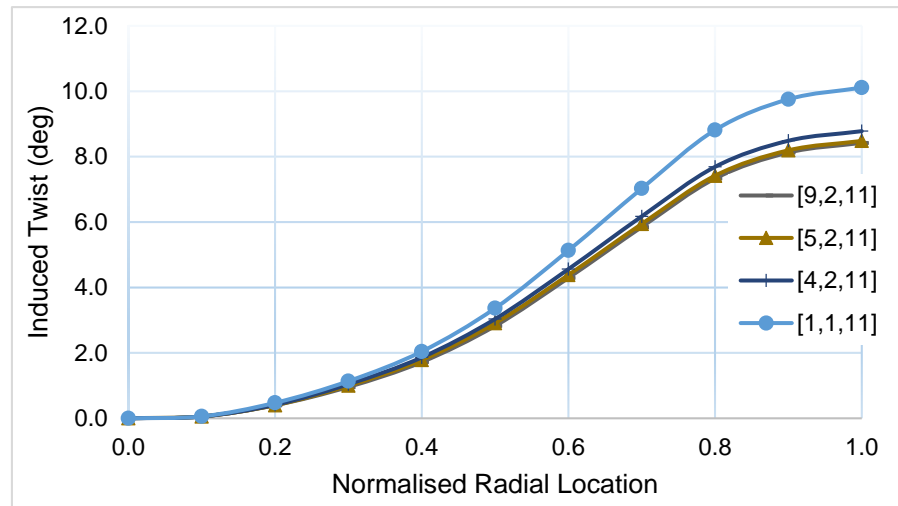


Figure 4.32. Effect of shear webs on the induced twist (NREL 5 MW Blade)

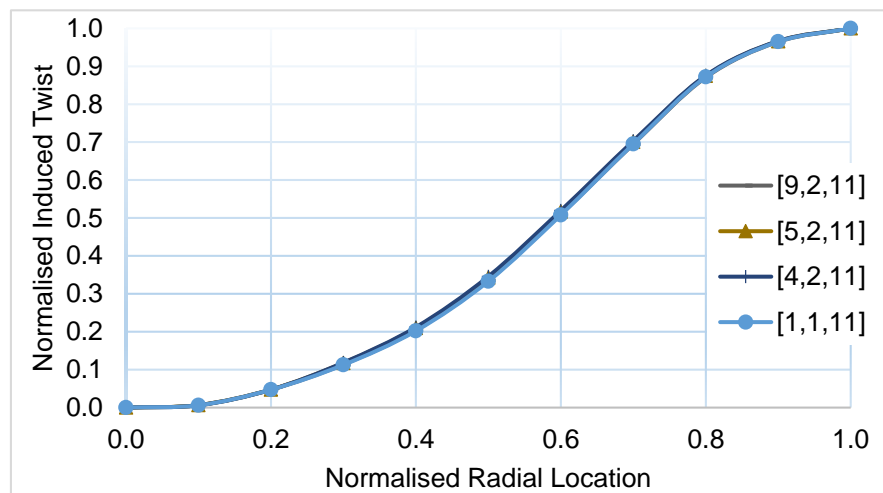


Figure 4.33. Effect of shear webs on β^* (NREL 5 MW Blade)

4.5.1 Effect of Fibre Angle variation distribution along the span on β^* (NREL 5 MW Blade)

From the previous study, section (4.4.1), it was shown that the fibre angle as long as it remains constant along the span of the blade [see Figure (4.13), Figure (4.14.b) & Figure (4.15.b) above], does not have any effect on the trend of the normalised induced twist. This

analysis is to investigate the effect of varying the fibre angle along the blade span on the normalised induced twist.

The equations for the fibre angle distributions are shown in Table (4.5), (4.6) & (4.7), giving different gradient of fibre angle variation distributions along the span of the blade. Considering linear and polynomial (quadratic and third degree) fibre angle variation, these cases are analysed [9,17, 25/20/22/24/21/23]. The results are shown in Figure (4.34). It can be seen from Figure (4.35.a) that the variation of the fibre angle distribution along the span of the blade has considerable effect on the trend of the normalised induced twist of the blade. This effect of the fibre angle variation on the normalised induced twist is expected because the elastic coupling of the configuration is extremely dependent on the fibre angle.

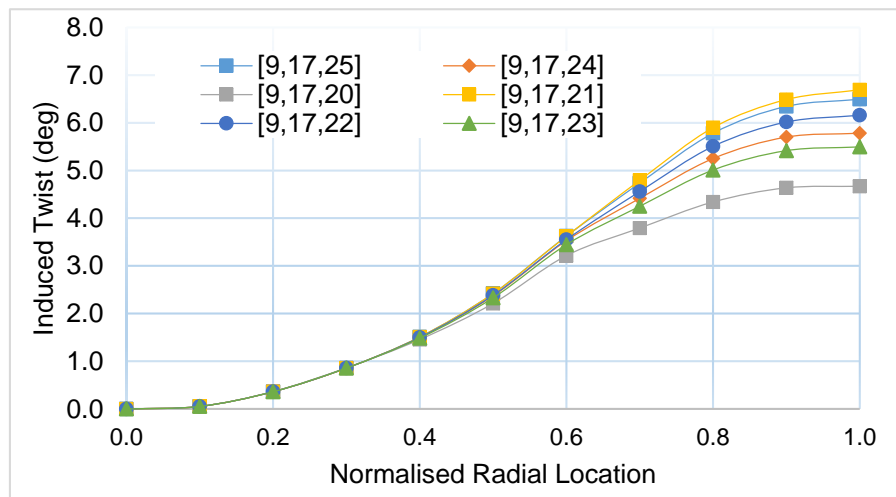


Figure 4.34. Effect of variation of fibre angle distribution on the induced twist (NREL 5 MW Blade)

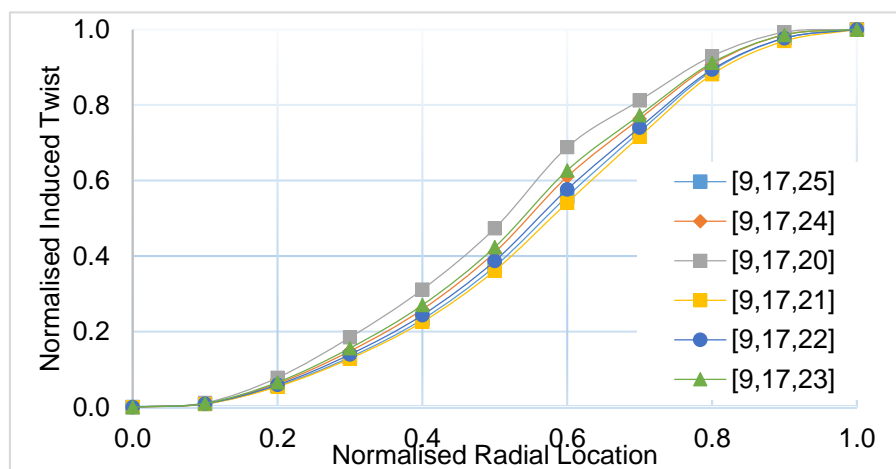


Figure 4.35.(a) Effect of variation of the fibre angle distribution on β^* (NREL 5 MW Blade)

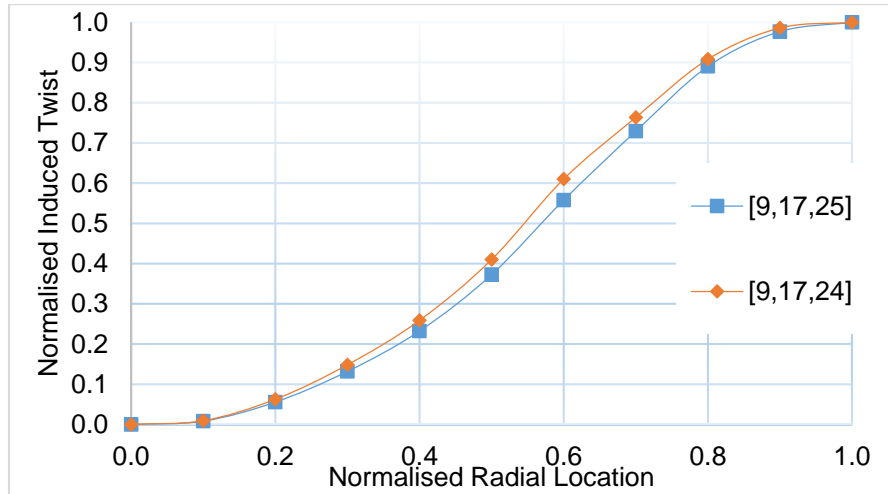


Figure 4.35.(b) Effect of polynomial variation of fibre angle distribution on β^* (NREL 5 MW Blade)

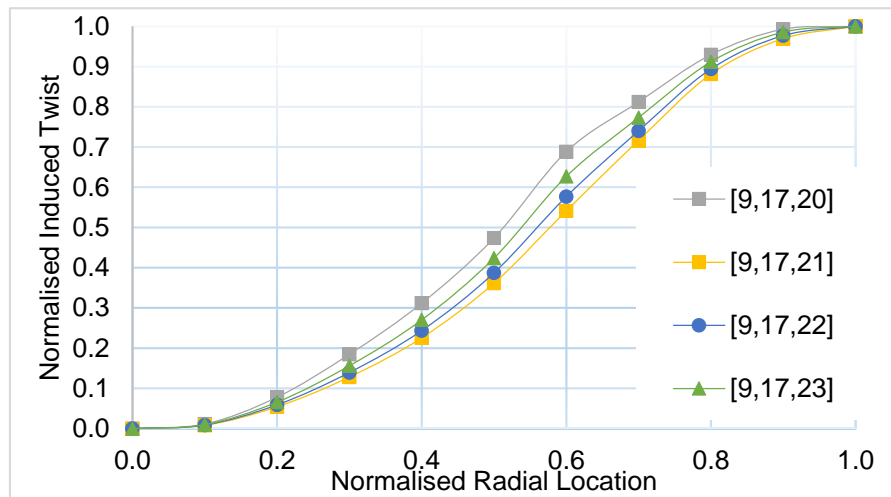


Figure 4.35.(c) Effect of linear variation of fibre angle distribution on β^* (NREL 5 MW Blade)

A further interesting observation from the results when plots for the linear and polynomial angle variation were separately carried out, the degree of the distribution steepness influences the value of the normalised induced twist [Figures (4.35.b) & (4.35.c)].

Similarly, cases of varying the fibre angle and shell thickness distribution along the blade span were carried out to observe the trend and to give proper insight in the general analytical model proposition. These cases are analysed [9, 8/15, 22] and the results are shown in the Figure (4.35.d).

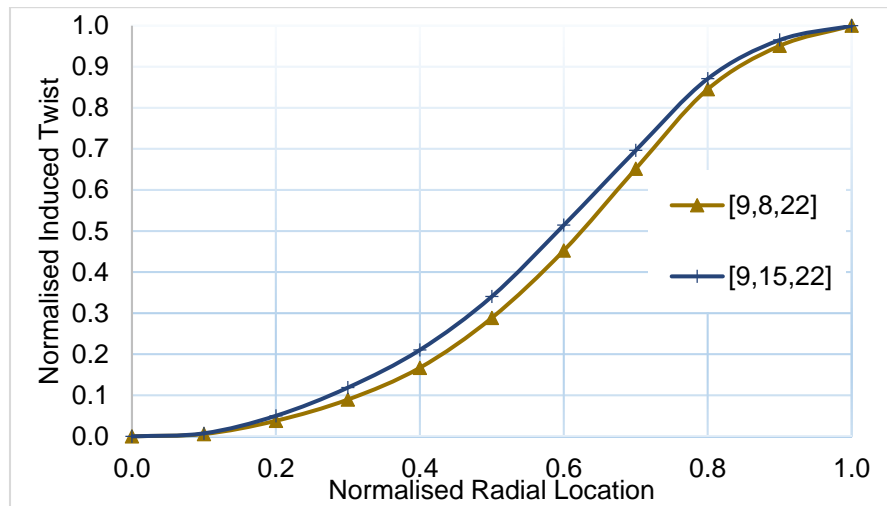


Figure 4.35-(d) Effect of varying shell thickness and varying fibre angle distribution on β^* (NREL 5 MW Blade)

4.5.2 Effect of Fibre Angle variation distribution along the span on β^* (AWT-27 Blade)

From the previous study section (4.4.2), it was shown that the fibre angle as long as it is uniform along the span of the blade [see Figures (4.19) to (4.21) above], does not have any effect on the trend of the normalised induced twist. This study is to investigate the effect of varying the fibre angle along the blade span on the normalised induced twist for an AWT-27 blade.

The equations for the fibre angle distributions are shown in Table (4.5), (4.6) & (4.7), giving different gradient of fibre angle variation distributions along the span of the blade. Considering linear and polynomial (quadratic and third degree) fibre angle variation, these cases [5,21, 20/21/22/23/24/25] were analysed. The results for these are shown in Figure (4.36). It can be understood from Figure (4.37.a) that the variation of the fibre angle along the span of the blade has considerable effect on the trend of the normalised induced twist of the blade. This effect of the fibre angle variation on the normalised induced twist is expected because the torsional stiffness of the material is influence by the fibre angle and consequently making the elastic coupling of the configuration to be extremely dependent on the fibre angle. Therefore, having varying angle along the span gives varying stiffness in the blade configuration.

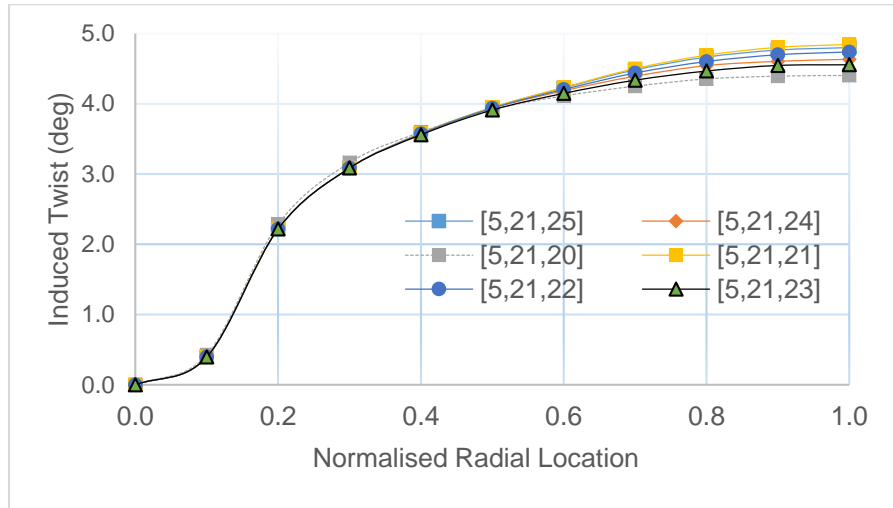


Figure 4.36. Effect of variation of fibre angle distribution on the induced twist (AWT-27 Blade)

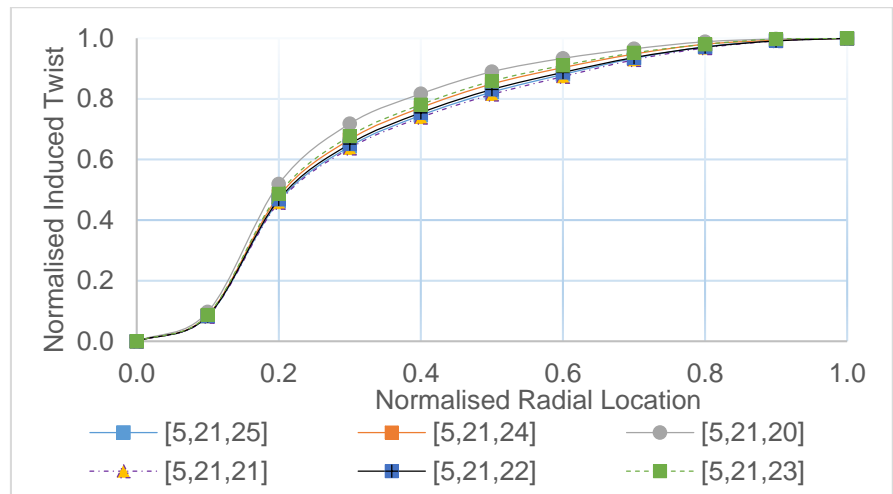


Figure 4.37.(a) Effect of variation of fibre angle distribution on β^* (AWT-27 Blade)

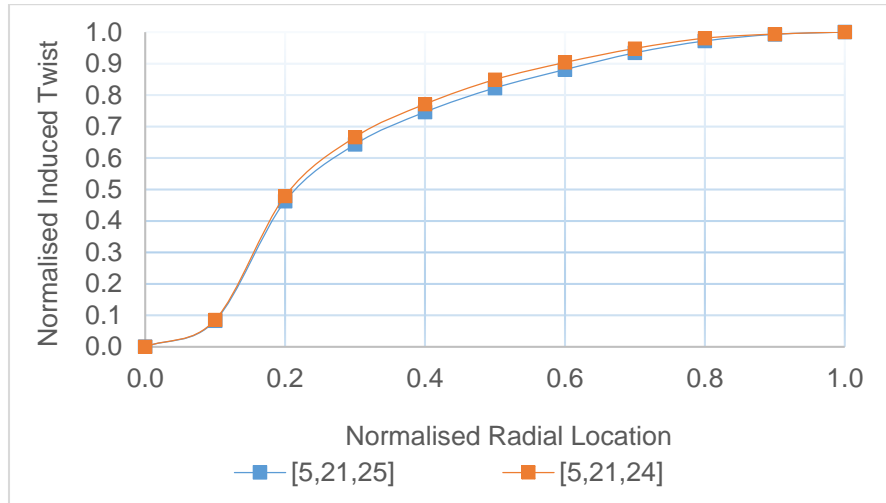


Figure 4.37(b) Effect of polynomial variation of fibre angle distribution on β^* (AWT-27 Blade)

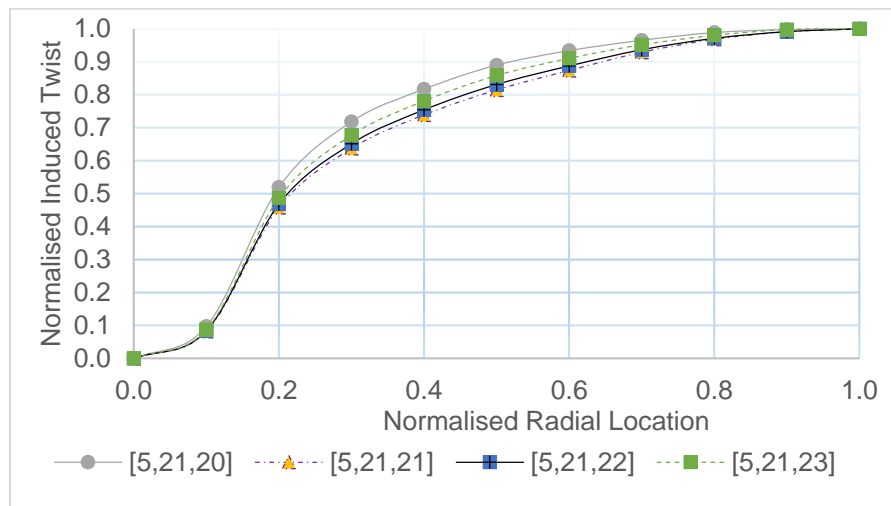


Figure 4.37(c) Effect of linear variation of fibre angle distribution on β^* (AWT-27 Blade)

A further interesting observation from the results like that using the NREL 5 MW blade, plotting the linear and polynomial variation results separately, the gradient of the variation influences the value of the normalised induced twist [Figures (4.37.b) & (4.37.c)].

Also studying cases of varying fibre angle and shell thickness distribution along the blade span to observe the trend, was carried out using cases [5,12,22] & [5,16,22]. The result is shown in the Figure (4.37.d). This gives a good situation in proposing the general analytical model.

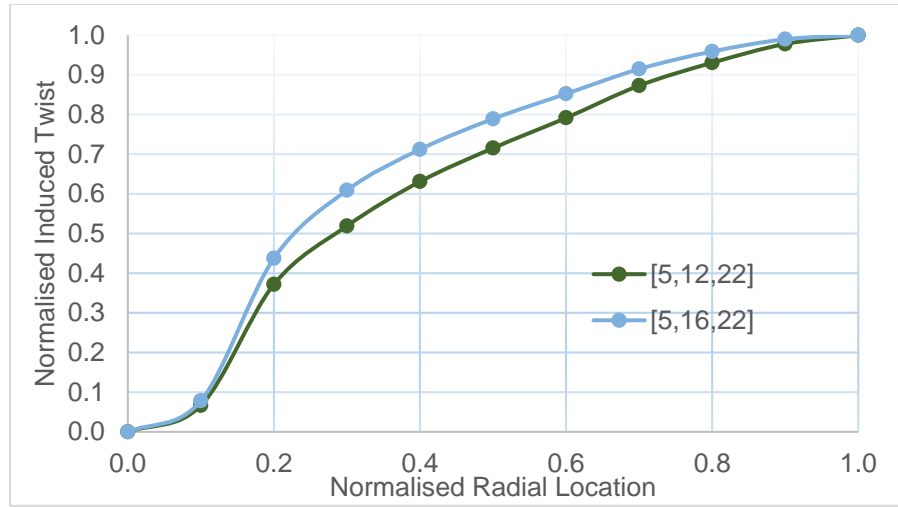


Figure 4.37(d) Effect of varying shell thickness and varying fibre angle distribution on β^* (AWT-27 Blade)

4.6 Extended Analytical Model for the blade Normalised Induced Twist

Using the data generated in previous sections, the analytical model Equation (4.15) for predicting the normalised induced twist in an adaptive blade with uniform shell thickness distributions along the blade span is used to propose an extended analytical model. This model could be used to predict the adaptive blade normalised induced twist with variable shell thickness and variable angle distribution along the span blade.

Relationships of the fibre angle and shell thickness to the behaviour of the normalised induced twist need to be established in order to propose the analytical model for predicting the normalised induced twist.

From stress-strain relations for a lamina of arbitrary orientation according to Jones [159], the apparent orthotropic moduli like the modulus of rigidity for an orthotropic lamina stressed at fibre angle to the principal material directions is a function of the angle as seen in Equation (4.16).

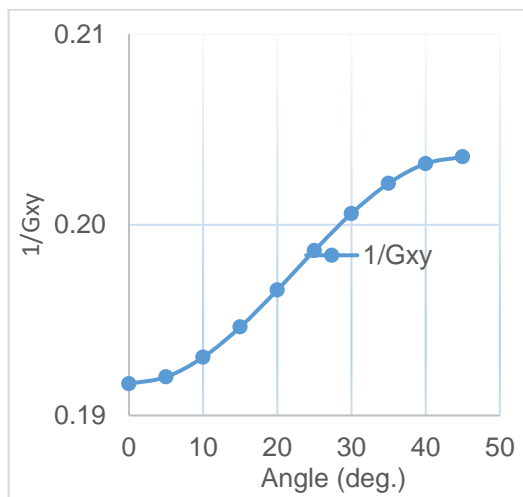
$$\frac{1}{G_{xy}} = 2 \left[\frac{2}{E_1} + \frac{2}{E_2} + \frac{4\nu_{12}}{E_1} - \frac{1}{G_{12}} \right] \sin^2 \theta \cos^2 \theta + \frac{1}{G_{12}} (\sin^4 \theta + \cos^4 \theta) \quad (4.16)$$

The modulus of rigidity determines the torsional stiffness of the blade, in order to establish the relationship and propose the general analytical model this equation will be analysed.

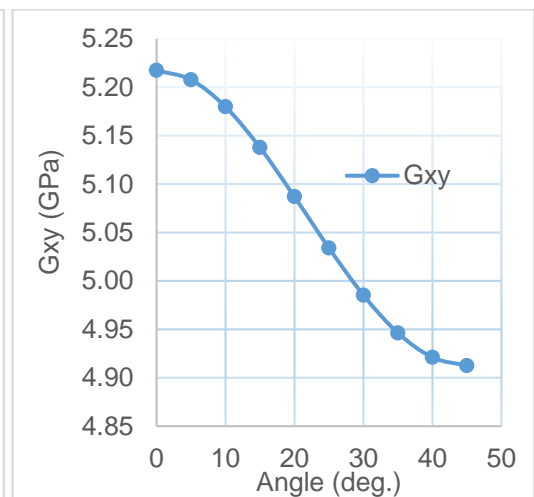
Considering the two terms of Equation (4.16), taking the first part to be term A and the second part to be term B as shown below; Figures (4.38.a) to (4.38.j) were plotted to establish the relation of the two terms to the induced twist.

$$\text{A: } 2 \left[\frac{2}{E_1} + \frac{2}{E_2} + \frac{4\nu_{12}}{E_1} - \frac{1}{G_{12}} \right] \sin^2 \theta \cos^2 \theta$$

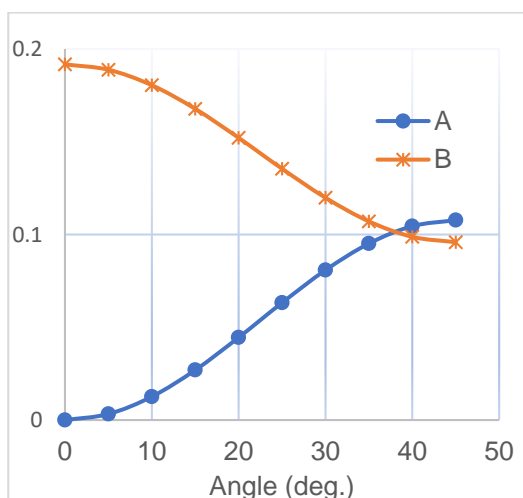
$$\text{B: } \frac{1}{G_{12}} (\sin^4 \theta + \cos^4 \theta)$$



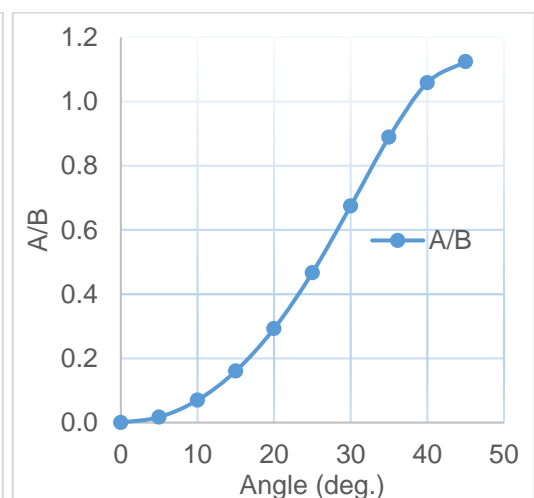
(a)



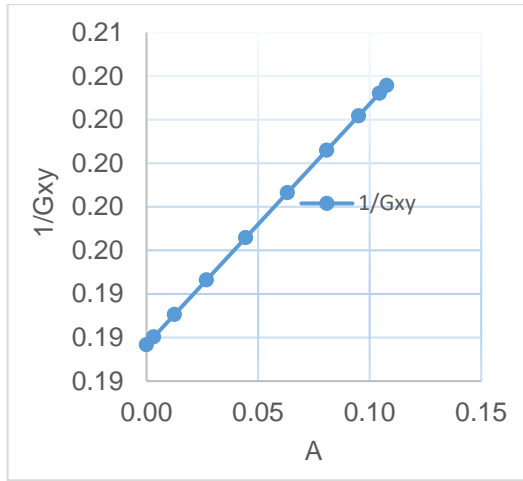
(b)



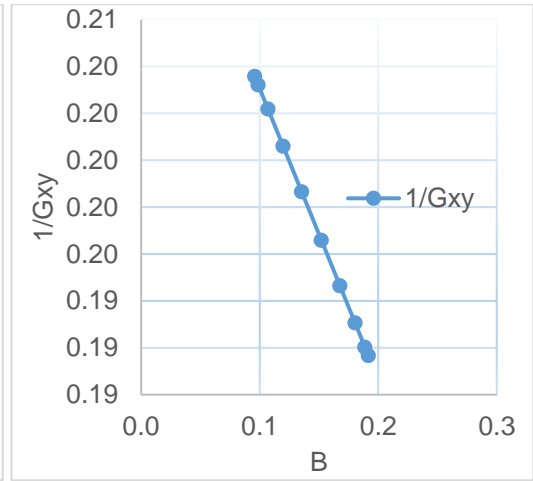
(c)



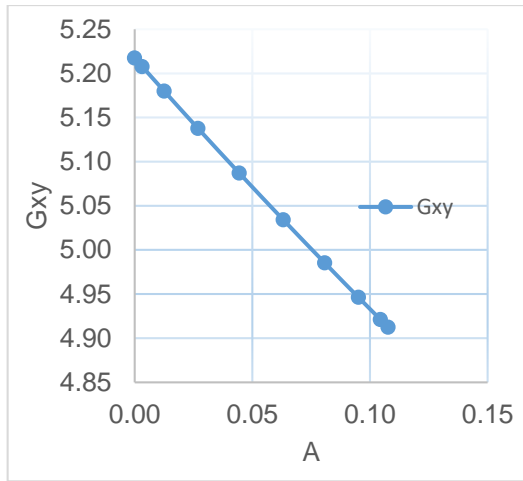
(d)



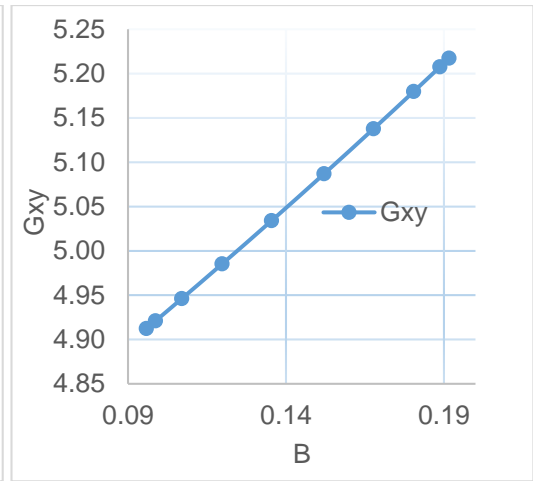
(e)



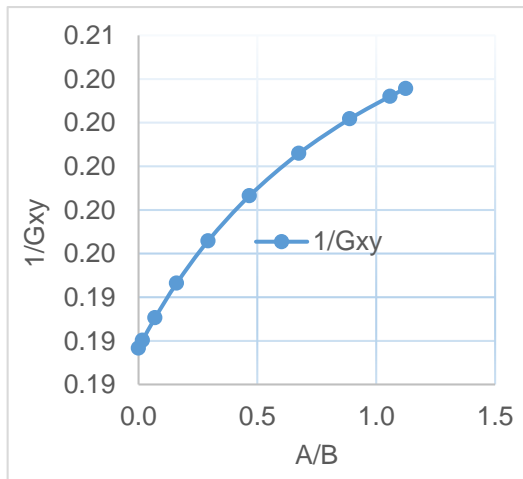
(f)



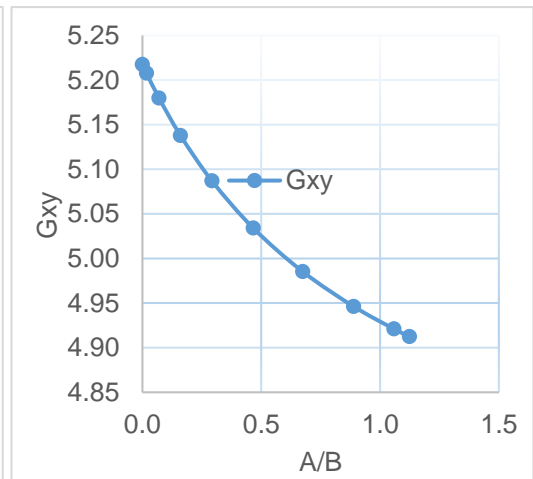
(g)



(h)



(i)



(j)

Figure 4.38.(a-j) Torsional stiffness/Fibre Angles relations

$$\theta_i = \frac{TL}{GJ} \quad (4.17)$$

where

θ_i = angle of twist in radian

T = applied torque

L = length of beam

J = torsional constant

The shear modulus G , is directly proportional to the torsional stiffness and also knowing from Equation (4.17), G is inversely proportional to the angle of twist. From the plots relationship, Figure (4.38.g), term A is inversely proportional to the torsional stiffness. Figure (4.38.h), term B is directly proportion to the torsional stiffness and from Equation (4.17), the torsional stiffness is inversely proportional to the elastic induced twist. Furthermore, it could be seen in Figure (4.38.j), the ratio of A/B is inversely related to the torsional stiffness, which indicates the stronger effect of term B on the torsional stiffness. It shows as the fibre angle increases, term B reduces and the torsional stiffness decreases.

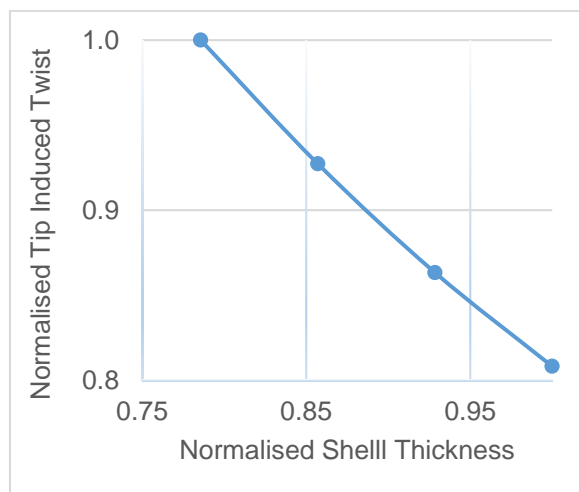


Figure 4.39. Normalised Tip Induced Twist

To determine the shell thickness relationship to the normalised induced twist, Figure (4.39) is plotted for the normalised tip induced twist for different shell thicknesses. It can be seen

that the normalised tip induced twist is linearly inversely proportional to the normalised shell thickness.

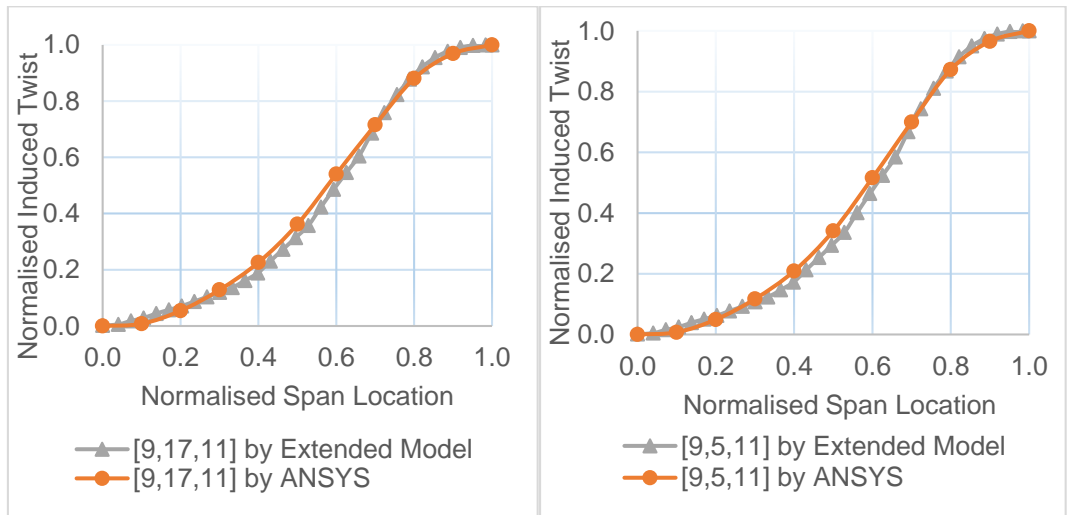
With these relationships established, the analytical model for the prediction of the normalised induced in an adaptive blade with variable shell thickness and fibre angle along the span is proposed.

$$\beta^*(r^*) = \frac{\int_0^{r^*} \frac{M^*(r^*)}{t_{\max}^3(r^*) t_s^*(r^*) (\sin^4 \theta + \cos^4 \theta)} dr^*}{\int_0^1 \frac{M^*(r^*)}{t_{\max}^3(r^*) t_s^*(r^*) (\sin^4 \theta + \cos^4 \theta)} dr^*} \quad (4.18)$$

where

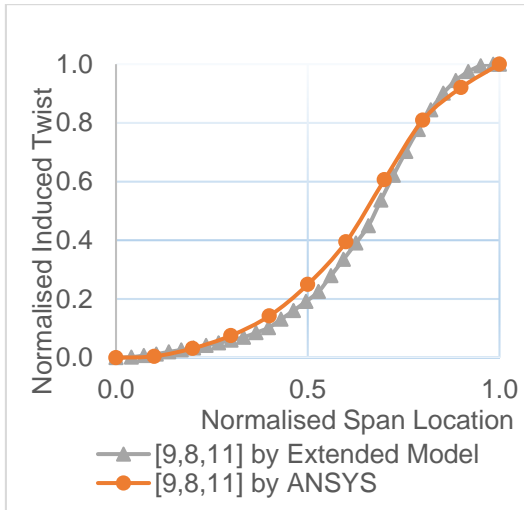
$$t_s^* = t_s / t_{s,\max}$$

In order to investigate the performance of the proposed analytical model of Equation (4.18), the normalised induced twist predicted by this model has been compared with the numerical results obtained by ANSYS for several sets of blade configurations. Results are shown in Figures (4.40.a) to (4.40.j) for NREL 5 MW Blade and Figures (4.41.a) to (4.41.j) for AWT-27 Blade.

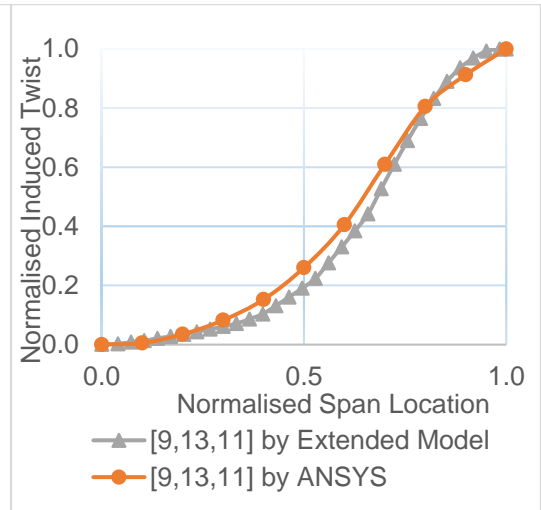


(a)

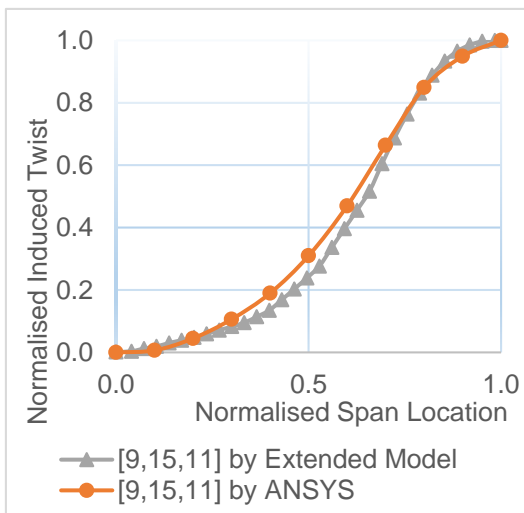
(b)



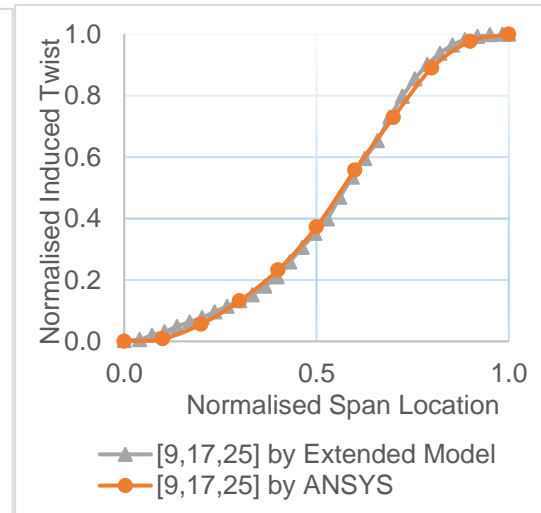
(c)



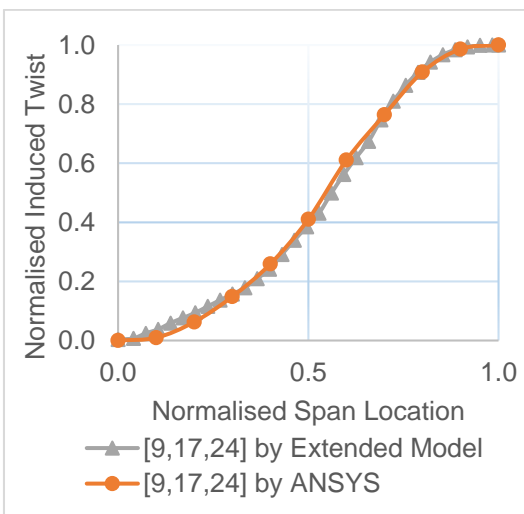
(d)



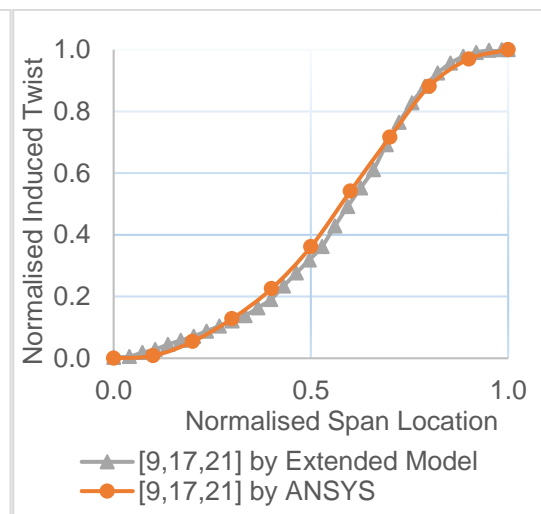
(e)



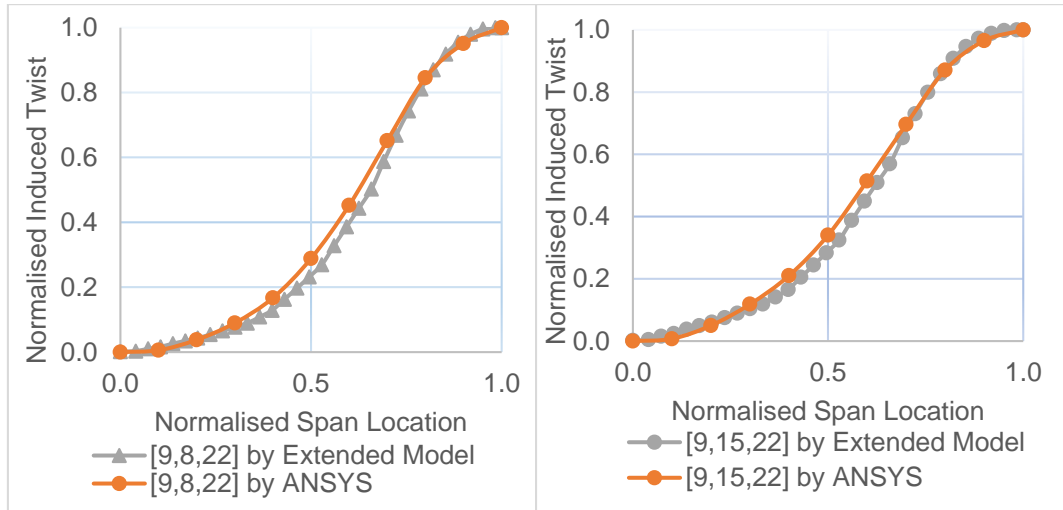
(f)



(g)



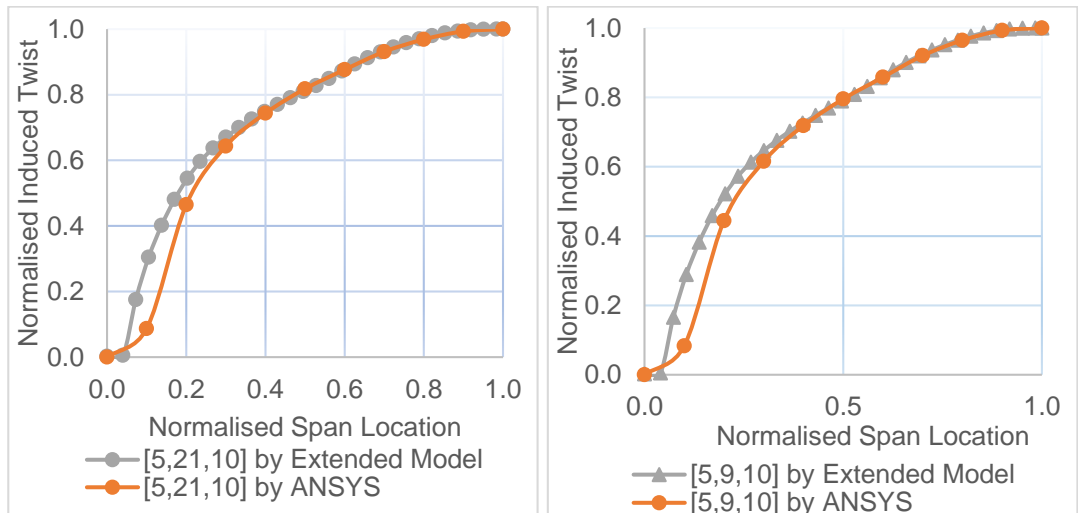
(h)



(i)

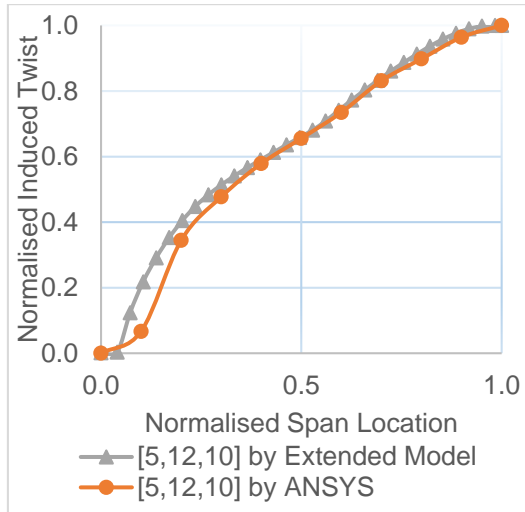
(j)

Figure 4.40.(a-j) Predicted Normalised Induced twist by Equation (4.18) and ANSYS (NREL 5 MW Blade)

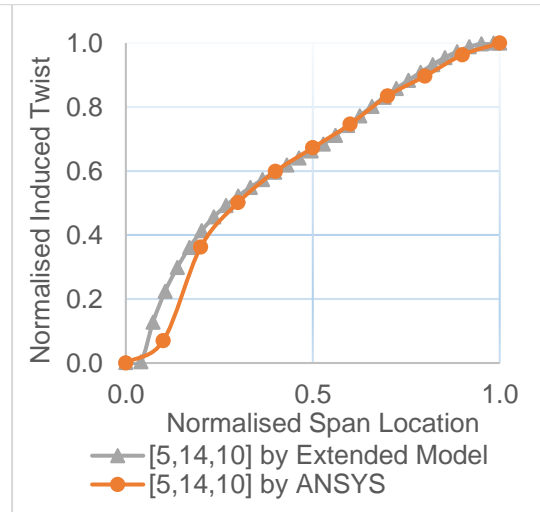


(a)

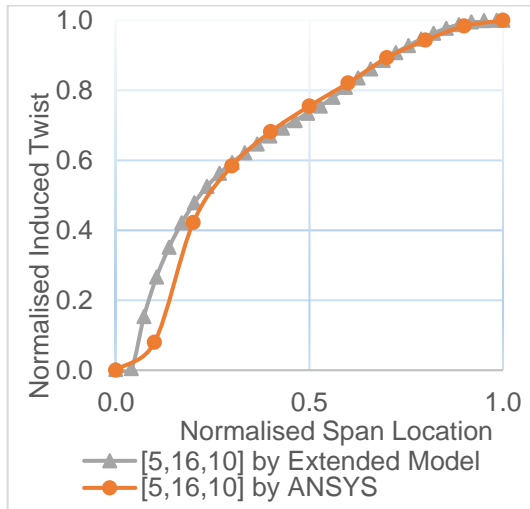
(b)



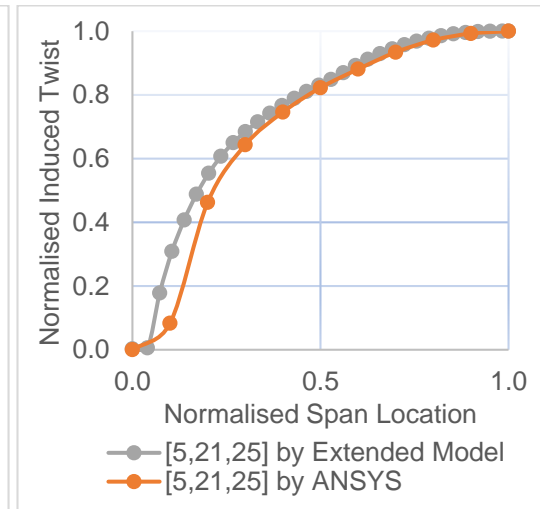
(c)



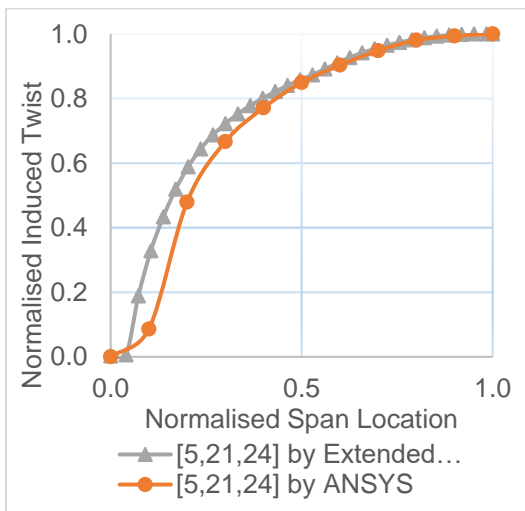
(d)



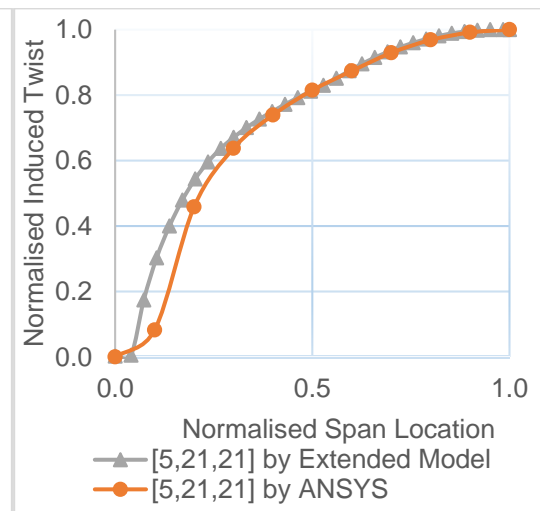
(e)



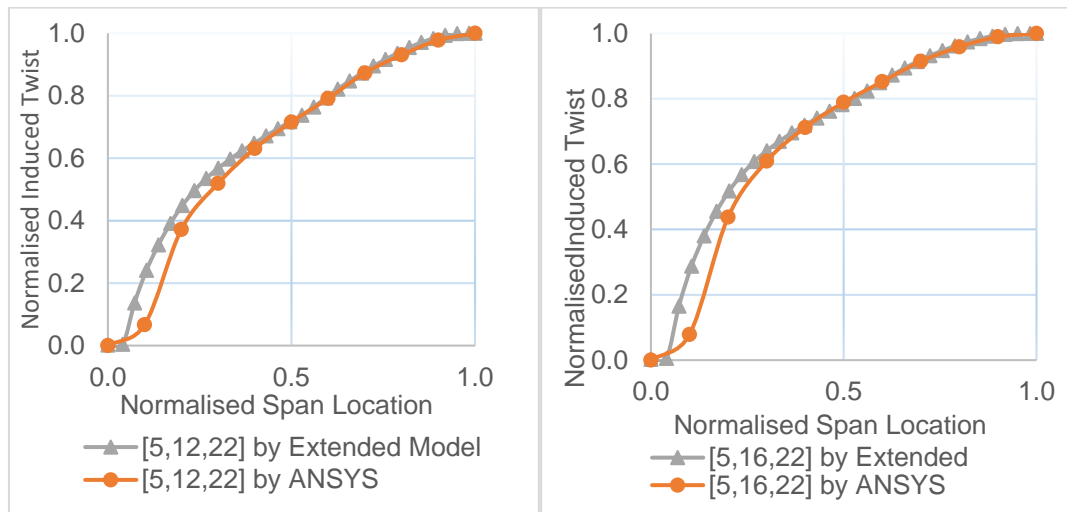
(f)



(g)



(h)



(i)

(j)

Figure 4.41.(a-j) Predicted Normalised Induced twist by Equation (4.18) and ANSYS (AWT-27 Blade)

As could be seen from the graphs, for the NREL 5MW, Figure 4.40 (a-j), there is slight difference in the values obtained using ANSYS and those obtained using the analytical model with maximum percentage error difference of 4.7% for the normalised induced twist. For the AWT-27, Figure 4.41 (a-j), the percentage error looks massive between the span region close to the root of the blade but the actual value of induced twist in this region of the blade is insignificant compared to the induced twist at the tip of the blade. The induced twist in this region is fraction of a degree. The actual induced twist values in this blade region are very small, thus difficult for ANSYS to accurately capture the induced twist. This does not have significant impact on the result because the deviation is towards the root of the blade where the blade is not aerodynamically active. The most effective part of blade is about one third of the blade towards the tip.

4.7 Conclusion

The purpose of this research work is to make the adaptive blade design more efficient and flexible by decoupling the aerodynamic and structural design by treating the elastic coupling induced twist as a variable. It is well known that span-wise distribution of the wind turbine adaptive blade induced twist due to bending/twist elastic coupling significantly affects its aerodynamic performance. In decoupled adaptive blade design, when the tip induced twist is treated as a design parameter, it is easy to obtain the induced twist distribution by use of normalised induced twist. Then investigating the effect of the

magnitude of shell thickness and fibre angle on the normalised induced twist is necessary and critical for decoupled adaptive blade design.

In this research work, the pattern of normalised induced twist for several combinations of shell thickness and layup configuration is investigated. The investigation is used to propose an analytical model for predicting the normalised induced twist in adaptive blades with variable shell thickness distribution and variable fibre angle distribution along the blade span based on the simple model proposed by Maheri et al [135]. The results obtained from numerical analysis using ANSYS are compared to those obtained using the proposed analytical model and it shows that the model is capable of predicting the normalised induced twist for wind turbine blade with variable shell thickness and variable fibre angle with reasonable accuracy.

From the results obtained, the following conclusions can be drawn:

- The normalised induced twist of the wind turbine blade is not a function of the shell thickness actual value and fibre angle if the layup configuration and thickness remain constant along the blade span.
- For constant layup configurations but variable distribution of shell thickness along the blade span, the normalised induced twist trend is a function of the variation of thickness slope rather than its actual value. In other words, it is the rate of the variation of shell thickness that decisively affects the trend of the normalised induced twist not the actual value of shell thickness.
- Normalised induced twist is not a function of the material and shear webs.

5 Adaptive Blades: Dynamic Analysis

5.1 Introduction

Wind turbine blade size is constantly increasing because the energy captured by the wind turbine is proportional to the swept area of the rotor blade. Designing of the wind turbine to have less weight is very vital to improve cost-effectiveness of the turbine. Resulting to having more slender, flexible and lighter rotor blades. Though the turbine power performance is affected due to the slenderness and flexibility of the blades making aeroelastic deformation to be inevitable resulting to vibratory loads [197]. These vibratory loads may induce adverse instability issues that could affect the turbine operational life [198]. It is therefore vital to have a good understanding of the aeroelastic behaviour of the turbine blades such that they are designed to be more efficient and reliable energy capturing system.

Wind turbine blades are the most expensive part and so their design is very critical to attain effective, robust and reliable systems. The blades have intricate geometry and should ensure material layup configurations that could endure severe loads over a long period of time. The blades normally receive stochastic loads of wind over a typical lifetime of approximately 20 years, making the blade buckling resistance, stiffness, flexibility and strength very important. The wind turbine blades rotate most of the time resulting to deflecting into different discrete patterns or vibration shapes as they are being acted on by different forces.

To comprehend and picture the intricate ways in which the blade deflects – for instance when and how the blade bends and also when and how the blade twists, the shapes are resolved into unique modes of vibration, each mode describing a distinctive vibration form. These modes have their associated natural frequencies and value of damping. The natural frequency, the mode shape and the value of damping are collectively known as the modal parameters. The modal properties of mechanical structures are directly altered by their physical properties. So, when there is any change in the physical properties of the structure, this will result to a change in its modal parameters. The natural frequencies of the structure are determined by its fundamental characteristics, such as the geometry, stiffness and density of the structure.

The value of damping has huge effect on the vibration decaying period. Thus, the blade response of a forced vibration will decay quicker when the value of damping is higher.

Excessive vibrations can considerably decrease the life span of the structure and which need to be circumvented. The wind turbine blades are severely exposed to wind loads, so it is important to determine the frequencies at which the vibration occur and understand the consequences of the vibration. In order to do this, a comprehensive knowledge of the different modes of the blade when excited during operation is essential. The natural frequencies which are associated with the low frequencies modes are of great interest to researchers and manufacturers of wind turbine. From research, it could be seen that the first natural frequencies of long wind turbine blades are very low even as low as fraction of 1 Hz, so to be able to successfully characterise them is important. The wind load excites the blade torsional modes as the blade cuts through the air thus good understanding of the blade dynamic response is crucial. This makes the knowledge of the lower torsional modes to designing a robust and safe pitch varying mechanism to be very important.

Modal analysis is the most common process used to provide the dynamic characteristics of mechanical systems, and it produces very descriptive and easy interpretable results and thus, helps in understanding of the comprehensive dynamic behaviour of the systems. It is used to analyse natural frequencies, and vibration modes of mechanical structures.

The problems of aeroelastic instability is becoming an increasing concern and of importance due to the increasing size of the wind turbines blades. The blade design process needs to include investigation of the dynamic stability of the blade in order to maintain these large blades in a stable mode. Therefore, modal analyses are performed with a focus on dynamic behaviour of the blade when adaptive blade is used. It has been established that the damping is significantly influenced by variations of the torsional stiffness.

5.2 Aeroelasticity

Aeroelasticity is now been considered as an important topic for wind turbine blade design. Therefore, there is need of aeroelastic modelling of wind turbine blades. As the size of wind turbine blades is increasing in order to increase the power capture, this reduces the cost of wind power generation in terms of levelized cost of energy (£/kWh) (LCOE) [199]. However, the larger the size of the blades, the more significant the aeroelastic adverse effects become of concern. Aeroelasticity which is the science of the interactions between aerodynamic loads, inertial dynamics, and elastic deflections that occur when a flexible

structure is exposed to fluid flow is one of the critical issues for wind turbine with longer and more flexible blade. Aeroelasticity is principally concerned with the physical phenomena which involve important reciprocal interaction between aerodynamic forces, inertial, and elasticity of the non-rigid body [200]. The interactions can be seen in Figure (5.1) below using the Collar Aeroelastic Diagram

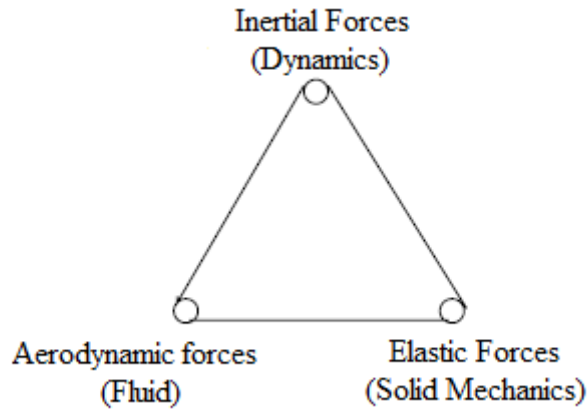


Figure 5.1. Collar Aeroelastic Diagram [201]

Most aeroelastic phenomena are of an adverse effect, resulting to design effectiveness loss or even at times colossal structural failure. Aeroelasticity effects could be catastrophic to the wind turbine; thus, it is important to ensure that wind turbine blades are designed taking into consideration the instabilities cause by aeroelasticity. Mathematically, aeroelasticity can be represented as shown in Equation (5.1).

$$M\ddot{x}(t) + C\dot{x}(t) + Kx(t) = f_a(v_\infty, \dot{x}(t), x(t)) + f_e(t) \quad (5.1)$$

where M, C and K are the dynamic properties of the system in terms of structural mass, damping and stiffness respectively. The term $f_a(v_\infty, \dot{x}(t), x(t))$ represents the aerodynamic loads on the structure, which depends on the airspeed v_∞ and motion of the body while $f_e(t)$ represents the external forces which are independent of the structural motion, for example the turbulent components of the wind due to its stochastic nature [201].

For wind turbines, the controls also have significant influence in the aeroelastic stability, so it will be reasonable to consider the control forces as a player in the forces interaction. Taking into cognisance the control forces in the aeroelastic interaction, the Collar aeroelastic diagram can be modify as shown in Figure (5.2) [202].

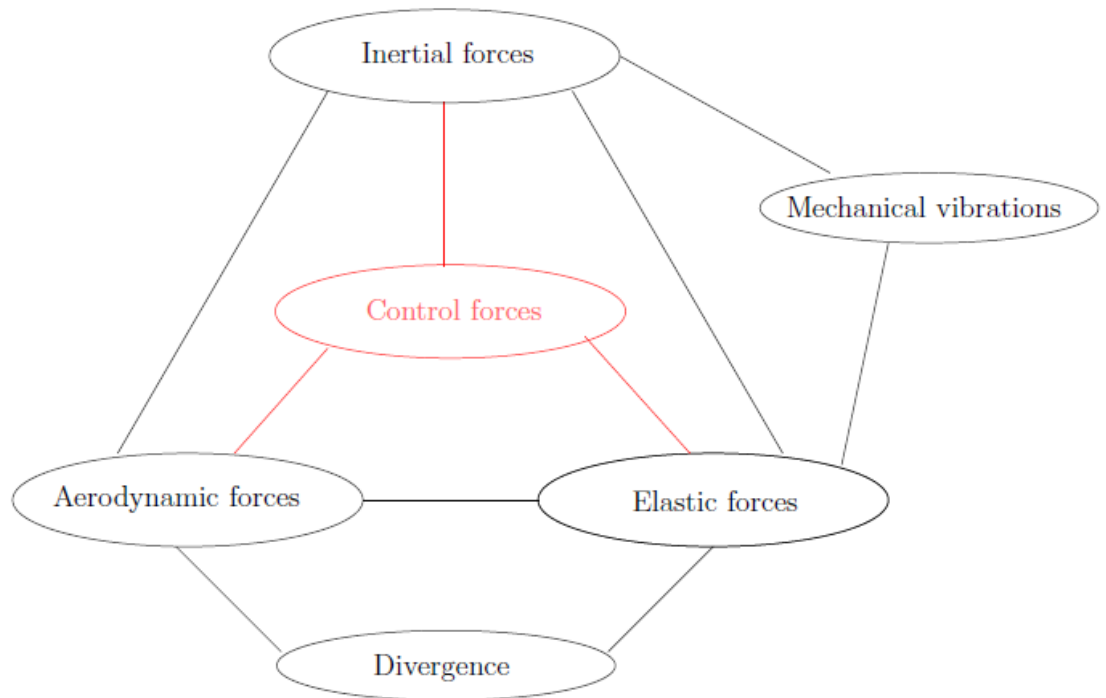


Figure 5.2. The Collar Triangle modified with the control forces added [202]

The aerodynamic forces acting on these structures depend on the relative velocities of the air the structure is exposed to. As forces are exerted on the structure, the structure is deformed which result to shape change due to the elastic bending and twisting consequently changing the angle of attack, therefore, affecting the aerodynamic forces. This now has a reciprocating effect with the resulting aerodynamic forces producing the deformation and the velocity of the structure as a cycle. There is significant mutual interaction role by inertial forces with the aerodynamic forces, elastic forces and the resulting accelerations. The forces interaction could produce an increase vibration, as a result making the structure to be unstable. Elastic body vibrates in discrete geometric patterns known as mode shapes of the body when subjected to periodic forcing functions [202]. These mode shapes have their corresponding mode frequency and the frequencies depend on the mass distribution, boundary conditions and the stiffness distribution. Blades are elastic structures and the arrival of longer, thinner and flexible wind turbine blades in endeavour to increase the energy capture and material cost reduction, makes it important to look into the mode shapes of the blades in the design process of the blades in order to mitigate the risk of occurrence of aeroelasticity problems.

Wind turbine is exposed to vagarious wind conditions which impose varying loading conditions on the blades. These varying loadings on the blades will cause some alterations to the blade geometry when certain speed is exceeded and then result to an increase stress level in crucial regions on the blades. The increase level of stress will tend to have negative impact on the fatigue life of the blades though it has been shown in reports that aeroelastic optimised flexible blades have some advantages over rigid blades. Some of the advantages include load shedding which increases the fatigue life of the blade and also higher energy capture [203].

Therefore, better understanding of aeroelasticity and developing of adequate design tool to mitigate its effects is imperative [204]. Some undesirable aeroelastic phenomena are Divergence (static aeroelastic phenomenon), Flutter (dynamic aeroelastic phenomenon), Vortex Shedding, Galloping, Buffeting and Limit Cycle Oscillations. Vortex Shedding, Galloping and Buffeting are all unsteady aerodynamic phenomena [205]. Divergence is concerned with the steady or static response of the non-rigid body while Flutter is concerned with vibrational response of the elastic body.

5.2.1 Divergence

Divergence occurs when the elastic twist of the lifting surface unexpectedly becomes theoretically infinite and could make the surface to fail in a catastrophic way. In this situation, the load deforms the structure to a state where the torsional loads surpass the structural restoring forces, that is the diverge point. The airspeed at which this happens is known as the divergence airspeed U_D . This can be determined theoretically using static equilibrium equation which is the summation of the aerodynamic forces and elastic moments about a particular point and it is equivalent to zero. In this occasion, the point is the elastic centre or elastic axis of the aerofoil. Figure (5.3) shows a simplified aeroelastic model (NACA0012 profile) mounted on a torsional spring, to demonstrate divergence phenomenon.

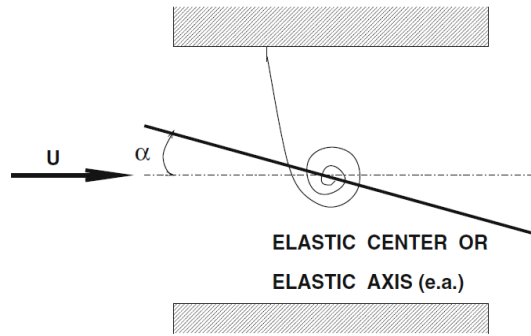


Figure 5.3. Simple aeroelastic model to demonstrate divergence phenomenon [200]

The increase in the aerodynamic angle of attack is controlled by the attached spring and the total aerodynamic angle of attack, α which is sum of the initial angle of attack α_0 and the angle due to the elastic twist α_e [200].

$$\alpha = \alpha_0 + \alpha_e \quad (5.2)$$

Furthermore, a point is defined on the aerofoil which is known as the aerodynamic centre. At this point the aerodynamic moment does not depend on the angle of attack, α . The moment about the elastic centre can be written as shown in Equation (5.3).

$$M_y = M_{AC} + Le \quad (5.3)$$

From aerodynamic theory,

$$L = C_L qS \quad (5.4.1a)$$

$$M_{AC} = C_{MAC} qcS \quad (5.4.1b)$$

where

$$C_L = C_{L_0} + \frac{\partial C_L}{\partial \alpha} \alpha, \quad \text{lift coefficient} \quad (5.4.1c)$$

$C_{MAC} = C_{MAC_0}$, a constant, elastic centre moment coefficient and the dynamic pressure is shown in Equation (5.4.1.d)

$$q = \frac{\rho U^2}{2} \quad (5.4.1d)$$

where

- M_y moment about the elastic centre or axis
- M_{AC} moment about aerodynamic centre, both moments are positive nose up
- L lift, net vertical force positive up
- C_L lift coefficient
- S aerofoil area
- e distance from aerodynamic centre to elastic centre, positive aft
- q dynamic pressure
- ρ air density

Equation (5.4.1.c) is a Taylor Series expansion of C_L for small α . C_{L_0} is the lift coefficient at $\alpha \equiv 0$.

These functions C_{L_0} , $\partial C_L / \partial \alpha$, C_{MAC_0} are non-dimensional functions of aerofoil shape, planform and Mach number.

Therefore, from Equations (5.3), (5.4.1a) and (5.4.1b)

$$M_y = C_{MAC_0} qcS + C_L eqS \quad (5.5)$$

Substituting Equations (5.2) and (5.4.1.c) into Equation (5.5) gives

$$M_y = C_{MAC_0} qcS + \left[C_{L_0} + \frac{\partial C_L}{\partial \alpha} (\alpha_0 + \alpha_e) \right] eqS \quad (5.6)$$

Considering it as a flat plate in 2-dimensional incompressible flow [201]

$$\frac{\partial C_L}{\partial \alpha} = 2\pi, \quad C_{MAC_0} = 0 = C_{L_0}$$

Thus, for simplicity $C_{L_0} \equiv 0$ and without any significant effect on the resulting equations.

Equation (5.6) results into

$$M_y = \left[\frac{\partial C_L}{\partial \alpha} (\alpha_0 + \alpha_e) \right] eqS + qcSC_{MAC_0} \quad (5.7)$$

Now let's consider the elastic moment. Assuming the spring has linear moment-twist characteristics, the elastic moment will be $-K_\alpha \alpha_e$ with K_α being the elastic spring

constant and has units of moment per twist angle [201]. Thus, the summation of the moments we give

$$\left[\frac{\partial C_L}{\partial \alpha} (\alpha_0 + \alpha_e) \right] e q S + q c S C_{MAC_0} - K_\alpha \alpha_e = 0 \quad (5.8)$$

For this aerofoil model considered, Equation (5.8) is the equation of static equilibrium. For simplicity $C_{MAC_0} = 0$ is assumed.

Hence, solving for the elastic twist, α_e , from Equation (5.8) gives

$$\alpha_e = \frac{qS}{K_\alpha} \left[\frac{e \frac{\partial C_L}{\partial \alpha} \alpha_0}{1 - q \frac{eS}{K_\alpha} \frac{\partial C_L}{\partial \alpha}} \right] \quad (5.9)$$

At a particular dynamic pressure, the denominator at the right hand side tends to zero

$$1 - q \frac{eS}{K_\alpha} \frac{\partial C_L}{\partial \alpha} = 0 \quad (5.10)$$

At this point the elastic twist tends to infinity and Equation (5.10) represents the ‘divergence condition’. From Equation (5.10), the ‘divergence dynamic pressure’, q_D , can be determined.

$$q_D \equiv \frac{K_\alpha}{eS \left(\frac{\partial C_L}{\partial \alpha} \right)} \quad (5.11)$$

With divergence dynamic pressure determined, the divergence velocity can be determined.

The meaningful dynamic pressures are positive which means $e > 0$ for divergence to occur, therefore, using Equation (5.11), Equation (5.9) can be rewritten as

$$\alpha_e = \frac{(q/q_D) \alpha_0}{1 - q/q_D} \quad (5.12)$$

5.2.2 Flutter

Flutter is a dynamic instability of an elastic structure in a fluid flow which occurs due to the interaction between the aerodynamic forces exerted by the fluid flow and the elasticity of the structure. Flutter is the condition where the phasing between the aerodynamic load variations and elastic deflections are such that a resonant condition is realised. This is an unfavourable phase and may lead to rapidly high amplitude vibrations of the structure and subsequently catastrophic failure of the structure [206]. It is a recognised phenomenon in the aircraft industry though no report of failure due to flutter has been reported on commercial wind turbines but there is cause for concern as a result of the increase in the size of wind turbine blades nowadays. As the size of the blade increases, the blade flexibility increases and the relative velocity at the blade tip increases making the blade to be inclined to flutter. Some other parameters that influence the critical flutter limit are centre of mass aft of the aerodynamic centre, blade aspect ratio, air-blade mass ratio, the bending/twist coupling and the material damping [206]. As the wind speed increases, the aerodynamic energy added to the structure increases. It gets to a speed where the flutter mode is attained which has a highly negative aeroelastic damping and the material damping will not be sufficient to damp out. Flutter is a dynamic aeroelastic phenomenon due to the coupling of two structural modes - the flap-wise bending and torsional modes [206-209]. At this speed, the frequencies of these modes couple together to form one mode at the flutter condition and flutter frequency which is called the flutter resonance [208].

5.2.3 Flutter Motion

The aircraft wing is used for the demonstration of a basic flutter. Flutter may possibly be started by a rotation of the aerofoil which can be seen starting at $t=0$ in Figure (5.4). With the increase in the force, the aerofoil tends to rise. The torsional stiffness of the structure returns the aerofoil to zero rotation ($t=T/4$ in Figure (5.4)). After which, the bending stiffness of the structure attempts to return the aerofoil to the neutral position, however, the aerofoil rotates in a nose-down position ($t=T/2$ in Figure (5.4)). The aerofoil plunges as a result of the increased force and the torsional stiffness returns the aerofoil to zero rotation ($t=3T/4$). The aerofoil returns to the neutral position with a nose-up rotation which is the completion of the cycle (T). The plunge motion tends to damp out as the time

increases, but the rotation motion diverges. If the motion continues, the forces as a result of the rotation will cause the structure to fail [209].

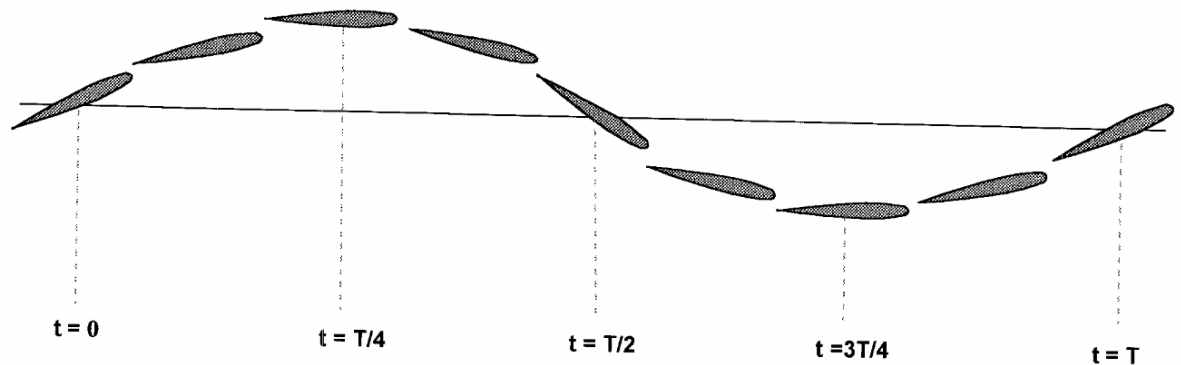


Figure 5.4. Aerofoil motion demonstrating flutter [209]

5.2.4 Classical Flutter Instability Mechanism

This two-dimensional instability which involves the interaction of the flap-wise bending and torsional blade vibration. In this flutter condition, the first torsional blade mode couples with a flap-wise bending mode and as a result of torsion, the aerodynamic lift fluctuates in an adverse phase with the flap-wise bending [206]. The aerodynamic lift force L is defined at the aerodynamic centre AC which is a distance ca_{AC} in front of the elastic axis and it usually lies a quarter of the chord length behind the leading edge. The elastic axis is a length ca_{CG} in front of the centre of gravity and it is in-between the centre of gravity and the aerodynamic centre. These can be seen in the simple blade section of a wind turbine Figure (5.5) which consists of two degrees-of-freedom (DOFs), flap-wise translation and torsional, to determine the classical flutter instability. The blade section is subjected to quasi-steady aerodynamic lift force [207].

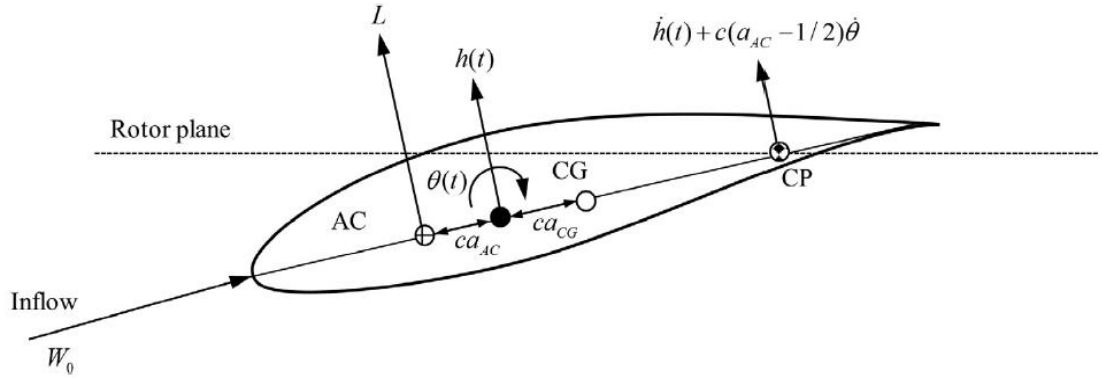


Figure 5.5. Blade section with 2 degrees-of-freedom [207]

The wind inflow is parallel to the chord of the blade while the flap-wise translation DOF is perpendicular to the direction of the wind inflow. The linear motion of equations of motion can be written as shown where the structural damping is disregarded [207 & 208].

$$\text{Forces in the flap-wise direction:} \quad m\ddot{h} - mca_{CG}\ddot{\theta} + k_f h = L \quad (5.13)$$

$$\text{Moments about the elastic axis:} \quad -mca_{CG}\ddot{h} - m(c^2 r_{CG}^2 + c^2 a_{CG}^2)\ddot{\theta} + k_t \theta = ca_{AC} L \quad (5.14)$$

where

- h flap-wise translation DOF
- θ torsional rotation DOF
- m mass per unit length of the blade section
- r_{CG} radius of gyration normalised by the blade chord length
- c blade chord length
- \ddot{h} second time-derivative of the flap-wise translation DOFs
- $\ddot{\theta}$ second time-derivative of the torsional rotation DOFs
- k_f flap-wise stiffness
- k_t torsional stiffness
- L aerodynamic lift force
- W_0 steady-state relative inflow wind speed

In order to solve the equation of motion, Equation (5.15) which is the quasi-steady aerodynamic lift force per unit length is required with the apparent mass terms in Equation (5.14) neglected:

$$L = \frac{1}{2} \rho c W^2 C_L(\alpha) \quad (5.15)$$

where

W relative inflow wind speed
 ρ air density
 C_L coefficient of lift

The coefficient of lift, C_L is a function of the angle of attack. To include the effects of the torsional velocity $\dot{\theta}$, the angle of attack is defined at the collocation point (CP) which is located at three-quarter of the chord length on the blade from the leading edge [207]. The relative inflow wind speed and the angle of attack are defined in Equation (5.16.a) and (5.16.b) respectively

$$W = \sqrt{W_0^2 + h^2} \quad (5.16a)$$

$$\alpha = \arctan \left[\frac{W_0 \sin \theta - \dot{h} - c \left(\frac{1}{2} - a_{AC} \right) \dot{\theta}}{W_0 \cos \theta} \right] \quad (5.16b)$$

W_0 is the steady-state relative inflow wind speed and it is parallel to the chord, at small values of angle of attack. Substituting Equation (5.16.a) & (5.16.b) for W and α into Equation (5.15) and linearising it about $\theta = \dot{h} = \dot{\theta} = 0$ gives the expression for the linear lift as shown in Equation (5.17)

$$L \approx L_0 + \frac{1}{2} \rho c W^2 C'_L \left[\theta - \frac{\dot{h}}{W_0} - \left(\frac{1}{2} - a_{AC} \right) \frac{c \dot{\theta}}{W_0} \right] \quad (5.17)$$

where

L_0 steady-state lift force
 C'_L gradient of the lift curve, (i.e. $dC_L/d\alpha$), evaluated at the angle of attack $\alpha_0 = 0$

Considering a thin aerofoil, the value of C'_L can be assumed to be 2π and the value for the steady-state lift force L_0 can be assumed to be zero because it has little influence on the instability of the aerofoil [206]. Therefore, the equations of motion (Equations (5.13) & (5.14)) with linearised lift can be written in this form:

$$\mathbf{M}\ddot{\mathbf{x}} + \mathbf{C}\dot{\mathbf{x}} + \mathbf{K}\mathbf{x} = \mathbf{0} \quad (5.18)$$

With the vector $\mathbf{x} = [h/c, \theta]^T$ comprises of non-dimensional DOFs and \mathbf{M} , \mathbf{C} , \mathbf{K} being matrices which are defined as:

$$\mathbf{M} = \begin{bmatrix} 1 & -a_{CG} \\ -a_{CG} & r_{CG}^2 + a_{CG}^2 \end{bmatrix}, \quad \mathbf{C} = \frac{ck}{W_0} \begin{bmatrix} 1 & \frac{1}{2} - a_{AC} \\ a_{AC} & a_{AC} \left(\frac{1}{2} - a_{AC} \right) \end{bmatrix}, \quad \mathbf{K} = \begin{bmatrix} \omega_f^2 & -k \\ 0 & r_{CG}^2 \omega_t^2 - k a_{AC} \end{bmatrix}$$

where

M blade structure mass matrix
C aerodynamic damping matrix
K aeroelastic stiffness matrix

where $\omega_f = \sqrt{k_f/m}$ is the natural frequency of flap-wise mode and $\omega_t = \sqrt{k_t/(mc^2 r_{CG}^2)}$ is the natural frequency of torsional mode, without inertial coupling which means that $a_{CG} = 0$ and $k = (\rho/2m)W_0^2 C_L'$ is the aerodynamic stiffness, which is dependent on the air-blade mass ratio ρ/m .

The aerodynamic damping matrix, \mathbf{C} , makes little contribution to the dissipative aerodynamic forces, which can be assumed to have no qualitative impact on the flutter instability mechanism. However, it is very significant when determining the exact critical flutter limit. Considering only the qualitative impact in this case, the aerodynamic damping matrix, \mathbf{C} , can be ignored to simplify the calculation and inserting $\mathbf{x} = \mathbf{v}e^{\lambda t}$ into Equation (5.18) where λ is the eigenvalue and \mathbf{v} is the eigenvector, results in the following single-blade eigenvalue problem Equation (5.19) [205 & 207].

$$(\lambda^2 \mathbf{M} + \mathbf{K})\mathbf{v} = \mathbf{0} \quad (5.19)$$

The determinant of Equation (5.19) must be zero in order to determine the non-trivial solutions and the following characteristics equation can be derived:

$$r_{CG}^2 \lambda^4 + [(r_{CG}^2 + a_{CG}^2)\omega_f^2 + r_{CG}^2 \omega_t^2 - k(a_{AC} + a_{CG})]\lambda^2 + \omega_f^2(r_{CG}^2 \omega_t^2 - k a_{AC}) = 0 \quad (5.20)$$

The eigenvalues are normally complex $\lambda = \beta + i\omega$. When the real part of the solution of one eigenvalue is positive, $\beta > 0$, then the section corresponds to unstable behaviour. Based on the Routh-Hurwitz stability criteria, the section is stable if

$$(r_{CG}^2 + a_{CG}^2)\omega_f^2 + r_{CG}^2\omega_t^2 - k(a_{AC} + a_{CG}) > 0 \quad (5.21a)$$

and

$$r_{CG}^2\omega_t^2 - ka_{AC} > 0 \quad (5.21b)$$

These limits (Equations (5.21.a) & (5.21.b)) can be used to define the critical flutter limit. Using the first limit, Equation (5.21.a), the imaginary part is non-zero when the eigenvalue real part is positive, this results to oscillations. Thus, the resulting flutter criterion can be deduced:

$$\frac{\rho}{2m} W_0^2 C'_L < \omega_f^2 \frac{r_{CG}^2 + a_{CG}^2}{a_{AC} + a_{CG}} + \omega_t^2 \frac{r_{CG}^2}{a_{AC} + a_{CG}} \quad \text{for} \quad a_{AC} + a_{CG} \geq 0 \quad (5.22)$$

From Equation (5.22), if the right hand side of the equation is less than the left hand side, then the danger of flutter instability is substantial. Based on Equation (5.22), it is assumed that wind turbine runs the risk of flutter occurring if the following four criteria are met [207-2010].

1. When there is attached flow condition $C'_L > 0$. If this is not the situation, the blade torsion will not lead to aerodynamic lift increased.
2. High tip speeds. This means that the relative wind speed W_0 must be sufficiently high for the aerodynamic forces to be large to overcome the structure dynamic elastic forces and resulting to classical flutter instability.
3. There must be low flap and torsion stiffness, making the values of the flap-wise frequency, ω_f and torsional frequency, ω_t to be sufficiently low so that they can couple in a flutter mode.
4. The location of the centre of gravity, CG must be aft of the aerodynamic centre, AC (i.e. $a_{AC} + a_{CG} > 0$), which will make certain the right phasing between the flap-wise and torsional modes of the flutter.

Modal analysis is the process of determining the modal parameters, which are then sufficient for formulating a mathematical dynamic model. The free dynamic response of the wind turbine blade can be reduced to a discrete set of modes. The modal parameters are the natural frequency, damping and mode shape of the wind turbine blade. Within the frequency range of interest, the modal parameters of all the modes constitute a complete dynamic description of the wind turbine blade. The modes of vibration represent the inherent dynamic properties of the wind turbine blade. The range of applications for modal data includes, checking the modal parameters, verifying and improving analytical models, predicting the response to assumed excitations, predicting the change in dynamic properties due to physical modifications, i.e. load or stiffness, predicting the necessary physical modifications required to obtain a desired dynamic property.

5.3 Effect of the Fibre Orientation on the Natural Frequencies (NREL 5 MW Blade)

In this section, a modal analysis is carried out on the adaptive blade to understand the dynamic response of the adaptive blade with change in the fibre orientation. Modal features are considered with reference to the stationary blade, therefore rotational effects are excluded [210].

Table 5.1 Layup Configurations

Case	Layup configuration, $\{[t_{layer}, mat_{ID}, \theta]_n\}$	Web 1	Web 2
1	$\{[1,3,0]_1, [1,2, \theta]_{56}\}$ both upper and lower surface	$[\pm 45]_{18}$ @ x/c=0.25	$[\pm 45]_{18}$ @ x/c=0.55
2	$\{[1,3,0]_1, [1,2, \theta]_{56}\}$ mirror lower surface	$[\pm 45]_{18}$ @ x/c=0.25	$[\pm 45]_{18}$ @ x/c=0.55
3	$\{[1,3,0]_1, [1,2, \theta]_{28}\}$ both upper and lower surface	$[\pm 45]_{16}$ @ x/c =0.46	–
4	$\{[1,3,0]_1, [1,2, \theta]_{28}\}$ mirror lower surface	$[\pm 45]_{16}$ @ x/c =0.46	–

where t_{layer} is the lamina thickness, mat_{ID} is the composite material used, θ is the fibre angle while n is the number of fibre layers.

The analysis is carried out using a uniform layer configuration, Case 1, seen in Table (5.1) and constant fibre angle along the blade span. This was done for angle 0° to 90° in an increment of 10° . The natural frequencies obtained from the modal analysis are presented and could be seen in Figure (5.6.a), the natural frequencies response to the fibre angle increment is positive, that is, the lowest six natural frequencies increase with increase in the fibre angle. The modal analysis was also used to obtain the mode shapes associated with the leading deflection direction for the blade related to the six lowest natural frequencies. For each mode, the modal deflection was resolved in a flap-wise, an edge-wise and a torsional deflection. It could be seen that the first natural frequency dominant deflection direction is flap-wise (1st flap-wise), the second is edge-wise (1st edge-wise) while the sixth natural frequency is torsional deflection (1st torsional). The mode shapes are shown in Appendix C.

From the obtained results, it could be noticed that the change in the natural frequencies with an increment in the fibre angle is higher in the frequencies associated with the higher modes which could be seen in Figure (5.6.b).

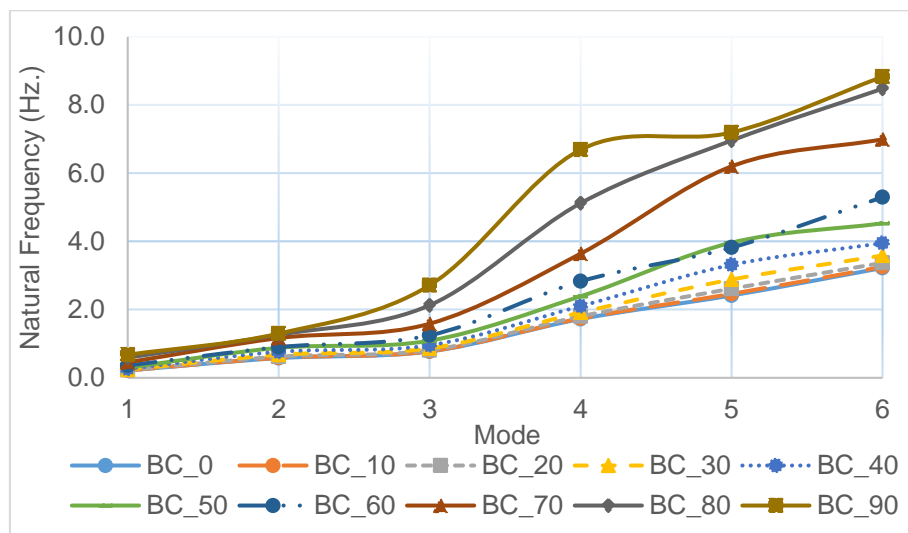


Figure 5.6.(a) Dynamic behaviour for a balanced layup configuration

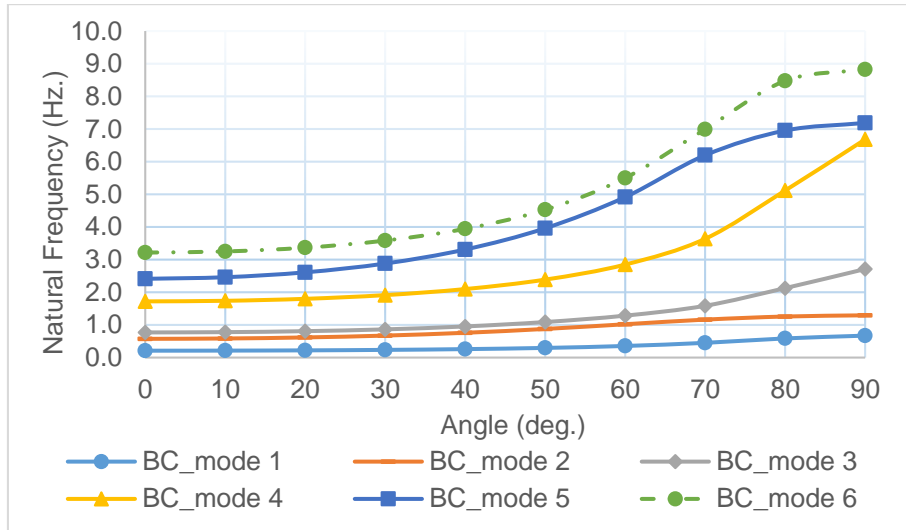


Figure 5.6.(b) Effect of the fibre orientation on the natural frequencies for a balanced layup configuration

Considering mirror configuration, Case 2 seen in Table (5.1), with the lower surface a mirror configuration of the upper surface, the results are shown in Figure (5.7.a). It shows that the natural frequencies increase with the increase in the fibre angle. The lowest or first natural frequencies increases with increment in fibre angle. When comparing the modes at different fibre angles, it is glaring in Figure (5.7.b), that the difference in the natural frequencies associated with the higher modes is higher when compared to that of the lower modes, showing same response as that of balanced layup configurations.

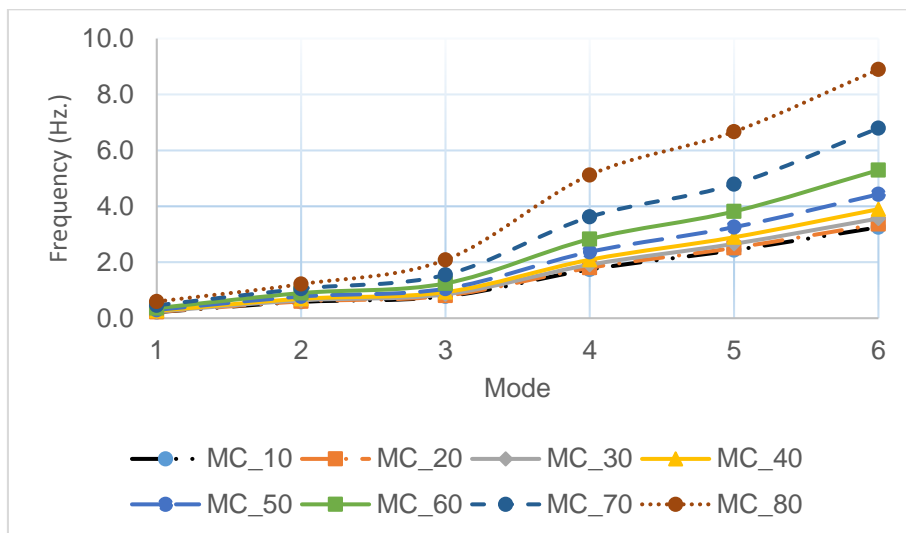


Figure 5.7.(a) Dynamic behaviour for a “mirror” layup configuration [NREL 5 MW Blade]

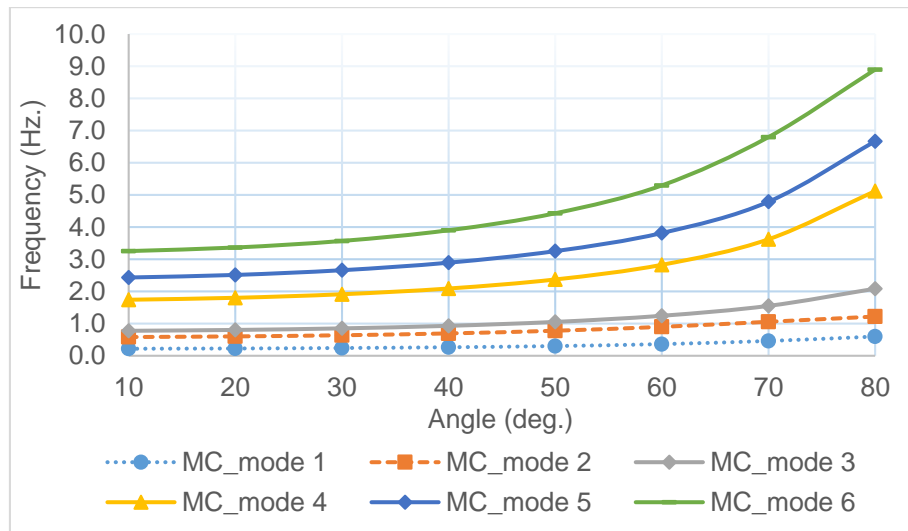


Figure 5.7.(b) Effect of the fibre orientation on the natural frequencies of a “mirror” layup configuration [NREL 5 MW Blade]

5.4 Effect of the Fibre Orientation on the Natural Frequencies (AWT-27 Blade)

This section investigates the dynamic response of the AWT-27 wind turbine blade to the fibre orientation. The analysis is performed using a uniform layer configuration Case 3 seen in Table (5.1) and constant fibre angle along the blade span. In order to determine the response, angle 0° to 90° in an increment of 10° was used. Figure (5.8.a) shows the natural frequencies of the blade to change in the fibre angle. The lowest first six natural frequencies were extracted, it could be seen that the natural frequencies increase as the fibre angle increases. Also, the associated mode shapes for the leading deflection for the first six natural frequencies were obtained. Furthermore, it could be seen that the first natural frequency leading deflection direction is flap-wise (1st flap-wise), the second is edge-wise (1st edge-wise) while the sixth natural frequency is torsional deflection (1st torsional) just like in the response gotten when the NREL 5 MW wind turbine blade was investigated.

From the obtained results, it could be observed as seen in Figure (5.8.b) that the variation in the natural frequencies with an increment in the fibre angle is higher in the frequencies associated with the higher modes.

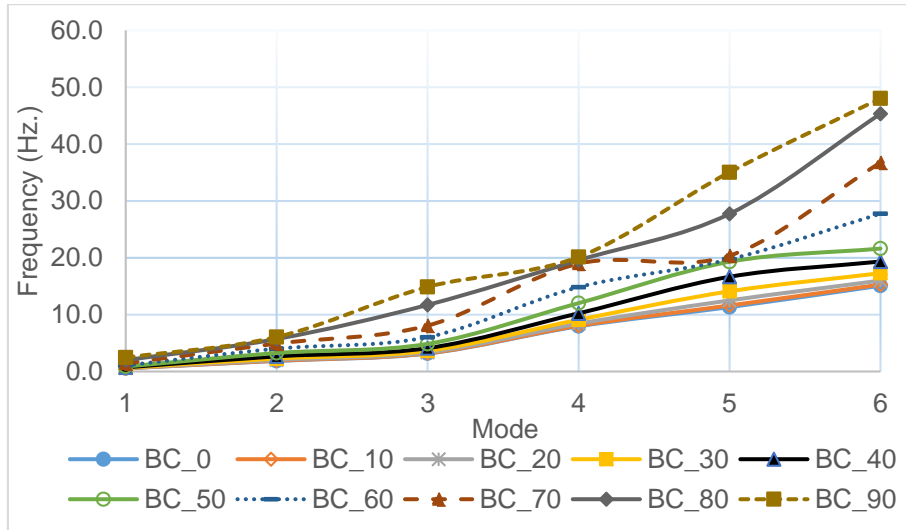


Figure 5.8.(a) Dynamic behaviour for a balanced layup configuration [AWT-27 Blade]

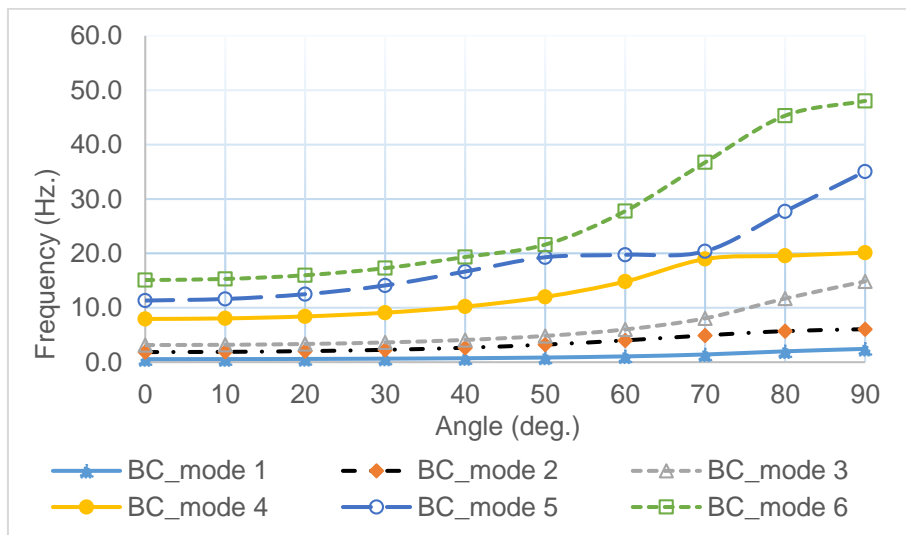


Figure 5.8.(b) Effect of the fibre orientation on the natural frequencies of a balanced layup configuration [AWT-27 Blade]

Investigating the blade response using mirror configuration, Case 4 in Table (5.1), with the lower surface of the blade a mirror surface of the upper surface was used, the results are plotted in Figure (5.9.a). It could be observed that the natural frequencies increase with the increase in the fibre angle. For different angles, when the natural frequencies for the modes are compared as shown in Figure (5.9.b), the difference in the natural frequencies associated with the higher modes are higher when compared to that of the lower modes and this is the same response gotten for the balanced lay-up configuration.

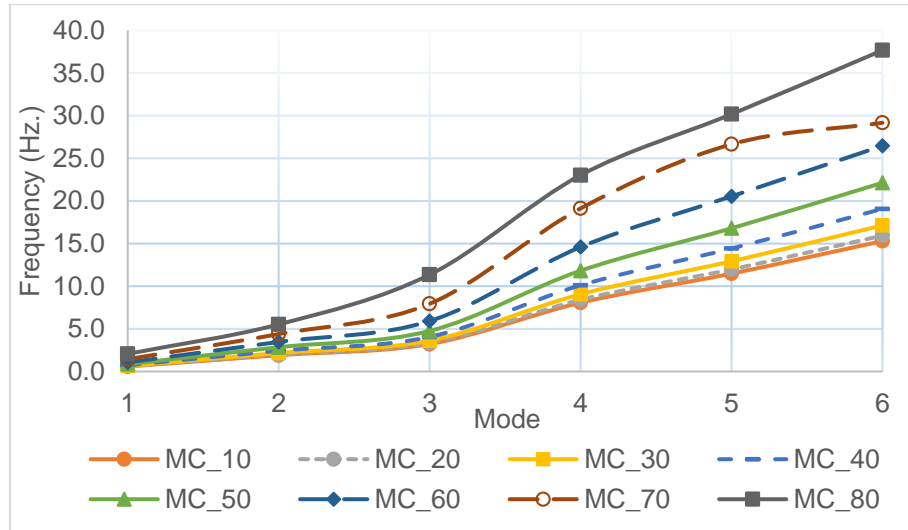


Figure 5.9.(a) Dynamic behaviour for a “mirror” layup configuration [AWT-27 Blade]

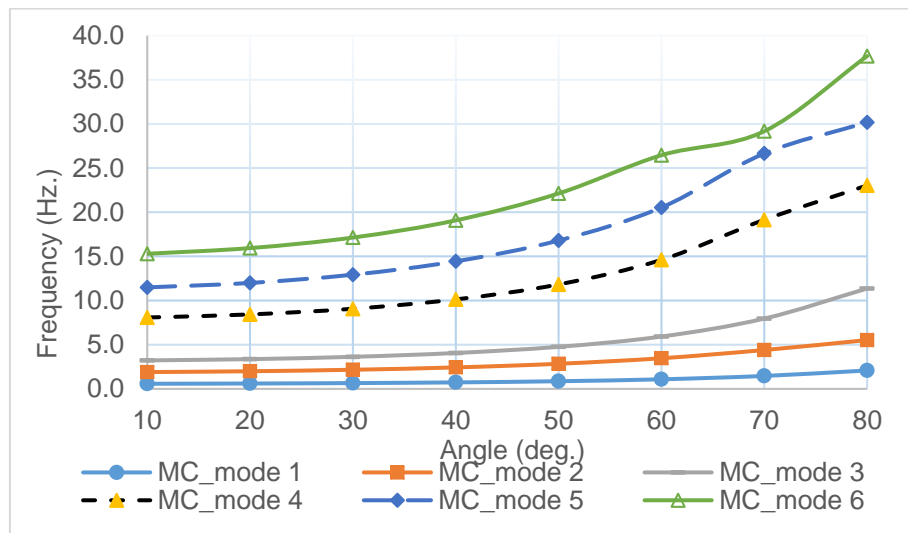
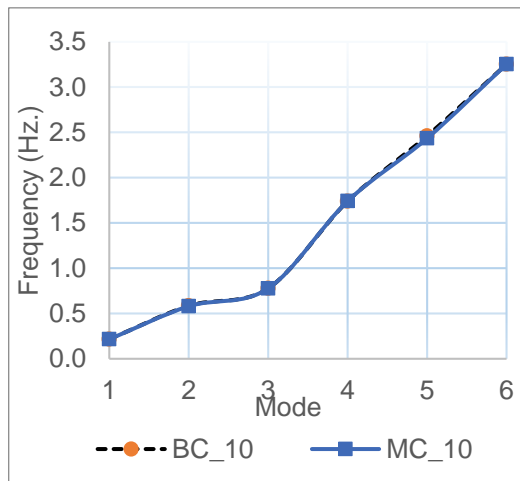


Figure 5.9.(b) Effect of the fibre orientation on the natural frequencies of a “mirror” layup configuration [AWT-27 Blade]

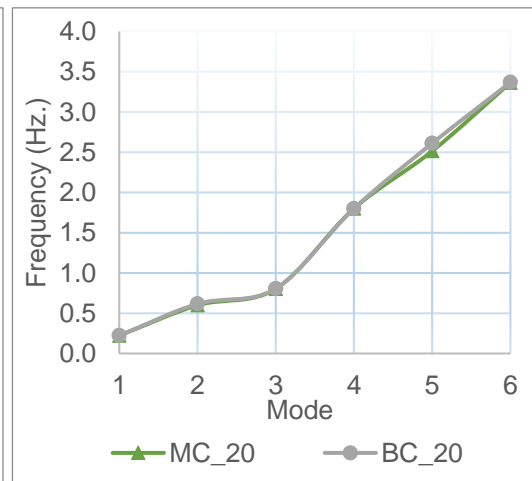
5.5 Effect of Unbalanced Layup Configuration on the Natural Frequencies (NREL 5 MW Blade)

The effect of material coupling on the statically deflected slope of the adaptive blades with laminates configurations having ply angles $\theta = 10^{\circ}$ to $\theta = 80^{\circ}$ in an increment of 10° presented in Case 2 is investigated. In order to facilitate the comparison of the response of the blade to the fibre orientation for an adaptive blade which is made from an elastic coupling configuration to that of balanced layers configuration for conventional blades,

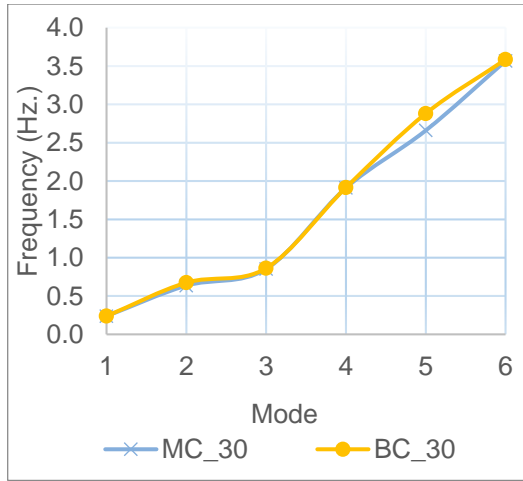
Case 2 and Case 1 in Table (5.1) were analysed and the results plotted for different fibre angles. It could be seen in the plots, Figure (5.10.a) to (5.10.h) that at some particular angles, comparing the balanced and the unbalanced layers configurations, the natural frequencies difference is insignificant. These could be observed in the cases shown in Figure (5.10.a), Figure (5.10.b), Figure (5.10.c) and Figure (5.10.f) while in the other fibre angle cases, there are significant difference in some of the natural frequencies. However, the agreement is better for the deflection components associated with low natural frequencies than for deflection components associated with higher natural frequencies. This plausibly could be as a result of the elastic coupling which is higher in these fibre angles mirror configurations. Comparing the balanced to the unbalanced layers configuration, despite the magnitude difference in these higher modes of natural frequencies, the same tendency was observed in the mode shapes, hence it follows that this flexibility does not affect the mode shapes for these configurations. Furthermore, in all of these cases, there is insignificant difference in the first four natural frequencies. This brings to the conclusion that the effect of the unbalanced fibre orientation configuration on the first four natural frequencies is negligible. The mode shapes are shown in Appendix C.



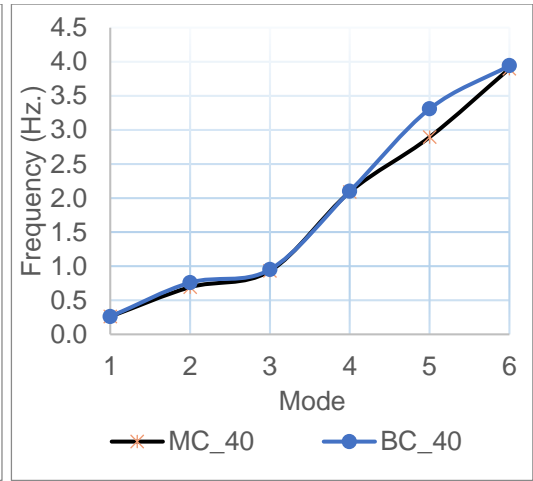
(a)



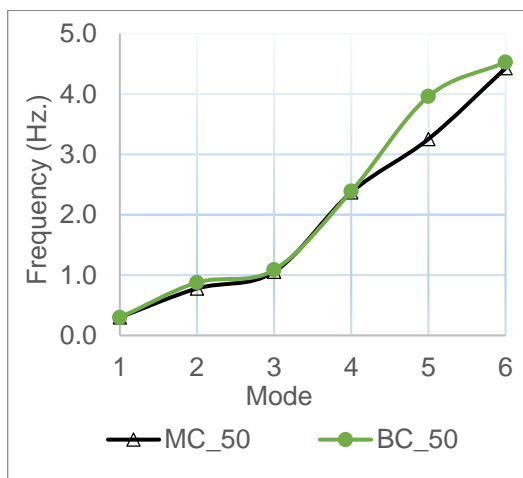
(b)



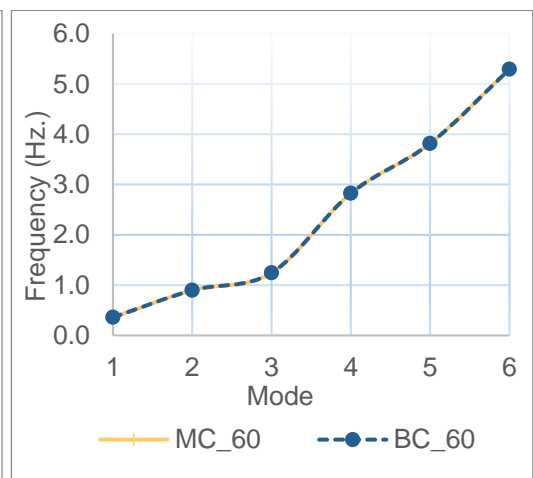
(c)



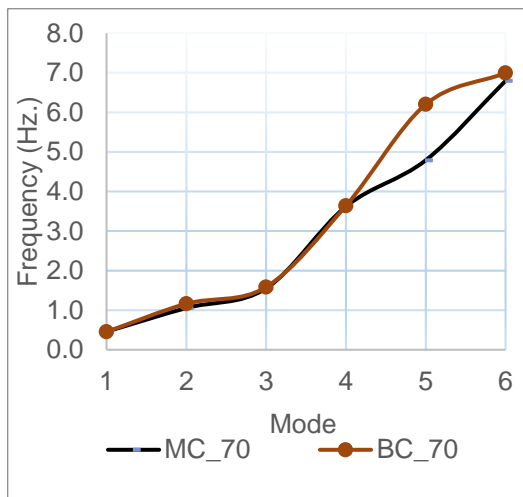
(d)



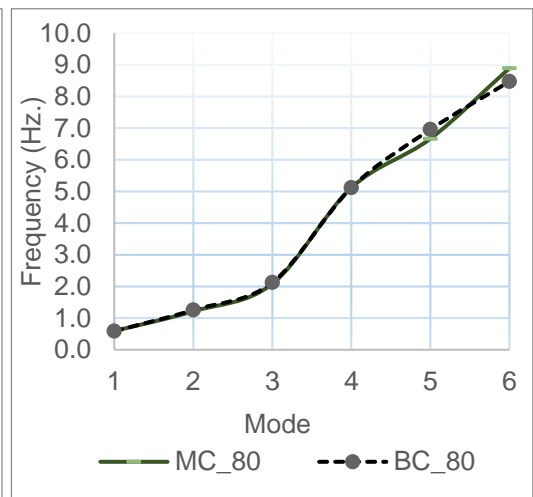
(e)



(f)



(g)



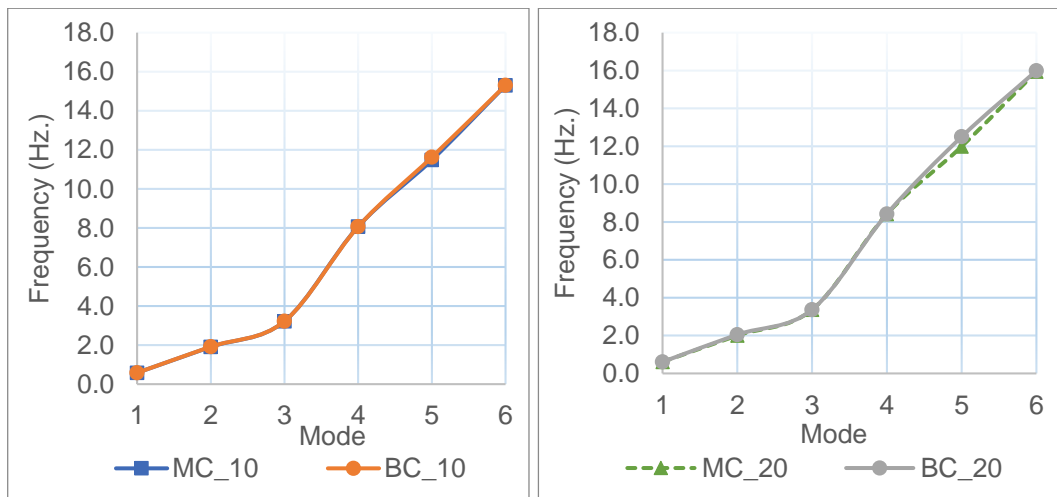
(h)

Figure 5.10.(a-h) Dynamic behaviour for unbalanced and balanced layup configuration compared [NREL 5 MW Blade]

5.6 Effect of Unbalanced Layup Configuration on the Natural Frequencies (AWT-27 Blade)

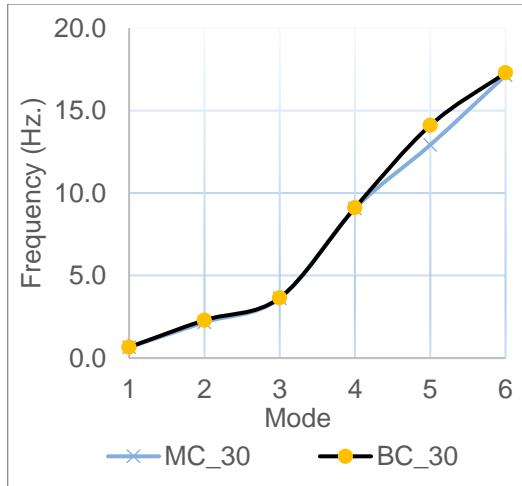
This section is same as that of Section (5.5) but the analysis is carried out using the AWT-27 Blade. Case 3 and Case 4 in Table (5.1) configurations were used for the balanced and the unbalanced configurations respectively. The results plotted are shown in Figure (5.11.a) to (5.11.h) and it could be observed when the natural frequencies obtained for the balanced layers configuration were compared to that of the unbalanced layers configuration, there is no significant difference in the magnitude for some particular angles. These could be observed in the cases shown in Figure (5.11.a), Figure (5.11.b), Figure (5.11.c) and Figure (5.11.f) while in the other fibre angle cases, there are significant difference in the natural frequencies of the higher modes. Though, the lower modes natural frequencies for the balanced and unbalanced layers configuration are almost the same in magnitude for all the fibre orientations analysed. The same deformation was observed for the mode shapes for both the balanced and unbalanced layers configuration despite the difference in the magnitude of the natural frequencies associated with the higher deflection mode. Thus, it follows that the flexibility these unbalanced configurations does not affect the mode shapes.

Same conclusion as when NREL 5 MW blade was used for the analysis can be drawn that the effect of the unbalanced fibre orientation configurations on the first four natural frequencies is negligible.

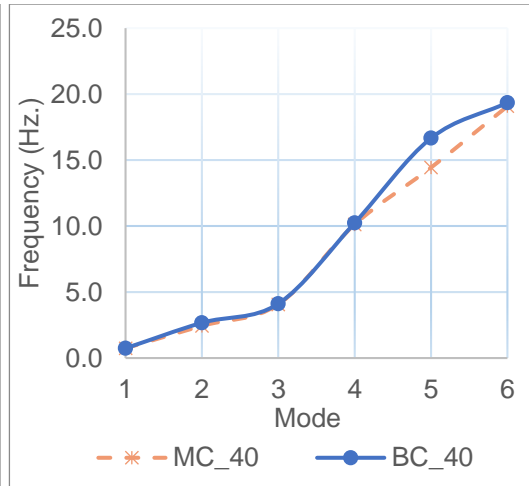


(a)

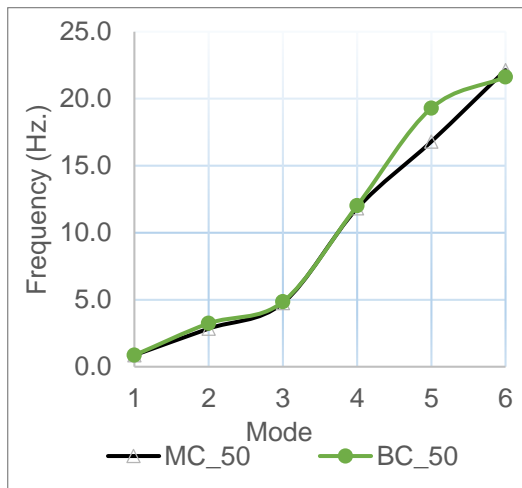
(b)



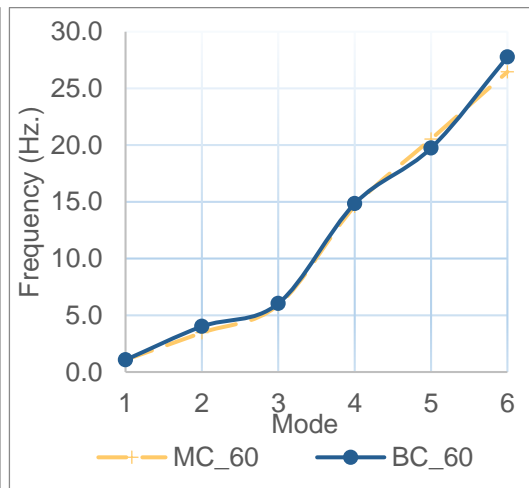
(c)



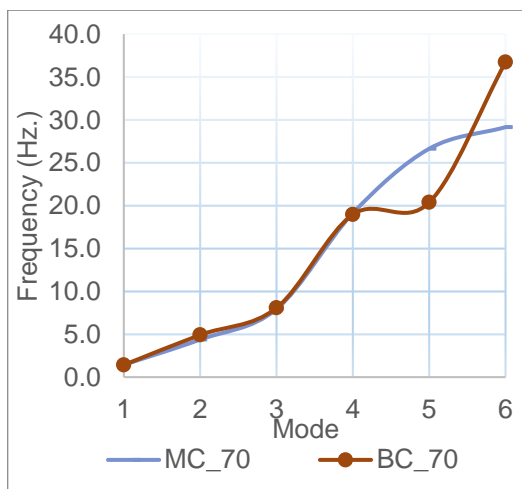
(d)



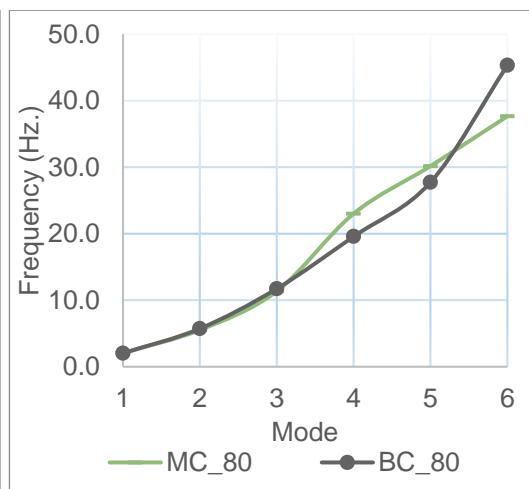
(e)



(f)



(g)



(h)

Figure 5.11.(a-h) Dynamic behaviour for unbalanced and balanced layup configuration [AWT-27 Blade]

5.7 Conclusion

The performed modal analysis gives evaluations of the dynamic behaviour; the natural frequencies and mode shapes for the investigated wind turbine blades. The investigation of the essential dynamic properties of the wind turbine blades; like natural frequencies and mode shapes, it can be seen that there is insignificant difference in the lowest natural frequencies for the balanced and the unbalanced configuration. These results bring to the conclusion that the adaptive blade configuration will not severely increase the dynamic instability of the blade.

6 Summary and Conclusion

6.1 Summary

Focus on enhancing energy extraction from renewable sources is on the increase, motivating wind energy researchers to investigate the design of wind turbines for high efficiency energy extraction. One of the primary objectives is to alleviate the aerodynamic loads on the wind turbine blade, which is one of the major components of the turbines. The wind turbine annual energy production (AEP) has revealed to increase by tailoring of the blade appropriately to give elastic respond to the aerodynamic loads while at the same time alleviating the extreme aerodynamic loading due to stochastic wind characteristics.

For greater energy capture, the sizes of blades are on the increase because theoretically the power produced by wind turbines is proportional to the square of the length of the blade. Increasing the blade size poses its peculiar challenges of increasing the weight, cost and susceptibility to greater aerodynamic loading. In this situation, the efficient design of the turbine blade that is mass efficient and capable of harnessing more energy is of a necessity. Thus, appropriate tailoring of the wind turbine blade is essential by decisively designing bending/twist elastic coupling into the blade, in order to have the blade twist suitably while flap-wise bending is taking place.

There are power enhancement and load control systems for wind turbines. Among the control approaches are the flapping blades by the use of functional materials and adaptive blades achievable by either geometrical adaptiveness or structural adaptiveness.

Flapping of the blades can enhance the lift generation but the appropriate motions (transition and rotation) of the blade are vital to allow positive angle of attack maintenance and higher lift generation. Furthermore, the response of the blade to oscillation frequencies and amplitude is also essential. Thus, the investigation of the effect of oscillation frequencies, oscillation amplitude and pitching amplitude on the blade.

Adaptive blades have controlled and bending/twist deformation produced as a result of purposefully designing the blades to exhibit bending/twist elastic coupling to the changes of the aerodynamic loading. From previous study, adaptive blades have proven to show enormous potentials for increasing the wind turbine annual energy production as well as reducing the extreme aerodynamic loads as a result, improving the fatigue performance. However, simulation of wind turbines using adaptive blades is more intricate. The major

reason being, the simulation is an iterative coupled aero-structural design process because of the aerodynamic performance dependency of the adaptive blade on its structural characteristics. The utilisation of finite element based commercial software for the structural deformation analysis as part of the aerodynamic performance evaluation of adaptive blades is time-consuming. For the aerodynamic performance simulation of the adaptive blade, the induced deformation as a result of the elastic coupling needs to be known as well as the blade structural characteristics. Thus, a high accuracy sophisticated structural analyser for accurately predicting the blade induced deformation is required.

Decoupling the coupled-aero-structure (CAS) process by use of the decoupled design method has shown to be very efficient in adaptive blades design though a more robust and general model needs to be developed which takes into account variation in the span-wise fibre angle and variation in the span-wise shell thickness of the blade.

Dynamic behaviour of adaptive blades is also of a concern with aeroelastic stability to be one of the main issue. Thus, the effect of elastically tailoring layup configuration on the natural frequencies of the blade is investigated

In view of the above, this research aimed at the establishment of an efficient and robust tool for the ease of efficient design of wind turbine adaptive blades.

6.2 Achievements and Original Contribution

The key achievements are listed as follows

- A ‘proof of concept’ using a flat plate to investigate the effect of oscillation frequencies, oscillation amplitude and pitching amplitude was done towards establishing the aerodynamic characteristics (lift coefficient and drag coefficient) and this was done by using numerical method (e.g. ANSYS CFX/FLUENT) and user defined function (UDF) for the motion, a rotating flapping flat plate in a uniform flow field was analysed to assess the effect of rotation on its aerodynamic characteristics.
- An auxiliary software tool was developed for robust and efficient structural analysis of an adaptive. This allows the material properties, layup configurations of the blade to be defined and static structural analysis performed efficiently using the tool and saved in APDL format for the results to be extracted using ANSYS

Mechanical APDL. This tool allows very high flexibility of layup configurations and material properties definition.

- An extended analytical model using the decoupled design method was proposed and validated for predicting the normalised induced twist of an adaptive blade for general case of variable shell thickness and variable fibre angle along the span of the blade. The results obtained using the proposed analytical model and those obtained using ANSYS were compared for validation, and it shows that the analytical model can be used to predict the normalised induced twist for blades with variable shell thickness and variable fibre angle with good level of accuracy. This was achieved by using numerical FEA Based commercial software packages ANSYS, running several cases (span-wise variable properties) for both blades (NREL 5 MW and AWT-27) with the modelling done via MATLAB. Classical Laminate Theory was used to obtain the material properties which was inputted into MATLAB for the blade modelling. WTAero, an in-house aerodynamic performance code for wind turbine was used to generate the external aerodynamic forces and the generated aerodynamic loads was applied on the blades to perform static analysis for the different case scenarios. The deformation result was obtained from which the induced twist was calculated. The results were used to establish the analytical model for predicting the normalised induced twist of adaptive blades.
- Dynamic analysis was performed to investigate the aeroelastic stability of the adaptive blade. It was found out that the aeroelastic tailoring does not have significant effect on the lowest natural frequencies of the blade. This was carried out using a high performance blade modelling tool, (HPBM), in conjunction with ANSYS ADPL to perform dynamic behaviour analysis to ascertain the dynamic performance of the bending/twist adaptive blades (BTABs). Using the auxiliary tool via MATLAB and in ANSYS Batch mode, several cases were simulated to determine the dynamic behaviour of the blades.

6.3 Critical Appraisal and Future Work

In running the computational fluid dynamics to simulate the kinematics of flapping blade in order to establish the aerodynamic characteristics some assumptions were made:

- Firstly, for simplicity, a flat plate was used which might not accurately represent a turbine blade, but it does not dispute the relationship of the flapping amplitude, flapping frequency and pitching amplitude but will possibly have effect on the magnitude of the lift generated because of the difference in geometries.
- Secondly, a simple harmonic motion equation was used to simulate the kinematic motions which is not actually the case for flapping wings.
- Thirdly, because of the computationally intensive nature of the analyses, simulating a rotating flapping flat plate as a wind turbine blade towards evaluating its aerodynamic performance as a substitute for conventional lift-driven blades was not completed.

As a future work, rotation of the flapping flat plate, using of the wings kinematic equations and also using of wind turbine blade for more realistic analysis should be performed to obtain correlations/charts/graphs for correlating flapping frequencies, rotating speed, flow field characteristics and aerodynamic performance.

References

1. Kumar Y., Ringenberg J., Depuru S.S., Devabhaktuni V.K., Lee J.W., Nikolaidis E., Andersen B. & Afjeh A. (2016) “Wind Energy: Trends and enabling technologies” *Renewable and Sustainable Energy Reviews* 53, pp 209-224
2. Wind Energy Foundation; (2014). <http://www.windenergyfoundation.org/about-wind-energy/history> Accessed date 20/03/2017
3. Islam M. R., Mekhilef S. and Saidur R. (2013) “Progress and recent trends of wind energy technology” *Renewable and Sustainable Energy Reviews* pp456-468
4. *Wind turbine design* <http://www.learnengineering.org/2013/08/Wind-Turbine-Design.html> Assessed: 09/08/2017
5. Saad M.M.M. & Asmuin A. (2014) Comparison of Horizontal Axis Wind Turbines and Vertical Axis Wind Turbines, *IOSR Journal of Engineering*, vol. 4 Issue 08
6. Seki K, Shimizu Y. & Zhu, K. (1996) “A design strategy for the improvement of an existing 300kW WTGs rotor blade” *Renewable Energy*, 9, pp 858-886
7. Ronold K.O. & Christensen C.J (2001) “Optimization of a design code for wind-turbine rotor blades in fatigue” *Engineering Structures*, 23 pp 993-1004
8. Maalawi K.Y. & Negm H.M. (2002) “Optimal frequency design of wind turbine blades” *Journal of Wind Engineering and Industrial Aerodynamics*, 90 pp 961-986
9. Jureczko M., Palwak M. & Mezyk A. (2005) “Optimisation of wind turbine blade” *Materials Processing Technology*, 167, pp 463-471
10. Mendez J. & Greiner D. (2006) “Wind blade chord and twist angle optimization using genetic algorithms” *Proceedings of the Fifth International Conference on Engineering Computational Technology*.
11. Tangler J. L. (2002) “The nebulous art of using wind-tunnel airfoil data for predicting rotor performance” *National Renewable Energy Laboratory*, Report NREL/CP-500-31243
12. Tangler J. L. & Kocurek J. D. (2004) “Wind turbine post-stall airfoil performance characteristics guidelines for blade element momentum methods” *National Renewable Energy Laboratory*, Report NREL/CP-500-36900
13. Jonkman J. M. (2003) “Modelling of the UAE wind turbine for refinement of FAST AD” *National Renewable Energy Laboratory*, Technical Report NREL/TP-500-34755
14. Ashwill T. & Laird, D. (2007) “Concepts to facilitate very large blades” *Proceedings of ASME/AIAA Wind Energy Symposium*, Reno, NV
15. Thumthae C. & Chitsomboon T. (2009) “Optimal angle of attack for untwisted blade wind turbine” *Renewable Energy* 34 pp1279–1284
16. Song F., Ni Y. & Tan Z. (2011) “Optimization Design, Modeling and Dynamic Analysis for Composite Wind Turbine Blade” *Procedia Engineering* 16 pp369 – 375
17. Sayed M. A., Kandil H. A. & Shaltot A. (2012) “Aerodynamic analysis of different wind-turbine-blade profiles using finite-volume method” *Energy Conversion and Management* 64 pp541–550

18. Lee J.-W., Lee J.-S., Han J.-H. & Shin H.-K. (2012) “Aeroelastic analysis of wind turbine blades based on modified strip theory” *Journal of Wind Engineering and Industrial Aerodynamics* 110 pp62–69
19. Liao C. C., Zhao X. L. & Xu J. Z. (2012) “Blade layers optimization of wind turbines using FAST and improved PSO Algorithm” *Renewable Energy* 42 pp227-233
20. Cox K. & Echtermeyer A. (2012) “Structural design and analysis of a 10MW wind turbine blade” *Energy Procedia* 24 pp194 – 201
21. Polat O. & Tuncer I. H. (2013) “Aerodynamic Shape Optimization of Wind Turbine Blades Using a Parallel Genetic Algorithm” *Procedia Engineering* 61 pp28-31
22. Bai C. J., Hsiao F. B., Li M. H., Huang G.Y. & Chen Y. J. (2013) “Design of 10 kW Horizontal-Axis Wind Turbine (HAWT) Blade and Aerodynamic Investigation Using Numerical Simulation” *Procedia Engineering* 67 pp279 – 287
23. Kim B., Kim W., Lee S., Bae S. & Lee Y. (2013) “Development and verification of a performance based optimal design software for wind turbine blades” *Renewable Energy* 54 pp166-172
24. Castelli M. R., Monte A. D., Quaresimin M. & Benini E. (2013) “Numerical evaluation of aerodynamic and inertial contributions to Darrieus wind turbine blade deformation” *Renewable Energy* 51 pp101-112
25. Vaz D. A. T. D., Vaz J. R. P., Pinho A. L. A. M. J. T. & Junior A. C. P. B. (2013) “Optimum aerodynamic design for wind turbine blade with a Rankine vortex wake” *Renewable Energy* 55 pp296-304
26. Sharifi A. & Nobari M. R. H. (2013) “Prediction of optimum section pitch angle distribution along wind turbine blades” *Energy Conversion and Management* 67 pp342–350
27. Buckney N., Pirrera A., Green S. D. & Weaver P. M. (2013) “Structural efficiency of a wind turbine blade” *Thin-Walled Structures* 67 pp144–154
28. Chen J., Wang Q., Shen W. Z. Pang X. Li S. & Guo X. (2013) “Structural optimization study of composite wind turbine blade” *Materials and Design* 46 pp247–255
29. Jeong M.-S., Kim S.-W., Lee I., Yoo S.-J. & Park K. C. (2013) “The impact of yaw error on aeroelastic characteristics of a horizontal axis wind turbine blade” *Renewable Energy* 60 pp256-268
30. Fischer G. R., Kipouros T. & Savill A. M. (2014) “Multi-objective optimisation of horizontal axis wind turbine structure and energy production using aerofoil and blade properties as design variables” *Renewable Energy* 62 pp506-515
31. Vesel Jr. R. W. & McNamara J. J. (2014) “Performance enhancement and load reduction of a 5 MW wind turbine blade” *Renewable Energy* 66 pp391-401
32. Hasnan <http://winds-energy.blogspot.co.uk/2009/04/effect-of-blade-number-on-aerodynamic.html> accessed date 29/06/2016
33. Maheri A., Noroozi S. & Vinney J. (2007d) “Application of combined analytical/FEA coupled aerodynamic aero-structure simulation in design of wind

- turbine adaptive blades” *Renewable Energy*, vol. 32, issue 12, pp2011-2018. ISSN 0960-1481.
34. Milborrow D. (2011) “Are three blades really better than two?” *Wind Power Monthly*, August 2011, <http://www.windpowermonthly.com/article/1083653/three-blades-really-better-two>
 35. National Renewable Energy Laboratory. Wind energy technologies. In: *Renewable electricity futures Study (chapter11)*, vol.2; 2012, pp.11-1–11-63.
 36. Mckenna R., Ostman P.v.d., & Fichtner L.W. (2016) “Key Challenges and prospects for large wind turbines” *Renewable and Sustainable Energy Reviews* 53, pp1212-1221
 37. Ahmed M.R (2012) “Blade sections for wind turbine and tidal current turbine applications – current status and future challenges” *International Journal of Energy Research* 36 pp 829-844
 38. Gao L., Zhang H., Liu Y. & Han S. (2015) “Effects of vortex generators on a blunt trailing-edge airfoil for wind turbines” *Renewable Energy* vol. 76 pp 303-311
 39. van Dam C.P., Chow R., Zayas J.R. & Berg D.E. (2007) Computational Investigations of Small Deploying Tabs and Flaps for Aerodynamic Load Control
 40. El-Khozondar H.J., Reyala A.S.A. & Muller M.S. (2014) “Load reduction in wind energy converters using individual pitch control” *JERT*, vol. 1, issue 1
 41. <http://www.energy.siemens.com/hq/en/renewable-energy/wind-power/platforms/d7-platform/> accessed date: 03/05/2016
 42. <http://www.telegraph.co.uk/finance/economics/12090394/Britain-abandons-onshore-wind-just-as-new-technology-makes-it-cheap.html> accessed date: 03/05/2016
 43. International Renewable Energy Agency (IRENA) (2012) “Renewable Energy Technologies: Cost Analysis Series, Wind Power” Volume 1: Power Sector Issue 5/5
 44. Lobitz D.W. & Veers P.S. (2003) “Load Mitigation with Bending/Twist-coupled Blades on Rotors using Modern Control Strategies” *Wind Energy* vol. 6, pp 105-117
 45. Capellaro M. (2008) “Bend twist coupled blades – Redux”. In: Proceedings of the IEA topical expert meeting on “the application of smart structures for large wind turbine rotor blades” Sandia National Labs, Albuquerque, USA
 46. Barlas, T.K., & van Kuik G.A.M. (2010) “Review of state of the art in smart rotor control research for wind turbines” *Progress in Aerospace Sciences* 46 pp 1-27
 47. Berg D.E. (2008) “Introductory Note”. In: Proceedings of the IEA topical expert meeting on “the application of smart structures for large wind turbine rotor blades” Sandia National Labs, Albuquerque, USA
 48. Hoffmann R.D (2002) “A comparison of control concepts for wind turbines in terms of energy capture” Dissertation
 49. Bossanyi E.A. (2000) “The Design of Closed Loop Controllers for wind turbines” *Wind Energy* 3, pp 149-163.
 50. Larsen T.J., Madsen H.A. & Thomsen K. (2005) “Active load reduction using individual pitch, based on local inflow measurements” 8, pp 67–80

51. Hand M.M., Wright A.D., Fingersh L.J. & Harris M. (2006) “Advanced wind turbine controllers attenuate loads when upwind velocity measurements are inputs”, AIAA 2006-603. In: Proceedings of the 44th AIAA/ASME, Reno, NV, USA, 2006.
52. Li C.F., Xu Y., X L Zhao X.L. & Xu J.Z. (2013) “Influence of trailing edge flap on wind turbine blade using three-dimensional computational fluid dynamics method” *Materials Science and Engineering* 52, 6th International Conference on Pumps and Fans with Compressors and Wind Turbines
53. Wilson D.G., Berg D.E., Barone M.F., Berg J.C., Resor B.R. & Lobitz D.W. (2009) “Active Aerodynamic Blade Control Design for Load Reduction on Large Wind Turbines” European Wind Energy Conference & Exhibition 2009 Parc Chanot, Marseille, France 16-19 March 2009.
54. Frederick M., Kerrigan E. C. & Graham J. M. R. (2010) “Gust alleviation using rapidly deployed trailing-edge flaps” *Journal of Wind Engineering and Industrial Aerodynamics* 98 pp712–723
55. Yen D.T., van Dam C.P., Bräeuchle F., Smith R.L. & Collins S.D. (2000) “Active load control and lift enhancement using MEM translational tabs” *Fluids* 2000, AIAA Paper 2000-2422
56. Macquart T. & Maheri A. (2015) “Integrated aeroelastic and control analysis of wind turbine blades equipped with microtabs” *Renewable Energy* 75, pp102-114
57. Wilson D.G., Berg D.E., Lobitz D.W. & Zayas J.R. (2008) “Optimized Active Aerodynamic Blade Control for Load Alleviation on Large Wind Turbines” AWEA WINDPOWER 2008 Conference & Exhibition, Houston, Texas
58. Barbarino S, Bilgen O, Ajaj R.M, & Friswell M.I, Daniel J.I (2011) “A Review of Morphing Aircraft”, *Journal of Intelligent Material Systems and Structures* 22 pp823-877
59. Barbarino S, Dettmer W.G, & Friswell M.I (2010) “Morphing Trailing Edges with Shape Memory Alloy Rods” *21st International Conference on Adaptive Structures and Technologies*
60. Coutu D, Brailovski V, & Terriault P (2010) “Optimized design of an active extrados structure for an experimental morphing laminar wing” *Aerospace Science and Technology* 14, pp451–458
61. Daynes S, & Weaver P.M (2013) “Stiffness tailoring using prestress in adaptive composite structures” *Composite Structures* 106 pp282–287
62. Ekanger J.V (2011) “Morphing skins to improve local flow behaviour in a hydroturbine context” MSc Thesis, Norwegian University of Science and Technology
63. Friswell M.I, Herencia J.E, Baker D, & Weaver P.M (2008) “The optimisation of hierarchical structures with applications to morphing aircraft” *Second International Conference on Multidisciplinary Design Optimization and Applications*
64. Gandhi F, & Anusonti-Inthra P (2008) “Skin design studies for variable camber morphing airfoils” *Smart Materials and Structures*, 17

65. Khoo C.K, Salim F, & Burry J (2012) “Designing Architectural Morphing Skins with Elastic Modular Systems” *International Journal of architectural computing*, 04 (09) pp 397-419
66. Kikuta M.T (2003) “Mechanical Properties of Candidate Materials for Morphing Wings” Virginia Polytechnic Institute and State University, MSc Thesis
67. Kuder I.K, Arrieta A.F, Raither , & Ermanni W.E.P (2013) “Variable stiffness material and structural concepts for morphing applications” *Progress in Aerospace Sciences* 63 pp33–55
68. Murugan S. & Friswell M.I (2012) “Morphing Wing Flexible Skins with Curvilinear Fiber Composites” *Elsevier*
69. Murugan S, Flores E.I.S, Adhikari S, & Friswell M.I (2012) “Optimal design of variable fiber spacing composites for morphing aircraft skins” *Composite Structures* 94 pp1626–1633
70. Schmitz A. & Horst P (2013) “Bending deformation limits of corrugated Morphing Skins” *The 19th International Conference on Composite Materials*
71. Schmitz A. & Horst P (2014) “Bending deformation limits of corrugated unidirectionally reinforced composites” *Composite Structures*, 107 pp103-111
72. Sofla A.Y.N, Meguid S.A, K.T. Tan K.T. & Yeo W.K (2010) “Shape morphing of aircraft wing: Status and challenges” *Materials and Design*, 31 pp1284-1292
73. Steenhuizen D. & van Tooren M (2012) “The implementation of a knowledge-based framework for the aerodynamic optimization of a morphing wing device” *Advanced Engineering Informatics* 26 pp207–218
74. Thill C., Etches J., Bond I., Potter K., & Weaver P. (2008) “Morphing Skins”, *The Aerodynamic Journal*, 112 pp117-139
75. Vocke III R.D, Kothera C.S, Woods B.K.S, Bubert E.A, & Wereley N.M (2012) “One Dimensional Morphing Structures for Advanced Aircraft” *Recent Advances in Aircraft Technology*
76. Xia Y, Friswell M.I, & Flores E.I.S (2012) “Equivalent models of corrugated panels” *International Journal of Solids and Structures* 49 pp1453–1462
77. Whitmer C.E. & Kelkar A.G. (2005) “Robust control of a morphing airfoil structure” *American control conference* [Portland, OR, USA]
78. Marques P. (2014) “A Review of Active Blade Twist Technology: Part II – Integral Twist Actuation” *International Journal of Unmanned Systems Engineering* 2, 2, pp26-36
79. Park J-S. & Shin S.J. (2007) “A Preliminary Design on the Second Generation Integral Twist-Actuated Blade” *ICCES* 4,4, pp265-269.
80. Hazen D.C. (1968) “Film Notes for Boundary-Layer Control” National Committee for Fluid Mechanics Films.
81. Hubler M., Nissle S., Gurka M. & Wassenaar J. (2016) “Active vortex generator deployed on demand by size independent actuation of shape memory alloy wires integrated in fiber reinforced polymers” *Industrial and Commercial Applications of Smart Structures Technologies*, Proceedings Volume 9801
82. Quackenbush T.R., Danilov P.V. & Whitehouse G.R (2010) “Flow Driven Oscillating Vortex Generators for Control of Boundary Layer Separation” 40th

- Fluid Dynamics Conference and Exhibit 28 June - 1 July 2010, Chicago, Illinois, AIAA 2010-4266
83. Paul A.R., Joshi S., Jindal A., Maurya S.P. & Jain A. (2013) "Experimental Studies of Active and Passive Flow Control Techniques Applied in a Twin Air-Intake" *Scientific World Journal* doi: [10.1155/2013/523759](https://doi.org/10.1155/2013/523759)
 84. Truab L.W., Miller A.C. & Rediniotis O. (2014) "Comparisons of a Gurney and Jet-Flap for Hinge-Less Control" *Journal of Aircraft* vol. 41, 2 pp 420-423
 85. Romain F. (2015) "Drag reduction using plasma actuators" Licentiate Thesis, Stockholm, Sweden
 86. Choi K-S., Jukes T. & Whalley R. (2011) "Turbulent boundary-layer control with plasma actuators" *b* 369, pp 1443-1458
 87. Liu, W. & Gong, J (2011) "Adaptive Bend-Torsional Coupling Wind Turbine Blade Design Imitating the Topology Structure of Natural Plant Leaves" South China University of Technology China
 88. Zhang P & Huang S. (2011) "Review of Aeroelasticity for wind turbine: Current status, research focus and future perspectives" *Front Energy* 5(4), pp419-434
 89. Kensch C. W. (2006) "Fatigue of Composites for Wind Turbines" *International Journal of Fatigue* 28 pp1363-1374
 90. Samborsky D. D., Wilson T. J., Agastra P. & Mandell J.F. (2008) "Delamination at Thick Ply Drops in Carbon and Glass Fiber Laminates Under Fatigue Loading" *Journal of Solar Energy Engineering* vol. 130 (3)
 91. Sakin R & Ay I. (2008) "Statistical analysis of bending fatigue life data using Weibull distribution in glass-fiber reinforced polyester composites" *Materials and Design* vol. 29 (6) pp1170-1181
 92. Ponta F.L., Otero A.D., Rajan A. & Lago L.I. (2014) "The adaptive-blade concept in wind-power applications" *Energy for Sustainable Development* 22 pp3-12
 93. Nelson R. C., Corke T. C. & Othman H. (2008) "A Smart Wind Turbine Blade Using Distributed Plasma Actuators for Improved Performance" *46th Aerospace Sciences Meeting, January 7-10, 2008, Reno, Nevada.*
 94. Tangler, J. L. & Somers, D. M., (1995) "NREL Airfoil Families for HAWTs" *AWEA 95, March, 1995.*
 95. Zuo D., Chen W., Peng S. & Zhang W. (2006) "Modeling and simulation study of an insect-like flapping-wing micro aerial vehicle" *Advanced Robotics* vol. 20, issue 7.
 96. Malik M. A. & Ahmad F. (2010) "Effect of Different Design Parameters on Lift, Thrust and Drag of an Ornithopter" *Proceedings of the World Congress on Engineering*, vol. 2, pp1460-1465.
 97. Sane S. & Dickinson M. H. (2002) "The aerodynamic effects of wing rotation and a revised quasi-steady model of flapping flight" *The Journal of Experimental Biology* vol. 205, pp1087-1098.
 98. Liebe R. (2007) *Flow Phenomena in Nature: Inspiration, learning and application*, vol. 2, WIT Press, pp428-430

99. Jones K. D. & Platzer M. F. (2001) "On the Use of Vortex Flows for the Propulsion of Micro-Air and Sea Vehicles" Naval Postgraduate School Monterey CA Dept. of Aeronautics and Astronautics
100. Platzer M.F & Jones K.D. (2008) "Flapping-Wing Aerodynamics: Progress and Challenges" *AIAA Journal* 46 (9) pp2136-2149
101. Shyy W., Ifju P. & Viieru D. (2005) "Membrane Wing-Based Micro Air Vehicles" *Applied Mechanics Reviews* vol. 58, pp283-301
102. Shyy W., Aono H., Chimakurthi S. K., Trizila P., Kang C,-K., Cesnik C.E.S & Liu H. (2010) "Recent progress in flapping wing aerodynamics and aeroelasticity" *Progress in Aerospace Sciences* vol. 46, pp284-327
103. Nakata T. & Liu H. (2012) "A fluid-structure interaction model of insect flight with flexible wings" *Journal of Computational Physics* vol. 231, pp1822-1847

104. von Ellenrieder K. D., Parker K. & Soria J. (2008) "Fluid mechanics of flapping wings" *Experimental Thermal and Fluid Science* vol. 32, pp1578-1589
105. Senda K., Obara T., Kitamura M., Nishikata T., Hirai N., Iima M. & Yokoyama N. (2012) "Modeling and emergence of flapping flight of butterfly based on experimental measurements" *Robotics and Autonomous Systems* vol. 60, pp670-678
106. Liu H. (2009) "Integrated modelling of insect flight: From morphology, kinematics to aerodynamics" *Journal of Computational Physics*, vol. 228, pp439-459
107. Razak N. A & Dimitriadis G. (2014) "Experimental study of wings undergoing active root flapping and pitching" *Journal of Fluids and Structures* vol. 49, pp687-704.
108. Wu D., Yeo K. S & Lim T. T. (2014) "A numerical study on the free hovering flight of a model insect at low Reynolds number" *Computers & Fluids* vol. 103, pp234-261.
109. Philips N. & Knowles K. (2011) "Effect of flapping kinematics on the mean lift of an insect-like flapping wing" *Proceedings of the Institution of Mechanical Engineers, Part G: Journal of Aerospace Engineering*, vol.225, pp723-736.
110. Djodjodhardjo H., Ramli A. S. S. & Wiriadidjaja S. (2012) "Kinematic and aerodynamic modelling of flapping wing ornithopter" *Procedia Engineering*, vol. 50, pp848-863.
111. Fenelon M. A. A. & Furukawa T. (2010) "Design of an active flapping wing mechanism and a micro aerial vehicle using a rotary actuator" *Mechanism and Machine Theory* vol. 45, pp137-146.
112. Hsiao F. Y., Yang T.M. & Lu W. C. (2012) "Dynamics of flapping-wing MAVs: Application to the Tamkang Golden Snitch" *Journal of Applied Science and Engineering* vol. 15, issue 3, pp227-238.
113. Persson P.-O, Willis D. J., & Peraire J. (2011) "Numerical Simulation of Flapping Wings using a Panel Method and a High-Order Navier-Stokes Solver" *International Journal for Numerical Methods in Engineering*

114. Young J. & Lai J.C.S. (2004) "Oscillation Frequency and Amplitude Effects on the Wake of a Plunging Airfoil" *AIAA Journal*
115. Isogai K. Y., Shinmoto Y. & Watanabe Y. (1999) "Effects of Dynamic Stall on Propulsive Efficiency and Thrust of Flapping Airfoil" *AIAA Journal* 37 (10) pp1145-1151.
116. Isogai K., & Shinmoto Y. (2001) "Study on Aerodynamic Mechanism of Hovering Insects," *AIAA Paper* pp2001-2470
117. Liu H., Ellington C. P., Kawachi K., Van Den Berg C. & Willmott A. P. (1998) "A Computational Fluid Dynamic Study of Hawk-Moth Hovering" *Journal of Experimental Biology*, 201 pp. 461–477
118. Lewin G. C., & Haj-Hariri H. (2003) "Modelling Thrust Generation of a Two-Dimensional Heaving Airfoil in a Viscous Flow" *Journal of Fluid Mechanics*, 492 pp339–362
119. Pedro G, Suleman A, & Djilali N. (2003) "A numerical study of the propulsive efficiency of a flapping hydrofoil" *International Journal for Numerical Methods in Fluids* Volume 42, Issue 5, pages 493–526
120. Hover F.S., Haugsdal O., Triantafyllou M.S. (2004) "Effect of angle of attack profiles in flapping foil propulsion" *Journal of Fluids and Structures* 19 (1) pp37–47
121. Tuncer I.H. & Platzer M.F. (2000) "Computational Study of Flapping Airfoil Aerodynamics" *Journal of Aircraft*, 37 (3) pp. 514-520
122. Tuncer I. H., & Kaya M. (2005) "Optimization of Flapping Airfoils for Maximum Thrust and Propulsion Efficiency" *AIAA Journal*, 43 (11) pp2329–2341
123. Tuncer I. H., Walz R. & Platzer, M. F. (1998) "A Computational Study of the Dynamic Stall of a Flapping Airfoil," *AIAA Paper* DOI: 10.2514/6.1998-2519, pp219-225
124. Koochesfahani M. M. (1989) "Vortical Patterns in the Wake of an Oscillating Airfoil" *AIAA Journal*, vol. 27, series 9, pp1200-1205.
125. Anderson J. M., Streitlien K., Barrett D. S. & Triantafyllou M. S. (1998) "Oscillating Foils of High Propulsive Efficiency" *Journal of Fluid Mechanics* 360, pp41-72
126. Jones K. D. & Platzer M. F. (1999) "An Experimental and Numerical Investigation of Flapping-Wing Propulsion" *AIAA Paper No. 99-0995*, Reno Nevada
127. Ho S., Nassef H., Pornsinsirak N., Tai Y.-C., & Ho C.-M., (2003) "Unsteady aerodynamics and flow control for flapping wing flyers" *Progress in Aerospace Sciences* 39 pp635–681
128. Young J. & Lai J. C. S. (2004) "Oscillation Frequency and Amplitude Effects on the Wake of a Plunging Airfoil" *AIAA Journal*.
129. Andro J.-Y. & Jacquin L. (2009) "Frequency effects on the aerodynamic mechanisms of a heaving airfoil in a forward flight configuration" *Aerospace Science and Technology* vol. 13, pp71–80.
130. Ren W., Hu H., Liu H. & Wu J. C. (2013) "An Experimental Investigation on the Asymmetric Wake Formation of an Oscillating Airfoil" *AIAA Journal*, 51st AIAA

Aerospace Sciences Meeting including the New Horizons Forum and Aerospace Exposition, 07 - 10 January 2013.

131. Amiralaei M. R., Alighanbari H. & Hashemite S. M. (2011) "Flow field characteristics study of a flapping airfoil using computational fluid dynamics" *Journal of Fluids and Structures*, vol. 27, pp1068–1085.
132. Shyy W., Berg M., & Ljungqvist D. (1999) "Flapping and flexible wings for biological and micro air vehicles" *Progress in Aerospace Sciences*, vol. 35, pp455-505.
133. Ansari S. A., Zbikowski R., & Knowles K. (2006) "Aerodynamic modelling of insect-like flapping flight for micro air vehicles" *Progress in Aerospace Sciences*, vol. 42, pp129–172.
134. Bos F. M., van Oudheusden B. W. & Bijl H. (2013) "Wing performance and 3-D vortical structure formation in flapping flight" *Journal of Fluids and Structures* vol. 42, pp130-151.
135. Maheri A., Noroozi S. & Vinney J. (2007a) "Decoupled aerodynamic and structural design of wind turbine adaptive blades" *Renewable Energy*, vol. 32 issue 10, pp1753-1767. ISSN 0960-1481.
136. Maheri A. & Isikveren A. (2010) "Performance prediction of wind turbines utilizing passive smart blades: approaches and evaluation" *Wind Energy*, vol. 12, issue (2-3), pp255-265. ISSN 1095-4244.
137. Kelkar A. G. & Whitner C. E. (2005) "Robust control of a morphing airfoil structure" *American control conference*, vol. 5, pp2863-2868.
138. Johnson S. J., Baker J. P., van Dam C. P. & Berg D. (2010) "An overview of active load control techniques for wind turbines with an emphasis on microtabs" *Wind Energy*, vol. 13, issue (2-3), pp239-253.
139. Castagnet D., Poulsen N. K., Buhl T. & Wedel-Heinen J. J. (2011) "Model predictive control of trailing edge flaps on a wind turbine blade" *American control conference*, pp4398-4403.
140. Macquart T., Maheri A. & Busawon K. (2014) "Microtab dynamic modelling for wind turbine blade load rejection" *Renewable Energy*, vol. 64, pp144-152 ISSN 0960-1481, 2014.
141. Knut, O. R., Wedel-Heinen, J. & Christensen, C. J. (1999) "Reliability-based fatigue design of wind-turbine rotor blades
142. Otero, A. D., Ponta, F. L. & Lago, I. L. (2012) "Structural Analysis of Complex Wind Turbine Blades: Flexo-Torsional Vibrational Modes"
143. Nicholls-Lee, R. F., Boyd, S. W. & Turnock, S. R. (2009) "Development of High Performance Composite Bend-Twist Coupled Blades for a Horizontal Axis Tidal Turbine" *Fluid Structure Interactions Research Group, University of Southampton*
144. Zhang H. (2013) "Wind Turbine Adaptive Blade Integrated Design and Analysis" PhD Thesis submitted in partial fulfilment of the requirements of the University of Northumbria at Newcastle upon Tyne.
145. Maheri, A., Noroozi, S. & Vinney, J. (2007c) "Combined Analytical/FEAbased Coupled-Aero-Structure Simulation of Wind Turbines with Bend/Twist Adaptive Blades", *Renewable Energy*, 32(6), pp916-930.

146. Maheri, A., Noroozi, S., Toomer, C. & Vinney, J. (2006c) 'WTAB, a Computer Program for Predicting the Performance of Horizontal Axis Wind Turbines with Adaptive Blades'. *Renewable Energy*, 31(11), 1673- 1685.
147. Maheri, A. & Isikveren, A. T. (2008) 'Variable-state design parameters in design of aero-structures made of intrinsically smart materials'. In: *High Performance Structures and Materials IV*. pp. 421-430.
148. Maheri, A., Noroozi, S., Toomer, C. A. & Vinney, J. (2007b) 'Efficient meshing of a wind turbine blade using force adaptive mesh sizing functions', *Renewable Energy*, Volume 32, Issue 1, January 2007, pp 95-104.
149. Maheri, A., Noroozi, S., Toomer, C. & Vinney, J. (2006b) 'A Simple algorithm to modify an ordinary wind turbine blade to an adaptive one'. In: *European Wind Energy Conference EWEC 2006*, 27 February-2 March 2006, Athens, Greece.
150. Maheri, A. & Isikveren, A. T. (2009a) "Design of wind turbine passive smart blades" *European Wind Energy Conference EWEC 2009*, Marseille, France
151. Maheri, A. (2014) "A typical design optimisation of structures: Case studies" *High Performance and Optimum Design of Structures and Materials*
152. Macquart, T. & Maheri, A. (2015) 'Integrated Aeroelastic and Control Analysis of Wind Turbine Blades Equipped with Microtabs.' *Renewable Energy*, 75. pp. 102-114.
153. Lobitz, D. W. & Laino, D. J. (1998) "Load Mitigation with Twist-Coupled HAWT Blades", *Proceedings of the ASME Wind Energy Symposium*, January 1998.
154. Lobitz, D. W., Veers, P. S., Eisler, G.R., Laino, D. J., Migliore, P. G., & Bir, G. (2001) "The Use of Twist-Coupled Blades to Enhance the Performance of Horizontal Axis Wind Turbines," SAND2001-1003, Sandia National Laboratories, Albuquerque, NM, May 2001
155. Lobitz, D. W. and Veers, P. S. (1998) "Aeroelastic Behaviour of Twist-Coupled HAWT Blades" *American Institute of Aeronautics and Astronautics*
156. Gibson R. F. (2004) "Principles of Composite Material Mechanics" Third Edition, CRC Press Taylor and Francis Group
157. Gay D., Hoa S. V. & Tsai S. W. (2003) "Composite Materials Design and Applications" CRC Press Taylor and Francis Group
158. Autar K. K. (2006) "Mechanics of Composite Materials" Second Edition, CRC Press Taylor and Francis Group
159. Jones R. M. (1999) "Mechanics of Composite Materials" Second Edition, Taylor and Francis Inc.
160. Mortensen A. (2007) "Concise Encyclopedia of Composite Materials" Second Edition, Elsevier
161. Locke, J. & Valencia, U. (2004) "Design studies for Twist-Coupled Wind Turbine Blades" Wichita State University National Institute for Aviation Research Wichita, Kansas 67260-0093.
162. Karaolis N. M., Jeronimidis G, & Mussgrove P. J. (1989) "Composite wind turbine blades: coupling effects and rotor aerodynamic performance" *Proceedings of EWEC'89*, European Wind Energy Conference, Glasgow, Scotland, 1989

163. Kooijman H. J. T. (1996) “Bending-Torsion Coupling of a Wind Turbine Rotor Blade” ECN-I 96- 060, Netherlands Energy Research Foundation ECN
164. Lobitz D. W. & Veers P. S. (1996) “Enhanced Performance of HAWTs Using Adaptive Blades” United States Department of Energy under Contract DE-AC04-94AL8500
165. Hayat K., Martinez de Lecea A. G., Moriones C. D. & Ha S.K. (2016) “Flutter Performance of bend-twist coupled large-scale wind turbines blades” *Journal of Sound and Vibration* 370 149–162
166. Stablein A. R., Tibaldi C. & Hansen M. H. (2016) “Using Pretwist to Reduce Power Loss of Bend-Twist Coupled Blades” AIAA 34th Wind Energy Symposium
167. Module 5 Laminate Theory, Lecture 16: Introduction to Classical Laminate Theory, http://nptel.ac.in/courses/101104010/lecture16/16_3.htm accessed date 03/04/2016
168. Classical Laminate Theory <http://www.isfk.at/en/1428/> accessed date 03/04/2016
169. Clyne T. W. (2016) “Course C16: Composite Materials” Department of Materials Science and Metallurgy
170. Maheri A. & Daadbin A. (2010) “High performance finite element analysis of composite aeroelastic structures” In: High Performance Structures and Materials V
171. Heathcote S. & Gursul I. (2007) “Flexible Flapping Airfoil Propulsion at Low Reynolds Numbers” *AIAA Journal*, 45 (5) pp1066-1079
172. Schouveiler L., Hover F.S, & Triantafyllou M.S. (2005) “Performance of flapping foil propulsion” *Journal of Fluids and Structures* 20 pp949–959.
173. Miao J.-M, & Ho M.-H. (2005) “Effect of flexure on aerodynamic propulsive efficiency of flapping flexible airfoil” *Journal of Fluids and Structures* 22 (3) pp 401–419
174. Ansari S.A, Zbikowski R, & Knowles K (2006) “Aerodynamic modelling of insect-like flapping flight for micro air vehicles” *Progress in Aerospace Sciences* 42 pp129–172
175. Truong T. Q., Phan V. H., Sane S. P. & Park H. C. (2014) “Pitching Moment Generation in an Insect-Mimicking Flapping-Wing System” *Journal of Bionic Engineering* 11 pp36–51
176. Andro J.-Y & Jacquin L., (2009) “Frequency effects on the aerodynamic mechanisms of a heaving airfoil in a forward flight configuration” *Aerospace Science and Technology*, 13, pp71–80.
177. Amiralaei M.R., Alighanbari H. & Hashemite S.M., (2011) “Flow field characteristics study of a flapping airfoil using computational fluid dynamics” *Journal of Fluids and Structures*, 27 pp1068–1085.
178. Bos F.M., van Oudheusden B.W. & Bijl H. (2013) “Wing performance and 3-D vortical structure formation in flapping flight” *Journal of Fluids and Structures* 42 pp130-151
179. Du G. & Sun M. (2012) “Aerodynamic effects of corrugation and deformation in flapping wings of hovering hoverflies” *Journal of Theoretical Biology* pp19–28

180. Wang X.-S., Li Y. & Shi Y.-F., (2008) “Effects of sandwich microstructures on mechanical behaviors of dragonfly wing vein” *Composites Science and Technology*, 68, pp186–192
181. Ren H., Wang X., Li X., & Chen Y., (2013) “Effects of Dragonfly Wing Structure on the Dynamic Performances” *Journal of Bionic Engineering* 10, pp28–38.
182. Mantia M.L. & Dabnichki P. (2011) “Effect of the wing shape on the thrust of flapping wing” *Applied Mathematical Modelling* 35, (10), pp4979–4990
183. Sun J. & Bhushan B. (2012) “The structure and mechanical properties of dragonfly wings and their role on flyability” *C. R. Mecanique*, 340, pp3–17.
184. Pourtakdoust S. H. & Aliabadi S. K. (2012) “Evaluation of flapping wing propulsion based on a new experimentally validated aeroelastic model” *Scientia Iranica B* 19 (3), pp472–482
185. Stanford B., Beran P., Snyder R. & Patil M. (2013) “Stability and power optimality in time-periodic flapping wing structures” *Journal of Fluids and Structures* 38 pp238–254
186. Ghommem M., Collier N., Niemi A. H. & Calo V. M. (2014) “On the shape optimization of flapping wings and their performance analysis” *Aerospace Science and Technology* 32 pp 274–292
187. Takizawa K., Henicke B. Puntel A. Kostov N. & Tezduyar T.E (2013) “Computer modelling techniques for flapping-wing aerodynamics of a locust” *Computers & Fluids* vol. 85, pp 125-134.
188. Gilmanov A. & Sotiropoulos F. (2005) “A hybrid Cartesian/immersed boundary for simulating flows with 3D, geometrically complex moving bodies” *Journal of Computational Physics* vol. 207, pp 457-492.
189. Wilmot A.P. & Ellington C.P. (1997) “The mechanics of flight in the Hawkmoth *Manduca sexta* I Kinematics of hovering and forward flight” *The Journal of Experimental Biology*, vol. 200, pp 2705-2722
190. Castelli M.R., Cioppa P. & Benini E. (2012) “Numerical Simulation of the flow field around a 30° Inclined Flat Plate” *World Academy of Science, Engineering and Technology International Journal of Aerospace and Mechanical Engineering*, vol. 6, No. 3.
191. Cengel Y.A. & Cimbala J.M. (2006) “Fluid Mechanics: Fundamental and Applications” ISBN 0-07-247236-7
192. Tsai, S. & Ong, C. H. (1998) *D-Spar Blade Design and Manufacture. unpublished contractor reports*. Sandia National Laboratories contract BB-6066 Stanford University.
193. Maheri, A., Noroozi, S., Toomer, C. & Vinney, J. (2006d) “Damping the fluctuating behaviour and improving the convergence rate of the axial induction factor in the BEMT-based rotor aerodynamic codes”. In: European Wind Energy Conference EWEC 2006, 27 February-2 March 2006, Athens, Greece.
194. Maheri, A. (2012) “A finite element suite for deformation analysis of composite aeroelastic structures subjected to operational aerodynamic loading”. In: *Proceedings of the Institution of Mechanical Engineers, Part C: Journal of Mechanical Engineering Science* 226(8), 2062-2076

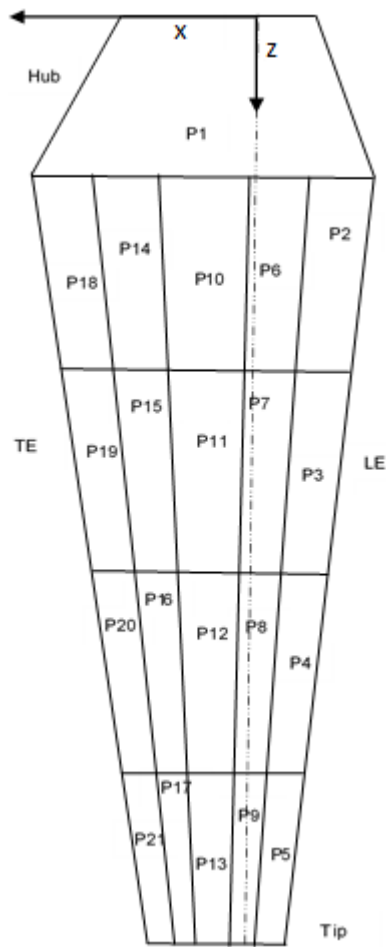
195. Nicholls-Lee, R. & Turnock, S. (2007) "Enhancing performance of a horizontal axis tidal turbine using adaptive blades". In: *Oceans '07. Aberdeen, Scotland: IEEE; 2007.*
196. Kim, C. & White, S. R. (1997) "Thick-walled composite beam theory including 3-d elastic effects and torsional warping". *International Journal of Solids and Structures*, 34(31–32), 4237-4259.
197. Dong O. Y. & Kwon J.O. (2014) "Predicting wind turbine blade loads and aeroelastic response using a coupled CFD-CSD method" *Renewable Energy* 70 pp184-196
198. Hansen H.M (2007) "Aeroelastic Instability Problems for Wind Turbines" *Wind Energy* vol. 10 pp 551-577
199. Wang L., Liu X., and Kolios A. (2016) "State of the art in the aeroelasticity of wind turbine blades: Aeroelastic modelling" *Renewable and Sustainable Energy Reviews* 64, pp195-210
200. Dowell E. (2015) "A Modern Course in Aeroelasticity" Fifth Revised and Enlarged Edition, Solid Mechanics and its Applications, (ISBN: 9783319094526)
201. Andrienne T. (2012) "Experimental and Numerical Investigations of the Aeroelastic Stability of Bluff Structures" PhD Thesis submitted to the Department of Aerospace and Mechanics, University of Liege
202. Holierhoek J. G. (2008) "Aeroelasticity of Large Wind Turbines" PhD Thesis submitted to de Technische Universiteit Delft
203. Verelst D. (2009) "Flexible Wind Turbine Blades: a FEM-BEM coupled model approach" Graduation Report to Delft University of Technology
204. Ramdenee D., Llinca A. & Minea I. S. (2012) "Aeroelasticity of Wind Turbines Blades Using Numerical Simulation" <http://dx.doi.org/10.5772/52281>
205. Andrienne T. (2016) "Aeroelasticity & Experimental Aerodynamics: Introduction- Equation of Motions" http://www.itsa-aea.ulg.ac.be/cms/uploads/AERO0032-1_2015-16_Lecture1.pdf Accessed date 01/07/2016
206. Vatne S. R. (2011) "Aeroelastic Instability and Flutter for a 10 MW Wind Turbine" MSc Thesis submitted to the Department of Energy and Process Engineering, Norwegian University of Science and Technology.
207. Hayat K. & Ha K. S. (2015) "Flutter performance of large-scale wind turbine blade with shallow-angled skins" *Composite Structures* 132 pp575-583
208. Aerodynamic Flutter http://dl.btc.pl/kamami_wa/hk_24474_2.pdf accessed date 17/07/2016
209. Baran R. P (2013) "Aeroelastic Analysis and Classical Flutter of a Wind Turbine using BLADEMODE V.2.0 and PHATAS in FOCUS 6" MSc Thesis submitted to Department of Sustainable Energy Technology, Delft University of Technology
210. Capuzzi M., Pirrera A. & Weaver P.M. (2015) "Structural design of a novel aeroelastically tailored wind turbine blade" *Thin-walled Structures*
211. Campbell F. C. (2010) "Introduction to Composite Materials" *Structural Composite Materials*, ASM International
212. Bryan H. (1999) "Engineering Composite Materials" The Institute of Materials, London

213. Koruche U. S. & Patil S. F. (2015) “Application of Classical Lamination Theory and Analytical Modelling of Laminates” International Research Journal of Engineering and Technology (IRJET), 2(2), e-ISSN: 2395-0056
214. Nettles A. T. (1994) “Basic Mechanics of Laminated Composite Plates” NASA Reference Publication 135
215. Conti-Ramsden J. & Dyer K. (2015) “Materials innovations for more efficient wind turbines” Renewable Energy Focus.

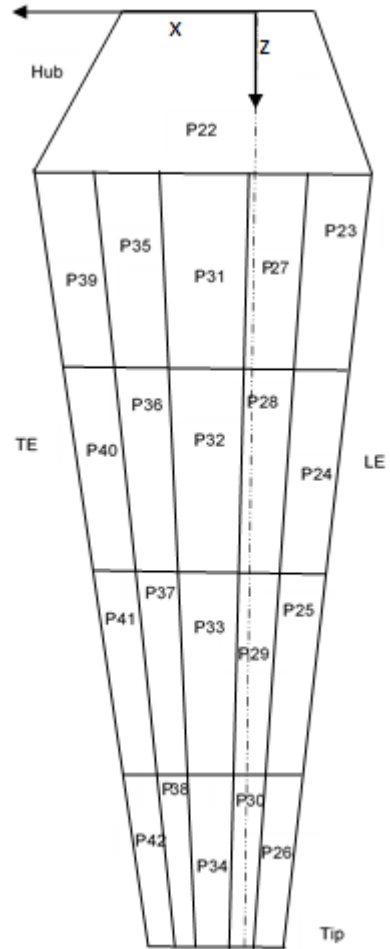
Appendix A

Table A1- The Blade Patches Configuration

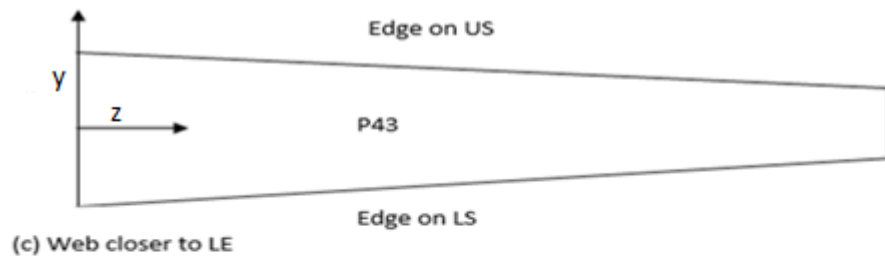
Patch #	Location index	Patch Coordinates In 2D Square system of coordinates
1	1	[0,0;1,0;1,0.13333;0,0.13333]
2	1	[0,0.13333;0.050,0.13333;0.050,0.35;0,0.35]
3	1	[0,0.35;0.050,0.35;0.050,0.60;0,0.60]
4	1	[0,0.60;0.050,0.60;0.050,0.90;0,0.90]
5	1	[0,0.90;0.050,0.90;0.050,1;0,1]
6	1	[0.050,0.13333;0.25,0.13333;0.25,0.35;0.050,0.35]
7	1	[0.050,0.35;0.25,0.35;0.25,0.60;0.050,0.60]
8	1	[0.050,0.60;0.25,0.60;0.25,0.90;0.050,0.90]
9	1	[0.050,0.90;0.25,0.90;0.25,1;0.050,1]
10	1	[0.25,0.13333;0.55,0.13333;0.55,0.35;0.25,0.35]
11	1	[0.25,0.35;0.55,0.35;0.55,0.60;0.25,0.60]
12	1	[0.25,0.60;0.55,0.60;0.55,0.90;0.25,0.90]
13	1	[0.25,0.90;0.55,0.90;0.55,1;0.25,1]
14	1	[0.55,0.13333;0.85,0.13333;0.85,0.35;0.55,0.35]
15	1	[0.55,0.35;0.85,0.35;0.85,0.60;0.55,0.60]
16	1	[0.55,0.60;0.85,0.60;0.85,0.90;0.55,0.90]
17	1	[0.55,0.90;0.85,0.90;0.85,1;0.55,1]
18	1	[0.85,0.13333;1,0.13333;1,0.35;0.85,0.35]
19	1	[0.85,0.35;1,0.35;1,0.60;0.85,0.60]
20	1	[0.85,0.60;1,0.60;1,0.90;0.85,0.90]
21	1	[0.85,0.90;1,0.90;1,1;0.85,1]
22	2	[0,0;1,0;1,0.13333;0,0.13333]
23	2	[0,0.13333;0.050,0.13333;0.050,0.35;0,0.35]
24	2	[0,0.35;0.050,0.35;0.050,0.60;0,0.60]
25	2	[0,0.60;0.050,0.60;0.050,0.90;0,0.90]
26	2	[0,0.90;0.050,0.90;0.050,1;0,1]
27	2	[0.050,0.13333;0.25,0.13333;0.25,0.35;0.050,0.35]
28	2	[0.050,0.35;0.25,0.35;0.25,0.60;0.050,0.60]
29	2	[0.050,0.60;0.25,0.60;0.25,0.90;0.050,0.90]
30	2	[0.050,0.90;0.25,0.90;0.25,1;0.050,1]
31	2	[0.25,0.13333;0.55,0.13333;0.55,0.35;0.25,0.35]
32	2	[0.25,0.35;0.55,0.35;0.55,0.60;0.25,0.60]
33	2	[0.25,0.60;0.55,0.60;0.55,0.90;0.25,0.90]
34	2	[0.25,0.90;0.55,0.90;0.55,1;0.25,1]
35	2	[0.55,0.13333;0.85,0.13333;0.85,0.35;0.55,0.35]
36	2	[0.55,0.35;0.85,0.35;0.85,0.60;0.55,0.60]
37	2	[0.55,0.60;0.85,0.60;0.85,0.90;0.55,0.90]
38	2	[0.55,0.90;0.85,0.90;0.85,1;0.55,1]
39	2	[0.85,0.13333;1,0.13333;1,0.35;0.85,0.35]
40	2	[0.85,0.35;1,0.35;1,0.60;0.85,0.60]
41	2	[0.85,0.60;1,0.60;1,0.90;0.85,0.90]
42	2	[0.85,0.90;1,0.90;1,1;0.85,1]
43	3	[0,0.13333;1,0.13333;1,1;0,1]
44	4	[0,0.13333;1,0.13333;1,1;0,1]



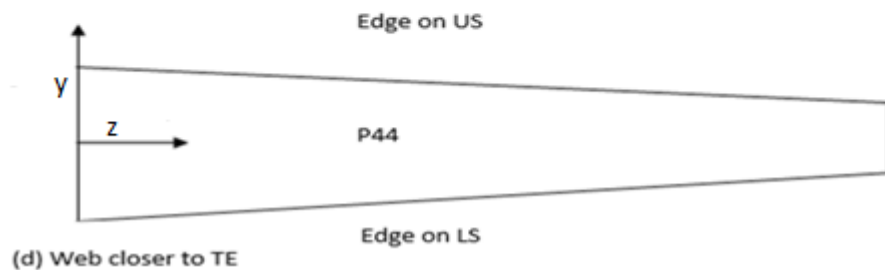
(a) Patch Numbering on upper surface



(b) Patch Numbering on lower surface



(c) Web closer to LE



(d) Web closer to TE

Figure A1-(a-d) -Blade Patches Configuration

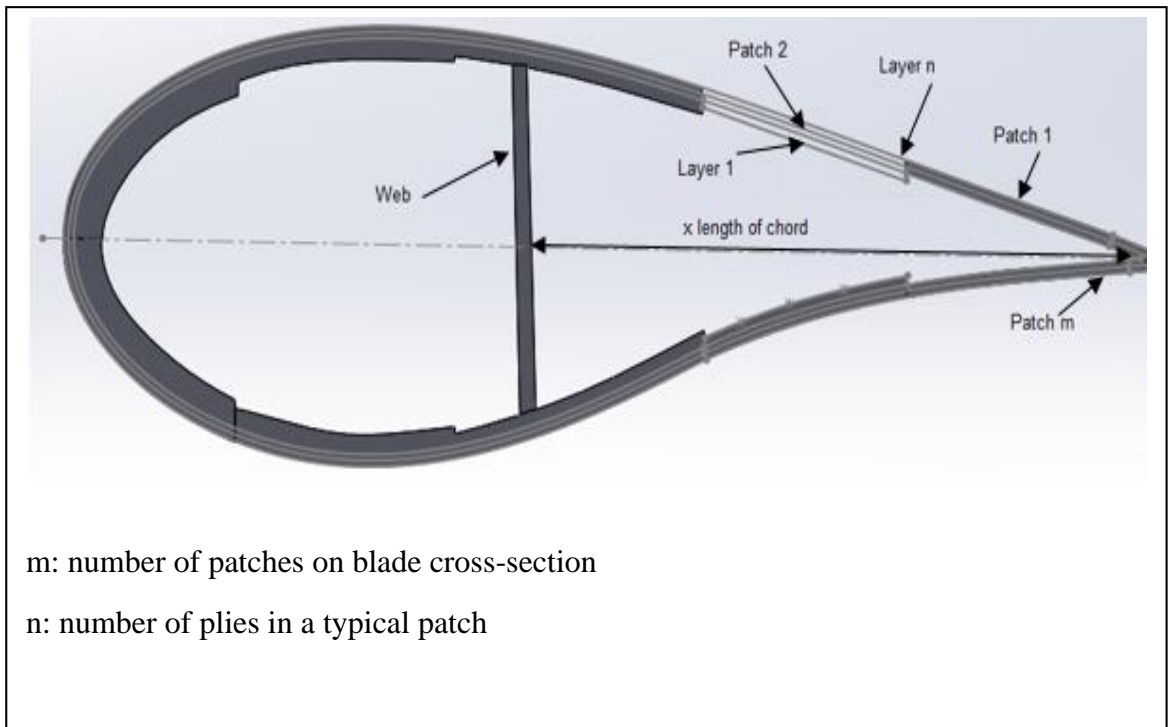


Figure A2 -A typical cross-section of an adaptive blade with varying thickness

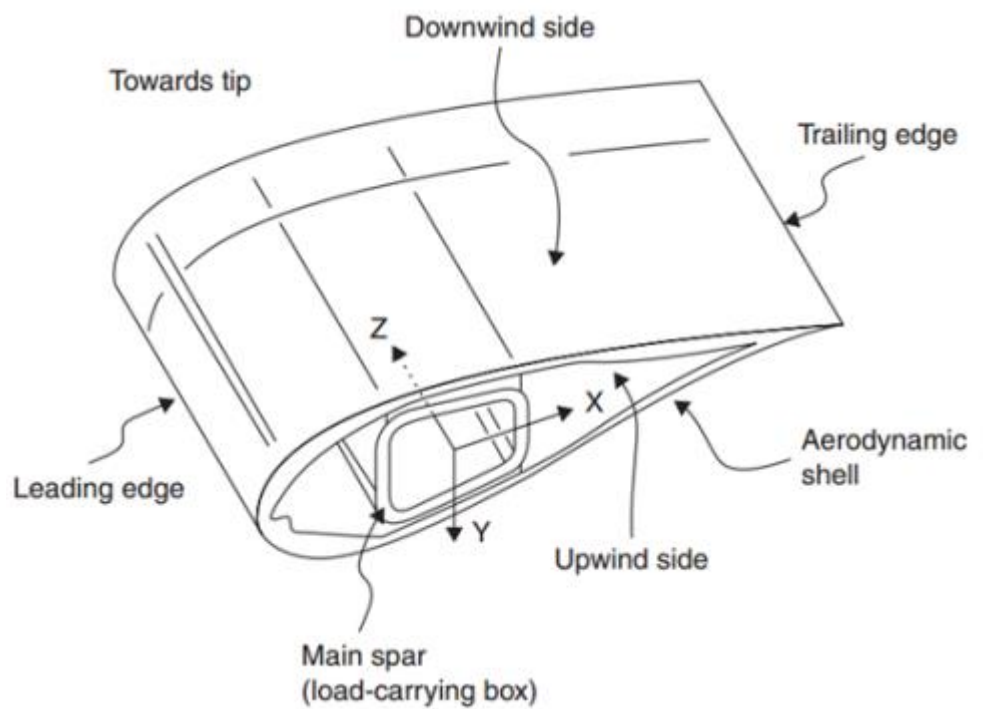


Figure A3 -A typical section of a wind turbine blade [215]

Appendix B

Using Rules of Mixture [211 & 212];

$$\begin{aligned}
 \text{Density of Composite} &= \rho_c = \sum_{i=1}^n \rho_i V_i \\
 \rho_c &= \rho_f V_f + \rho_m V_m \\
 E_1 &= E_f V_f + E_m V_m \\
 \nu_{12} = \nu_{13} &= \nu_f V_f + \nu_m V_m
 \end{aligned} \tag{B.1a-d}$$

Using the Halpin-Tsai model for the transverse moduli

$$E_2 = E_3 = \frac{E_m (1 + \xi \eta V_f)}{(1 - \eta V_f)}, \quad \text{where } \eta = \frac{(E_f - E_m)}{(E_f + \xi E_m)} \tag{B.2}$$

ξ is close to unity

Using the Halpin-Tsai equations for the shear moduli

$$G_{12} = G_{13} = \frac{G_m (1 + \xi \eta V_f)}{(1 - \eta V_f)}, \quad \text{where } \eta = \frac{(G_f - G_m)}{(G_f + \xi G_m)} \tag{B.3}$$

$$\nu_{23} = \nu_f V_f + \nu_m (1 - V_f) \left[\frac{1 + \nu_m - \nu_{12} \left(\frac{E_m}{E_{11}} \right)}{1 - \nu_m^2 + \nu_m \nu_{12} \left(\frac{E_m}{E_{11}} \right)} \right]$$

$$\nu_{23} = \nu_f V_f + \nu_m V_m \left[\frac{1 + \nu_m - \nu_{12} \left(\frac{E_m}{E_{11}} \right)}{1 - \nu_m^2 + \nu_m \nu_{12} \left(\frac{E_m}{E_{11}} \right)} \right]$$

$$\text{where } V_m = 1 - V_f \tag{B.4a-c}$$

$$G_{23} = \frac{E_{22}}{2(1 + \nu_{23})} \tag{B.5}$$

The stress-strain relationship for an orthotropic material using Hooke's Law in terms of strain is

$$\begin{bmatrix} \varepsilon_1 \\ \varepsilon_2 \\ \varepsilon_3 \\ \nu_{23} \\ \nu_{31} \\ \nu_{12} \end{bmatrix} = \begin{bmatrix} \frac{1}{E_1} & -\frac{\nu_{21}}{E_2} & -\frac{\nu_{31}}{E_3} & 0 & 0 & 0 \\ -\frac{\nu_{12}}{E_1} & \frac{1}{E_2} & -\frac{\nu_{32}}{E_3} & 0 & 0 & 0 \\ -\frac{\nu_{13}}{E_1} & -\frac{\nu_{23}}{E_2} & \frac{1}{E_3} & 0 & 0 & 0 \\ 0 & 0 & 0 & \frac{1}{G_{23}} & 0 & 0 \\ 0 & 0 & 0 & 0 & \frac{1}{G_{31}} & 0 \\ 0 & 0 & 0 & 0 & 0 & \frac{1}{G_{12}} \end{bmatrix} \begin{bmatrix} \sigma_1 \\ \sigma_2 \\ \sigma_3 \\ \tau_{23} \\ \tau_{31} \\ \tau_{12} \end{bmatrix} \quad (\text{B.6})$$

For thin unidirectional lamina which is assumed not to carry any out-of-plane loads, the plane stress condition can be assumed for the lamina. Therefore, $\sigma_3 = 0$, $\tau_{31} = 0$ and $\tau_{23} = 0$. This assumption reduces the three dimensional stress-strain equations to two dimensional stress-strain equations [212-214]. Thus, Equation (B.6) can be written as:

$$\begin{bmatrix} \varepsilon_1 \\ \varepsilon_2 \\ \nu_{12} \end{bmatrix} = \begin{bmatrix} S_{11} & S_{12} & 0 \\ S_{12} & S_{22} & 0 \\ 0 & 0 & S_{66} \end{bmatrix} \begin{bmatrix} \sigma_1 \\ \sigma_2 \\ \tau_{12} \end{bmatrix} \quad (\text{B.7})$$

where

$$S_{11} = \frac{1}{E_1} \quad , \quad S_{12} = -\frac{\nu_{12}}{E_1} = -\frac{\nu_{21}}{E_2} \quad , \quad S_{22} = \frac{1}{E_2} \quad , \quad S_{66} = \frac{1}{G_{12}}$$

Inverting Equation (B.7), the stress-strain relationship will be:

$$\begin{bmatrix} \sigma_1 \\ \sigma_2 \\ \tau_{12} \end{bmatrix} = \begin{bmatrix} Q_{11} & Q_{12} & 0 \\ Q_{12} & Q_{22} & 0 \\ 0 & 0 & Q_{66} \end{bmatrix} \begin{bmatrix} \varepsilon_1 \\ \varepsilon_2 \\ \nu_{12} \end{bmatrix} \quad (\text{B.8})$$

The reduced stiffness coefficients Q_{ij} for the material in terms of engineering constants are shown below:

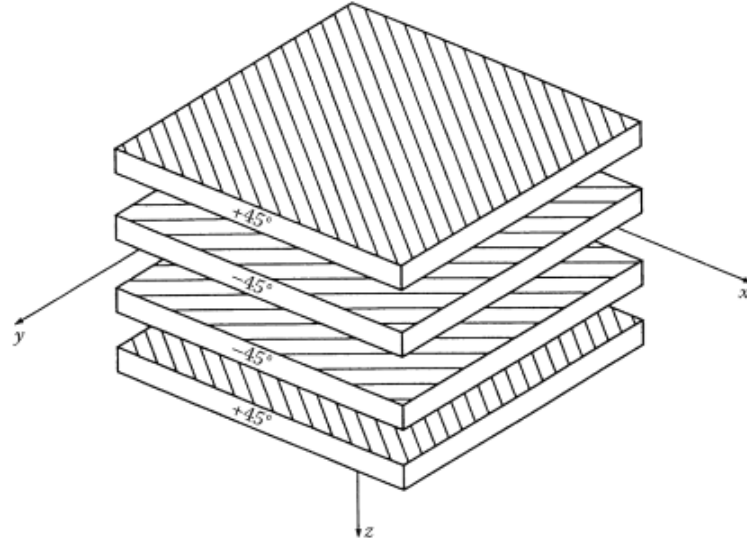


Figure B1 -Exploded view of [-45/+45/-45/+45] symmetric laminate [156]

$$Q_{11} = \frac{E_1}{1 - \nu_{12}\nu_{21}}$$

$$Q_{22} = \frac{E_2}{1 - \nu_{12}\nu_{21}}$$

$$Q_{12} = \frac{\nu_{21}E_1}{1 - \nu_{12}\nu_{21}} = \frac{\nu_{12}E_2}{1 - \nu_{12}\nu_{21}}$$

$$Q_{66} = G_{12} \quad (\text{B.9a-d})$$

The relationship between the transformed reduced stiffness coefficients \bar{Q}_{ij} for each ply based on the reduced stiffness coefficients and fibre angle are shown in Equations (B.10.a) to (B.10.f) [214]

$$\bar{Q}_{11} = Q_{11}m^4 + 2(Q_{12} + 2Q_{66})m^2n^2 + Q_{22}n^4$$

$$\bar{Q}_{12} = (Q_{11} + Q_{22} - 4Q_{66})m^2n^2 + Q_{12}(m^4 + n^4)$$

$$\bar{Q}_{22} = Q_{11}n^4 + 2(Q_{12} + 2Q_{66})m^2n^2 + Q_{22}m^4$$

$$\bar{Q}_{16} = (Q_{11} - Q_{12} - 2Q_{66})m^3n + (Q_{12} - Q_{22} + 2Q_{66})mn^3$$

$$\bar{Q}_{26} = (Q_{11} - Q_{12} - 2Q_{66})mn^3 + (Q_{12} - Q_{22} + 2Q_{66})m^3n$$

$$\bar{Q}_{66} = (Q_{11} + Q_{22} - 2Q_{12} - 2Q_{66})m^2n^2 + Q_{66}(m^4 + n^4) \quad (\text{B.10a-f})$$

where $m = \cos \theta_k$, $n = \sin \theta_k$

The laminate extensional stiffness matrix A , coupling stiffness matrix B and bending stiffness D are defined below [214]:

$$\begin{aligned}
 A_{ij} &= \sum_{k=1}^n \left[\bar{Q}_{ij} \right]_k t_k \\
 B_{ij} &= \sum_{k=1}^n \left[\bar{Q}_{ij} \right]_k t_k \frac{(h_k + h_{k-1})}{2} \\
 D_{ij} &= \sum_{k=1}^n \left[\bar{Q}_{ij} \right]_k \left(\frac{t_k^3}{12} + t_k \bar{z}_k^2 \right)
 \end{aligned} \tag{B.11a-c}$$

where $\frac{(h_k + h_{k-1})}{2} \equiv \bar{z}_k$

From the ABD matrices, the laminate elastic properties are defined [214]:

$$\begin{aligned}
 E_{xx} &= \frac{\begin{bmatrix} A_{11} & A_{12} & A_{16} & B_{11} & B_{12} & B_{16} \\ A_{12} & A_{22} & A_{26} & B_{12} & B_{22} & B_{26} \\ A_{16} & A_{26} & A_{66} & B_{16} & B_{26} & B_{66} \\ B_{11} & B_{12} & B_{16} & D_{11} & D_{12} & D_{16} \\ B_{12} & B_{22} & B_{26} & D_{12} & D_{22} & D_{26} \\ B_{16} & B_{26} & B_{66} & D_{16} & D_{26} & D_{66} \end{bmatrix}}{h}, & E_{yy} &= \frac{\begin{bmatrix} A_{11} & A_{12} & A_{16} & B_{11} & B_{12} & B_{16} \\ A_{12} & A_{22} & A_{26} & B_{12} & B_{22} & B_{26} \\ A_{16} & A_{26} & A_{66} & B_{16} & B_{26} & B_{66} \\ B_{11} & B_{12} & B_{16} & D_{11} & D_{12} & D_{16} \\ B_{12} & B_{22} & B_{26} & D_{12} & D_{22} & D_{26} \\ B_{16} & B_{26} & B_{66} & D_{16} & D_{26} & D_{66} \end{bmatrix}}{h} \\
 & & & \frac{\begin{bmatrix} A_{22} & A_{26} & B_{12} & B_{22} & B_{26} \\ A_{26} & A_{66} & B_{16} & B_{26} & B_{66} \\ B_{12} & B_{16} & D_{11} & D_{12} & D_{16} \\ B_{22} & B_{26} & D_{12} & D_{22} & D_{26} \\ B_{26} & B_{66} & D_{16} & D_{26} & D_{66} \end{bmatrix}}{h}, & & \frac{\begin{bmatrix} A_{11} & A_{16} & B_{11} & B_{12} & B_{16} \\ A_{16} & A_{66} & B_{16} & B_{26} & B_{66} \\ B_{11} & B_{16} & D_{11} & D_{12} & D_{16} \\ B_{12} & B_{26} & D_{12} & D_{22} & D_{26} \\ B_{16} & B_{66} & D_{16} & D_{26} & D_{66} \end{bmatrix}}{h} \\
 \\
 G_{xy} &= \frac{\begin{bmatrix} A_{11} & A_{12} & A_{16} & B_{11} & B_{12} & B_{16} \\ A_{12} & A_{22} & A_{26} & B_{12} & B_{22} & B_{26} \\ A_{16} & A_{26} & A_{66} & B_{16} & B_{26} & B_{66} \\ B_{11} & B_{12} & B_{16} & D_{11} & D_{12} & D_{16} \\ B_{12} & B_{22} & B_{26} & D_{12} & D_{22} & D_{26} \\ B_{16} & B_{26} & B_{66} & D_{16} & D_{26} & D_{66} \end{bmatrix}}{h}, & \nu_{xy} &= \frac{\begin{bmatrix} A_{12} & A_{26} & B_{12} & B_{22} & B_{26} \\ A_{16} & A_{66} & B_{16} & B_{26} & B_{66} \\ B_{11} & B_{16} & D_{11} & D_{12} & D_{16} \\ B_{12} & B_{26} & D_{12} & D_{22} & D_{26} \\ B_{16} & B_{66} & D_{16} & D_{26} & D_{66} \end{bmatrix}}{\begin{bmatrix} A_{22} & A_{26} & B_{12} & B_{22} & B_{26} \\ A_{26} & A_{66} & B_{16} & B_{26} & B_{66} \\ B_{12} & B_{16} & D_{11} & D_{12} & D_{16} \\ B_{22} & B_{26} & D_{12} & D_{22} & D_{26} \\ B_{26} & B_{66} & D_{16} & D_{26} & D_{66} \end{bmatrix}}
 \end{aligned}$$

$$v_{yx} = \frac{\begin{matrix} - \\ \begin{bmatrix} A_{12} & A_{16} & B_{11} & B_{12} & B_{16} \\ A_{16} & A_{66} & B_{16} & B_{26} & B_{66} \\ B_{12} & B_{16} & D_{11} & D_{12} & D_{16} \\ B_{22} & B_{26} & D_{12} & D_{22} & D_{26} \\ B_{16} & B_{66} & D_{16} & D_{26} & D_{66} \end{bmatrix} \end{matrix}}{\begin{bmatrix} A_{11} & A_{16} & B_{12} & B_{22} & B_{26} \\ A_{16} & A_{66} & B_{16} & B_{26} & B_{66} \\ B_{11} & B_{16} & D_{11} & D_{12} & D_{16} \\ B_{12} & B_{26} & D_{12} & D_{22} & D_{26} \\ B_{16} & B_{66} & D_{16} & D_{26} & D_{66} \end{bmatrix}}$$

Appendix C

This section shows the mode shape of the blade deformation for NREL 5MW and AWT-27 blades for mirror configurations of fibre orientation 50 degrees and 45 degrees respectively.

Mode Shape for NREL 5MW

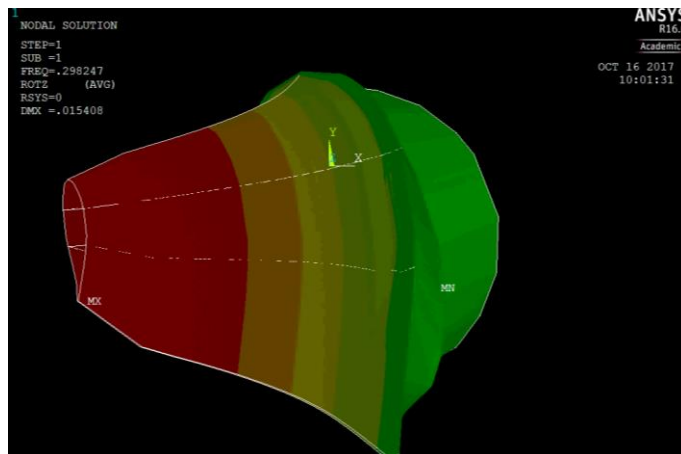


Figure C1-(a) -1st Mode Shape NREL 5MW [1st Flap-wise deformation]

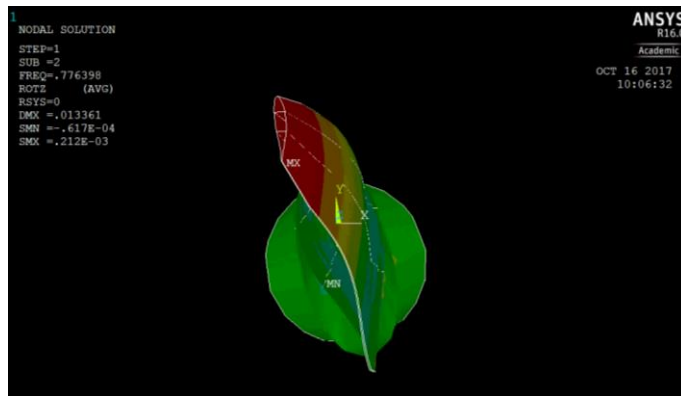


Figure C1-(b) -2nd Mode Shape NREL 5MW [1st Edge-wise deformation]

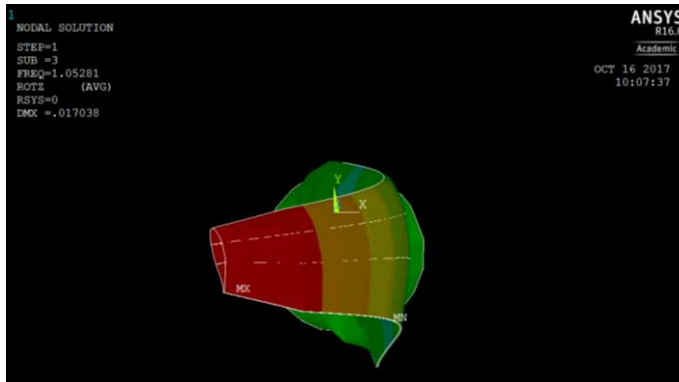


Figure C1-(c.) -3rd Mode Shape NREL 5MW [2nd Flap-wise deformation]

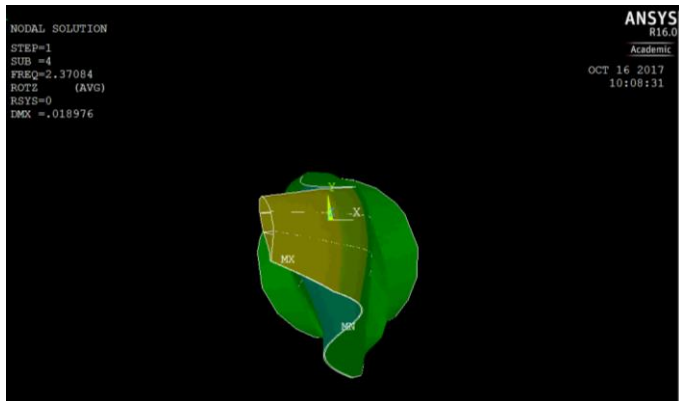


Figure C1-(d) -4th Mode Shape NREL 5MW [3rd Flap-wise deformation]

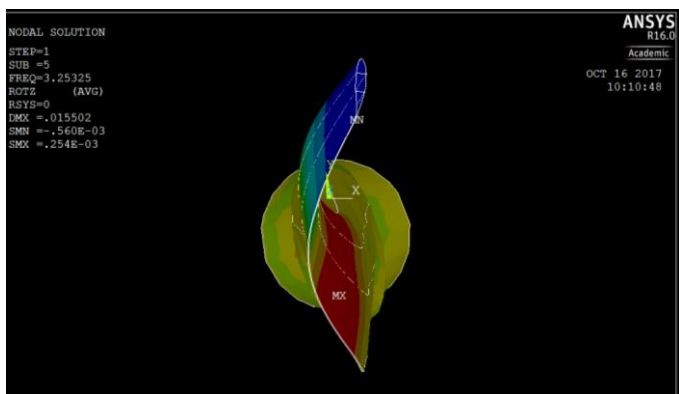


Figure C.1-(e) -5th Mode Shape NREL 5MW [2nd Edge-wise deformation]

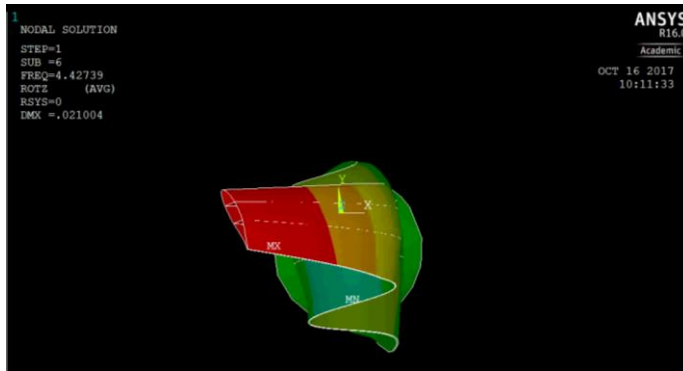


Figure C1-(f) -6th Mode Shape NREL 5MW [1st Torsional deformation]

Mode Shape for AWT-27

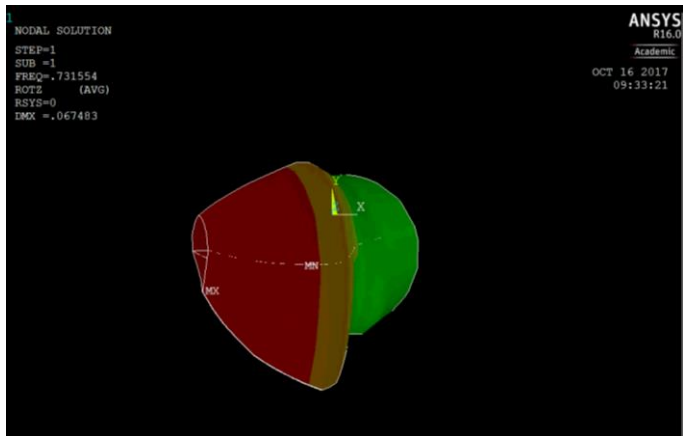


Figure C2-(a) -1st Mode Shape AWT-27 [1st Flap-wise deformation]

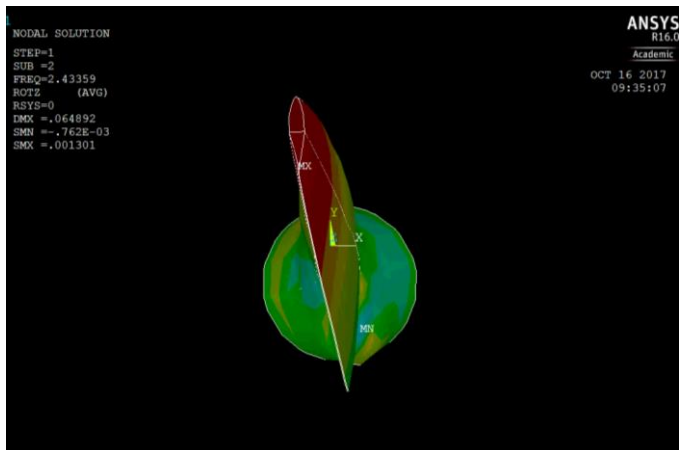


Figure C2-(b) -2nd Mode Shape AWT-27 [1st Edge-wise deformation]

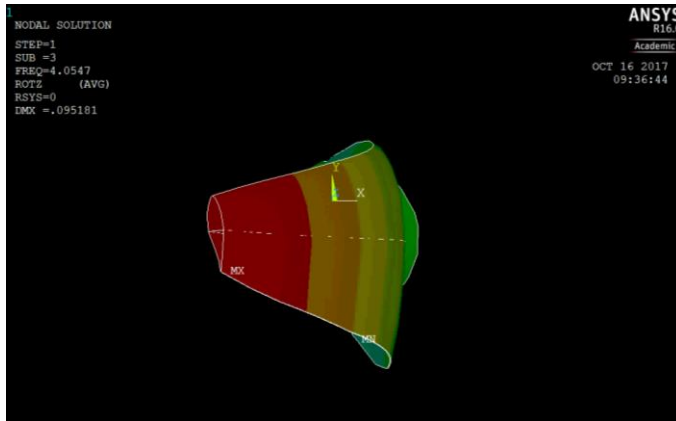


Figure C2-(c) -3rd Mode Shape AWT-27 [2nd Flap-wise deformation]

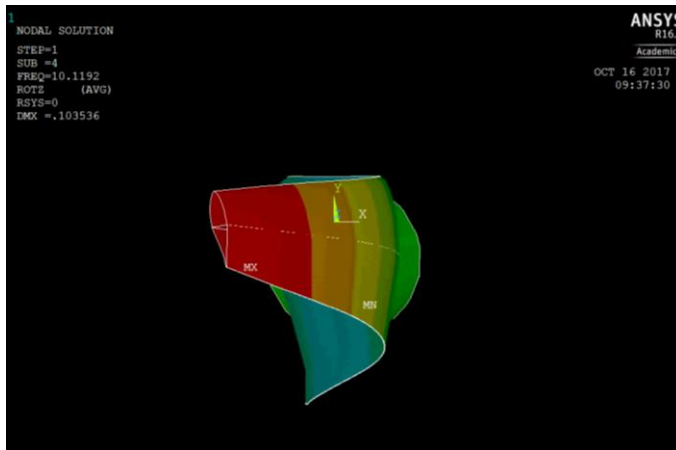


Figure C2-(d) -4th Mode Shape AWT-27 [3rd Flap-wise deformation]

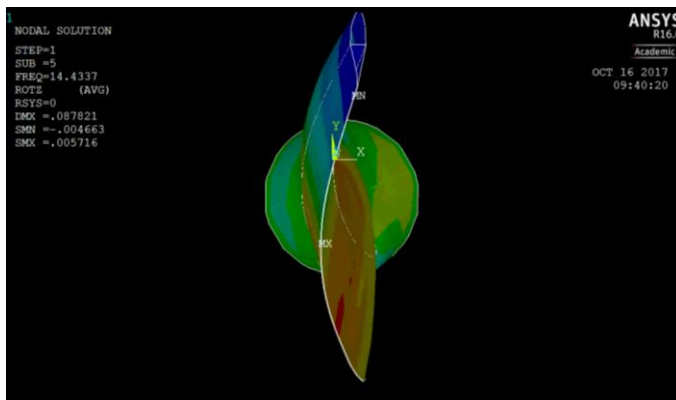


Figure C2-(e) -5th Mode Shape AWT-27[2nd Edge-wise deformation]

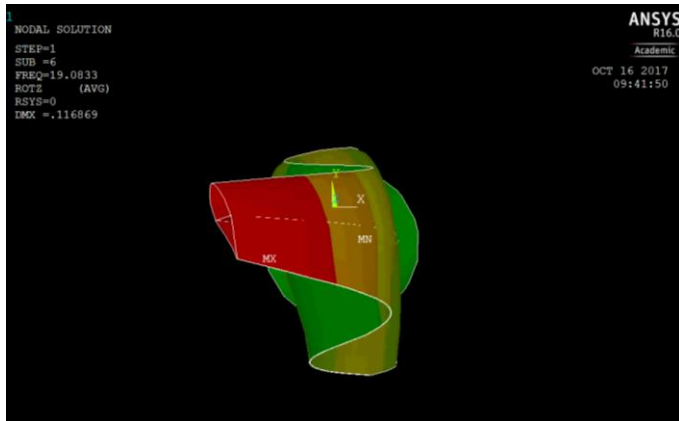


Figure C2-(f) -6th Mode Shape AWT-27 [1st Torsional deformation]